

HUMAN IN-VIVO CARDIAC PHOSPHORUS NMR SPECTROSCOPY AT 3.0 TESLA

By

ANGELA PROPERZIO BRUNER

A DISSERTATION PRESENTED TO THE GRADUATE SCHOOL
OF THE UNIVERSITY OF FLORIDA IN PARTIAL FULFILLMENT
OF THE REQUIREMENTS FOR THE DEGREE OF
DOCTOR OF PHILOSOPHY

UNIVERSITY OF FLORIDA

1999

Copyright 1999

by

Angela Properzio Bruner

This work is dedicated to my loving husband, Thom Bruner, and my parents, Sharon and Bill Properzio, without whom I would not have had the loving support I needed to complete this work.

ACKNOWLEDGMENTS

I would like to thank the following individuals for their assistance and for making this work possible. The greatest thanks go to my advisor and mentor, Dr. Kate Scott, who encouraged and advised me through this project. Thanks also goes to Dr. Hee-Won Kim, who taught me the basics of the ISIS pulse sequence, shared experiences in working on the General Electric (GE) Sigma™, and offered valuable pulse programming support. Credit must be given to David Peterson and Bryan Wolverton, under the direction of Dr. Fitzsimmons, who built the coils that were used in this study. Thanks also go to the combined efforts of Dr. Scott, Dr. Fitzsimmons, Dr. Ballinger, Shands at UF, the VA Hospital, and the Brain Institute for their efforts in getting a 3.0 T whole body magnet to the University of Florida. Thanks are also well deserved for Jim Scott who taught me the chemistry for the phantom preparations.

After starting this project, I was lucky to begin collaborative work with a number of individuals in cardiology both here at the University of Florida (UF) and at the University of Alabama at Birmingham (UAB). Great appreciation goes to Dr. Carl Pepine, currently the division chief of cardiology, Shands at UF, who fully supported my efforts and encouraged greater work. Also, countless thanks and appreciation are well deserved for Alice Boyette, the Women's Ischemic Syndrome Evaluation (WISE) research cardiology technologist. Alice not

only attended all the WISE meetings and scheduled the cardiac patient studies on the 1.5 and 3.0 T, but also provided patient handholding and technical support during the studies. In addition, WISE research nurse Eileen Handberg-Thurmond was very supportive and made sure that all financial issues were under control and the necessary equipment purchased. It was through the efforts of cardiology at UF that the Dinamap™ vital signs monitor was purchased and that all patient studies were financially compensated. I was also fortunate to have my protocol and my study results analyzed by a group at UAB who already had a published history in doing cardiac phosphorus spectroscopy as well as some experience with higher Tesla whole body systems (a 4.1 Tesla). The expertise, careful analysis, and approval of my data by Dr. Steven Buchthal, Dr. Jan den Hollander, and Dr. Gerald Pohost provided excellent feedback that I was on the right track and succeeding in my methodology.

I would especially like to thank all of the members of my committee, Dr. Katherine Scott (Chair), Dr. Jeffrey Fitzsimmons, Dr. J Ray Ballinger, Dr. Richard Briggs, Dr. Christine Stopka and Dr. David Hinterlang. These individuals took time out of their busy scheduled to review my work and support my efforts.

I would also like to sincerely thank those who believed in me and helped me achieve my doctorate through their continuous moral support. This includes a long list of family members (Thom Bruner, Sharon Properzio, Bill Properzio, Tom Bruner Sr, Jess Bruner, Dee Dee Haun, Carter Haun) and friends (Manuel Arreola, Libby Brateman, Lynn Rill, Michelle Werner, Cathy Carruthers, Mark Knudsen, Beth Knudsen, Sheila Marks).

TABLE OF CONTENTS

	page
ACKNOWLEDGMENTS.....	iv
LIST OF TABLES.....	ix
LIST OF FIGURES.....	xi
ABSTRACT.....	xvi
CHAPTERS	
1 INTRODUCTION.....	1
Statement of Problem.....	2
Spectroscopy's Contribution to Diagnosing Myocardial Ischemia.....	3
Research Hypotheses.....	4
Specific Objectives.....	5
Assumptions.....	6
Scope of the Project.....	7
Significance.....	8
2 REVIEW OF LITERATURE.....	10
P-31 Spectroscopy Pulse Sequence Options for the Heart.....	13
Slice Localization Techniques.....	14
Multi-Voxel Localization Techniques.....	15
Single Voxel Localization Techniques.....	17
Cardiac P-31 Spectroscopy Results in the Literature.....	22
Animal studies.....	22
Human Studies.....	24
Post-Processing Calculations and Corrections.....	48
Skeletal Muscle Contamination.....	49
Blood Contamination.....	49
Relaxation Corrections.....	52
Calculation of pH.....	56
3 PHANTOM P-31 SPECTROSCOPY ACQUISITION TECHNIQUES.....	60
Phantom Design.....	61
Gate-able and Depth Phantoms.....	61
Slice Profile Phantom.....	64
GE Phosphoric Acid Phantom.....	64
Radio Frequency Coil Design.....	65
3.0 Tesla Square Proton Coil Paired with Quadrature Phosphorus Coil.....	65
3.0 Tesla Phosphorus Single-Turn Coil.....	66

3.0 Tesla Coil Comparisons	67
1.5 Tesla Coils.....	69
Coil Ideas for Future Cardiac Spectroscopy Studies.....	70
Imaging.....	70
Spectroscopy.....	71
Localized Proton Spectroscopy.....	72
Localized Phosphorus Spectroscopy.....	73
Phosphorus STEAMCSI and PRESSCSI.....	74
Phosphorus ECHOCSI.....	74
Phosphorus SPINECHO.....	75
Phosphorus ISISCSI.....	76
Phosphorus FIDCSI.....	78
1.5 Tesla to 3.0 Tesla Phosphorus Spectroscopy Comparisons.....	82
Phantom Results.....	84
 4 HUMAN CARDIAC P-31 SPECTROSCOPY ACQUISITION TECHNIQUES	112
 Imaging.....	113
Spin-Echo Imaging.....	113
Gradient-Echo Imaging.....	114
Human Positioning.....	114
Gating.....	116
Shimming with Localized Proton Spectroscopy.....	119
Cardiac Phosphorus Spectroscopy In-Vivo Acquisition.....	120
Localized P-31 Multivoxel CSI.....	120
Localized P-31 ISISCSI.....	121
Slice Localized P-31 FIDCSI (DRESS).....	122
Single Turn versus Quadrature Surface P-31 Coil at 3.0 T.....	123
Human Test Participants.....	123
In-Magnet Exercise.....	128
Spectroscopy Post-Processing.....	129
Post-Processing Software.....	130
Skeletal Muscle.....	136
Blood Contamination.....	136
T ₁ Relaxation Corrections.....	137
Calculations of pH.....	139
Analysis.....	140
 5 HUMAN DATA REPRODUCIBILITY.....	156
 T ₁ Relaxation Corrections	157
Overall Reproducibility of the Oblique DRESS Method.....	159
Adequacy of the Hydraulic, In-Magnet, Handgrip Exerciser.....	165
Reproducibility of the Hydraulic Handgrip.....	167
No Drop in [PCr]/[ATP] During Exercise with Reference Volunteer.....	168
Drop in [PCr]/[ATP] Seen with the Handgrip Exerciser with Ischemia.....	170
Myocardial pH Measured at 3.0 T.....	171
 6 SUMMARY AND CONCLUSIONS.....	174
 Implications for Future Research.....	176
 APPENDICES	
 A IRBS AND SCREENING FORMS.....	180

B FIGURE ACQUISITION PARAMETERS.....	193
C HYDRAULIC HANDGRIP.....	224
D 3.0 T CARDIAC ACQUISITION PROTOCOL.....	228
E SPECTROSCOPY POST-PROCESSING INSTRUCTIONS.....	236
F HUMAN T ₁ RELAXATION DATA	256
G T ₁ RELAXATION RATES OF DEPTH PHANTOM	259
REFERENCES	260
BIOGRAPHICAL SKETCH.....	281

LIST OF TABLES

<u>Table</u>	<u>page</u>
1. Nuclear Spin Parameters	13
2. Research Published on Human, In-Vivo Cardiac P-31 NMR Spectroscopy of Studies on Normal-Controls or Patients and Related Work	26
3. Cardiac [PCr]/[ATP] Ratio of Healthy Volunteers (Normal Controls) at Rest and During Stress	36
4. Cardiac [PCr]/[ATP] Ratio of Patients with Myocardial Infarction at Rest and During Stress	38
5. Cardiac [PCr] and [ATP] Amounts at Rest in Patients with Myocardial Infarction, Ischemia and in Normal Controls.....	39
6. Cardiac [PCr]/[ATP] at Rest and Stress in Patients with Myocardial Ischemia.....	43
7. Cardiac [PCr]/[ATP] at Rest and Stress in Patients with Myocardial Ischemia with Some Type of Intervention.....	44
8. Literature Review of In-Magnet Handgrip Exercise Response	48
9. Published Spin-Lattice Relaxation Times of Myocardial PCr and ATP.....	55
10. Myocardial pH in the Literature as Measured by Human, In-vivo Phosphorus NMR Spectroscopy	57
11. Gate-able and Depth Phantom Compartment Sizes and Concentrations	62
12. A Comparison of 3.0 Tesla Coil Parameters.	67
13. Comparison of 1.5 Tesla Coil Parameters.	69
14. Participants at 3.0 T for Cardiac P-31 Spectroscopy	126
15. In Magnet Hydraulic Exercise Handgrip Participants	127
16. Oblique DRESS Acquisition P-31 Metabolite area Values Obtained with Different TR gating Intervals for the Purpose of Relaxation Measurements.....	158
17. Summary of Resulting T ₁ values for PCr and ATP _{sc}	159

18.	WISE 1.5 T Cardiac Spectroscopy Acquisition Success Rate	161
19.	3.0 T Cardiac P-31 Spectroscopy at Rest Only, 3xRR Gating	162
20.	3.0 T Cardiac P-31 Results Categorized by P-31 Surface Coil	165
21.	Heart rate (HR) and Systolic Blood Pressure (SBP) Response from 30% of Maximum Effort Isometric Hydraulic Handgrip.....	166
22.	Handgrip exercise compared to dobutamine and treadmill responses for known WISE studies.....	167
23.	Handgrip 30% Maximum Effort Isometric Exercise Results of K.S. Subject Tested Repeatedly.....	168
24.	Results from 1.5 T Cardiac P-31 Exercise Study on Reference Normal Volunteer.....	170
25.	Ischemic and WISE Studies at 3.0 T Show Drop in [PCr]/[ATP] with Handgrip Exercise.....	171
26.	Mycardial pH as Measured on Human Volunteers Using Oblique DRESS Cardiac P-31 MRS on the GE 3.0 T SIGNA™ for those Studies where the Pi Peak was Discernible due to Adequate SNR	172
27.	Comparison of Cardiac P-31 Post-Processing Software.	252

LIST OF FIGURES

<u>Figure</u>	<u>page</u>
1. STEAM Pulse Sequence	58
2. PRESS Pulse Sequence	58
3. ISIS Volumes for 8 Acquisition Voxel Localization.	59
4. Gate-able-Phantom (a) photograph and (b) position in magnet, without the liquids and with movement direction demonstrated... .	87
5. Gate-able-Phantom images, (a) axial, (b) coronal and (c) sagittal views, as imaged with 25cm square proton coil....	87
6. The Depth-Changing-Phantom (a) photograph with top open and (b) position in magnet, with movement direction demonstrated... .	88
7. Depth-Changing-Phantom images, (a) axial, (b) coronal and (c) sagittal views, as imaged with 25cm square proton coil....	88
8. Axial slice image of Slice Profile Phantom and details on how oblique DRESS slices were placed within phantom to estimate the amount of potential contamination from outside the localized slice.....	89
9. Photographs of GE's 14.7 M P-31 Phantom from (a) front, (b) back and relative position in magnet.....	89
10. Photographs of quadrature phosphorus and square proton coil as (a) a paired set and (b) separated onto individual platforms for 3.0 Tesla.....	90
11. Schematic diagrams of (a) the 25 x 25 cm ² square proton coil set (tuned to 127.75 MHz) used with (b) the 10 cm phosphorus quadrature coil at 3.0 T (tuned to 51.71 MHz)	90
12. Photograph of the single turn, 9.5 cm diameter, phosphorus transceive coil tuned to 51.71 MHz (3.0 Tesla).....	91
13. Schematic diagram of the single-turn phosphorus transceive 9.5 cm diameter coil at 3.0 T tuned to 51.71 MHz.....	91
14. Comparisons of single-turn versus quadrature P-31 RF coils in terms of relative signal based on 25 mm thick DRESS acquisitions of 14.7 M phantom at 0.5 cm intervals with TG optimized at each position.....	92

15.	Photograph of the single turn, 9.5 cm diameter, phosphorus transceive coil tuned to 25.87 MHz (1.5 Tesla) with three small vials that are used to locate the coil in the proton images.....	93
16.	Schematic diagram of the single-turn phosphorus transceive 10 cm diameter coil at 1.5 T tuned to 25.87 MHz.....	93
17.	Photograph of 1.5 T quadrature P-31 coil.	94
18.	Schematic diagram of the quadrature phosphorus transceive 10 cm diameter coil at 1.5 T tuned to 25.87 MHz.....	94
19.	Axial images of gate-able phantom comparing images obtained on 3.0 T using a 25 cm square proton surface coil with the image pulse-sequences of (a) spin echo, (b) fast spin echo, (c) gradient echo and (d) fast gradient echo imaging.....	95
20.	The STEAMCSI pulse sequence, GE's version of STEAM for spectroscopy voxel localization.....	96
21.	The PRESSCSI pulse sequence, GE's version of PRESS for spectroscopy voxel localization.....	96
22.	Frequency domain of (a) PRESSCSI voxel localized phosphorus spectroscopy with (b) diagram demonstrating localization.....	97
23.	Frequency domain of (a) STEAMCSI voxel localized phosphorus spectroscopy with (b) diagram demonstrating localization.....	97
24.	The ECHOCSI pulse sequence, one of GE's versions of Spin Echo for spectroscopy acquisition.....	98
25.	Frequency domain of (a) ECHOCSI voxel localized phosphorus spectroscopy with (b) diagram demonstrating localization.....	98
26.	Chemical shift imaging (CSI) voxel sizes versus time of slice plus 2D CSI acquisition on GE Sigma Advantage".....	99
27.	The SPINECHO pulse sequence, one of GE's versions of Spin Echo for spectroscopy acquisition.....	100
28.	Frequency domain of SPINECHO CSI multivoxel localized phosphorus spectroscopy.....	100
29.	The ISISCSI pulse sequence (as shown for one gradient), GE's versions of ISIS for volume, slice, column or voxel localization.....	101
30.	Frequency domain of (a) ISISCSI slice localized phosphorus spectroscopy with (b) diagram demonstrating localization.....	101
31.	Frequency domain of (a) ISISCSI column localized phosphorus spectroscopy with (b) diagram demonstrating localization.....	102
32.	Frequency domain of (a) ISISCSI voxel localized phosphorus spectroscopy with (b) diagram demonstrating localization.....	102

33.	Visual display example of the acquisition where the total number of acquisitions is 32 performed by (a) the current GE ISISCSI technique, and (b) the modified ISIS technique.....	103
34.	Frequency domain of (a) modified ISISCSI localized voxel sequence for phosphorus (created from eight separate acquisitions, added and subtracted appropriately during post-processing) with (b) diagram demonstrating localization..	104
35.	The FIDCSI pulse sequence without phase encoding gradients turned on, GE's versions of the simple single RF pulse necessary to produce an FID for a spectroscopy acquisition....	104
36.	Charts comparing (a) relative signal obtained by varying transmitter gain (TG) values at various depths for slice localized FIDCSI at 1.5 Tesla, using the quadrature coil and (b) relative optimized TG value versus depth for the single turn coil	105
37.	Charts comparing relative signal obtained by varying transmitter gain (TG) values at various depths for slice localized FIDCSI at 3.0 Tesla, using (a) the quadrature coil, or (b) the single turn coil.....	106
38.	Frequency domain of FIDCSI slice localized phosphorus spectroscopy of (a) gate-able phantom and (b) depth phantom... .	107
39.	Multivoxel phosphorus FIDCSI plus CSI of the (a) gate-able phantom (b) depth phantom	108
40.	Comparison of 1.5 to 3.0 Tesla results of phosphorus FIDCSI plus CSI localized voxel scaled by noise level.....	109
41.	Comparison of 1.5 to 3.0 Tesla results of phosphorus, modified ISISCSI localized voxel (created from eight separate acquisitions, added and subtracted appropriately during post-processing)	109
42.	1.5 T, P-31 single turn RF coil signal from a set of 25 mm thick, oblique DRESS slices (FIDCSI oblique slice) moved across the internal phosphoric acid vial in the Slice Profile Phantom.....	110
43.	3.0 T, P-31 single turn RF coil signal from a set of 25 mm thick, oblique DRESS slices (FIDCSI oblique slice) moved across the internal phosphoric acid vial in the Slice Profile Phantom.....	110
44.	3.0 T, P-31 quadrature RF coil signal from a set of 25 mm thick, oblique DRESS slices (FIDCSI oblique slice) moved across the internal phosphoric acid vial in the Slice Profile Phantom.	111
45.	Human cardiac imaging with the spin-echo pulse sequence at (a) 1.5 T with the body coil and at (b) 3.0 T with a surface coil	141

46.	Human cardiac imaging with the fast gradient echo pulse sequence at (a) 1.5 T with the body coil and at (b) 3.0 T with a surface coil.....	142
47.	Prone positioner for in-magnet cardiac spectroscopy	143
48.	A comparison of the heart's position in the (a) prone and (b) supine positions, as shown from a 3.0 T axial slice.....	144
49.	Waveforms of (a) peripheral gating and (b) ECG gating on the 3.0 T from a normal human volunteer (TEB) on Sept 20, 1998, displayed at a rate of 21 mm/sec.....	144
50.	A comparison of peripheral gating (pg) versus ECG gating, and breathing during the image versus breath-hold images.....	145
51.	Human proton voxel localized spectroscopy of the heart and chest wall obtained during one volunteer's shim using the techniques of GE's (a) STEAMCSI and (b) PRESSCSI.....	146
52.	P-31 FIDCSI with CSI of a human subject at 3.0 T	147
53.	DRESS localization via oblique slice select combined with sensitivity region of coil.....	148
54.	Examples of 1.5 T cardiac phosphorus spectra localization problems resulting in (a) liver contamination, or (b) skeletal muscle contamination, in comparison with (c) a non-contaminated cardiac spectrum.....	149
55.	P-31 FIDCSI oblique slice localized human cardiac spectroscopy (oblique DRESS) of the same subject, at 1.5 and 3.0 T, on different days showing examples of resting and exercise spectra, raw and fitted.....	150
56.	Series of cardiac region oblique DRESS spectra representing decreased skeletal muscle contamination with increase in depth of spectroscopy slice localization....	151
57.	Relative size of oblique DRESS slice with (a) a 10-cm diameter single-turn P-31 surface coil and (b) a 16 x 10 cm ² quadrature P-31 surface coil.....	152
58.	Water, hydraulic, hand-squeeze ergometer/static-exerciser, modified from original design by North Coast Medical	153
59.	The linear response of the hydraulic handgrip to added weight on the rubber bulb is illustrated.....	154
60.	Dinamap™ blood pressure and pulse monitoring equipment	154
61.	Myocardial pH is proportional to the frequency difference of the Pi and PCr peaks in the human, in-vivo phosphorus NMR spectrum.....	155

62.	Relaxation correction factors at 3.0 T for cardiac [PCr]/[ATP] values based on repetition time (TR) values.	173
63.	ECG lead placement for 3.0 T gating.	230
64.	Example 3.0 T data set analyzed by FITMASTER™.	238
65.	Example 3.0 T data set analyzed by Sage_IDL™.	241
66.	Example 3.0 T data set analyzed by Sage_IDL™ with baseline correction points selected.	241
67.	Example 3.0 T data set analyzed by Sage_IDL™ with baseline correction.	242
68.	Example 3.0 T data set processed by MRUI™.	244
69.	Example 3.0 T data set analyzed by MRUI™.	245
70.	Example 3.0 T data set processed by FELIX™.	248
71.	Example 3.0 T data set processed by FELIX™ with peaks picked. ...	249
72.	Example 3.0 T data set processed by FELIX™ with baseline correction.	250
73.	Example 3.0 T data set analyzed by FELIX™.	250
74.	Example 1.5 T data set with low SNR analyzed by SAGE_IDL™.	252
75.	Example 1.5 T data set with low SNR analyzed by FITMASTER™.	254
76.	1.5 T T ₁ relaxation curve for MDPA (T _r = 5.53 sec)	259
77.	3.0 T T ₁ relaxation curve for MDPA (T _r = 6.04 sec)	259

Abstract of Dissertation Presented to the Graduate School
of the University of Florida in Partial Fulfillment of the
Requirements for the Degree of Doctor of Philosophy

HUMAN IN-VIVO CARDIAC PHOSPHORUS NMR SPECTROSCOPY AT 3.0 TESLA

By

Angela Properzio Bruner

August 1999

Chairman: Katherine N. Scott

Major Department: Nuclear and Radiological Engineering

One of the newest methods with great potential for use in clinical diagnosis of heart disease is human, cardiac, phosphorus NMR spectroscopy (cardiac P-31 MRS). Cardiac P-31 MRS is able to provide quantitative, non-invasive, functional information about the myocardial energy metabolites such as phosphocreatine (PCr), adenosinetriphosphate (ATP) and pH. In addition to the use of cardiac P-31 MRS for other types of cardiac problems, studies have shown that the ratio of [PCr]/[ATP] and pH are sensitive and specific markers of ischemia at the myocardial level. In human studies, typically performed at 1.5 Tesla, [PCr]/[ATP] has been relatively easy to measure but often requires long scan times to provide adequate signal-to-noise (SNR). In addition, pH which relies on identification of inorganic phosphate (Pi), has rarely been obtained.

Significant improvement in the quality of cardiac P-31 MRS was achieved through the use of the General Electric SIGNA™ 3.0 Tesla whole body magnet, improved coil designs and optimized pulse sequences.

Phantom and human studies performed with many types of imaging and

spectroscopy sequences identified breathhold gradient-echo imaging and oblique DRESS P-31 spectroscopy as the best compromises among SNR, flexibility and quality of localization. Both single-turn and quadrature 10-cm diameter, P-31 radio frequency coils were tested. The quadrature coil provided greater SNR, but had to be used at a greater depth to avoid skeletal muscle contamination. Gated cardiac P-31 MRS obtained in just 6 to 8 minutes, showed both improved SNR and discernment of Pi allowing for pH measurement.

A handgrip, in-magnet exerciser was designed, created and tested at 1.5 and 3.0 Tesla on volunteers and patients. In ischemic patients, this exercise was adequate to cause a repeated drop in [PCr]/[ATP] and pH with approximately eight minutes of isometric exercise at 30% maximum effort. As expected from the literature, this exercise did not cause a drop in [PCr]/[ATP] for reference volunteers.

CHAPTER 1 INTRODUCTION

The statistics placing heart disease as a leading killer are remarkable. Considering all age groups and genders, heart disease is the number one killer, above other common killers such as cancer, accidents, and diabetes.¹ Cardiovascular disease kills about 2,500 people each day or more than one million each year in the United States.² Some form of heart disease affects one in four persons, with the combination of costs from treatment and loss of productivity approaching 50 billion dollars annually.²

One of the most common types of heart disease is myocardial ischemia. In myocardial ischemia, individual cells in affected areas of the myocardium can no longer function due to significant decreases in blood flow to the region, which results in chest pain (angina pectoris). The blood flow reduction is typically due to a gradual blockage in the large and/or small vessels, which substantially increases the risk for acute and total blockage (infarction). Ischemia limited to the small vessels is termed microvascular ischemia or microvascular dysfunction (MVD). MVD seldom results in death but is very disabling due to fatigue and anxiety resulting from the chest pain.³ Although patients with chest pain are usually checked for heart disease, asymptomatic patients are also tested based on risk factors such as age, weight, life-style (high fat diet, smoking) and family history. Ischemia is often clinically silent or associated with

atypical symptoms. Unfortunately its presence is a significant risk factor for a fatal heart attack. The American Heart Association estimates that as many at 3 to 4 million Americans have silent or asymptomatic ischemic episodes that are eventually diagnosed by testing for reasons unrelated to the symptoms.¹

Statement of Problem

None of the current clinical methods for diagnosing cardiac ischemia is 100% accurate. This is especially true of the most common cardiac test, measurement of the heart's electrical function via electrocardiogram (ECG). Most especially for women, but also for men, the ECG often does not assist in the diagnosis of cardiac dysfunction.⁴ In addition, although large vessel ischemia is commonly quantified by the degree of stenosis in the coronary arteries via a coronary angiography (CA) catheterization study, microvascular ischemia cannot be diagnosed with CA because the vessels are too small to resolve.

Of all the tests clinically available to diagnose myocardial ischemia, most do not provide a direct quantitative measure of ischemia in the affected myocardial tissue. Most of the tests that look directly at the myocardial tissue are qualitative imaging studies, such as clinical nuclear medicine, ultrasound, computed tomography, and magnetic resonance imaging methods, where information such as wall motion and perfusion defects can be qualitatively determined. However, these evaluations do not provide quantitative information about levels of ischemia, although the technique of MR tagging (now at a research stage only) may be used in the near future to quantify wall motion.

Those tests that do provide quantitative information do so indirectly, rather than as a direct measure of the myocardial tissue, such as the electrical signal measured via ECG or the percent stenosis of the coronary arteries as measured in a CA study. Individually, none of these tests can provide a direct diagnosis of ischemia. In this context, it is common practice to perform multiple tests for added accuracy in diagnosing myocardial ischemia.

Spectroscopy's Contribution to Diagnosing Myocardial Ischemia

Human, cardiac phosphorus NMR spectroscopy (cardiac P-31 MRS) is a non-invasive technique that directly measures pH and the levels of intracellular myocardial phosphocreatine (PCr), adenosine triphosphate (ATP), phosphodiester (PDE), and inorganic phosphate (Pi) in a non-destructive manner. Both the reduction in the ratio of [PCr]/[ATP] and pH have been shown to be sensitive and specific markers of ischemia at the tissue level in animal models^{1,2} and in humans.^{3,4} Cardiac P-31 MRS is an additional tool that can add to the degree of sensitivity and specificity in diagnosis of ischemic heart disease by providing quantitative information as a measure of the myocardial tissue directly, regardless of whether it is caused by macro- or micro-vascular ischemia.

Cardiac P-31 MRS is currently in limited use clinically. The reasons for this pertain partially to the degree of difficulty in obtaining cardiac P-31 MRS in a reasonable amount of time and uncontaminated by non-cardiac signal. Useful cardiac P-31 MRS requires obtaining a phosphorus spectrum with good signal-to-noise ratio (SNR),

with the Pi peak discernible in order to measure pH, and without contamination from skeletal muscle or liver. The spectrum must be obtained from the heart, which is moving in a rhythmic motion with the cardiac cycle. In addition, spectral acquisitions are sensitive to B_0 homogeneity and generally require more shimming than do images to enhance the SNR. Shimming of a moving, heterogeneous object is more difficult than a stationary one. To compound the difficulties, the anterior region of the heart is only 10 to 18 mm thick and at a depth of 4 to 8 cm from the P-31 surface coil. The distance between the heart and the surface P-31 radio frequency (RF) coil limits the acquisition volume to the anterior wall of the heart because of attenuation of B_1 and low SNR. Between the heart and the P-31 surface coil is the chest wall skeletal muscle, below the heart is the liver, and in the cardiac chambers is blood. Care must be taken so that neither the skeletal muscle nor liver will contaminate the spectra obtained from the cardiac muscle. Blood contamination can be corrected for after the acquisition. The result of a cardiac P-31 acquisition is typically a low SNR spectrum with an acquisition time of around 10 to 40 minutes. Because in-magnet exercise and/or drug-induced stress are required for P-31 MRS studies of ischemic heart disease, a scan time of more than 10 minutes is undesirable.

Research Hypotheses

The following hypotheses will be tested in this dissertation.

1. Human, phosphorus NMR spectroscopy of the heart can be implemented at 3.0 Tesla (T) by overcoming technical problems to produce spectra of higher quality than obtained at 1.5 T.

2. Mild exercise from an isometric, hydraulic handgrip, designed and produced for this study, provides adequate stress on the heart to cause a significant drop in [PCr]/[ATP] in the ischemic myocardium and thus differentiates ischemic from non-ischemic myocardium.

Specific Objectives

Localized phosphorus spectra will be obtained from both phantoms and the anterior myocardium of human participants. All human participants will be screened for MR incompatibility and will sign an approved Institutional Review Board Informed Consent Form (Appendix A).

The optimal pulse sequence for obtaining human, cardiac phosphorus spectroscopy will be determined from phantom and human studies. All spectroscopy pulse sequences available on the General Electric (GE) 3.0 T whole-body magnet will be compared using phantom studies. Measurement of SNR and degree of localization will be made for each pulse sequence. Select pulse sequences will then be tested and compared using human subjects. Human study comparisons will be based on SNR and the degree of contamination of cardiac muscle signal from other sources (skeletal muscle and liver).

A 10-cm diameter, single-turn P-31 RF coil will be compared with a 16 x 10-cm, quadrature P-31 RF coil (two, 10-cm diameter RF coils overlapping). Comparisons will be based on quality factors, isolation, SNR at different depths, and degree of signal contamination.

Select tests will be performed on both 1.5 and 3.0 T GE Signa Advantage™ systems to compare the resulting SNR and spectral dispersion obtained using the same pulse sequence, coil, and sample studied

(phantom or human). The human cardiac phosphorus spectra obtained at 3.0 T should show greater SNR and spectral dispersion allowing for the discernment of the Pi peak and thus the measurement of pH.

A hydraulic handgrip exerciser, designed and produced for this study, will be tested for adequacy as a cardiac stressor that should cause a drop in $[PCr]/[ATP]$ in ischemic myocardium but not in non-ischemic myocardium. The adequacy will be demonstrated by obtaining data on heart rate and blood pressure changes with isometric handgrip exercise of 30% maximum effort. These data will be compared with literature values where similar devices were used during cardiac phosphorus spectroscopy acquisitions as well as compared with the responses to clinical cardiac tests (treadmill and dobutamine) obtained locally.

Assumptions

This work will build on past knowledge and technology for assessing cardiac metabolites and thus heart function. It will be assumed, in most cases, that data from previous publications are correct, especially at 1.5 T, and this data will be used to help validate the work developed in this dissertation by comparing it with past publications and work on similar patients and procedures performed locally.

In order to assess the procedure used to stress the participants in the magnet, both suspected ischemic and non-ischemic subjects will be tested. It will be assumed that these participants will be properly

categorized by risk factor assessment, current symptoms, and when available ECG treadmill and cardiac catheterization results.

Scope of the Project

This work will be limited to creating a procedure for obtaining human, in-vivo cardiac P-31 NMR spectroscopy optimized for the GE Signa Advantage™ 3.0 T whole body magnet located in the tunnel between Shands at UF and the Veterans Affairs hospitals in Gainesville, FL. The ability to improve the results of acquisitions on the 3.0 T scanner is limited by the capabilities of the system, such as gradient strength (1 Gauss/cm) and specific absorption rate (SAR) limitations.

This work also will not use extensive pulse programming to improve the system performance. Instead, the available sequences on the 3.0 T system will be optimized, most often via the choice of parameters and protocols. When necessary, small pulse programming changes may be performed by Dr. Hee-Won Kim.

The numbers of subjects in the studies will be limited but should still be adequate to demonstrate the feasibility and reproducibility of the technique. A true set of controls free of ischemic heart disease would first have to be evaluated by a cardiologist, at a cost that is not available for this project. Taking any willing volunteer would potentially introduce bias into the results as some might have silent ischemia. In addition, a cardiologist will refer all participants identified with ischemic heart disease. This work is intended as a feasibility study where the results could then be used to justify further research.

Significance

Human cardiac spectroscopy has been commonly performed at 1.5 T⁸⁻¹¹ and occasionally at 4.0 T,^{16,17} but never before at 3.0 T. With all other factors the same, an increase in magnet field strength will theoretically result in a linear increase in the spectral dispersion and at least a linear increase in the SNR. In addition, the use of a quadrature surface coil is expected to further increase the SNR compared to the simpler single loop surface coil currently used in previously reported human cardiac spectroscopy studies.¹⁸⁻²⁴

Finally, the use of in-magnet exercise while non-invasively measuring human cardiac phosphorus metabolites has been accomplished by just a few research groups.^{11,21,25-28} In-magnet exercise with our technique and device is easy to incorporate and looks very promising for helping to distinguish normal from diseased cardiac muscle, especially in cases of myocardial ischemia.

In terms of potential research and clinical use of human cardiac phosphorus spectroscopy, there are many potential future benefits. First, this test may provide increased accuracy of diagnosis of ischemia and microvascular ischemia, for which new treatment modalities may exist. Because cardiac P-31 MRS is a quantitative measure of ischemia at the tissue level, it could be used to monitor or follow-up treatment regimes or to help develop new treatments for ischemic heart disease. In addition, a noninvasive MR diagnostic test of ischemia may eliminate unnecessary invasive cardiac catheterization procedures, reducing both risk of medical complications and cost. Based on data from the Health Care Finance Administration, National Physician Fee

Schedule Relative Value File,²⁹ a cardiac catheterization study costs four times as much as a cardiac MR exam.

CHAPTER 2
REVIEW OF LITERATURE

Magnetic resonance (MR) is a technique for using the interactions of atoms and molecules with external magnetic fields to extract image and chemical data from a sample. Using the classical description, the proton possesses a spin angular momentum, \vec{S} , and a gyromagnetic ratio, γ , where the product is the magnetic dipole moment, $\vec{\mu}$.

$$\vec{\mu} = \gamma \vec{S}$$

Equation 1

Hydrogen and nuclei with either an odd number of protons (such as phosphorus-31 with 15 protons and 16 neutrons) or an odd number of neutrons possess magnetic moments whereas even-even nuclei have zero magnetic moment. NMR takes advantage of the spin magnetic moment to obtain a signal from these nuclei, especially if they are already somewhat plentiful in the human body like proton (H-1) and phosphorus (P-31).

Placing a bulk of material, having nuclei with spin magnetic moments, into a strong and uniform external magnetic field (B_0) causes the nuclei's magnetic moment to attempt to align with the applied magnetic field. This results in the spin precessing around the magnetic field analogous to a spinning top.¹⁰ The precession of the nuclei in response to an applied magnetic field proceeds at a known frequency described by the Larmor equation:

$$\omega_0 = \gamma B_0$$

Equation 2

where ω_0 is the rate of precession in radians per second, and B_0 is the main magnetic field. The application of radio frequency energy at the Larmor frequency for a nucleus constitutes a condition of resonance, hence explaining the terms of Nuclear Magnetic Resonance or NMR.

In practice, the distribution of electrons about any given nucleus provides some shielding of the nucleus from the B_0 field. Since the distribution of electrons is a function of the molecular structure in which the atoms (and their nuclei) are located, the actual field experienced by the nucleus differs from the B_0 field by some small amount.¹⁰ Equation 2 can be modified to include the shielding constant for chemical shift, σ , for a nucleus in a specific molecular environment¹⁰:

$$\omega_0 = \gamma B_0 (1 - \sigma)$$

Equation 3

A basic NMR experiment consists of placing a sample in a constant external magnetic field (B_0) where the nuclei's magnetic moment attempts to align with B_0 , also called the equilibrium condition. After applying an oscillating radio-frequency (B_1) identical to the precession frequency of the nucleus of interest (the Larmor frequency), the nuclei absorb energy and tip away from their alignment with the external magnetic field. This displacement with the B_1 field causes the individual spins to coalesce, creating a combined magnetic moment in the transverse plane. Once the B_1 field is removed, the magnetic moment rotates at the Larmor frequency, slowly losing phase coherence due to

magnetic field variations affecting the individual spins.¹¹ A signal is induced in a receiver RF coil (either the same or different from the RF transmitting coil) by the rotating magnetic moment in the transverse plane. This produces a damped sinusoidally varying signal of positive and negative polarity at the Larmor frequency, known as the free induction decay (FID). Only when the net magnetic moment in the transverse plane is nonzero, and the spins are in phase coherence will a signal be generated.¹¹

The MR technique is both non-invasive and sensitive to the molecular environments of the atoms. These factors have led to the use of MR in several areas, primarily for imaging and spectroscopy. In MR imaging (MRI) the signals from fat and water hydrogen atoms are mapped according to their location and their characteristics. The second area of use, MR spectroscopy (MRS), is a technique that was first used in chemistry and physics laboratories in the analysis and identification of chemical compounds.¹² Biologically, MRS has also been used in the identification and analysis of protein and macromolecular structures and conformation using high resolution NMR.¹³ Another biological use of MRS has been the examination of cell samples or organs, *ex vivo*.¹⁴ The most clinically relevant use of MRS, however, is *in vivo* where the patient's tissue metabolites can be examined directly and non-invasively using techniques to localize to the region of interest within the body.

The two main isotopes that are most studied in human, *in-vivo* spectroscopy are proton (H-1) and phosphorus (P-31) because of their natural abundance, relative sensitivity and chemical significance within the body. H-1 MRS is the most commonly performed clinical MRS

patient examination because it can be done using standard MRI equipment and software available on most clinical systems. It has been shown to be useful in measuring markers of a variety of brain abnormalities such as stroke,¹⁶ tumors¹⁶ and epilepsy,¹⁷ through the relative increase or decrease of the metabolites (such as NAA, choline, and creatine). P-31 has a larger chemical shift range (~30 ppm) than H-1 (~10 ppm) and a much lower sensitivity, as shown in Table 1. Water suppression is not necessary in P-31 MRS, but lower spatial resolution and/or increased scan times are required to obtain the same signal to noise (SNR) as with H-1 MRS. P-31 MRS can detect a number of metabolites involved in cellular energy metabolism, such as phosphocreatine (PCr), adenosinetriphosphate (ATP) and inorganic phosphate (Pi). The chemical shift of the Pi peak is pH dependent. In addition, relative peak areas of PCr, Pi and ATP peaks have been used to evaluate fatigue and/or ischemia in muscle, as will later be discussed in this chapter.

Table 1. Nuclear Spin Parameters¹⁸.

Isotope	% Natural Abundance	Gyromagnetic Ratio (MHz/T)	Resonance Frequency at 1.5 T	Resonance Frequency at 3.0 T	Relative Sensitivity
H-1	99.985	42.58	63.86	127.74	100
P-31	100	17.25	25.88	51.75	6.6518

P-31 Spectroscopy Pulse Sequence Options for the Heart

A variety of pulse sequences have been employed to localize to the myocardium when performing in-vivo cardiac spectroscopy. The most basic pulse sequence, a square excitation pulse, uses no gradients and thus performs no localization, but instead takes in all signal within

the sensitive volume of the coil. This sensitive volume is generally defined, for a surface coil, as the volume of a sphere of one coil diameter.¹⁹ Such unlocalized acquisition methods have been used with animal studies where open chest experiments allow for small surface coils to be placed directly on the heart.^{40,41} This uses the surface coil as a localizer. For human studies, where we prefer to work non-invasively, a combination of coil and pulse sequence localization techniques have been used. This presents a technical challenge to optimize a localization technique for obtaining spectra from a moving heart, at a depth into the body, without adding signal from the chest skeletal muscle that lies between the coil and the heart.

Slice Localization Techniques

Slice selection is accomplished in MR by simultaneously turning on a slice-selective RF pulse and a gradient along the direction of the slice. The gradient is on for just a few milliseconds. The RF pulse designed for slice selection has a time-varying shape in the form of a $\sin t/t$ or "sinc" function,⁴²⁻⁴⁴ which is used for both spectroscopy and imaging. The RF pulse is generated at the resonance frequency of the nuclei of interest. With the gradient on, this allows the sinc RF pulse to excite just those frequencies in a narrow bandwidth to either side of the center resonance frequency. A sinc pulse can produce a sharp cutoff of frequencies thus exciting just within a slice region. The thickness of the excitation slice is related to the bandwidth of the RF pulse and the gradient strength. For example, the steeper the gradient or the narrower the RF pulse bandwidth (the longer the RF

pulse) the thinner the selected slice. In terms of spectroscopy acquisitions, the shorter the RF transmit pulse the larger the range of frequencies acquired.

Slice localized pulse sequences, such as DRESS (Depth Resolved Surface Coil Spectroscopy),⁴⁵ SLIT-DRESS (SLice INterleaved DRESS),^{46,47} Rotating Frame MR,⁴⁸ FROGS (Fast Rotating Gradient Spectroscopy),⁴⁹ and 1D-CSI (chemical shift imaging),⁵⁰ allow for acquisition of signal from a slice at a depth parallel to the coil. DRESS for cardiac studies involves acquiring from a coronal or oblique slice through the cardiac muscle at a depth from the chest, thus avoiding contamination from the skeletal muscle directly under the surface coil. Sometimes it requires outer volume suppression to avoid contamination of the signal from the adjacent skeletal muscle at the sides of the body. Most studies have not used outer volume suppression, but relied on reduced regions of coil sensitivity to prevent contamination from the sides of the body. Because it is simple and not extremely motion sensitive,⁵⁰ DRESS has been widely used for obtaining spectroscopy slice profiles of human cardiac muscle.^{12,13,15,27,45,51-56}

Multi-Voxel Localization Techniques

The spectrum of the cardiac muscle is easily contaminated by the surrounding skeletal muscle and blood, therefore localization and suppression of unwanted signal outside the volume of interest is important and accomplished with single- or multi-voxel localization techniques. Multiple voxel acquisition via chemical shift imaging (CSI) involves the use of the gradients to split up the selected slice or slices into a number of smaller voxel areas. Spatial localization

is done by phase encoding gradients in one (1D-CSI), two (2D-CSI) or three dimensions (3D-CSI).¹⁸ There are no gradients on, however, during signal acquisition. The advantage of CSI is that multiple voxels are sampled as part of the same acquisition protocol. However, this is accomplished at the cost of increased scan time for the phase encoding for each axis. CSI is generally utilized to further partition a volume already selected by another pulse sequence.

There are a number of technical problems associated with acquiring spectra with CSI. One problem is achieving a good shim over a large region of interest and possible changes in magnetic susceptibility encompassing the multivoxel acquisition volume. In addition, the point-spread function from the spatial Fourier transform reconstruction implies that any given voxel in the multivoxel acquisition contains contributions from neighboring voxels.¹⁸ This leads to lesser ability to prevent contamination outside the voxel of interest, such as the skeletal muscle contaminating the cardiac muscle.

In addition, depending on the size of the voxel of interest and size of the field of view, the time of the acquisition can be dramatically increased beyond the reasonable limit for performing in-magnet exercise during the study. This is primarily due to the increased time necessary for the CSI phase encoding steps. For example, the total measurement time for a 3D CSI acquisition is given by

$$\text{Time (seconds)} = \text{TR} \cdot N_{\text{acq}} \cdot N_x \cdot N_y \cdot N_z \quad \text{Equation 4}$$

where TR is the repetition time, N_{acq} is the number of acquisitions, and N_x , N_y and N_z are the number of phase encoding steps in the x, y and z directions.³⁸

Despite these faults with CSI, a number of studies of cardiac phosphorus spectroscopy have utilized 1D,^{11,23,27,57-61} 2D,^{10,65-72} and 3D CSI,^{64,73-75} and techniques similar to CSI such as 3D fourier series window.⁷⁶ Among these studies, some were performed on animals alone,^{67,69,73,74} but the majority were performed on humans.

Single Voxel Localization Techniques

Single voxel localization techniques rely on the pulse sequence to obtain a localized voxel of data, selected from within a larger volume. This protocol of obtaining a single voxel of data per acquisition typically takes less time than the CSI multivoxel approach because of the added phase encoding steps needed for CSI. Single voxel acquisition pulse sequences that have been reported include PRESS (Point Resolved Spectroscopy Sequence),⁷⁷ PROGRESS (a version of PRESS),⁷⁸ STEAM (Stimulated Echo Acquisition Mode),⁷⁹ ISIS (Image Selective In-Vivo Spectroscopy),^{16,17,30-41} and modified ISIS pulse sequences such as CRISIS (combination of ISIS and DRESS with x- and z-selective 180° pulses followed by a 90° y-slice selection pulse; which eliminates y-direction motion artifacts and benefits from reduced cycle time),⁴⁴ FLAX-ISIS,⁴¹ and 2D ISIS plus Outer Volume Suppression (OVS).⁴⁵

With PRESS and STEAM, three slice selective RF pulses are used to select three intersecting orthogonal planes. Only spins in the voxel defined by the intersection of the three planes experience the three RF pulses and contribute to the final signal. Both STEAM and PRESS

acquire a voxel with each acquisition (also called single-shot localization),⁵⁵ thus being less motion sensitive than techniques requiring multiple acquisitions to localize. STEAM uses a 90° RF pulse for all three excitations thus creating a stimulated echo, as shown in Figure 1. PRESS creates a double echo by using a 90° and two 180° RF pulses, as shown in Figure 2.^{56,57} Echo time (TE) for STEAM is designated as twice the time between the first and second RF pulse. PRESS has two echo times, TE1 and TE2, where TE1 is equal to twice the time between the first (90°) and second (180°) pulses and the total time to produce the first signal echo.⁵⁸ TE2 is twice the time from the first echo to the second 180° RF pulse and the full time between the first and second signal echo. In general, each TE for both STEAM and PRESS must be relatively short to successfully acquire phosphorus spectra, so that the signal losses due to transverse relaxation (T_2) are small. PRESS offers the advantage of having twice the SNR of STEAM, but cannot be run with short TE's,⁵⁵ while STEAM can handle some shorter TE's down to the system limit.

PRESS and STEAM differ primarily in the nature of the echo signal created. PRESS forms the echo from 180° RF refocusing of the net magnetization, whereas in STEAM, only part of the available signal is used to form the stimulated echo via the use of 90° RF pulses. This theoretically results in a factor of 2 increase in SNR for PRESS over STEAM. Experimentally, the factor of 2 increase in SNR has also been documented.^{56,57}

Both PRESS and STEAM have occasionally been accomplished successfully at the phosphorus frequency, but never on the heart. STEAM has been shown to work on a phantom (400 mmolar solution of

$\text{Na}_5\text{P}_3\text{O}_{10}$ in H_2O) at 1.5 T using a TE of 3.1 msec.⁶⁸ and on human brain at 2.0 T using a TE of 3.0 msec.⁶⁹ PRESS has also been used to obtain phosphorus spectroscopy of a newborn human brain at 2.4 T using a TE of 10 msec.⁷⁰ Note that in each of these cases, the TE was set at a minimum value. Neither PRESS nor STEAM are well suited for phosphorus MR spectroscopy due to reasons related to the characteristically short T_2 times of phosphorus metabolites, but STEAM does work marginally better than PRESS.^{41,71} The echo times achievable with PRESS are too long for the acquisition of signals from nuclei with short T_2 relaxation times.⁵¹ In contrast, STEAM's shorter TE values reduce signal loss from T_2 relaxation and allow some observation of short T_2 metabolites, such as P-31 metabolites.⁷²

ISIS allows for volume, slice, column or voxel selection based on one, two, four or eight acquisitions.⁷³ Zero to three selective-inversion pulses in the presence of gradients precedes each acquisition exciting different areas within the volume. A combination of areas, added and subtracted, results in the localization achieved with ISIS as shown in Figure 3.^{74,75} ISIS has proved to be one of the best voxel localization techniques for P-31 spectroscopy. Unlike PRESS and STEAM, ISIS is not sensitive to the T_2 values of the acquired resonances but is sensitive to the T_1 values, as part of the time delay between the selective excitation and signal acquisition.⁷⁶ Most P-31 biological T_1 values are on the order of a few seconds, therefore obtaining in vivo ISIS spectra from living tissue should not be a problem in terms of relaxation times.⁷⁷ Also, for any localized spectroscopy pulse sequence, when long repetition times are used to allow for T_1 relaxation, there is no T_1 error in terms of signal cancellation. ISIS

may require eight separate acquisitions in order to localize to a voxel, but the final SNR is still equivalent to an acquisition taken with eight acquisitions (i.e. no signal is lost due to localization). This is also true for CSI acquisitions. ISIS is also flexible in that fewer than eight acquisitions can be used to obtain a volume (1 acquisition), a slice (2 acquisitions), a column (4 acquisitions), or a voxel (8 acquisitions).

ISIS uses an adiabatic RF pulse that allows for uniform excitation of signals over a larger volume of the sample.³⁴⁻³⁶ The adiabatic pulse, a modification of the sinc pulse, was specially designed for use with surface coils where uniform excitation is difficult to obtain.³⁴

The adiabatic pulse is frequency selective and B_1 insensitive, and can achieve uniform excitation in an area of B_1 field inhomogeneities. The adiabatic pulse is designed using frequency modulation to satisfy two constraints. First, the RF pulse is designed to cause negligible decay of the transverse magnetization during the pulse. Second, the rate of change of the net magnetization orientation is considerably slower than its rate of precession.³⁴

In addition, adiabatic pulses are different from sinc or square RF pulses in that they are designed to excite maximally at a high gain and remain maximal even when the gain is further increased.^{34,36} Sinc or square RF waves excite an area based on the gain of the signal with an optimal signal peaking at some point between low and high levels of gain. Unfortunately, the ISIS adiabatic pulse require a greater power than sinc or square pulses, therefore it is important to have a quality amplifier designed for the higher requirements. Since power

requirements increase with field strength, special consideration needs to be made to provide enough power for ISIS while still remaining within the safety guidelines. Specifically, the Food and Drug Administration (FDA) has limited the specific absorption rate (SAR) of the RF power to a maximum of 8 Watts/kg in the head or torso for any period of 5 minutes.⁵⁷ This applies to all pulse sequences and all field strengths used on human subjects.

ISIS is prone to many possible causes of signal contamination.⁵⁸ As ISIS selects outside the volume of interest and attempts to subtract this signal, only partial cancellation of the unwanted signal is achieved.⁵⁹ This effect is greater when the volume of interest (VOI) is much smaller than the complete volume detected by the coil. Since signal is detected from a large volume after each acquisition, the receiver gain cannot be optimized for the smaller VOI.⁶⁰ In addition, the adiabatic pulse does not acquire equally all the chemically shifted resonance's at the acquired frequency.⁶¹ Finally, T_1 smearing⁶² caused by residual magnetization left from the observation pulse from the previous acquisition, also results in less than total subtraction of unwanted signal outside the ISIS selected volume of interest.⁶³ ISIS is also motion sensitive due to its volume subtraction method of localization involving eight separate acquisitions to obtain the spectrum from one voxel.⁶⁴ In addition, ISIS is affected by spatial displacement of chemically shifted species in the slice selection at high field at the P-31 frequency.⁶⁵

The issues of contamination with ISIS have been tested in a computer simulation and published.⁶⁶ Despite its faults, only ISIS and ISIS derived pulse sequences are useful as single-voxel localization

pulse sequence techniques for P-31 MRS. A number of cardiac spectroscopy studies have been done using ISIS or ISIS derived pulse sequences.^{14,15,17,23,28,69-82,130-137} All except one¹¹⁵ of this list of studies was performed on humans.

Cardiac P-31 Spectroscopy Results in the Literature

Animal studies

Animal studies have been essential for predicting potential areas for human use. A majority of cardiac spectroscopy animal studies have been done with the animal's chest open, thus allowing the surface coil to be placed directly on the heart,^{40,41} via a catheter coil inside the heart,¹¹⁸ or by excising the heart and maintaining it artificially in an isolated heart perfusion study^{5,119-122}. There have also been closed-chested animal experiments^{67,123,124} that more closely match what would happen if the same test were performed on humans. The promise of the open-chested experiments is that a great deal of information from the heart via spectroscopy can be obtained when SNR is maximized. Unfortunately, outstanding SNR is generally only achieved when the RF receive coil is placed directly on the heart, allowing for unlocalized acquisitions. The open-chested *in situ* mode can also take advantage of the increased SNR and use localization acquisition methods, such as 2D ISIS, 1D spectroscopic imaging (SI), or PLAX-ISIS, to obtain spectroscopic information about discrete layers of the myocardium, sub-endocardium and sub-epicardium individually.^{41,125,126}

Animal hearts can be stressed to a much greater degree while under anesthesia¹²⁷ than we would ethically stress a human volunteer.

Although most human studies of normal myocardium have shown no change in the phosphorus metabolites with the stress levels that do produce changes in ischemic hearts, normal animal hearts have often been stressed beyond what can be done in humans to the point where a change in the phosphorus metabolites can be induced. Care must be taken, therefore, when making extrapolation to humans based on these animal studies, because often the heart is damaged by the level of stress or by the deliberate infarction.^{124,125}

Animal studies allow for tighter control of the disease state and measurement than can be ethically accomplished in humans and therefore reveal the potential for P-31 MRS to provide feedback of specific cardiac disease states. Studies of permanent coronary occlusion in dogs with open chest, measured up to 6 hours after occlusion¹²⁶ and up to 5 days after occlusion¹²⁴ show that residual Pi remains in the region of the infarction for a period of days although tissue pH returns to normal within a day.⁷ Human cerebral infarction measured by phosphorus MRS has shown similar behavior.^{7,127} A study on open-chested dogs showed that phosphorus spectroscopy could differentiate between viable and non-viable myocardium from 6 to 54 hours after an ischemic insult based on measurements of PCr and [Pi]/[PCr].¹²⁸ Another animal study of assayed myocardium after coronary occlusion or low-flow ischemia showed a depletion of PCr and ATP with irreversible injury.¹²¹ Animal studies have shown reduced phosphorus metabolites in cases of hereditary cardiomyopathy,^{122,123} cardiomyopathy from chronic chemical exposure,^{124,125} dietary deficiencies,¹²⁶ and diabetes¹²⁷. In another animal study, PCr was shown to be preserved until the blood flow was reduced to about 50% of that in an originally healthy heart.¹²⁸ This is another example of

the type of understanding that can be achieved with animal studies but would be unethical for human studies.

Specifically, both a decrease in the [PCr]/[ATP] ratio and a downfield shift of the inorganic phosphate resonance due to acidosis have been measured occurring with the onset of ischemia.^{5,6} In cases with mild reductions in blood flow (approximately 17%), only the Pi and pH changed significantly when compared to a control group. When the blood flow reduction was more substantial (on the order of 50% or more), the [PCr]/[ATP] ratio was also shown to decrease while ECG monitoring was also abnormal (reduction in segment shortening).^{139,140}

Human Studies

Nuclear medicine thallium scans clinically show a reversible thallium defect where the area fills with thallium during rest but does not during stress indicating an area of ischemia. If the defect is not reversible, meaning the area doesn't fill with thallium during rest or stress, then the area is infarcted. P-31 exercise tests on subjects with severe CAD and/or reversible thallium defects showed a significant decrease in the [PCr]/[ATP] ratio.^{22,49} Although a change in the [PCr]/[ATP] ratio is seen in the ischemic heart with stress, tests on normal controls and patients with non-coronary cardiomyopathy show no significant change with exercise. In patients with stenosis of the macrovessels, a drop in the [PCr]/[ATP] ratio is no longer present after revascularization.⁴³ These findings prove that in the absence of blood flow reduction or scar to an area of the myocardium, the metabolite energy values will remain constant. These studies showed a

direct correlation between ischemia and a decrease in [PCr]/[ATP] and pH with stress as measured via phosphorus NMR spectroscopy.

A number of research groups from a variety of locations around the world have been utilizing human, in-vivo cardiac NMR P-31 spectroscopy. Assorted magnet systems, coils and techniques have been employed. In addition, a wide number of patient types have been studied. Even though there is a wide variation in heart problems studied, some trends in the type of techniques and RF coils used have started to appear that may prove diagnostically and clinically feasible. In the least, P-31 MRS should provide information that scientists and physicians can utilize to better understand the workings of the human heart under all types of disease conditions.

A condensed summary of all the research locations that have conducted in-vivo cardiac phosphorus NMR spectroscopy acquisitions of the human heart are listed in Table 2. This table is given in an effort to simultaneously demonstrate how much and how little work has been done since the late 1980s. Since each type of cardiac problem will have its own trends and results in terms of cardiac P-31 MRS, research on each of the main types of heart disease has also been detailed in the remainder of this chapter.

Table 2. Research Published on Human, In-Vivo Cardiac P-31 NMR Spectroscopy of Studies on Normal-Controls or Patients and Related Work.

Location	Major Players	Magnet Tesla	P-31 Method	P-31 Coils	References
Erlangen, Germany	Neubauer Loeffler Sieverding Siemens	1.5 T Philips 1.5 T Siemens	ISIS CSI CSI/SLOOP DRESS	10-15cm diam R/T diam R/T 12cm R	117 141 142 82 14 71 105 68 100 143 111 109 65 104 10 144 113 145 18 146
Otsu, Mie, Toyko, Tsukuba, Japan	Mitsunami Okada Yabe Sakuma	1.5 T GE GE	DRESS CSI	5-15cm diam R/T, 20cm T +	56 55 147 148 52 54 13 51 12 27 60 53 19
Baltimore, Maryland, Schenectady, New York	Bottomley Weiss Hardy GE	1.5 T Bruker	DRESS CSI	40cm T + 7cm R, 7cm diam R/T	9 149 70 63 67 49 11 150 151 152 153 154 20
Oxford, England	Rajogopalan Conway Radda Blackledge	2.0 T	PMRFI CSI DANTE	5-6.5 cm diam R/T, 15cm T + 7cm R	48 155 25 156 157 57 58 158 159 59 21 160
San Francisco, California	Matson Schaefer Aufferman	1.5 T 2.0 T Philips	ISIS CSI	9-14cm diam R/T	83 15 161 64 162 163
Leiden, Netherlands	Lamb de Roos den Hollander Philips	1.5 T Philips	CSI ISIS	10-14cm diam R/T	116 164 108 165 28 22 166 167 112 114 168
Birmingham, Alabama	Evanochko Hetherington den Hollander Buchthal Pohost	1.5 T Philips 4.1 T	ISIS	10-14cm diam R/T	103 106 169 81 102 170 171 80 28 16 23
Minneapolis Minnesota	Menon Ugurbil	4.0 T Siemens	CSI ISIS	11cm diam R/T	17 76
Philadelphia Pennsylvania	Whitman Oxford	1.9 T	Coil localized	5cm diam R/T	172
Durham, North Carolina	Herfkens	1.5 T	CSI	6cm diam R/T	24
Paulo, Brazil	Kalik-Filho	1.5 T Philips	ISIS	Not Listed	173
Gainesville, Florida	Bruner Scott, Kim	1.5T GE 3.0T GE	Oblique DRESS	10cm diam, Quadrature	174 175

P-31 Spectroscopy Acquisition Techniques. In terms of techniques for acquiring human, *in vivo*, cardiac P-31 MRS, there is a trend that emerges. For those locations with clinical Philips systems, the most common technique used is ISIS followed by CSI. For clinical GE sites, the most common technique is DRESS followed by CSI. The two Siemens sites conducting human, *in-vivo* P-31 MRS primarily utilize CSI.^{144,176}

This chapter summarizes the results from studies of various types of cardiac diseases. When available, the acquisition times are listed in Table 3 through Table 7. Notice that DRESS^{12,149} and 1D-CSI^{49,161} are the shortest duration sequences, generally being under 10 minutes, although running them for longer further increases SNR. ISIS typically is run for slightly longer periods of time at around 20 minutes,^{32,103,105,173} although it can be run the same amount of time as DRESS at around 10 minutes¹⁶⁷. Two dimensional and 3D-CSI are the longest duration,¹⁴⁴ with some scans lasting an hour for just a single P-31 acquisition¹⁸¹.

A few truly unique techniques for obtaining human cardiac P-31 MRS, SLOOP and PMRFI, are utilized only at their originating locations. Spectral localization with optimal pointspread function or SLOOP was created and used by a group in Germany, utilizing a Siemens 1.5 T system.^{18,68,161,143,144} The SLOOP technique is a combination of a 3D-CSI acquisition with sophisticated post-processing that uses anatomical information from the proton image to group the spectra by tissue type. Anatomical compartments, such as for cardiac muscle, skeletal muscle, and liver are defined with the proton image. The overlaying P-31 spectral data is then separated into each of these compartments. The papers that have been published from this group using SLOOP seem

outstanding as they achieve cardiac spectra with greater SNR, due to the larger volume they can utilize to obtain the signal. In addition, they seem to have solved the problems with contamination. Unfortunately, until the technique is tried and evaluated at other locations, judgment on the true accuracy of the method cannot be fully established.

Phase modulated rotating frame-depth imaging selection technique or PMRFI is a technique used for cardiac P-31 MRS solely at Oxford, England.^{48,57,58,155} PMRFI allows for a 2D-spectroscopy signal to be collected from the sample within the sensitivity of the coil via a set of free induction decays. The data is collected from a volume formed by a stack of disc shaped slices at various depths into the chest with the entire data set taking approximately 35 minutes to acquire.⁴⁸ The PMRFI technique claims to produce high-resolution, high SNR spectral images with limited spatial distortion.⁴⁸

In addition, at Oxford, they have also utilized DANTE for cardiac P-31 MRS of human volunteers.¹⁵³ DANTE allows for the selective excitation/suppression of individual peaks in the frequency domain in this case used to distinguish the intracellular and extracellular Pi. This group also utilized an initial saturation pulse to eliminate any contamination from skeletal muscle.¹⁵⁹ Many of these types of unique pulse sequences were originally developed on research magnets for animal studies and then recently extended to human use on a Bruker research magnet system. This may be the reason why these techniques have not been published for use on clinical 1.5 T systems, such as from GE, Philips or Siemens. Users often have the ability to pulse program

clinical systems, but with less flexibility and ease in programming options.

P-31 Radio Frequency Coils. Surface coils have been used for all human cardiac spectroscopy studies to date. The reasons are simple. Compared to a volume coil that would need to encompass the chest, surface coils provide a much greater signal-to-noise ratio (SNR) than the volume coil. The simplest surface coil, a single loop of wire, provides a means of obtaining spectra from a volume of tissue adjacent to the coil.⁴¹ The sensitivity of the surface coil is greatest for the tissue closest to the coil, with sensitivity decreasing rapidly with depth.⁴¹ This sensitivity range extends approximately one radius away from the center of the surface coil,⁴² with the majority of the signal obtained from a disc-shaped region at the plane of the coil and decreasing in size with depth.⁴¹ Typically, the result is relatively good SNR from the anterior wall of the heart, but not enough depth penetration to cover the entire heart. Surface coils can be adapted to a variety of specific tasks by changing the size and shape of the coil.

Surface coils are commonly used in both MRI and MRS as receivers because of their high sensitivity, providing good SNR. In spectroscopy, especially with nuclei other than H-1, surface coils are frequently used both as RF transmitters and receivers.⁴³ Their applications evolved from small animal P-31 spectroscopy studies¹⁷ to spectroscopy investigations of muscle and superficial organs in humans.⁴⁴ Unfortunately, surface coils suffer from non-uniform RF excitation and inadequate spatial localization when used without a localized pulse sequence. The sensitivity of the surface coil to a point in the sample is proportional to the B₁ field achieved by the coil

at that point, with the most signal received from sample points closest to the coil.^{41,178} Fortunately, pulse sequences designed for localization, utilizing selective RF pulses or gradients such as ISIS^{179,180} and CSI,¹⁸¹⁻¹⁸³ or multiple RF pulses¹⁸⁴ can localize spectra to regions where the B_1 field is relatively constant such as in a localized voxel volume.¹⁷⁸ For example, the ISIS pulse sequence uses an adiabatic excitation pulse that with enough power is specifically designed to excite spins in a manner that is independent of the B_1 field for more uniform excitation.⁴¹ Such a pulse has been shown to improve the localization abilities when used with a surface coil.¹⁸⁴ In addition, there is the option of using a larger transmit coil to provide better homogeneity of the B_1 field, with a smaller receive coil for optimal SNR.

The B_1 inhomogeneity inherent with using a surface coil can degrade the performance of the RF pulses resulting in an incorrect tipping angle, decreasing signal from the volume of interest (VOI), and potentially increasing signal contamination from regions outside the VOI.^{15,93,185} Contamination is most probable from the tissue closest to the coil since such tissue will have the highest degree of sensitivity by the coil.⁹³ In the case of cardiac spectroscopy, the skeletal muscle has a large potential to contaminate the cardiac muscle signal in this manner. Larger coils provide higher homogeneity at the expense of reduced sensitivity to small, shallow VOI's.^{51,185} This compromise between increased-size resulting in increased homogeneity versus decreased-size resulting in increasing sensitivity has led to many different sizes of transceive and a few combinations of transmit and receive coils being built.

A trend that appears when looking at Table 2 involves the design of the P-31 coils. The greater majority (over 95%) of human, in-vivo, cardiac P-31 MRS patient studies are conducted using a simple single turn P-31 coil of 5 to 15 cm diameter to act as a transceive radio frequency (RF) coil. Beyond this, the next largest minority uses a larger transmit (15 to 40 cm) to excite and a smaller 6.5 or 7 cm diameter coil to receive.

The purpose of a larger RF transmit coil used with a smaller receive coil is to improve the homogeneity and still have a small spatial sensitivity.⁷ The two coils can be arranged coplanar¹⁸⁶ or slightly displaced.⁴⁵ The sensitive volume is determined by the overlap region of the two coils.⁷ Unfortunately, there are more drawbacks to using separate transmit and receive coil for localized phosphorus spectroscopy. The complexity of the setup creates difficulties when trying to control accurately the position and thickness of a plane or volume of a voxel. Multiple acquisitions are required in order to localize the signal.⁷ This is due to the fact that the placement of the RF coil is critical within a few centimeters over a prime spot anterior to the heart. Often, the placement is not correct the first time and/or the pulse sequence localization position and/or transmitter gain must be modified for better localization to the cardiac muscle.

There are also designs in the literature for quadrature coils and array designs for human P-31 cardiac spectroscopy with a theoretical $\sqrt{2}$ improvement in SNR, but there is no known literature on such coils being used with patient studies to date. Phased array and quadrature coils offer the advantage of a larger sensitive coil region without increased acquisition time or a decrease in SNR.^{152,157} Quadrature and

phased array coils have been used more extensively in imaging than spectroscopy modes of human in-vivo data acquisitions. Several experimental designs have been considered for cardiac imaging and spectroscopy including (1) a 4-coil, diamond shaped design by Hardy et al.,¹⁵² (2) two pairs of surface coils placed on the chest and back, surrounding the heart by Constantinides et al.,¹⁵³ (3) a single pair of coils designed for placement on the chest,^{155,150} and (4) a double-tuned quadrature surface coil by Menon et al.¹⁵⁶ There has also been a theoretical study performed to determine the optimum configuration of 2 to 10 circular coils combined in a phased array system designed for cardiac imaging.¹⁵⁰ This paper argued that theoretically the best results would be obtained from a 4 coil array, producing 560% signal improvement relative to a whole body coil and up to 360% improvement over some commercial cardiac imaging coils.¹⁵⁰

Cardiac RF surface coils are placed on the front of the chest, over the heart. Coil placement is critical for optimum signal from the intended volume of interest. Incorrect coil placement can result in decreased signal from the desired VOI.⁷ This is especially true of small (5 to 10 cm diameter), transceive, single-turn surface coils. Incorrect coil placement can also increase contamination from areas outside the VOI.⁷ The problem with positioning can be theoretically minimized by using a phased array or quadrature coil that will cover a larger area with the improved SNR up to square root of two.^{7,152,151}

Patient Studies. In a normal, disease-free heart, a phosphorus spectrum will show a consistent level of each of the phosphorus metabolites^{25,49,157,161} of phosphomonoester (PME), inorganic phosphate (Pi), phosphodiester (PDE), phosphocreatine (PCr), and the three

adenosine triphosphate peaks (γ , α , β -ATP). Conversely, in patients and animals with myocardial infarction or myocardial ischemia, in vivo phosphorus cardiac spectroscopy will demonstrate either a reduction in the overall amounts of each metabolite^{192,193} or a change from the normal ratios of one metabolite to another^{12,49,60,124,194}. Such a measurement has the potential to differentiate a healthy heart from one with myocardial infarction or ischemia. In addition, some cardiac diseases, such as cardiomyopathy or hypertrophy, both involving thickness changes of the heart wall, are easier to diagnose with cardiac images. Even these types of heart problems can potentially benefit diagnostically from the added feedback of the chemical information provided by P-31 MRS.

Patient studies have proven over and over again that P-31 spectroscopy is a sensitive marker for clinical cardiac disease states.^{82,149} A quick overview will be presented here to prove how solid the P-31 spectroscopy measurement has been shown to be. As part of a study on patients with severe stenosis of the left anterior descending coronary artery (greater than 70% blockage), the [PCr]/[ATP] ratio decreased significantly with exercise.⁴⁹ A group of normal controls and patients with non-ischemic heart disease showed no significant change in the [PCr]/[ATP] ratio when they underwent the same stress as part of the same study. A repeat P-31 NMR spectroscopy measurement was made of five of the patients with severe stenosis of the left anterior descending coronary artery after revascularization. In all five cases, a significant improvement in the [PCr]/[ATP] measurement was seen in terms of a smaller decrease in [PCr]/[ATP] during in-magnet stress. In a similar study by Yabe et al.,¹² P-31 NMR spectroscopy with in-magnet exercise was performed on patients with ischemia, patients with

blockages (infarction), and normal controls. The patients were first categorized based on results from radionuclide testing with thallium-201. Those patients with reversible thallium defects (ischemia), showed a reduction in $[PCr]/[ATP]$ during in-magnet handgrip exercise, that normalized during rest. Those patients with irreversible thallium defects (infarction or dead myocardial tissue) and normal controls showed no change in the $[PCr]/[ATP]$ ratios with exercise. It is believed that the $[PCr]/[ATP]$ ratio does not change in cases of pure infarction because the affected tissue is completely dead while the remaining tissue is essentially sound. Therefore, the resulting signal is less overall due to a lesser amount of viable tissue, but the ratio remains the same. It is theorized that more complex techniques that would measure the absolute quantity of the metabolite levels would be able to differentiate even myocardial infarction as the overall amounts would be lower, assuming measurement of a known volume of cardiac muscle.

Healthy Volunteers. Multiple studies have confirmed that for healthy volunteers free of substantial coronary artery disease, in-magnet exercise stress tests with non-drug stimuli have not produced a significant change in the anterior myocardial $[PCr]/[ATP]$ ratio.^{12,23,49,54,157,163} Such results are shown in Table 3 where both leg and handgrip exercises show no drop in $[PCr]/[ATP]$ with normal control groups. These results have been repeated in animal studies, without handgrip exercise. No significant change in the $[PCr]/[ATP]$ ratio was found in the normal intact dog heart over a five-fold range of rate-pressure products.¹²⁷ In this case the stress was in the form of a

pacemaker which increased the rate of the heartbeats by threefold and increased the rate-pressure product by 1.5.

There is however, the potential to use drug stimulus to stress the healthy human heart to the point that a drop in [PCr]/[ATP] can be seen. The first attempt at doing this was by Schaefer et al.¹⁶³ where 2 to 16 $\mu\text{g}/\text{kg}/\text{min}$ of dobutamine was used. Dobutamine has the effect of increasing the heart rate, contractility and blood pressure. In this case, this amount of dobutamine alone was enough to increase the rate-pressure product (heart rate times systolic blood pressure) in normal controls from 7,000 to 15,000. Despite this increase of stress on the heart with dobutamine, the [PCr]/[ATP] at stress was not significantly different from [PCr]/[ATP] at rest for the normal control group, as shown in Table 3. In the same study a group of dilated cardiomyopathy patients under the same stress also did not produce a significant change in [PCr]/[ATP] with dobutamine stress ([PCr]/[ATP] at rest = 1.63 ± 0.24 , with drug = 1.57 ± 0.24 , $p=0.38$). Two other published studies repeated these experiments with a slightly different protocol and succeeded in dropping the [PCr]/[ATP] ratio even in normal controls. Lamb et al.^{162,167} and Pluim et al.,¹⁶⁸ both of Oxford, England, first utilized 10 $\mu\text{g}/\text{kg}$ and 0.03 mg/kg, respectively, of atropine sulfate to block the cholinergic nervous system which will allow for increased heart rates. They then both used 10 to 40 $\mu\text{g}/\text{kg}/\text{min}$ of dobutamine to achieve a steady heart rate, based on subject age. This protocol produced a significant drop in the [PCr]/[ATP] ratio of the normal controls being studied.

Table 3. Cardiac [PCr]/[ATP] Ratio of Healthy Volunteers (Normal Controls) at Rest and During Stress.

[PCr]/[ATP] at Rest	[PCr]/[ATP] at Stress	Stress Form	Magnet Tesla	P-31 Method	Reference
1.5±0.2 (n=6)	1.58±0.14	leg exercise	1.9 T	Not listed	25, 157
1.51±0.03 (M=6)	1.51±0.03	Bicycle ergometer	1.5 T	DRESS	13
1.72±0.15 (n=11)	1.74±0.17	handgrip exercise	1.5 T	1D-CSI 5-14 min	49
1.77±0.16* (n=8)	1.74±0.19*	handgrip exercise	1.5 T	1D-CSI 8-16 min	63
1.80±0.28* (n=11)	1.84±0.26*	handgrip exercise	1.5 T	DRESS	54
1.85±0.28* (n=11)	1.90±0.23*	handgrip exercise	1.5 T	DRESS 7-8 min	12
1.86±0.17 (M=14)	1.90±0.22	dobutamine (drug)	2.0 T	1D-CSI 7 min	163
1.42±0.18* (F=2, M=18)	1.22±0.20*	Atropine/ dobutamine (drugs)	1.5 T	3D-ISIS 10 min	112, 167
1.41±0.18* (M=12)	1.16±0.13*	Atropine/ dobutamine (drugs)	1.5 T	3D-ISIS	168

* blood corrected; M = Male; F = Female

There has been one interesting study by Lamb et al.^{28,166} where reproducibility of each method and comparisons of the results from different methods were determined for the Philips 1.5 T system. Using 16 normal controls, the same area of the anterior left ventricle produced a [PCr]/[ATP] ratio of 1.31±0.19 for ISIS alone, 0.98±0.20 for CSI alone and 1.41±0.20 for ISIS plus CSI. Lamb et al. concluded that the CSI contained liver contamination resulting in a low [PCr]/[ATP] ratio. In addition, the intra-examination difference of repeated studies of each volunteer produced a smaller difference than the inter-examination, volunteer-to-volunteer [PCr]/[ATP] difference.

Myocardial Infarction. In some of the studies in patients with myocardial infarction, the phosphorus spectrum shows a normal ratio of $[PCr]/[ATP]$,^{82,149,153} but the overall concentrations of the phosphorus metabolites are lower than normal^{152,153} as described by Bottomley et al.¹ and Luney et al.⁸¹ These characteristics are theorized to occur since the dead myocytes can not contribute a metabolic signal to the observed spectrum.⁷ The observed PCr and ATP signals are derived from surviving myocytes surrounding or interspersed with the infarcted myocytes.^{20,149} More recent publications are providing evidence that the $[PCr]/[ATP]$ ratio can be lower for infarction than in normal controls,^{12,54,60,61} and reduce $[PCr]/[ATP]$ slightly during stress^{12,54}. It has been suggested that the reduction in the $[PCr]/[ATP]$ ratio for the patients with myocardial infarction represents an ongoing metabolic stress in the myocytes remaining within the scarred region of the myocardium.⁸¹ It is still not clear how the expected ratio of the myocardium with infarction should present, but it is known that the amounts of the metabolites will differ significantly from normal. Therefore, measurements of the absolute concentrations of the phosphorus metabolites, rather than the ratios, should provide appropriate characterization of myocardial infarction.

The published results for $[PCr]/[ATP]$ of myocardial infarction are summarized in Table 4. Notice that there is not a significant change in $[PCr]/[ATP]$ with handgrip exercise. Table 5 compares the amounts of $[PCr]$ and $[ATP]$ in normal controls to patients with myocardial infarction. Observe that in more than one case the overall amount of each metabolite ($\mu\text{mol/g}$) is significantly reduced for cases of myocardial infarction^{60,152,153} compared to normal controls.^{20,60,67} There

is even a slight reduction in the amount of [PCr] and [ATP] for the case of myocardial ischemia.⁶³ This data shows that P-31 cardiac spectroscopy has the potential to evaluate myocardial viability.

Table 4. Cardiac [PCr]/[ATP] Ratio of Patients with Myocardial Infarction at Rest and During Stress.

Degree of Disease	[PCr]/[ATP] at Rest	[PCr]/[ATP] at Stress	Magnet Tesla	P-31 Method	Reference
Infarction After angioplasty and drug therapy	1.6 ± 0.2 (M=2, F=2)	-	1.5 T	DRESS 2.5-9 min	149
Infarction After angioplasty and drug therapy	1.8 ± 0.2 (EPI) (M=2, F=2)	-	1.5 T	DRESS 2.5-9 min	149
Myocardial "Scar"	0.48 ± 0.21 *	-	1.5 T	2D-ISIS + 1D-CSI	81 **
Chronic anterior wall infarction	Normal (M=6)	-	1.5 T	ISIS 32 min	82
Chronic posterior wall infarction	Normal (M=4)	-	1.5 T	ISIS 32 min	82
Fixed Tl-201 defects	0.94 ± 0.41 * (M=8, F=4)	-	1.5 T	DRESS 12-15min	60
Fixed Tl-201 defects	1.18 ± 0.28 (n=12)	1.12 ± 0.24 (handgrip)	1.5 T	DRESS	54
Fixed Tl-201 defects	1.24 ± 0.28 * (M=9, F=3)	1.19 ± 0.28 * (handgrip)	1.5 T	DRESS 7-8 min	12

* = blood corrected; M = Male; F = Female

ENDO = localized to endocardium; EPI = localized to epicardium;

** = 3 out of 5 patients had a prior history of heart failure

Table 5. Cardiac [PCr] and [ATP] Amounts at Rest in Patients with Myocardial Infarction, Ischemia and in Normal Controls.

Patient Type	[PCr] μmol/g	[ATP] μmol/g	Magnet Tesla	Quantify to:	P-31 Method	Reference
Infarction	< normal	< normal	1.5 T	External Standard	DRESS	193
Infarction	< normal	< normal	1.5 T	External Standard	DRESS	192
Infarction	3.94±2.21 (M=8, F=4)	4.35±1.52	1.5 T	External Standard	DRESS 12-15 min	60
Ischemia	7.64±3.00 (M=22, F=7)	6.35±3.17	1.5 T	External Standard	DRESS 12-15 min	60
Normal	11.7±2.5	7.2±1.2	1.5 T	External Standard	1D-CSI + 2D-Phase Encode	67
Normal	12.14±4.25 (n=11)	7.72±2.97	1.5 T	External Standard	DRESS 12-15 min	60
Normal	10±2 (n=21) (M=21)	5.8±1.6	1.5 T	Internal Water	1D-CSI	20

M= Male; F = Female

There is also potential value in observing the Pi and pH of patients with myocardial infarction. One study at 1.5 T of six patients with anterior myocardial infarction, with blood contamination corrections performed on the spectra, showed a slight but non-significant elevation of Pi in the patient set.⁴⁹ This study was early on in human, cardiac P-31 MRS, used only a simple 1D-CSI acquisition, and may have mistaken blood contamination for Pi. There are not many studies that follow this one in identifying changes with Pi at 1.5 T. Despite this fact, there is interest in identifying the Pi peak as a means of identifying a decrease in the pH of the myocardium that would also be a sign of ischemia.

Difficulty with blood contamination has made the measurement of Pi more complicated in human cardiac spectroscopy studies. This is due to the fact that at 1.5 T or below, the Pi is most often overlapped by the 2,3-DPG (2,3-diphosphoglycerate) peaks from the blood contamination. The Pi has been repeatedly seen at 1.5 T with the use of specialized pulse sequences such as DANTE selective excitation,¹⁵ nuclear Overhauser effect (NOE) for signal enhancement, magnetization transfer,¹⁶ and proton decoupling for enhanced spectral resolution.¹⁷ These options are not currently available on the GE 3.0 T system. Also, long acquisition times can increase the probability of visualizing the Pi peak by increasing the SNR. These problems are overcome at 3.0 T. Work at 3.0 T allows for the Pi peak to be distinguished even over relatively short scan times (i.e. 6 to 8 minutes) due to the enhanced SNR and wider spectral dispersion achieved at the higher field strength.

Myocardial Ischemia. One of the most common types of heart disease is cardiac ischemia. In the diseased heart affected by myocardial ischemia, individual cells in affected areas of the myocardium can no longer function due to significant decreases in blood flow to the region. The blood flow reduction is typically due to a gradual blockage forming in the coronary arteries. These patients have symptoms of angina which are usually temporary and brought on by stress when the required blood flow to the heart is inadequate. Although typically these patients will suffer from angina and fatigue without triggering a deadly heart attack, a diagnosis of ischemia does substantially increase the risk of a heart attack. Since the blood flow is already reduced, there is greater potential for acute and total

blockage (infarction). The result is a disorder that is very disabling partially due to the fatigue but also due to the anxiety related to the chest pain.

The typical diagnosis of cardiac ischemia is based on signs, symptoms and laboratory tests that can be performed by a family-practice or emergency room physician. Cardiologists and radiologists at the local hospital can also perform further diagnostic exams. In addition to patients with angina being tested for ischemia, asymptomatic patients at risk for heart problems based on risk factors such as age, weight, life-style (high fat diet, smoking) and family history are also tested. This is due to the fact ischemia is often clinically silent or associated with atypical symptoms. The AHA estimates that as many as 3 to 4 million Americans have silent or asymptomatic ischemic episodes that are eventually diagnosed by testing for reasons unrelated to the symptoms, such as a routine physical examination.²

Ischemia is primarily quantified by the identification of stenosis in the larger vessels of the coronary arteries, but ischemia can also be confined to the microvessels. Microvascular ischemia can involve angina-like chest pain that is coincidental with exertion and thus may resemble typical angina pectoris but without stenosis of the main coronary arteries. More often, however, the chest pain associated with microvascular ischemia has characteristics that differentiate it from typical angina. For example, the pain is generally prolonged, repetitive, occurring at night, and poorly responsive to rest and medications. Dr. Carl Pepine, a cardiologist at the University of Florida, was one of the first to observe that patients' with symptoms

of microvascular disease are most often not predictive of a life threatening disorder. Whereas in age-matched patients with coronary artery disease such symptoms are indications of a life-threatening event.³ Despite microvascular disease not being life threatening, it still has a great impact on the quality of life. In addition, undiagnosed conditions, lethal or not, traditionally place added costs on the medical system as the patient will continue to seek diagnosis, go to new physicians and have more and more tests performed. Often the quality of life is diminished to an extent that many remain unemployed or retire from work and limit their activities, with obvious socioeconomic implications. From a clinical and financial point of view, these patients need to be diagnosed and treated.

In cases of myocardial ischemia, the localized phosphorus spectrum will show a small level of depletion in the [PCr]/[ATP] ratio at rest, compared with reference normal controls (i.e.: Ischemic Anterior Myocardium [PCr]/[ATP]: 1.45 ± 0.31 , n=16; Disease-Free Controls [PCr]/[ATP]: 1.72 ± 0.15 , n=11).⁴⁹ A more significant difference occurs when comparing the [PCr]/[ATP] ratio during minor stress test (leg or handgrip exercise) to that with the resting value, as shown in Table 6. Similar results have been shown in both animal^{126,134} and human experiments^{12,54,69}.

Table 6. Cardiac [PCr]/[ATP] at Rest and Stress in Patients with Myocardial Ischemia.

Degree of Ischemia	[PCr]/[ATP] at Rest	[PCr]/[ATP] at Stress	Magnet Tesla	P-31 Method	Reference
>= 70% stenosis	1.45±0.31 (n=16)	0.91±0.24 (handgrip exercise)	1.5 T	1D-CSI 5-14 min	49
>=70% stenosis	1.46±0.39* (M=14)	0.94±0.28* (handgrip exercise)	1.5 T	1D-CSI 8-16 min	150
>=75% stenosis	1.56±0.19 (n=15)	0.94±0.27 (handgrip exercise)	1.5 T	DRESS	54
>75% stenosis	1.60±0.19* (M=11, F=4)	0.96±0.28* (handgrip exercise)	1.5 T	DRESS 7-8 min	12

* = blood corrected; M = Male; F = Female

Table 7 demonstrates the descriptive value of cardiac P-31 MRS for ischemia that has been treated. The first two rows show a study where five ischemic patients were tested with and without in magnet exercise (handgrip) after revascularization surgery. In the case of the patients with revascularization, the [PCr]/[ATP] ratio does not drop when exercised, although the same patients did drop their [PCr]/[ATP] ratio prior to surgery.⁴⁹ This provides a quantitative means for evaluating the success of revascularization surgery. Another method for treating a heart attack that is thought to be primarily ischemic is to provide drug therapy intravenously, such as thrombolytic agents. The third row shows such a study where the region of the heart, even after being treated, remained in a stunned state, where the wall motion in the region is still impaired even after intervention.¹⁷³ In this case, investigators were able to show that despite the myocardium remaining stunned, the tissue [PCr]/[ATP] values were not

significantly depleted as they would normally be under an ischemic situation under stress, showing the potential of cardiac P-31 MRS as a feedback measure after treatment.¹⁷³ Unfortunately, no pre-treatment data was obtained so it is difficult to conclude that the ratio of [PCr]/[ATP] alone was a marker for ischemia. The last two rows show a study done only at rest of ischemic patients before and after angioplasty, which showed no change in [PCr]/[ATP]. This study would have been more effective if in magnet exercise or drug stress was used during the [PCr]/[ATP] acquisition.

Table 7. Cardiac [PCr]/[ATP] at Rest and Stress in Patients with Myocardial Ischemia with Some Type of Intervention.

Disease Description	[PCr]/[ATP] at Rest	[PCr]/[ATP] at Stress	Magnet Tesla	P-31 Method	Source
Ischemia before revascularization (n=5)	1.51±0.19 normal	1.02±0.26 < normal	1.5 T	1D-CSI 5-14 min	49
Postischemic after revascularization (n=5)	1.60±0.20 normal	1.62±0.18 normal	1.5 T	1D-CSI 5-14 min	49
Drug infused Postischemic, Stunned Myocardium (M=15, F=6)	1.51±0.17* normal	-	1.5 T	ISIS 22 min	173
Ischemia ≥ 75% stenosis before angioplasty (n=7)	1.5±0.7* normal	-	1.5 T	DRESS 15 min	51
Postischemic after angioplasty (n=7)	1.4±1.0* normal	-	1.5 T	DRESS 15 min	51

* blood corrected; M = Male; F = Female

Microvascular Ischemia Study: WISE. An NIH sponsored study concentrated on women's ischemic syndrome evaluation (WISE) is studying microvascular ischemia in women with phosphorus NMR spectroscopy as part of a multi-center study including the University of Florida. The

specific feasibility of phosphorus NMR spectroscopy to look at microvascular ischemia was initially demonstrated during a pilot study performed on a 1.5 T Philips system at the University of Alabama at Birmingham (UAB).¹³⁵ In this study, women were identified who had angina-like chest pain characteristic of ischemia and CA tested to measure the degree of stenosis in their macrovessels. The patients with insignificant stenosis (less than 30% stenosis) were also evaluated for all other possible causes for their chest pain, without diagnosis. UAB's study identified micro-vascular dysfunction (MVDS) in 30% of the women with previously unidentified chest pain. This data was also compared with 17 normal volunteers (ages 21 to 53 years; average age 32 ± 10; 10 males, 7 females), who underwent 8 minutes of isometric handgrip exercise at 30% maximum force. There was no significant change (-0.1% ± 10.3%) in the [PCr]/[ATP] ratio as compared to rest. These values are consistent with similar handgrip exercise literature where Weiss et al.¹³⁶ and Yabe et al.¹³² have similar estimated percent change statistics in their normal population samples of 1.9% ± 7.0% and 0.5% ± 9.0%. The determination of significance was set at two standard deviations (20.4%) of a percent drop in the [PCr]/[ATP] ratio of the normal volunteers with handgrip exercise.¹³⁵ In eight patients (7 male, 1 female) with CA proven stenosis greater than 70% blockage, the same amount of exercise resulted in a -24% ± 2% drop in [PCr]/[ATP]. This comparison of normal volunteers versus patients with proven stenosis proves that the phosphorus NMR spectroscopy test is viable for differentiating non-ischemic versus highly ischemic hearts. The Birmingham study also evaluated 17 women with less than 30% stenosis (very little blockage) and undiagnosed chest pain (suspected

microvascular ischemia). The same amount of exercise produced little [PCR]/[ATP] change ($-2\% \pm 7\%$) in 12 of these women, but 5 women had a PCR change of -27% . This change is attributed to MVDF, because of what is expected by the ischemic angina-like symptoms and the lack of macrovascular disease.¹⁴⁶ Accordingly, cardiac P-31 MRS shows significant potential as a quantitative test for myocardial ischemia that does not depend on the presence of macrovascular disease. No other current diagnostic modality is able to quantitatively assess the degree of ischemia of the heart in this way.

In-Magnet Exercise. For patients with myocardial ischemia, there is a significant difference between phosphorus cardiac spectra obtained at rest and during stress (in-magnet exercise).⁴⁹ It is clearly valuable to use some type of in-magnet exercise during one period of the cardiac spectroscopy acquisition protocol. Studies using in-magnet exercise have been done by exercising the legs,^{11,25,157,159} arms with a hand-grip,^{49,54,60,138,159} and drug-induced (dobutamine infusion) cardiac stress¹⁶¹. The leg exercises can allow for prone position exercises (prone position is best for cardiac imaging and spectroscopy to reduce respiratory motion artifacts). One design by Conway et al.¹⁵⁷ has the subject lie in a prone position, lifting 5-kg weights with the legs by bending at the knee. This stress test tends to produce an increase in the heart rate pressure product of around 70%.^{25,157} Isometric, hand-grip exercise, where the subject squeezes continuously at a constant 30% of the subject's maximal force,⁴⁹ can also be performed simply in any position. In-magnet exercise tests have been also done with devices as simple as a bottle of water. Widmaier et al.¹⁵⁹ successfully implemented

a dynamic hand-grip finger flexion exercise consisting of squeezing a 50-mm diameter, water-filled, plastic bottle at a Maximum Voluntary Contraction (MVC) approximately once every second for a 130 seconds acquisition. Such an exercise increases the heart rate pressure product by approximately 30 to 35%, which is still enough to increase coronary vasoconstriction in the presence of critical levels of coronary stenosis.¹¹⁸ The two types of handgrip exercise used are either dynamic, where the grip is released and regrabbed up to the 30% maximum level repeatedly during the test, or isometric, where the handgrip is held constant at the 30% of maximum effort level. As can be seen from Table 8, both dynamic and isometric handgrip raise the heart rate and blood pressure, but the isometric method is a harder level of work and therefore responds with a greater heart rate and blood pressure response. Finally, dobutamine infusion (drug infusion) has the ability to increase the rate-pressure product by 60 to 130%.^{7,142}

Table 8. Literature Review of In-Magnet Handgrip Exercise Response.

	Avg Rest & 30% Max Handgrip Exercise	Avg Rest & 4 Handgrip Exercise	Pressure Product (HRxSBP)	Avg Rest & Exercise [PCr]/[ATP]	Patient Type	Reference
dynamic	67±8 77±11	117±12 131±13	7839 10087	1.85±0.28 1.90±0.23	control	12
dynamic	68±12 75±13	118±13 134±16	8024 10050	1.60±0.19 0.96±0.28	ischemia ≥ 75% stenosis	12
dynamic	63±11 74±13	115±14 128±13	7245 9472	1.24±0.30 1.19±0.28	infarction ≥ 75% stenosis	12
isometric	67±12 81±10	143 156	9600 12600	1.72±0.15 1.74±0.17	control	49
isometric	77±13 89±16	132 151	10200 13400	1.45±0.31 0.91±0.24	CAD and ischemia ≥ 70% stenosis	49
isometric	75±13 85±14	132 159	9900 13500	1.59±0.31 1.55±0.24	Non-ischemic	49

F = Female; M = Male

Post-Processing Calculations and Corrections

Simply obtaining a phosphorus spectrum from a voxel in the myocardium is not enough to ensure useful spectral data. The cardiac spectrum is generally contaminated from unwanted signal from surrounding blood and skeletal muscle. Also, T_1 relaxation corrections must be made when $TR < 5 \times T_1$ and T_2 relaxation corrections when acquiring an echo instead of an FID. Finally, calculation of absolute concentrations of metabolites may show changes undetected by metabolite ratios.

Starting with the first human study of cardiac phosphorus spectroscopy, the techniques for gathering phosphorus cardiac spectra

have gradually changed and improved. The first cardiac spectrum was obtained by Bottomley et al. in 1984,⁴⁵ corrections for relaxation by 1987 by Bottomley et al.,⁴⁶ and blood contamination corrections as early as 1991 by Sakuma et al.⁵⁵ The pulse sequences and post-processing methods have been gradually refined and duplicated by different research groups and yielded very comparable results. In each case the ratio of myocardial [PCr]/[ATP] was comparable for reference controls during rest: 1.80 ± 0.21 (n=12),⁵¹ 1.93 ± 0.21 (n=17),⁵⁵ 1.95 ± 0.45 (n=19),⁵² 1.65 ± 0.26 (n=9).¹⁶⁵ Uncorrected cardiac spectra produce unreliable results,⁷ therefore studies of human cardiac spectroscopy are no longer publishable without corrections for blood contamination and relaxation effects. In addition, since there is no method for correcting for skeletal muscle contamination, such contamination invalidates the study results.

Skeletal Muscle Contamination

Skeletal muscle contains the same phosphorus peaks as cardiac muscle, but in different quantities. The primary method for ensuring that there is no skeletal muscle contamination in the cardiac spectrum is to use good methods of localization with an appropriate pulse sequence.⁵⁰ This dissertation project will evaluate ISIS and CSI derived pulse sequences for elimination of skeletal muscle contamination.

Blood Contamination

Blood contains ATP and PDE as does myocardium, but no PCr.⁶⁰ Blood also contains 2,3-DPG (2,3-diphosphoglycerate), which produces a

doublet in the phosphorus spectrum at chemical shift positions of 5.4 and 6.3 ppm, near Pi and phosphomonoester resonances. Blood contamination causes the [PCr]/[ATP] ratio to appear reduced.¹¹ Also, the myocardial Pi peak in normal heart is small and difficult to resolve from the blood DPG signal.^{7,148}

The correction method for blood contamination is to determine the relative signal contributions of 2,3-DPG and ATP from blood and use this knowledge to correct for blood's contribution to ATP. This is accomplished with the use of a correction factor, which is the ratio of blood [ATP]/[2,3-DPG]. Such a correction factor for the cardiac muscle [PCr]/[ATP] ratio typically increases its value by 13%¹¹ at 1.5 T.^{7,11,82,148,150,155} The blood correction is considered small enough that a substantial error in [ATP]/[DPG]_{blood} ratio will not severely compromise the final [PCr]/[ATP]_{cardiac spectrum} ratio, although the final value of myocardial [PCr]/[ATP]_{cardiac spectrum} will still be better than the uncorrected value.⁷ The ratio of blood ATP to DPG obtained from basic spectrometer methods is 0.30.²⁰⁰⁻²⁰²

Spectra from pure blood are usually obtained *in vitro* using heparinized (anti-coagulant) blood samples. Unfortunately, one study using proton decoupling of blood samples resulted in spectra with the contribution from 2,3-DPG overestimated and ATP underestimated.²⁰³ In addition, most of these types of blood studies were conducted days and weeks after the sample was obtained, since most studies were performed to test the survival of stored blood. These studies showed increased Pi which indicate the breakdown of 2,3-DPG. However, ATP was shown to remain constant when the cells were maintained under appropriate conditions of 37° C temperature and the appropriate gas mixture.²⁰²⁻²⁰⁶

The excess Pi signal appears as soon as two hours after obtaining the blood sample.²²⁷ As the 2,3-DPG breaks down over time the ATP/2,3-DPG ratio increases.²²² Consequently, the published ratio of 0.30 may be elevated due to the delay before acquisition. There are thus several reasons to distrust the results of these experiments when determining the proper ratios to correct for blood contamination in the *in vivo* cardiac muscle spectrum.

At least two human cardiac NMR research groups have dealt with the problems of obtaining adequate blood spectra by determining their own correction factors for blood ratios. They extracted venous blood (~50 milliliters) from their volunteers and obtained phosphorus spectra of the blood in the same magnet used for the cardiac study,^{22,148} in one case using the same NMR acquisition techniques as well.¹⁴⁸ In both cases studies were conducted at 1.5 T and the blood [ATP]/[2,3-DPG] concentration was much lower than the reported values from the standard spectrometer experiments: 0.11 ± 0.02^{22} and 0.14 ± 0.02^{148} . These research groups were also able to correct for the blood 2,3-DPG contamination of the muscle PDE peak with correction ratios of [PDE]/[DPG] of 0.19 ± -0.03^{22} and 0.21 ± -0.02^{148} . Theoretically, the blood could be measured *in-vivo* directly from inside the heart, but has not been documented in the literature to date.

Ischemia causes a reduction in systolic wall thickness. It has been debated that because of the reduced volume of myocardium, the phosphorus spectrum will be more contaminated with blood for ischemic patients. As blood contains ATP, blood contamination can alter the [PCr]/[ATP] ratio. Fortunately, the amount of blood contamination can be corrected for, and it has been shown that the [PCr]/[ATP] ratio is

still reduced with exercise for ischemic patients even after blood correction.¹²

Relaxation Corrections

Two components of the macroscopic magnetization in NMR are subject to time dependent exponential relaxation effect. The longitudinal magnetization or spin-lattice relaxation along the z-axis is an increasing exponential function (T_1 , dependent) with a maximum of magnetization of Mo. The transverse magnetization or spin-spin relaxation in the x,y plane is a decreasing exponential function (T_2 , dependent) with a minimum magnetization of near zero.¹⁰⁸

The relaxation time T_1 , is the time required for the net magnetization (M) to return to 63% of its original value following an excitation pulse.¹³ T_1 relaxation rates depend on the presence of molecular interactions in the vicinity of the excited spin that modulates with an intrinsic frequency (w_L).¹³ When w_L is near in frequency to the resonance frequency (w_0), the interaction will more readily absorb the resonant energy and this energy transfer will occur more frequently. This allows the collection of spins to return to the equilibrium configuration sooner, resulting in a shorter T_1 value.¹³ In-vivo metabolites as studied with P-31 spectroscopy are usually small molecules where the rate of molecular motion is rapid. This results in a poor match between w_L and w_0 and thus relatively long T_1 relaxation times.¹³ In addition, because of the relationship with resonant frequency, T_1 is also dependent on the main magnetic field strength.

In a typical P-31 MR spectroscopy experiment, the time between successive radio frequency pulses (TR) is usually insufficient for

complete T_1 relaxation. Successive acquisitions applied at a short TR result in a steady state of M where the spins are partially saturated and the resulting MR signals are reduced from their completely relaxed values.²⁸ This situation makes quantitation difficult since the correct MR signal from each P-31 metabolite is directly proportional to the number of spins only when the collection of spins is at equilibrium. Different metabolites relax at different rates. For example, the [PCr]/[ATP] ratio will typically be too small due to the faster relaxation of ATP. Fortunately, there is a way to correct this situation.

T_1 relaxation corrections are necessary for cardiac spectroscopy studies since the pulse repetition time, TR, is generally much shorter (minimum 1 sec when gated) than the total time for complete relaxation, five times T_1 .²⁹ ($T_1 = -4$ sec for PCr and -2 sec for β -ATP at 1.5 T).³⁰

The method for determining the relaxation factor for cardiac spectroscopy is to obtain two sets of phosphorus spectra, one at short TR ($TR < T_1$) and one at a fully relaxed TR ($TR \gg T_1$). Then a simple division of the ratio of [PCr]/[ATP] measured at the fully relaxed T_1 , over the [PCr]/[ATP] ratio measured at the shorter TR, provides the relaxation factor, assuming the same TR for each relaxation corrected experiment.²⁹ This factor can in turn be multiplied by the [PCr]/[ATP] ratio of the localized spectra obtained with the shorter TR value to obtain the relaxation corrected results.

The relaxation correction factor (RCF) ideally should be obtained directly from the myocardium, with localized techniques. This requires a set of volunteers be used to gather data to estimate the relaxation correction factor for all studies at that field strength and frequency.

This is because it would take an extra 30 minutes to an hour to gather data for RCF for each subject, an unreasonable request to be tacked on after a current two-hour study. However, Bottomley et al.^{67,209,210} obtains the relaxation data from each subject by using unlocalized acquisitions at long and short TR times, adding only six minutes of scan time²⁰⁹ and allowing the calculation of RCF for each participant. This method also assures that the flip angle, pulse power, RF coils, and patient is the same for the localized spectrum and for the measurement of the correction factor.²⁰⁹ In doing so, a large assumption is made that the P-31 metabolites of skeletal and cardiac muscle have the same relaxation rates and thus the same RCFs. This assumption is based on animal studies in rat skeletal muscle²¹¹ and canine cardiac muscle.²¹²

Those research groups that have measured animal and human localized cardiac P-31 metabolite T₁ values directly have shown that it is possible to obtain relatively consistent values although there are still discrepancies between research sites. This is demonstrated in Table 9 where the standard deviations of some published values of T₁ are relatively low with greater discrepancies between reports, such as between Neubauer et al.¹⁴ and most of the other human studies^{164,177,212} at 1.5 T. There is no need to rely on assumptions about cardiac and skeletal muscle metabolites, when the T₁ relaxation values of the P-31 metabolites can be measured from the cardiac muscle directly. A correction factor of 1.28, has been measured at UAB¹⁹³ and is used in the WISE study to correct for relaxation effects at 1.5 T. To use this correction factor, simply multiply it by the blood corrected [PCr]/[ATP] ratio.

Table 9. Published Spin-Lattice Relaxation Times of Myocardial PCr and ATP.

Subject	Field (Tesla)	T_1 (PCr) (sec)	T_1 (γ -ATP) (sec)	T_1 (β -ATP) (sec)	Reference
Dog	1.9	4.4 ± 0.1	1.8 ± 0.2	1.6 ± 0.1	118
Pig	4.7	4.8 ± 0.9	3.0 ± 1.7	2.6 ± 1.7	213
Pig	2.0	6.3 ± 0.4	2.2 ± 0.8	2.2 ± 0.7	213
Human	4.0	5.3 ± 1.6	$2.7 \pm .6$	-	17
Human	1.5	4.2	-	1.7	193
Human	1.5	4.0	-	1.8 ± 0.2	212
Human	1.5	4.1	-	2.7 ± 0.8	164
Human	1.5	6.1	5.4 ± 0.5	5.8 ± 1.0	14

The relaxation time T_2 , is the time required for the transverse component of M to decay 37% of its initial value. At equilibrium, M_0 is oriented only along the z (B_0 = main magnetic field) axis and no portion of M_0 is in the x,y plane. The coherence or uniformity of the spins is entirely longitudinal with no transverse component.¹⁸ A 90° radio frequency pulse causes M_0 to rotate entirely into the xy plane, so that the coherence is in the transverse plane at the end of the pulse. After the pulse, the coherence gradually disappears, the spins lose phase coherence, and reorient themselves along B_0 . The disappearing coherence produces the free induction decay (FID) with a dephasing time of T_2 or T_2^* , where T_2 is always less than T_1 and T_2^* is less than T_2 .¹⁸

After the application of the 90° radio frequency pulse, when M is oriented in the transverse plane, each spin precesses at the same frequency ω_0 , and the spins are in phase. Each nearby spin of the same

type and the same molecular environment will have the same ω_0 . The ω_0 will not remain the same, however, as intra- and inter-molecular interactions will cause the local magnetic field to modulate around each spin causing ω_0 to vary. The variations will produce a gradual, irreversible loss of phase coherence and a reduction in the transverse magnetization.³⁷ In addition, non-uniformity in the B_0 field and magnetic susceptibility differences can cause additional loss in transverse phase coherence and T_2^* relaxation.³⁸ Fortunately, neither T_1 nor T_2^* are factors that need to be corrected for quantitation of a P-31 spectrum using ISIS or DRESS, but they can affect the quality of the spectrum. The T_1 component of relaxation determines the amplitude of the metabolite signal while the T_2 or T_2^* has an effect on the decay of signal with time and the linewidth. Shimming of the region of interest can attempt to correct for some losses in phase coherence, but P-31 metabolites have inherently fast and unalterable T_2 times.

Calculation of pH

Some values of cardiac pH as found in the literature are shown in Table 10. The pH is proportional to the frequency difference of the Pi and PCr P-31 metabolite peaks. In the literature it is well stated that it is not always possible to see the Pi peak in every case due to SNR differences between cases. None of the publications listed were able to obtain pH values on every single subject. There are also no known publications of human cardiac pH during in-magnet stress.

Table 10. Myocardial pH in the Literature as Measured by Human, In-vivo Phosphorus NMR Spectroscopy.

Type of patient	n	pH at rest	Reference
Normal Control	4	7.15±0.03	165
Normal Control	?	7.15±0.02	149
Normal Control	1	7.17	159
Infarction	4	7.15±0.06	149

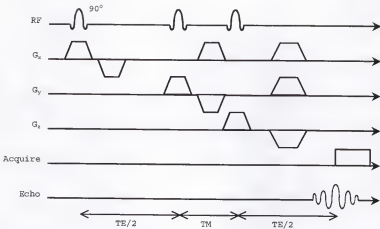


Figure 1. STEAM Pulse Sequence

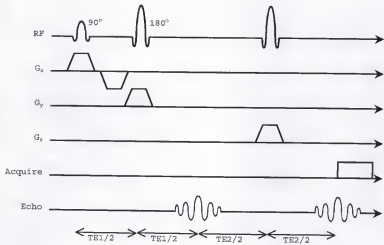


Figure 2. PRESS Pulse Sequence

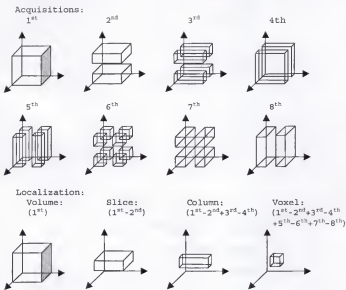


Figure 3. ISIS Volumes for 8 Acquisition Voxel Localization.

CHAPTER 3
PHANTOM P-31 SPECTROSCOPY ACQUISITION TECHNIQUES

This chapter covers the design and implementation of the phantom techniques for evaluating the 3.0 Tesla GE Signa Advantage™ magnet in Gainesville, Florida for purposes of performing cardiac spectroscopy on human subjects. The 3.0 Tesla magnet located in the tunnel between Shands at the University of Florida (UF) and the Veterans Affairs Medical Center (VAMC) is owned by the VAMC, Shands at UF, and the Brain Institute at UF. Phantom and coil combinations were tested with a variety of imaging and spectroscopy pulse sequences. The purpose of utilizing a phantom is to take the opportunity to test all the possible pulse sequences and options with a standard sample (the phantom) to compare each method. In addition having a phantom prevents the need to have an endless supply of human volunteers to test out each pulse sequence and option. In addition, it is often difficult for humans to lie perfectly still in the magnet for a long period of time, as they are generally required to do for all MRI and MRS studies (with the exception of exercise studies, where special procedures are implemented). When new protocols are initially being tested, they tend to take longer to run than after they are better defined, again pointing to the advantage of using a constant, stationary phantom. Although there is not enough room in each figure caption to capture the full protocol under which each image and spectrum were obtained, this

information can be found in the appendix, identified with its reference figure.

Phantom Design

Four phosphorus phantoms have been identified or built for the purpose of initially testing the parameters for each pulse sequence and protocol, before use on human subjects.

Gate-able and Depth Phantoms

Two phantoms, the gate-able and depth phantoms consist of two compartments, each containing a different phosphorus compound, which present as separate chemical peaks in the phosphorus spectrum. Photographs and images of the gate-able and depth phantoms, in each of the three planes can be found in Figure 4, Figure 5, Figure 6, and Figure 7. The outer and inner compartments (OC and IC) are filled with the phosphorus containing chemicals of sodium dihydrogen phosphate (NaH_2PO_4) and methylenediphosphonic acid (MDPA), respectively, each diluted in distilled water. The compartment sizes and concentrations for each phantom are described in Table 11. Two sections are necessary to test the ability of each pulse sequence to localize to the desired voxel (represented by the IC) and exclude the outer voxel signal (represented by the OC).²¹⁴ The OC represents the unwanted signal from skeletal muscle and blood that surrounds the myocardium. The IC represents the phosphorus signal from the myocardium. In addition, the depth phantom's IC is surrounded by a layer of water (compartment 2 in Table 11) which is just thick enough to eliminate most of the contamination from just outside the selected volume. For this reason

the depth phantom is especially useful in demonstrating complete elimination of the OC signal of NaH_2PO_4 when the pulse sequence is able to do so. Both phantoms were designed to load the H-1 and P-31 coils similar to a human chest load. The estimation of loading equivalency is demonstrated by the resulting quality factors (Q-factor) values of the loaded H-1 and P-31 coils compared to a human chest load, as shown in

Table 12. The Q-factor will be explained further in the section of this chapter on coil designs. The center of the gate-able phantom's IC is at a depth of 5 cm, to approximate the depth of the anterior wall of the heart, while the depth phantom has variable depth IC.

Table 11. Gate-able and Depth Phantom Compartment Sizes and Concentrations.

Phantoms	Inner Compartment Size	Inner Compartment Concentration	Outer Compartment Size	Outer Compartment Concentration
Gate-able	Container: 4.7-cm length, 2.7-cm ID*; 35 ml	80 mM MDPA	Container: 11-cm max height, 28-cm ID*; partially filled with 4 liters	80 mM NaH_2PO_4
Depth	Container 1: 3-cm length, 2.3 cm ID*	-80 mM MDPA	Container: 16-cm max height, 30-cm ID*; partially filled with 7 liters	30 mM NaH_2PO_4 plus 70 mM NaCl
	Container 2: 3-cm length, 3.6 cm ID*	water barrier		

Abbreviations: ID* = inside diameter

The gate-able phantom was initially designed to test the degree of localization of each pulse sequence and to do this while the IC was moved in and out of the volume of acquisition in a gated fashion. A volunteer standing outside of the magnet would gate the magnet acquisition with a peripheral-gating device reading the pulse rate in

the volunteer's finger. While viewing the pulse waveform, the volunteer would use an extension rod attached to the IC of the gate-able phantom to coincide the movement of the IC with the peripheral pulse gating, pushing and pulling the IC in or out of the acquisition volume (AV) with each beat. The system gated the sequence to the peak of the peripheral pulse waveform. It was found that placement of the IC in the AV at the peak of the pulse waveform resulted in a signal that was equivalent to that achieved by placing the IC in the AV without movement. In addition, when the cycle was reversed such that the IC was outside of the AV at the peak of the peripheral pulse, and moved inside between gated pulses, the result was equivalent to having the IC outside of the AV for the entire sequence without movement. Therefore, the gating was found to be predictable and accurate.

The depth-changing phantom (or simply "depth phantom") was borrowed from Hee-won Kim's dissertation work. This phantom is designed with an inner compartment that can be moved to different depths away from the coil surface, thus simulating different cardiac depths. Unlike the gate-able phantom, the IC position is fixed before the start of acquisition and cannot be moved during acquisition, although it can be moved to different depths between acquisitions. The IC of the depth phantom consists of two separate containers, an inner container of MDPA surrounded by a second container providing a layer of water between the IC and OC. The water layer is thin (~0.7 mm) but large enough to help eliminate a majority of signal just outside the selected volume of interest. This phantom is therefore ideal to use when demonstrating the ideal localization ability of a pulse sequence and to show virtually no external contamination from the external

NaH_2PO_4 . The primary use of the depth phantom, however, is to estimate the optimal transmitter gain (TG) which determines the optimal flip angle at each depth. For the human studies, these phantom measurements will provide initial guesses of TG values for human cardiac P-31 MRS acquisitions.

Slice Profile Phantom

A third phantom, the slice profile phantom, as shown in Figure 8, consists of a 2 ml vial of 14.7 M phosphoric acid (H_3PO_4), placed at an angle of 4° at depth of 5.5 cm with a plastic arch that is glued in place. The vial is surrounded by an outer compartment (22 x 22 cm^2 base x 10 cm tall) of 4 to 5 liters of 70 mM sodium chloride to load the coil. This phantom was used to more precisely detect the degree of contamination in a slice from a source (the 2 ml vial of H_3PO_4) just outside the slice.

GE Phosphoric Acid Phantom

A GE plastic bottle phantom consisting of a larger volume (~450 ml) of phosphoric acid (H_3PO_4) provided a strong P-31 signal for use in comparing the different types of P-31 coils. This phantom provided enough P-31 signal for adequate imaging at the P-31 frequency. It was used for quick working checks of coils and equipment, as well as to verify dimensionally the depth ranges of each phosphorus coil used in this work. The bottle is 18 cm tall (including cap) and has a 7.3 cm diameter at its widest. GE's 14.7 M Phosphorus Phantom is labeled as "GE Medical Systems, 46-317299G2, Spectroscopy Service Phantom, 14.7 M H_3PO_4 , Phosphoric Acid" as shown in Figure 9.

Radio Frequency Coil Design

Sets of proton and phosphorus radio frequency coils were selected in order to obtain the best performance from a study. The proton coil is used for imaging, shimming and ensuring correct positioning of the phosphorus coil. To prevent changes in shim values and localization due to patient movement, it is essential to have the proton coil and phosphorus coils in place during the entire study, independent of whether the magnet is set at the proton or phosphorus frequency. In terms of RF coils, this means having proton and phosphorus coil(s) that are compatible and maximize the SNR for the phosphorus spectrum. The coils were designed dimensionally by the author, with the author sometimes providing the platform and placing the copper tape on the coil former with proper dimensions. All of the capacitor, resistor and cable placements for proper coil tuning and usage, in addition to some initial platform creations, were performed by Dave Peterson and Bryan Wolverton in Dr. Fitzsimmons' coil lab, at the Veterans Affairs Medical Center, Gainesville, FL. In addition, Dave Peterson provided assistance in measuring coil parameters as are shown in Table 12 and Table 13.

3.0 Tesla Square Proton Coil Paired with Quadrature Phosphorus Coil

The GE 3.0 Tesla magnet does not have a body coil, therefore it is necessary to build a proton surface coil in addition to the phosphorus surface coil. A $10 \times 16 \text{ cm}^2$ quadrature transceive phosphorus coil (two 10-cm diameter coils overlapping), coplanar with a 25-cm square transceive proton coil was created and was shown to provide adequate imaging and spectroscopy performance. The quadrature coil

provides an advantage over the basic single-turn coil. Theoretically, a quadrature coil will provide up to $\sqrt{2}$ times the signal to noise of a single turn coil.¹⁸⁹ In practice, the signal to noise improvement can be better or worse depending on the quality of the coils that are compared. A quadrature coil, acting as receive only, provided 1.4 times the signal-to-noise ratio of a single turn coil having the same shape and total dimension, in a cardiac imaging acquisition.¹⁹⁰ Originally, the quadrature phosphorus coil and the square proton coil were permanently positioned together on one holder as shown in Figure 10a. A schematic diagram of the proton square coil is shown in Figure 11a, whereas a schematic diagram of the phosphorus quadrature coil is shown in Figure 11b. It was found that this pairing, when positions were permanently placed, offered limited flexibility in centering the quadrature coil over the heart, where the coil holder was often protruding into the chin of the volunteer. A modification was made to mount the two RF coils on separate holders so each could be optimally and comfortably positioned. This modification is shown in Figure 10b.

3.0 Tesla Phosphorus Single-Turn Coil

Most cardiac spectroscopy work is currently done with a simple, single turn surface coil. It is for this reason that tests were performed with a single-turn phosphorus coil for comparison with the quadrature coil results. The single turn coil is a 10 cm diameter transceive design tuned to 51.71 MHz for phosphorus at 3.0 Tesla. A photograph of this coil is shown in Figure 12, and a schematic diagram of this coil is found in Figure 13.

3.0 Tesla Coil Comparisons

Phantom tests with the GE 14.7 M phantom show that the quadrature coil overall performs significantly better than the single turn phosphorus coil, especially at greater depth.

Table 12 lists values of the basic coil parameters of quality (Q-factor = quality factor) and isolation for each of the 3 Tesla tuned coils. The quality factor is defined as the center frequency over bandwidth, where the bandwidth is the frequency +3dB and -3dB from the center frequency.²¹⁵ The parameters were measured with help from David Peterson in Dr. Fitzsimmons' coil lab, using the HP 8752A Network Analyzer.

Table 12. A Comparison of 3.0 Tesla Coil Parameters.

	Square H-1	Quadrature P-31	Single-Turn P-31
Q-factor Unloaded:	16	44	30
Q-factor Human* Chest Load:	2.2	24	19
Q-factor Depth Phantom Load:	2.8	12	13
Q-factor Gate-able Phantom Load:	2.5	16	16
Isolation of Quadrature:	-	15.4 dB	-
Isolation of P-31 coplanar with H-1:	-	36 dB	42 dB

* human chest load of 29 year old male with body mass index of 25.5.

In addition to measurements of the quality factor and isolation, each phosphorus coil's performance was mapped. Comparative mapping of the quadrature versus single-turn coil performance was achieved by a series of P-31 spectroscopy slice acquisitions where the TG was optimized at each slice. Using a larger proton slab phantom beneath the coil for loading, and placing the 14.7 M phantom on top of the coil, which provided excellent SNR, a DRESS slice (25 mm thick) was obtained at 5 mm intervals from each coil, as shown in Figure 14. At

each slice, the TG was optimized. The maximum distance from each coil measured was at 96 mm, just under 10 cm, where the 14.7 M P-31 phantom bottle's neck formed. The bottle also had curved edges at the bottom and top as well as a slight concave area at the bottom, which can explain part of the reduction in signal in the first few slices from the RF coils. Based on the results, the single-turn RF coil has optimal SNR at a depth of 25 mm while the quadrature RF coil has an optimal SNR at a depth of 42 mm. This data reinforces the fact that the quadrature coil penetrates deeper with greater SNR and is therefore more ideal for reaching the depths of hearts of thicker chested individuals. This result is duplicated when the ratio of quadrature to single-turn signal is plotted, showing the quadrature coil peaks with the greater signal at both the coil surface and at a depth of 42 mm. In addition, until the depth of 60 mm, the quadrature coil outperforms the single-turn coil in terms of relative signal. Increase in signal from the depth of zero to 3 cm in Figure 14 can also be explained. Starting at the coil position (zero distance from the coil), only half of the first slice contains the phantom material. As the depth increases, the entire phantom is in the slice by a depth of 1.25 cm. Acquisition of a spectroscopy slice is not 100% accurate at the edges, where a Gaussian like function describes the contamination of signal from outside the slice. At the first slice depth where the entire phantom is in the selected slice, only one edge is contributing signal contamination. As the depth increases, eventually both edges will contribute a small bit of contamination. In addition, although the 14.7 M P-31 phantom is only 73 mm in diameter, this test is not 100%

accurate because the profile of each coil (single turn and quadrature) may not have equally obtained signal from each slice.

1.5 Tesla Coils

One main argument for using the 3.0 Tesla magnet is its superior performance when compared to 1.5 Tesla. All comparisons between the 1.5 Tesla and 3.0 T were done on GE scanners with identical software (version 5.4) and with components as similar as possible. The 1.5 Tesla GE Signa Advantage™ has a body coil, therefore no proton coils were created. A single turn phosphorus coil of 10 cm diameter was created. In addition, a quadrature coil of the same dimensions as the 3.0 Tesla P-31 quadrature coil was constructed. The same parameter measurements taken from the 3.0 Tesla coils, were also performed on the 1.5 Tesla coils as shown in Table 13, with the exception of the 1.5 Tesla body coil, which cannot be moved for such testing in the coil lab. In addition, a photograph of each of the coils can be found in Figure 15 and Figure 17, and a schematic for each can be found in Figure 16 and Figure 18.

Table 13. Comparison of 1.5 Tesla Coil Parameters.

	Quadrature P-31	Single-Turn P-31
Q-factor Unloaded:	77	48
Q-factor Human* Chest Load:	45	33
Isolation:	-18.6 dB	not applicable
Match:	68 pF per side	not applicable
reflections:	-18 dB / -29 dB	not applicable

* human chest load of 29 year old male with body mass index of 25.5.

Coil Ideas for Future Cardiac Spectroscopy Studies

Future coil sets may consist of a smaller proton coil or a set of phosphorus coils with a separate, larger transmit coil, thus reducing spatially dependent spectral distortions from the excitation field.^{216,7} There is also the possibility of other coil designs, if one is found to significantly improve the performance of the cardiac imaging and spectroscopy acquisition.

Imaging

Both Spin Echo and Gradient Echo imaging pulse sequences are the most common MRI techniques for proton imaging on the GE system. The goal of the phantom imaging was to predict which pulse sequence would provide the best image uniformity and depth of penetration, when used with a simple surface coil. In this chapter, imaging is briefly examined at 3.0 T and only in phantoms, but in the next chapter images taken at 1.5 Tesla will be compared with 3.0 T and explained in greater depth. Imaging with the spin echo pulse sequence on the 3.0 Tesla with a surface coil has its limitations. Even with a maximum transmitter gain (TG) the signal depth is not as good as the gradient echo images. This is shown in Figure 19 where the top corners of the phantom are cut off when spin echo imaging is used, but are still visible when gradient echo imaging is used. In contrast, the spin echo pulse sequence works better at producing images than the gradient echo sequence on the 1.5 T, where a body coil provides more uniform excitation of the axial slice and requires less overall power. Human cardiac images shown in the next chapter emphasize this point. Also note the slight asymmetry

in signal brightness in the gradient echo images, which is due to the slightly off center placement of the 25 cm proton coil with the center of the gate-able phantom. Gradient echo imaging, especially with a flip angle of less than 90° (60° was used) was found to work best for imaging an axial slice with a simple surface coil.

Phosphorus imaging can only been done with a phosphorus sample of extremely high concentration, such as with the GE 14.7 M phosphorus phantom. The phosphorus concentrations in the human body, or in the depth or gate-able phantoms, are not high enough to produce an image within the standard phase and frequency steps designed for proton imaging. The result of imaging a phosphorus sample with normal tissue amounts of phosphorus in the millimolar range was simply an image of noise. The only phosphorus imaging that is presented in this write-up is of the GE 14.7 M phosphorus phantom. The GE 14.7 M phantom images were used to compare the depth penetration abilities of each of the phosphorus coils.

Spectroscopy

GE offers a number of spectroscopy pulse sequences of different characteristics and qualities. Due to characteristic differences of metabolites at different frequency ranges, there are pulse sequences that are more appropriate for either H-1 or P-31. In addition, some pulse sequences are designed to acquire spectra unlocalized, while others can slice, column or voxel localize. There is no direct purpose for using unlocalized H-1 or P-31 spectroscopy acquisitions, assuming T_1 corrections will be based on spectra localized to the cardiac muscle. The discussion will be limited to localized spectroscopy sequences that

would be of use in a cardiac MRS protocol. Using phantom studies the GE pulse sequences will be described and evaluated for the later purposes of H-1 localized acquisition for shimming and P-31 localized acquisition for evaluation of cardiac disease. Quality of the phosphorus spectra from the phantom studies will be determined based on acquisition time, SNR, and degree of localization (i.e. increased signal from the VOI and reduction of signal outside the VOI).

Note that most figures of complex P-31 spectral data in the figures of this dissertation are graphed as real, phased data, as noted by "REAL" as labeled by GE's SAGE IDL™ spectral post-processing software.

Localized Proton Spectroscopy

Although the magnet's homogeneity is optimized upon installation, any individual person or object that goes in the magnet will distort the main magnetic field to some degree. SNR and the resolution of peaks with frequencies that are close together depend partially on good field homogeneity. Homogeneity can be increased in a region of interest with a technique called shimming. Shimming involves obtaining an unsuppressed H-1 MRS signal from the region of interest and adjusting the gradients to optimize the H-1 MRS signal. The H-1 MRS signal is used because the water peak provides high SNR and optimizing the magnetic field for the water protons will also improve the signal for the P-31 metabolites. Since the linewidth of a resonance peak is inversely proportional to T_2^* , the homogeneity can be optimized by either minimizing the full width at half maximum (FWHM) of the water

peak or maximizing the extension of the T₂* dependent free induction decay (FID) of the H-1 MRS signal.

The two spectroscopy pulse sequences on the GE system most appropriate for voxel localized H-1 spectroscopy are STEAMCSI and PRESSCSI, based on the standard STEAM and PRESS techniques in the literature. GE's STEAMCSI pulse sequence incorporates three slice-selective 90° RF pulses and a set of crusher gradients, as shown in Figure 20. GE's PRESSCSI voxel localized pulse sequence is obtained through three slice-selective RF pulses and utilizes a spin-echo with 90°, 180° and 180° pulses and two sets of crusher gradients, as shown in Figure 21. The PRESSCSI pulse sequence was preferred because of its general ability to provide twice the SNR of the STEAM sequence, as explained previously in the literature review. The FWHM values of the water peak from the phantom studies with PRESSCSI and STEAMCSI were 5.78 Hz (0.045 ppm) and 14.09 Hz (0.110 ppm), respectively.

Localized Phosphorus Spectroscopy

Using the best possible scenario for obtaining a phosphorus spectrum, namely using a phantom, it is easy to definitively compare the quality of the results of each of the available GE pulse sequences, and some modified GE pulse sequences. The use of a phantom is ideal because it allows for a standardized cross-comparison of pulse sequence acquisition results with a non-moving, non-changing phantom. Each of the available GE pulse sequences, PRESSCSI, STEAMCSI, ECHOSCI, SPINECHO, ISISCSI, and FIDCSI are compared in increasing order of quality of localized results within a reasonable amount of time (usually less than ten minutes per acquisition). Such an increase in

quality of MDPA localization can be seen through the progression of quality of all GE spectroscopy pulse sequences via progressively smaller localization volumes, as seen in Figure 22 through Figure 32, and Figure 34 through Figure 38. Also presented are some modifications of the most viable phosphorus localized pulse sequences, ISISCSI and FIDCSI, which produce even better results.

Phosphorus STEAMCSI and PRESSCSI

GE's STEAMCSI and PRESSCSI pulse sequences, as explained previously, allow for the acquisition of a single voxel with each TR acquisition. In addition, both of GE sequences can be used along with CSI phase encoding gradients to further divide the field of view into multivoxels. As expected from the literature on PRESS and STEAM, PRESSCSI doesn't work as well as STEAMCSI, although neither was ideal for obtaining localized phosphorus spectra, as shown in Figure 22 and Figure 23, respectively. Note that the STEAM sequence was acquired in a fourth of the time of the PRESS sequence, but is better able to display the P-31 peaks.

Phosphorus ECHOCSI

ECHOCSI is GE's modification of the standard spin echo 90-180° pulse sequence combined with 2-D CSI, as shown in Figure 24.³¹ GE's version of ECHOCSI for localized spectroscopy employs a slice selection and CSI option. The use of a surface coil with this pulse sequence combines an inhomogeneous B_1 field with a pulse sequence requiring somewhat accurate 90° and 180° pulses. In addition, the reliance on CSI for voxel localization leads to intervoxel signal bleed. The result of

a P-31 ECHOCSI CSI voxel localized acquisition is shown in Figure 25 and demonstrates low SNR and inadequate localization to the MDPA inner compartment of the phantom.

In addition, reliance on CSI is done at an additional cost of increased scan time. A specific example of acquisition times, for various field of views and voxel sizes is shown in Figure 26 for a sample data set of 128 acquisitions and TR of 2 seconds with the ECHOCSI pulse sequence. These parameters were chosen based on the same parameters being used to obtain a localized P-31 spectrum successfully with GE's FIDCSI pulse sequence, as described later in this chapter. Notice when the voxel sizes are decreased to reasonable values for localizing to the cardiac muscle ($2 \times 2 \times 2 \text{ cm}^3$ or less) the scan time increases substantially from 18 to over 60 minutes, depending on the field of view (FOV). The FOV is centered with the magnet bore so the region of interest must be within the FOV to obtain spectral data. Considering this protocol will be used for cardiac spectroscopy acquisitions, the heart is not centered but to the left of the center 5 to 10 cm (depending on the person). In addition, this figure does not take into account the increased number of acquisitions that would be needed to keep the SNR constant as the voxel size decreases, thus further increasing the scan time.

Phosphorus SPINECHO

GE has available a second spectroscopy pulse sequence based on the spin echo idea. Like, ECHOCSI, GE's SPINECHO is based on the 90-180° spin-echo pulse sequence, except that the pulse and the parameters associated with the sequence have been optimized with the RF pulse

reformed, as shown in Figure 27. The oddly shaped amplitude (Rho1) and phase (Theta) modulated RF pulses are the result of a back calculation of the RF pulse based on an input of the echo time and slice profile²¹. The pulse is a composite of the initial 90° pulse and the refocusing 180° pulse. These pulses are combined together because if these two pulses are optimized separately, the resulting echo time is limited by the length of each individual pulse. The SPINECHO pulse available on the GE system has been calculated for a specific set of parameters and is not available for the user to change. The excitation pulse has an effective flip angle of 60° and an echo time of 2.5 msec. The radio-frequency pulse is optimized for the acquisition of phosphorus spectra from $3.0 \times 3.0 \times 3.0 \text{ cm}^3$ CSI volumes. The reported benefit of the optimization was the elimination of the need for baseline correction during post-processing. A test of this sequence on 3.0 T is shown for a CSI experiment in Figure 28. The limitations of a $3 \times 3 \times 3 \text{ cm}^3$ voxel areas positioned with CSI would make it difficult to localize to the anterior myocardium, where a rectangle would be more appropriate. It is also not clear that this pulse sequence was optimized for use at 3.0 T.

Phosphorus ISISCSI

The ISISCSI pulse sequence, GE's version of ISIS, is the most appropriate voxel localization pulse sequence for phosphorus as provided by GE for the 3.0 Tesla scanner, as shown in Figure 29. On the GE system, ISISCSI uses an adiabatic RF pulse that allows for uniform excitation of signals over a larger volume of the sample.²⁴

The ISISCSI sequence allows for various options in acquisition areas such as volume, slice, column, and voxel acquisition. As the acquisition volume size decreases, the ISISCSI sequence is successful in eliminating more and more of the outer phantom volume (NaH_2PO_4). This causes the NaH_2PO_4 signal to decrease with increasingly smaller localized volumes, such as the slice and column and shown in Figure 30 and Figure 31. One step smaller than the column is the voxel. The voxel acquisition is the most desirable localization technique for cardiac spectroscopy, because of the need to avoid contaminating the cardiac muscle signal with signals from skeletal muscle and blood.

ISISCSI, however, is plagued by poor localization due to short TR times between acquisitions of the next of eight separate volumes, not allowing for complete relaxation to occur between volume acquisitions. If the localization was ideal, the spectrum shown in Figure 32 would show just the peak on the left, MDPA, with no added signal from the outer volume signal of NaH_2PO_4 .

A modified ISISCSI sequence can be developed to overcome the relaxation error problems of the original GE pulse sequence. The original GE pulse sequence gathers each of the eight volumes (for a voxel acquisition) that will be added and subtracted from each other in sequence, with the same TR between each. The acquisition proceeds in the manner that all eight parts are acquired, and then the process is repeated until the number of acquisitions (a number divisible by eight) has been acquired. Without rewriting the ISISCSI pulse sequence, a modification that improves the ISISCSI localization results has been made. By acquiring an average of each of the eight volumes separately, with a delay time of at least 15 seconds between acquisition of each

volume, a much improved voxel acquisition can be acquired with very little compromise in overall acquisition time. This idea is explained visually in Figure 33 for an acquisition example of 32 NEX. When all eight volumes were acquired separately with a short TR time during each acquisition, but a longer TR between acquisitions, the localization results were significantly improved, as shown in Figure 34.

Phosphorus FIDCSI

GE's FIDCSI spectroscopy pulse sequence is the most basic of the spectroscopy sequences involving a single RF pulse, as shown in Figure 35.³³ In addition, CSI is an option to gather multivoxel acquisitions. The FIDCSI pulse sequence provides a good signal and slice localization. Slice localization without phase encoding can be done at a minimum thickness of 25 mm (also called depth resolved surface coil spectroscopy or DRESS). FIDCSI can do multi-voxel acquisition via phase encoded CSI. Slice localized spectroscopy that is acquired in the manner of FIDCSI is often referred to by the general term of DRESS (depth resolved surface coil spectroscopy), regardless of the machine or pulse sequence designer. This technique is often used for cardiac spectroscopy because it is a simple sequence with one spectrum output per acquisition. As long as the slice is sufficiently deep, the surface coil sufficiently narrow, and the slice properly positioned, there is only a small risk of skeletal muscle contamination. In addition, the transmitter gain (TG) must be optimized to ensure maximum signal from the slice. The proper TG values have been pre-measured using the depth phantom, as shown in Figure 36 at 1.5 Tesla and Figure 37 at 3.0 T. These measurement can then be used as a first estimate in

optimizing the signal from human FIDCSI slice localized studies at the same distance from the coil.

The DRESS slice localized spectrum of a phantom as obtained using the standard GE FIDCSI pulse sequence is shown in Figure 38. Unfortunately, the pulse sequence suffers from a significant delay time before the free induction decay is recorded. Some delay, 1 to 4 msec, is essential to prevent eddy current signals from contaminating the signal of interest. Long delays, as 20 msec for human FIDCSI oblique slice acquisitions at 3.0 T, are less desirable because they cut off too much signal from the ATP part of the phosphorus spectrum, which has the shortest T_1 relaxation time. Fortunately, there are post-processing programs, such as FITMASTER™ (Philips) which can estimate the missing part of the FID and provide excellent results.

All parameter options were evaluated for oblique and coronal FIDCSI slice selections. The oblique slice uses more than one gradient set to specify the slice and therefore can have more conservative parameter limits. Available parameter options with the FIDCSI slice selection protocol include changing a parameter called SQUEEZE, which reduces or increases the overall time taken for the RF pulse. If the time is reduced, as it is for SQUEEZE = 2, the delay time until the start of the FID is also reduced. A delay in the FID creates an increase in the frequency dependent phase shift (first order phase correction). A 180° phase shift will be created for each dwell period.²³ The delay time issue is even greater with the oblique slice as the system must be "tricked" by changing the variable pw_gph to 4 msec to even do an oblique slice localization. This is due to oblique slice using multiple gradients and having the GE software at the most

conservative level for error messages. The pw_gph variable actually increases the delay time to 20 msec when used at 3.0 Tesla with a spectral width of 4000, and with the SQUEEZE parameter set to 1.

After careful evaluation of the FIDCSI pulse sequence and after speaking with both Napapon Sailasuta and Ralph Hurd, both of GE, a rewriting of the FIDCSI pulse sequence was necessary to fix this delay problem. The FIDCSI pulse sequence program file was modified (by Dr. Hee-Won Kim using GE's EPIC) to decrease the delay time for an oblique slice and renamed FIDOBL on the GE console. This modification basically allows for a larger gradient strength, still within the system and safety limits, so that the RF and gradient pulses are as tall as possible, with the area and thus power remaining the same. A taller pulse takes less time, therefore, the delay time before acquisition was reduced. In addition, the need to change the pw_gph control variable is eliminated.

The FIDCSI pulse sequence can be utilized in one other way. The sequence can be set up to obtain a localized slice, which is segmented into multiple voxels. The limitations of this procedure come from inflexible placement of the multivoxels, timing necessary to acquire CSI phase encoding steps, and unwanted spectral bleed due to point-spread function inherent with CSI and the Fourier transform. As shown in Figure 39, the multivoxel FIDCSI with CSI option allows for a set of voxels to be placed within a set field of view. The field of view is centered on the image and the voxel placement within the field of view is dependent on how many times in the x and y direction the field of view is broken up by phase encoding gradient steps. It should also be noted that the standard GE FIDCSI pulse sequence on the 3.0 Tesla does

not allow for less than a 36 cm FOV if you let the console continue to think it is operating at the proton frequency while the acquisition is at a phosphorus frequency. This was the initial setup recommended by GE. In this case it is also necessary to change control variables "asfov" to 48 and "GAM" to 1723.5 to ensure the correct localization dimensions. It was found that with a few tricks with the control variables, a minimum FOV of 14 cm can be achieved. This is accomplished by setting the console to run at the P-31 frequency and then changing the following control variables to prevent system errors: "pibbandfilt" equals 0 and "pixmthband" equals 1. These control variables correct for the absence of a separate RF amplifier for P-31. The 3.0 Tesla system uses one amplifier for all frequencies, unlike the default of separate amplifiers expected by the software.

Finally, with some pulse programming corrections, as has been done with the modified FIDCSI protocol locally called FIDFOVH, FOVs below 14 cm can be achieved. Dr. Hee-Won Kim performed the modification of the FIDCSI pulse sequence program with EPIC pulse programming. The modification basically removed the protection limits for the gradient amplifiers. The FIDFOVH, modified FIDCSI pulse sequence, should only be used without the autoprescan, as parts of the autoprescan (where transmitter gain and receiver amplifiers are maximized) will exceed the limits of the gradients and do so without warning. Autoprescan is generally useless for phosphorus spectroscopy, therefore it would be a mistake to use autoprescan with phosphorus. This allows the FIDFOVH modified sequence to be used safely.

1.5 Tesla to 3.0 Tesla Phosphorus Spectroscopy Comparisons

One of the main arguments for using 3.0 T over using a 1.5 T magnet is the significant improvement in the amount of signal that is obtained with an increase in field strength. To prove this point, proton and phosphorus spectra of the depth phantom were taken at 1.5 T and 3.0 T with similar parameters and compared. In addition, the same parameter was again compared at 3.0 T to compare the single-turn and quadrature RF coils.

The first comparison was of an FIDCSI acquisition with CSI voxel localization of the depth phantom, as shown in Figure 40. In each case the parameters were set as follows: 256 acquisitions, 25 mm thick slice, $8 \times 8 \times 1$ CSI, 16 cm field of view, $2 \times 2 \times 2.5 \text{ cm}^3$ voxels, scan times = 4:26, and 10Hz line-broadening. In each case the phantom was positioned so that one of the voxels would select just the inner compartment of the depth phantom, at a depth of 5.5 cm. Experimentally, the resulting SNR of the MDPA peak of the P-31 spectrum for the single turn RF coil at 1.5 T was 7.4 while at 3.0 T it was 21.65, and the SNR of the quadrature RF coil at 3.0 T was 26.1. This shows a significant improvement in signal from 1.5 T to 3.0 T, but only a moderate improvement of the quadrature over the single turn coil. The MDPA T₁ relaxation rate was also measured at 1.5 T and 3.0 T and found to be 5.52 and 6.04 seconds, respectively (Appendix G). These relaxation rates are negligibly different from each other and do not significantly alter the MDPA SNR at each field strength.

The second comparison was of the modified ISISCSI acquisition of a voxel positioned over the center compartment (5.5 cm depth) of the depth phantom, as shown in Figure 41. The parameters used for the

ISISCSI acquisitions were as follows: 256 acquisitions, 16 cm field of view, $2 \times 2 \times 2 \text{ cm}^3$ voxel, scan times = 2:13 for each of 8 acquisition, and 10Hz line-broadening. Experimentally, the resulting SNR of the MDPA peak of the P-31 spectrum for the single turn RF coil at 1.5 T was 6.2 while at 3.0 it was 10.1, and the SNR of the quadrature RF coil at 3.0 T was 14.5. This shows a moderate improvement in signal from 1.5 T to 3.0 T and another moderate improvement in the results of the quadrature over the single turn coil.

To verify the extent to which the slice profile of the oblique, FIDCSI modified slice selection is accurate, a series of tests on the 1.5 and 3.0 Tesla were conducted using the slice profile phantom. Slices of 25 mm thick, tilted at an angle though the vial, were obtained across the vial, as shown in Figure 8. The results of the signal profile over the slice are shown in Figure 42 for the 1.5 Tesla with the single turn P-31 coil and Figure 43 and Figure 44 for the 3.0 Tesla for the single turn and quadrature P-31 coils, respectively. The slice profile tails (where none of the H₂PO₄ phantom was in the slice) widened slightly more at 3.0 T, most likely due to the same gradient pulse from the same pulse sequence on both systems despite different magnet field strengths. This is shown via slightly larger area of signal when no part of the phantom was in the slice (representing potential contamination by skeletal muscle or blood) at 3.0 T, as shown in Figure 43 and Figure 44, and compared to 1.5 Tesla as shown in Figure 42.

The volume where the slice selection was below the phantom represents the potential contamination from skeletal muscle. This is due to the fact that the phantom, in that case being above the selected

slice represents the skeletal muscle which would be above the selected cardiac slice. In the same way, the volume where the slice selection was above the phantom represents potential contamination from blood, typically concentrated below the cardiac muscle slice selection. At 1.5 T, at the first point where the prescribed acquisition slice does not contain the phantom, there is -9% potential contamination by skeletal muscle and blood. This increases slightly at 3.0 T, where for the single turn coil, the contamination at the first point where the prescribed acquisition slice does not contain the phantom is 19% and 12%, for skeletal muscle and blood. For the quadrature coil at 3.0 T, the numbers are similar with 17% and 12% potential skeletal muscle and blood contamination, at the point just beyond the slice prescription. The 1.5 and 3.0 T percent contamination numbers for the quadrature and single turn coils are not significantly different. Considering the distance away from the prescribed slice, the amount of potential contamination drops off quickly with near 0% contamination within approximately 8 mm at 1.5 Tesla and 10 mm at 3.0 T. In summary, the oblique DRESS pulse sequence slice profile has some signal contamination at both 1.5 T and 3.0 T but it is not significantly different on each system.

Phantom Results

In summary of the phantom results, proton imaging was performed at 3.0 T, whereas both proton and phosphorus spectroscopy techniques were tried at 1.5 and 3.0 T. Proton phantom images were obtained with spinecho, fast spinecho, gradient echo and fast gradient echo pulse sequence techniques, with fast gradient echo being the best option for

3.0 T imaging with a surface coil. In the next chapter, further evaluation of imaging will be done based on the clinical image quality of the human heart.

In terms of voxel localized proton spectroscopy, PRESSCSI without water suppression offers the best water signal for evaluation of the shim quality.

The evaluation of phosphorus spectroscopy included all available spectroscopy pulse sequences and some modifications of these sequences to improve their quality. For voxel localized phosphorus spectroscopy a number of pulse sequences were evaluated. The worst voxel localized phosphorus spectra resulted from the PRESSCSI and STEAMCSI pulse sequences. The ECHOCSI provided only slight improvement in signal to noise ratio (SNR), over the STEAM and PRESS sequences. The SPINECHO sequence, similar to the FIDCSI but promising no phase post-processing, was an optimized sequence for 1.5 Tesla but did not provide the expected phase attributes at 3.0 T. The ISISCSI voxel localization, run as a single sequence with a reasonable repetition time (under 15 seconds), suffered from volume localization inaccuracies due to relaxation effects. This problem could, in part, be fixed by acquiring eight separate acquisitions, with a 15-second or more delay time between acquisitions, and post-processed to create a significantly improved voxel localization result. Unfortunately, for patients, this would be difficult to acquire, therefore a modified ISIS sequence should be implemented. The modified ISIS sequence could automate what the eight separate acquisitions plus delay time between acquisition accomplished but without the need to do many multiple button presses. Finally, FIDCSI plus CSI for multivoxel acquisition, allows for

localization that is even better than the best ISIS voxel localization in terms of quality of localization and overall signal to noise. Unfortunately, for the current GE software some flexibility limits exist in terms of scan areas, voxel position and scan timing, in addition to extended post-processing. This may make CSI more difficult to use clinically.

In comparing 1.5 and 3.0 T performance it was clear from CSI localized FIDCSI and modified ISISCSCI that the 3.0 T provided substantially more signal than the 1.5 T, and the quadrature coil improved the signal of the localized voxels slightly more. Unfortunately, the human body is multi-compartmental, so evaluations done on phantoms must be extended to humans for a true test of the optimal pulse sequence and coil combination for human cardiac use. The two most viable GE pulse sequences for phosphorus spectroscopy use on the GE 3.0 T magnet are ISISCSCI and FIDCSI.

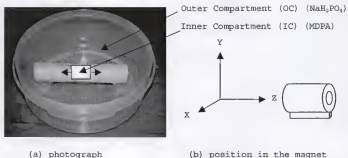


Figure 4. Gate-able-Phantom (a) photograph and (b) position in magnet, without the liquids and with movement direction demonstrated (Lid not shown).

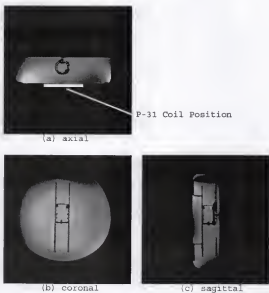


Figure 5. Gate-able-Phantom images, (a) axial, (b) coronal and (c) sagittal views, as imaged with 25cm square proton coil.

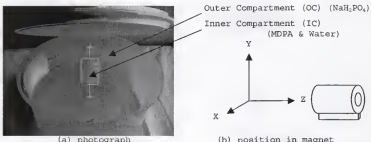


Figure 6. The Depth-Changing-Phantom (a) photograph with top open and (b) position in magnet, with movement direction demonstrated (Note: The phantom was created by Dr. Heewon Kim).

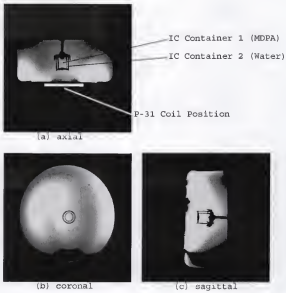


Figure 7. Depth-Changing-Phantom images, (a) axial, (b) coronal and (c) sagittal views, as imaged with 25cm square proton coil.

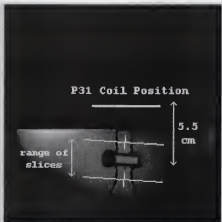


Figure 8. Axial slice image of Slice Profile Phantom and details on how oblique DRESS slices were placed within phantom to estimate the amount of potential contamination from outside the localized slice.



Figure 9. Photographs of GE's 14.7 M P-31 Phantom from (a) front, (b) back and relative position in magnet.

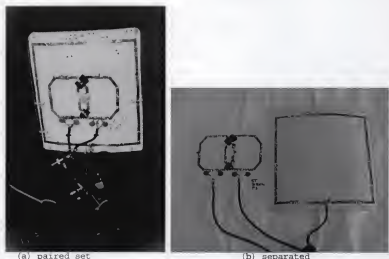


Figure 10. Photographs of quadrature phosphorus and square proton coil as (a) a paired set and (b) separated onto individual platforms for 3.0 Tesla.

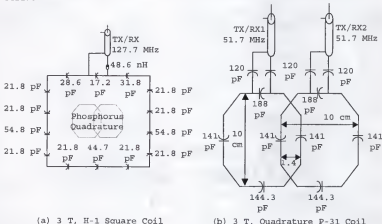


Figure 11. Schematic diagrams of (a) the $25 \times 25 \text{ cm}^2$ square proton coil set (tuned to 127.75 MHz) used with (b) the 10 cm phosphorus quadrature coil at 3.0 T (tuned to 51.71 MHz) (numerical parameters obtained from David Peterson and Bryan Wolverton, Coil Lab).

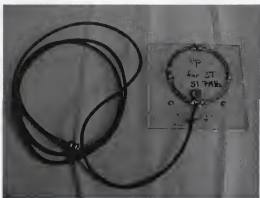


Figure 12. Photograph of the single turn, 9.5 cm diameter, phosphorus transceive coil tuned to 51.71 MHz (3.0 Tesla).

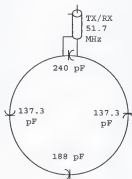


Figure 13. Schematic diagram of the single-turn phosphorus transceive 9.5 cm diameter coil at 3.0 T tuned to 51.71 MHz (numerical parameters obtained from David Peterson and Bryan Wolverton, Coil Lab).

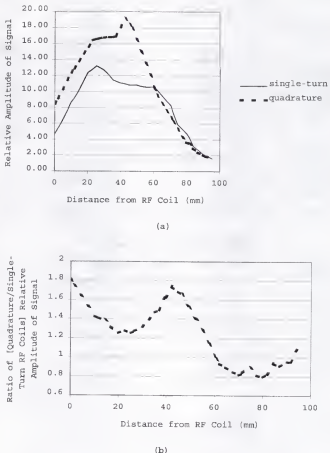


Figure 14. Comparisons of single-turn versus quadrature P-31 RF coils in terms of relative signal based on 25 mm thick DRESS acquisitions of 14.7 M phantom at 0.5 cm intervals with TG optimized at each position. (a) Relative amplitude of signal from single-turn and quadrature coils, with noise level at 0.02. (b) Ratio of signal from quadrature over single-turn coils showing optimal SNR from the quadrature coil.



Figure 15. Photograph of the single turn, 9.5 cm diameter, phosphorus transceive coil tuned to 25.87 MHz (1.5 Tesla) with three small vials that are used to locate the coil in the proton images.

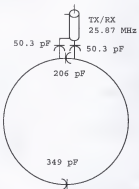


Figure 16. Schematic diagram of the single-turn phosphorus transceive 10 cm diameter coil at 1.5 T tuned to 25.87 MHz (numerical parameters obtained from David Peterson and Bryan Wolverton, Coil Lab).



Figure 17. Photograph of 1.5 T quadrature P-31 coil.

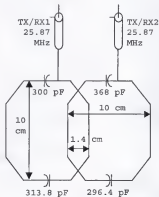


Figure 18. Schematic diagram of the quadrature phosphorus transceive 10 cm diameter coil at 1.5 T tuned to 25.87 MHz (numerical parameters obtained from David Peterson and Bryan Wolverton, Coil Lab).

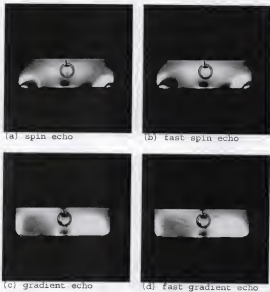


Figure 19. Axial images of gate-able phantom comparing images obtained on 3.0 T using a 25 cm square proton surface coil with the image pulse-sequences of (a) spin echo, (b) fast spin echo, (c) gradient echo and (d) fast gradient echo imaging. Asymmetry of image due to non-centered placement of phantom on 25 cm square proton surface coil.

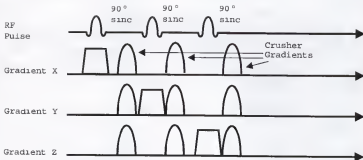


Figure 20. The STEAMCSI pulse sequence, GE's version of STEAM for spectroscopy voxel localization.

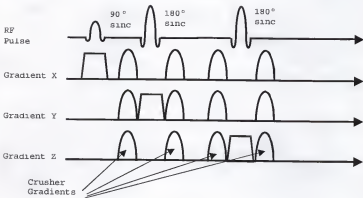


Figure 21. The PRESSCSI pulse sequence, GE's version of PRESS for spectroscopy voxel localization.

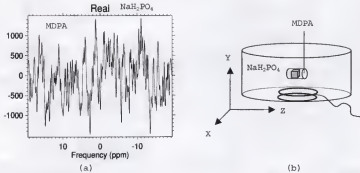


Figure 22. Frequency domain of (a) PRESSCSI voxel localized phosphorus spectroscopy with (b) diagram demonstrating localization. (Parameters: 128 acquisitions, 2000 Hz spectral width, 2 sec TR, $2 \times 2 \times 2 \text{ cm}^3$ voxel, scan time of 4:24, 3 T, quadrature RF coil and 10Hz line-broadening; see Appendix B for more detail).

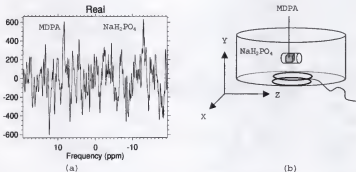


Figure 23. Frequency domain of (a) STEAMCSI voxel localized phosphorus spectroscopy with (b) diagram demonstrating localization. (Parameters: 32 acquisitions, 2000 Hz spectral width, 2 sec TR, $2 \times 2 \times 2 \text{ cm}^3$ voxel, scan time of 1:14, 3 T, quadrature RF coil and 10Hz line-broadening; see Appendix B for more detail).

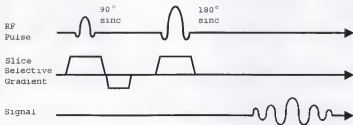


Figure 24. The ECHOCSI pulse sequence, one of GE's versions of Spin Echo for spectroscopy acquisition.

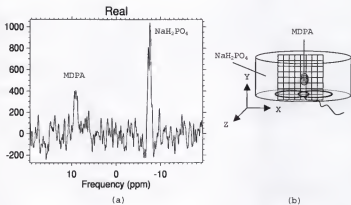


Figure 25. Frequency domain of (a) ECHOCSI voxel localized phosphorus spectroscopy with (b) diagram demonstrating localization. (Parameters: 256 acquisitions, 2000 Hz spectral width, 2 sec TR, $4.5 \times 4.5 \times 2 \text{ cm}^3$ voxel, scan time of 8:44, 3 T, quadrature RF coil and 30Hz line-broadening; see Appendix B for more detail).

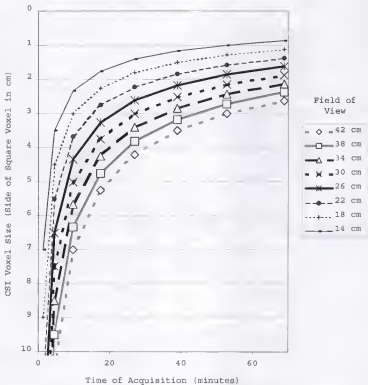


Figure 26. Chemical shift imaging (CSI) voxel sizes versus time of slice plus 2D CSI acquisition on GE Sigma Advantage™ (*TR = 2 seconds, 128 acquisitions, and 8 NEX). The figure demonstrates the long times necessary to obtain smaller voxel sizes with CSI.

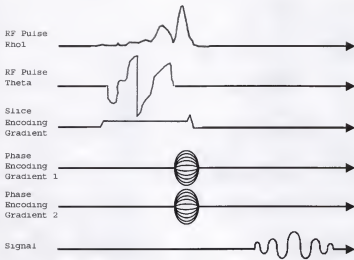


Figure 27. The SPINECHO pulse sequence, one of GE's versions of Spin Echo for spectroscopy acquisition.

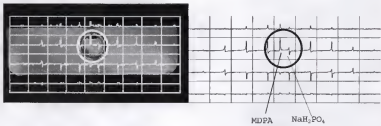


Figure 28. Frequency domain of SPINECHO CSI multivoxel localized phosphorus spectroscopy. (Parameters: 512 acquisitions, 2000 Hz spectral width, 2 sec TR, $3 \times 3 \times 3 \text{ cm}^3$ voxel, scan time of 32:40, 3 T, quadrature RF coil and 30Hz line-broadening; see Appendix B for more detail).

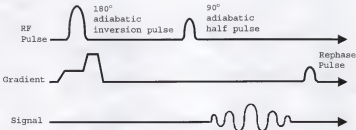


Figure 29. The ISISCSI pulse sequence (as shown for one gradient), GE's versions of ISIS for volume, slice, column or voxel localization.

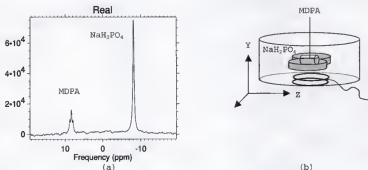


Figure 30. Frequency domain of (a) ISISCSI slice localized phosphorus spectroscopy with (b) diagram demonstrating localization. (Parameters: 256 acquisitions, 2000 Hz spectral width, 2 sec TR, 2 cm thick slice, scan time of 8:44, 3 T, quadrature RF coil and 10Hz line-broadening; see Appendix B for more detail).

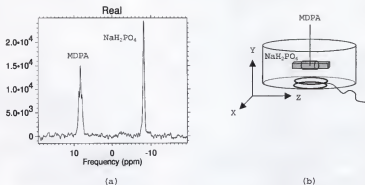


Figure 31. Frequency domain of (a) ISISCSI column localized phosphorus spectroscopy with (b) diagram demonstrating localization. (Parameters: 256 acquisitions, 2000 Hz spectral width, 2 sec TR, $2 \times 2 \text{ cm}^2$ column, scan time of 8:44, 3 T, quadrature RF coil and 10Hz line-broadening; see Appendix B for more detail).

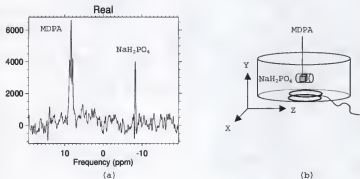
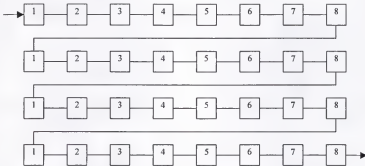
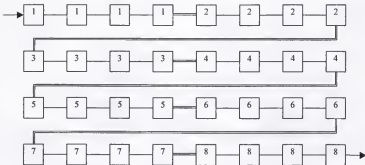


Figure 32. Frequency domain of (a) ISISCSI voxel localized phosphorus spectroscopy with (b) diagram demonstrating localization. (Parameters: 256 acquisitions, 2000 Hz spectral width, 2 sec TR, $2 \times 2 \times 2 \text{ cm}^3$ voxel, scan time of 8:52, 3 T, quadrature RF coil and 10Hz line-broadening; see Appendix B for more detail).



(a) Total Acquisition Time = $32 \times$ Short TR (or $32 \times$ Long TR)
Result: Poorly Localized Voxel Acquisition with Short TR
(Good Localization but Long Acquisition Time with Long TR)



(b) Total Acquisition Time = $(32 \times$ Short TR) + $(7 \times$ Long TR)
Result: Well Localized Voxel Acquisition



= ISIS volume acquisition 1 to 8

— = short TR

===== = long TR

Figure 33. Visual display example of the acquisition where the total number of acquisitions is 32 performed by (a) the current GE ISISCSI technique, and (b) the modified ISIS technique.

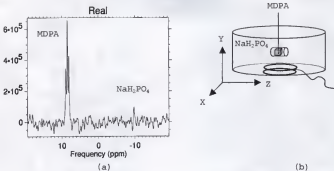


Figure 34. Frequency domain of (a) modified ISISCSI localized voxel sequence for phosphorus (created from eight separate acquisitions, added and subtracted appropriately during post-processing) with (b) diagram demonstrating localization. (Parameters: 64 acquisitions, 2000 Hz spectral width, 2 sec TR, $2 \times 2 \times 2 \text{ cm}^3$ voxel, scan time of 2:13 for each of 8 acquisitions, and 10Hz line-broadening; see Appendix B for more detail).

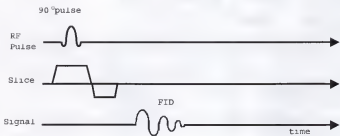
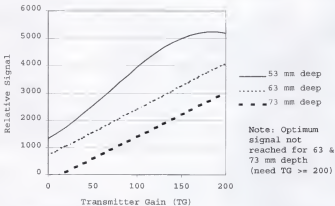
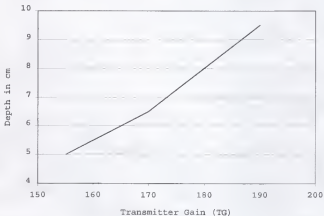


Figure 35. The FIDCSI pulse sequence without phase encoding gradients turned on, GE's versions of the simple single RF pulse necessary to produce an FID for a spectroscopy acquisition.

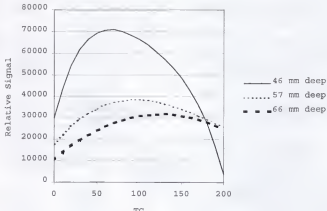


(a) quadrature coil at 1.5 T

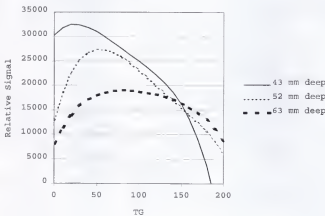


(b) single turn coil at 1.5 T

Figure 36. Charts comparing (a) relative signal obtained by varying transmitter gain (TG) values at various depths for slice localized FIDCSI at 1.5 Tesla, using the quadrature coil and (b) relative optimized TG value versus depth for the single turn coil (measurements done by Dr. Hee-Won Kim). These phantom values can be used to estimate proper TG values at depth in human studies.



(a) Quadrature Coil at 3.0 T



(b) Single turn coil at 3.0 T

Figure 37. Charts comparing relative signal obtained by varying transmitter gain (TG) values at various depths for slice localized FIDCSI at 3.0 Tesla, using (a) the quadrature coil, or (b) the single turn coil. These phantom values can be used to estimate proper TG values at depth in human studies.

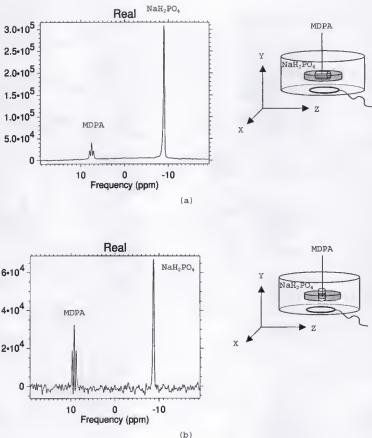


Figure 38. Frequency domain of FIDCSI slice localized phosphorus spectroscopy of (a) gate-able phantom and (b) depth phantom. (Parameters: 128 acquisitions, 2000 Hz spectral width, 2 sec TR, 2.5 cm thick slice, scan time of 4:26, 3 T, single-turn RF coil and 10Hz line-broadening; see Appendix B for more detail).

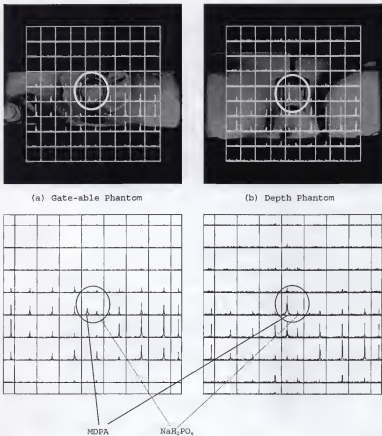


Figure 39. Multivoxel phosphorus FIDCSI plus CSI of the (a) gate-able phantom (b) depth phantom. (Parameters: 256 acquisitions, 2000 Hz spectral width, 2 sec TR, $2 \times 2 \times 2.5 \text{ cm}^3$ voxels, scan time of 4:59, and 10Hz line-broadening; see Appendix B for more detail).

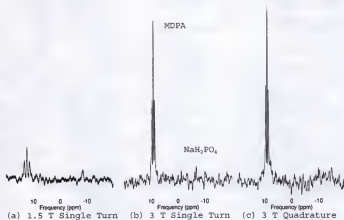


Figure 40. Comparison of 1.5 to 3.0 Tesla results of phosphorus FIDCSI plus CSI localized voxel scaled by noise level. (Parameters: 256 acquisitions, 1000 & 2000 Hz spectral width at 1.5 & 3 T, 2 sec TR, 2 \times 2 \times 2.5 cm³ voxels, scan time of 4:59, and 10Hz line-broadening; see Appendix B for more detail).

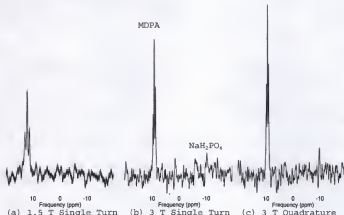


Figure 41. Comparison of 1.5 to 3.0 Tesla results of phosphorus, modified ISISCSI localized voxel (created from eight separate acquisitions, added and subtracted appropriately during post-processing). (Parameters: 256 acquisitions, 1000 & 2000 Hz spectral width at 1.5 & 3 T, 2 sec TR, 2 \times 2 \times 2 cm³ voxels, scan time of 2:13 each of 8, and 10Hz line-broadening; see Appendix B for more detail).

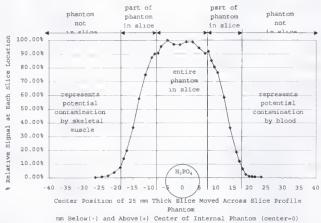


Figure 42. 1.5 T, P-31 single turn RF coil signal from a set of 25 mm thick, oblique DRESS slices (FIDCSI oblique slice) moved across the internal phosphoric acid vial in the Slice Profile Phantom. The data obtained when the entire slice was outside the H_3PO_4 phantom represents the amount of potential contamination from above or below the slice.

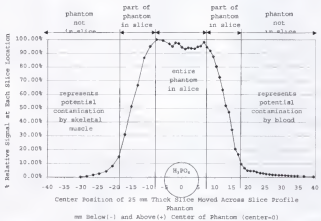


Figure 43. 3.0 T, P-31 single turn RF coil signal from a set of 25 mm thick, oblique DRESS slices (FIDCSI oblique slice) moved across the internal phosphoric acid vial in the Slice Profile Phantom. The data obtained when the entire slice was outside the H_3PO_4 phantom represents the amount of potential contamination from above or below the slice.

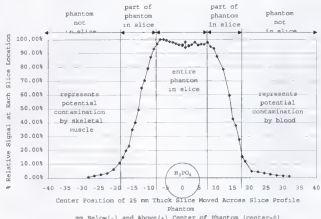


Figure 44. 3.0 T, P-31 quadrature RF coil signal from a set of 25 mm thick, oblique DRESS slices (FIDCSI oblique slice) moved across the internal phosphoric acid vial in the Slice Profile Phantom. The data obtained when the entire slice was outside the H₃PO₄ phantom represents the amount of potential contamination from above or below the slice.

CHAPTER 4
HUMAN CARDIAC P-31 SPECTROSCOPY ACQUISITION TECHNIQUES

Even after conducting phantom measurements to optimize the techniques for the human studies, further work must be done to maximize the quality of the human acquisitions and results. This chapter summarizes the tests and qualifications of the methods for looking non-invasively at the human heart with MR imaging and spectroscopy. First, the imaging is optimized for viewing the heart, via patient position, pulse sequences, and RF coils. Second, the spectroscopy acquisition techniques are optimized for the more complex human proton and phosphorus spectra, again based on patient position, pulse-sequences and coils. The optimization for each also includes looking at the best methods for gating the images and spectroscopy acquisitions from the heart. Next, the comfortable positioning of the participants was enhanced through ergonomic placement during the long study. A magnet-safe handgrip was designed for inducing stress on the heart via a steady grip. First, volunteers were tested to evaluate the quality of the protocol. The results of the studies were post-processed to eliminate blood contamination, evaluated for skeletal muscle contamination, and corrected for relaxation due to short repetition times during data acquisition. The results of the studies were evaluated in terms of peak amplitude ratios and peak area ratios.

Imaging

Images in this study are not used for diagnostic accuracy but instead to find landmark anatomical positions for purposes of localized phosphorus spectroscopy acquisitions. A simple, fast image is all that is needed to determine the proper location of the heart so that the phosphorus phantom can be positioned properly over the anterior of the heart, near the left ventricle. Gating is also important to keep the acquisitions timed with the cardiac cycle. Images are cardiac gated but not respiratory gated. Both spin echo and gradient echo images were obtained and compared at 1.5 T (GE Signa Advantage™ at Shands at UF) and 3.0 T (GE Signa Advantage™ in VAMC tunnel). Chest imaging was performed with the transceive body coil on the 1.5 T and with the 25 cm square proton surface coil at 3.0 T.

Spin-Echo Imaging

In the GE spin-echo imaging pulse sequence, a 90° RF pulse is followed by a 180° phase reversal pulse every TE/2, with the 90° pulse repeated every TR milliseconds. The 90° pulse creates transverse magnetization which is read in the form of a spin echo TE milliseconds after the initial 90° pulse.²¹ At 1.5 T the combination of the transceive body coil and spin echo imaging technique provided very homogeneous images over an axial slice of the heart, as shown in Figure 45(a). This image was achieved with a transmitter gain (TG) of 120. At 3.0 T, the combination of the 25-cm proton surface coil and the spin echo imaging technique, required a TG value above 200, although 200 is the system limit, to penetrate to the depth of the heart. There was not

enough power, therefore, to penetrate to the depth of the heart, as shown in Figure 45(b). Breathhold imaging was not required.

Gradient-Echo Imaging

The gradient echo uses a single partial flip-selective RF pulse, which is then rephased by an inverted slice-selection gradient. As such, the 180° pulse in the spin echo sequence is replaced by actions of the gradients. The gradient echo can produce an image quicker by allowing shorter TR and TE times, but with less SNR than the spin echo sequence, due to the smaller tip angle. As shown in Figure 46 the image quality of the gradient echo with a 60° tip angle is reasonable at both 1.5 T and 3.0 T, although the breathhold is necessary to reduce motion artifacts.

Human Positioning

The total time a volunteer must remain in the GE Signa Advantage™ magnet to obtain cardiac localized phosphorus spectra, with in-magnet exercise, runs from about 1.5 to 2 hours total time. As this is much longer than the typical MRI clinical study, which runs from 20 minutes to 1 hour, it is critical that the person be positioned in the magnet as comfortably as possible, especially to ensure minimal motion during the study (due to restlessness).

Both prone and supine positions were tried in the magnet at optimal comfort levels for each. The supine position was easily accomplished with a few added amenities. The magnet table was padded with an additional layer of egg-crate foam and a pillow was added for head and neck support. A second pillow was placed under the knees to

relieve pressure from the lower back. This position has proved very comfortable based on the number of volunteers who had fallen asleep. Some even snored during the study.

The prone position was maintained via the use of a foam, portable massage-bed (the M.A.T. by A2Z Possibilities, Inc.) which elevated the shoulders and chest, positioning the head in a cradle and putting the neck at an ergonomic angle, as shown in Figure 47. This mat was designed to keep the spinal column in the proper muscular-skeletal position when face down. It includes a face cradle with a large breathing passage, a pelvic tilt in the main body support to alleviate lower back compression, and a foam roll for the ankles to lessen stress to the calves or shins. This setup was magnet safe, and the width was cut to fit into the magnet with a person. Unfortunately, this bed was not equally comfortable for all subjects: two subjects were able to stay in the magnet for the entire time, but another two subjects could not stay in the magnet for more than 20 minutes. This orientation also made it difficult to adjust the position of the surface coils (both proton and phosphorus) once the session had started, as it required that the volunteers lift themselves up while the coil was repositioned beneath them. This could also potentially be a major problem with women with large breasts, where other modifications in the massage bed would probably have to be made.

Because of the heart's position, there are advantages and disadvantages for both prone and supine positioning of the person within the magnet, as shown in Figure 48. In the prone position, face down, there is a shorter distance from the heart to the chest wall. Rotating a person to a 30° angle can move the heart even closer to the

chest wall, thereby minimizing the lung/air gap created between the heart and chest wall.¹⁴⁹ Prone positioning thus allows for placement of the heart closer to the phosphorus surface coil, thereby increasing SNR. In addition, the shim is better over a consistent region of tissue (chest skeletal muscle and cardiac muscle layered), without the air gap. The respiratory motion artifacts will also be at a minimum in the prone position. Unfortunately, the positioning of the heart so close to the skeletal muscle in the chest wall puts more stringent requirements on the localization of the P-31 spectroscopy pulse sequence to eliminate skeletal muscle from the cardiac muscle acquisition. The supine position does allow the heart to fall back away from the chest wall, creating an air gap. This air gap, in addition to the motion of the heart, makes shimming more difficult, but localization to the cardiac muscle is more easily achieved. Therefore the supine position was used for most of the cardiac trial acquisitions in this chapter and for all of the repeated tests in the results chapter.

Gating

Gating is a method of monitoring the heart's cyclic behavior and using that signal to trigger the scanner acquisition in synchrony with the heartbeat, thus allowing multiple measurements to occur at the same time point in the cardiac cycle. Two options for gating can be used on the GE Signa Advantage™ 1.5 and 3.0 T systems, peripheral gating (via finger clip) or electrocardiogram (ECG) cables. Each option has its advantages and disadvantages. Both the ECG and peripheral gating (PG) provide a periodic up and down signal that represents the cycles of the

heart's beats, as shown in Figure 49. PG is a measure of the pulse, or the mechanical action of the blood pulsing through the body. PG is obtained via a finger clip using a photopulse sensor to monitor the pulse within a person's finger. Conversely, the ECG directly measures the heart's electrical activity during the heart cycle. The signal measured by PG tends to produce a broad peak, while the ECG signal produces a narrow peak as part of the QRS complex of the signal. In addition, PG can be slightly delayed by the time it takes the pulse to travel from the heart to the finger. This delay time was shown to be negligible by comparing images gated with ECG and PG, where the same part of the cardiac cycle was frozen in time, as shown in the sagittal images of Figure 50.

In ideal circumstances where the quality of both the ECG and PG signals are perfect, the ECG pulse is optimal. The PG uses a fiber optic cable and thus its signal is not compromised by the fluctuating magnetic fields in the bore. Conversely, the ECG cables are copper cables that can induce a signal, just like a radio frequency coil, especially when any curvature exists in the ECG cable line. It is very difficult to place the cables perfectly straight, in addition to getting the optimal signal from the electrodes that are placed on the body. In reality, the resulting signal from the PG is often of higher quality than that of the ECG due to the interactions with the magnetic field. In addition, the peripheral gating takes less time to set-up. At 1.5 T, the ECG signal is lost mostly during the use of the gradients, but at 3.0 T, just the act of sliding the patient into the main magnetic field is enough to reduce the quality and SNR of the ECG signal. The system uses the cyclic signal to predict when the next

heart beat will occur, therefore the signal providing better SNR will allow for more accurate gating. Images can be further improved by performing a quick breathhold of 10 to 20 seconds, depending on heart rate, and using fast gradient echo imaging. This explains why the sagittal and axial peripheral gated images are sharp, during breathhold imaging, as shown in Figure 50.

The option of respiratory gating was not considered optimal for this study. Respiratory gating relies on adequate use of a baffle that is stretched over the chest or abdomen and produces an oscillatory signal, corresponding to the breathing cycle. Combining gating of the heart and breathing produces a very long acquisition time, in addition to problems due to typically non-regular breathing rates if both the cardiac and respiratory gating cycles are to coincide to trigger acquisition. Since imaging can be done with fast gradient echo in less than 20 seconds, breathhold imaging makes more sense. Spectroscopy acquisitions, however, are too long (6 minutes or more) to allow for breathhold. If the sequence acquisition were triggered based on the heart rate and respiratory rate coinciding, an irregular and longer TR time would result, substantially increasing the total scan time. A possible future option is to record the heart rate and respiratory motion along with the spectrum acquisition and use post-processing techniques to compensate for the signal changes caused by the cardiac gating and respiratory motion. Advanced signal processing is being developed, such as independent component analysis (ICA), which can deconvolve the components of a complex signal into separate signals that are independent of each external contribution.²²⁰

An alternative would be to eliminate gating and attempt to correct for the blood/skeletal muscle contamination that occurs even in the ungated data. This would be similar to the approach used in some nuclear medicine cardiac exams where gating is not used since the overall signal is small and would require long acquisition times.⁷ Such an approach could only be done in conjunction with multi-voxel CSI, as single voxel localization techniques such as ISIS are motion sensitive, depending on the subtraction of identical areas to suppress signal outside the voxel of interest. Even with multi-voxel CSI, the lack of gating would blur the signal into less precise volumes of interest.

Shimming with Localized Proton Spectroscopy

As explained in the last chapter, localized proton spectroscopy is necessary to perform shimming of the volume of interest before acquisition of the P-31 spectrum. From theory, it is expected that PRESS will provide twice the SNR of STEAM. On a single subject (Female, age 46), both the GE PRESSCSI and STEAMCSI were acquired from the same voxel. The PRESSCSI sequence was first used to acquire a voxel 41.0 x 59.1 x 30.0 mm³ voxel, with a majority over the anterior heart and a minority in the chest wall for added signal for shim. The PRESSCSI protocol was as follows: 1000 Hz spectral width, 1024 points, 16 acquisitions, 40 msec TE, TR peripheral gated to every other heart beat, TG 70, scan time 40 seconds and a depth of 66 mm. With no change in the shim settings or selected voxel, a second localized proton spectrum was then acquired with STEAMCSI, with all other parameter settings the same. The result of this human experiment comparing GE's PRESSCSI and STEAMCSI is shown in Figure 51. The resulting FWHM for

the water peak for the PRESSCSI and STEAMCSI spectra are 40.8 Hz (0.32 ppm) and 43.4 Hz (0.34 ppm), respectively. In addition, the SNR for the water peak is 2330 for PRESSCSI and 1100 for STEAMCSI. This data was obtained from a Gaussian fit of the peaks.

Cardiac Phosphorus Spectroscopy In-Vivo Acquisition

All 1.5 T and 3.0 T cardiac phosphorus spectroscopy results shown in this dissertation were obtained with either the P-31 single turn or quadrature RF coils. The P-31 RF coils were held in place on the anterior chest with an elastic and Velcro strap.

Localized P-31 Multivoxel CSI

Proceeding with introducing phosphorus spectra in order of increasing optimal acquisition results, the next sequence to consider is multivoxel chemical shift imaging (CSI). Multivoxel CSI is the acquisition of a slice of interest, which is then broken down into a set of voxels by additional phase encoding gradients. The finer the desired resolution, the greater the acquisition time, assuming a constant field of view (FOV). Smaller voxels within the CSI can be achieved in less time by reduction in the overall FOV. One of the main advantages of using multivoxel CSI is that spectra from several voxels can be obtained simultaneously although at the cost of increased scan time. In addition, compared to other phosphorus voxel localization techniques, CSI is able to obtain higher quality localization within each voxel although some signal bleed still does exist, especially along the same horizontal or vertical direction of voxels away from the voxel of interest. Additional problems with CSI include long

acquisition times to achieve the desired small areas of localization and non-flexibility in moving voxel positions over the desired anatomy. (The CSI grid is centered in FOV). An example of how multivoxel CSI can be used to obtain cardiac spectra is shown in Figure 52, which shows a 6 x 6 CSI obtained in 12 minutes with a FOV of 20 cm, resulting in 35 x 35 x 30 mm³ voxels.

Localized P-31 ISISCSI

It has been shown via a phantom study that the ISISCSI protocol that comes standard on the 3.0 T system does not do an adequate job of localizing in a simple non-moving phantom. A protocol was created whereby the user could obtain 8 separate acquisitions and, via post-processing, co-add and -subtract the acquisitions properly to obtain excellent localization of a cubic area predefined by the user within the FOV. Although this protocol works, it is not practical to use during human, in-vivo cardiac P-31 spectroscopy acquisitions for several reasons. First, the user must be able to see the spectra at the time of acquisition to be sure that the acquisition voxel is optimally placed to get maximal SNR from the cardiac muscle while minimizing the skeletal muscle contamination. Second, the acquisition of 8 separate spectra would be difficult to be coordinated enough to acquire while at the same time taking patient blood pressure and/or coaching the patient to exercise in the magnet. For these reasons, Dr. Hee-Won Kim has been attempting to create a more automated pulse program that would accurately acquire 8 or more separate spectra and, co-add and subtract the results in real time for display during the acquisition.

Slice Localized P-31 FIDCSI (DRESS)

The best possible working localization method on the 3.0 T system can be achieved with a slice select FIDCSI sequence that has been modified to allow oblique acquisitions close to the coronal plane. The pulse sequence modifications were performed by Dr. Hee-Won Kim using GE's EPIC pulse programming. This method of localized spectroscopy acquisition is based on the Depth Resolved Surface Coil Spectroscopy (DRESS) method. This method localizes via a combination of the oblique slice localization in combination with the sensitivity range of the phosphorus surface coil, as shown in Figure 53. This method of slice localized spectroscopy is a bit tricky to use for localization. As will be dealt with further in the next chapter, it is easy to obtain contaminated spectra, as shown in Figure 54. The results of slice localized spectroscopy at both 1.5 T and 3.0 T with rest and exercise are shown in Figure 55.

At 3.0 T, due to the increased spectral dispersion, is it often easy to view the skeletal muscle contamination as a split in the PCr peak as shown in Figure 56. This figure shows slice localized phosphorus spectroscopy acquisitions, increasing with depth. It demonstrates how the skeletal muscle PCr peak dominates in the shallower slices. As the slices go deeper into the chest, the cardiac muscle PCr dominates, and the overall SNR decreases. This split of the PCr peak in cardiac phosphorus spectroscopy has been previously noted by Dr. Jan den Hollander¹³⁵ and Yabe et al⁶⁶.

Single Turn versus Quadrature Surface P-31 Coil at 3.0 T

The single turn coil is the most often used coil for obtaining in-vivo, human cardiac spectra as posted in the literature. Improved SNR can be achieved by using a quadrature coil in its place, as was demonstrated in the last chapter with phantom studies. The problem with using the quadrature coil for looking at the heart is that it has a large volume of sensitivity and thus greater potential for contamination. With localized pulse sequences such as multivoxel CSI and ISIS, the added SNR that the quad coil provides produces optimal results. Unfortunately, with DRESS, where the surface coil is used to help localize, there can be added skeletal muscle contamination unless the slice of interest is placed much deeper in the chest than would be done with a single turn coil on the same volunteer, as shown in Figure 57. A statistical comparison of the single and quadrature P-31 surface coils is available in the chapter on reproducibility.

Human Test Participants

Two main groups of participants were used. The first group was those used to obtaining cardiac P-31 MRS at 3.0 T. The second group was used to test the hydraulic handgrip exerciser at a 30% maximum exertion.

To test the protocol of obtaining localized cardiac P-31 spectra at 3.0 T, three types of volunteers were used, as shown in Table 14. The first person listed is a referred cardiac patient from the WISE study with suspected microvascular ischemia. The second participant listed is a person who was asymptomatic, but had a recent treadmill ECG and was found to have a 1 mm ST segment depression indicating mild

myocardial ischemia. Third, a group of participants (4 Male, 4 Female) who were not clinically tested for ischemia, but were non-symptomatic were also tested. These participants were also questioned about possible risk factors for heart disease (smoking, family history, exercise level, height/weight) and had their resting heart rate and blood pressure measured. Based on the results of height and weight, a body mass index (BMI) factor was calculated for each participant who had not been medically evaluated for ischemia. The BMI is a numerical factor that allows comparison, regardless of height, of the relative weight of individuals.²²

$$\text{BMI} = \frac{\text{Weight(pound)} \cdot 703}{\text{Height(inches)}^2} \quad \text{Equation 5}$$

Any BMI value far above 25 is considered overweight, a risk factor for heart disease. This group was used to obtain localized cardiac P-31 spectra at 2 to 3 different TR intervals for estimating T₁ relaxation corrections at 3 T. The third group was not used to obtain any exercise cardiac P-31 MRS since although they were asymptomatic, their non-ischemic status was had not been verified by medical tests.

The second group of participants, as shown in Table 15, was used to evaluate the adequacy of the hydraulic handgrip in producing sufficient changes in heart rate and blood pressure to adequately stress the heart. The hydraulic handgrip is used isometrically at 30% of maximum exertion. Four participants were non-symptomatic although one of the four had been tested clinically for myocardial ischemia and was found to have mild ischemia, based on an ECG treadmill test. The remaining 28 subjects were patients referred from cardiology based on

chest pain, "low" percent stenosis (as measured in a coronary angiogram study), and suspected microvascular ischemia (the WISE study). Less than 50% stenosis is considered "low".⁴ Two participants had tests at both 1.5 and 3.0 T, as noted. Since most of these tests were performed at 1.5 T and not at 3.0 T, the data that is relevant to cardiac spectroscopy at 3.0 T is limited to the use of the hydraulic handgrip cardiac response.

Human participants signed an IRB consent form (examples found in Appendix A) and were screened individually for potential health risks associated with 3.0 T magnetic resonance proton imaging and phosphorus spectroscopy (metal in the body, peripheral vascular disease, heart disease etc.). Volunteers were positioned in the magnet and made as comfortable as possible. Although the phantom work is useful for determining the quality of the pulse sequence acquisitions, human volunteers are necessary at an early stage. Human volunteers were used to test techniques designed to obtain a phosphorus spectrum from a moving heart, and to apply post-processing techniques that correct for blood and skeletal muscle contamination and relaxation effects.

Table 14. Participants at 3.0 T for Cardiac P-31 Spectroscopy.

Initials	Age & Gender	Heart disease?	BMI
E.O.	54 y.o. Female	WISE referral: chest pain with suspected microvascular ischemia, low 39% stenosis	25.9
K.S.	66 y.o. Female	non-symptomatic, mild myocardial ischemia, treadmill ECG showing 1 mm depression of ST segment indicating mild ischemia	23.9
T.B.	29 y.o. Male	non-symptomatic, mildly physically active, not clinically evaluated for ischemia	25.7
C.M.	26 y.o. Female	non-symptomatic, average physically activity, family history of heart disease, not clinically evaluated for ischemia	19.2
W.P.*	59 y.o. Male	non-symptomatic, highly physically activity, family history of heart disease, not clinically evaluated for ischemia	25.1
D.P.	29 y.o. Male	non-symptomatic, average physically activity, family history of heart disease, not clinically evaluated, ischemia	25.5
L.R.	28 y.o. Female	non-symptomatic, average physically activity, family history of heart disease, not clinically evaluated for ischemia	20.2
L.B.	50 y.o. Female	mitral valve prolapsed, average physically activity, family history of heart disease, not clinically evaluated for ischemia	23.8
C.S.**	46 y.o. Female	heart murmur, possible leak of mitral valve, highly physically active, family history of heart disease, not clinically evaluated for ischemia	27.41
R.B.	48 y.o. Male	non-symptomatic, average physically activity, family history of heart disease, not clinically evaluated for ischemia	24.5

* poor SNR with W.P. study resulted in data that Fitmaster* was unable to process

** study not completed on C.S. due to claustrophobia while in the magnet

Table 15. In Magnet Hydraulic Exercise Handgrip Participants.

Initials	Age & Gender	Heart disease?	Cardiac Site
E.Q.	25 y.o. F	non-symptomatic	1.5 T
S.P.	56 y.o. F	non-symptomatic	1.5 T
A.B.	43 y.o. F	non-symptomatic	1.5 T
K.S.	66 y.o. F	non-symptomatic, mild myocardial ischemia	1.5 & 3T
E.O.	54 y.o. F	WISE (39% stenosis)	1.5 & 3T
G.N.	55 y.o. F	WISE (0% stenosis)	1.5 T
B.H.	51 y.o. F	WISE (29% stenosis)	1.5 T
S.E.	60 y.o. F	WISE (0% stenosis)	1.5 T
S.H.	58 y.o. F	WISE (60% stenosis)	1.5 T
E.K.	65 y.o. F	WISE (36% stenosis)	1.5 T
E.B.	54 y.o. F	WISE (no CA data available)	1.5 T
H.P.	74 y.o. F	WISE (24% stenosis)	1.5 T
S.J.	53 y.o. F	WISE (75% stenosis)	1.5 T
S.A.	53 y.o. F	WISE (0% stenosis)	1.5 T
J.G.	65 y.o. F	WISE (57% stenosis)	1.5 T
L.C.	49 y.o. F	WISE (0% stenosis)	1.5 T
J.F.	67 y.o. F	WISE (0% stenosis)	1.5 T
H.T.	55 y.o. F	WISE (0% stenosis)	1.5 T
J.D.	72 y.o. F	WISE (no CA data available)	1.5 T
R.S.	40 y.o. F	WISE (0% stenosis)	1.5 T
M.P.	66 y.o. F	WISE (0% stenosis)	1.5 T
G.O.	56 y.o. F	WISE (no CA data available)	1.5 T
E.W.	50 y.o. F	WISE (no CA data available)	1.5 T
G.A.	60 y.o. F	WISE (0% stenosis)	1.5 T
A.S.	61 y.o. F	WISE (36% stenosis)	1.5 T
K.G.	39 y.o. F	WISE (no CA data available)	1.5 T
N.W.	62 y.o. F	WISE (no CA data available)	1.5 T
M.A.	52 y.o. F	WISE (no CA data available)	1.5 T
L.H.	51 y.o. F	WISE (no CA data available)	1.5 T
D.M.	69 y.o. F	WISE (no CA data available)	1.5 T

Abbreviations: WISE = chest pain with suspected microvascular ischemia, F = female, - = measurement not made, * = blood pressure measured from ankle instead of forearm, CA = coronary angiogram where % stenosis is measured

In-Magnet Exercise

The design criterion of the in-magnet exerciser includes getting the most value for the least cost. In addition, the selected exercise device must not cause added motion to the chest region that would interfere with the signal acquisition, effectively decreasing the SNR. The exercise must be sustainable for the duration of the time necessary to obtain one set of data (i.e. averaged and gated). Studies have shown this time period can vary from three¹⁴ to 40 minutes,¹⁵ depending on the voxel size and selected pulse sequence, due to the small volume of the myocardium and the extended acquisition time necessary for gating.

An isometric handgrip ergometer has been created that is simple and cost effective. A hydraulic system was designed with a rubber bulb at one end of 30 feet of plastic tubing, with a 30 psi, hydraulic, analog gauge at the other end, as shown in Figure 58. The rubber bulb is placed in the participant's hand while in the magnet. A maximum contraction of the bulb is recorded as a pressure difference on the analog gauge. The linear response of the handgrip was tested by placing a gradient of weights on the bulb and it was verified that the handgrip does respond linearly, as shown in Figure 59. Thirty percent of that maximum exertion is used as the level of work to keep the participant isometrically squeezing the handgrip to put a stress on the heart. The stress level is monitored both by the level of isometric grip and via vital signs measurements. Specifically, the blood pressure and heart rate are recorded every two minutes during rest, exercise and two recovery periods. The hand chosen to squeeze the bulb

is the opposite to which the blood pressure is taken via a Dinamap™ monitor, as shown in Figure 60. The analog gauge on the exercise equipment could be replaced at some point with a digital gauge that would allow for recording of the pressure levels during rest and isometric exercise. Details on how to construct the hydraulic handgrip exerciser can be found in Appendix C.

To test the adequacy of the hydraulic handgrip exerciser, all participants listed in Table 15 were monitored for heart rate and blood pressure during rest and during exercise. The exercise consisted of isometrically squeezing the hydraulic handgrip to a level at 30% of the subject's individual maximum squeeze effort. The results of these studies can be found in the next chapter.

Spectroscopy Post-Processing

Simply obtaining a phosphorus spectrum from a voxel in the myocardium is not enough to ensure useful spectral data. The spectra must be post-processed using specialized software such as Sage_IDL™, MRUI™ or FELIX™. This software allows the spectrum to be measured to quantitatively produce ratios of different metabolites. The results of these ratios can then be examined for skeletal muscle contamination. Also, since the localization procedure obtains signal from cardiac muscle and blood, the spectrum must be corrected for blood contamination. Finally, relaxation corrections that account for acquisitions taken at times shorter than five times T_1 (i.e. not fully relaxed) must be made. In addition, methods for calculating millimolar (mM) amounts will be evaluated.

Post-Processing Software

A number of spectroscopy post-processing programs are available for use; four different types were examined for this project: FITMASTER™ (Philips), Sage_IDL™ (GE), MRUI™ (funded by European Community) and FELIX™ (Molecular Simulations, Inc.). Most human spectra obtained in the study for both 1.5 and 3.0 T were analyzed and evaluated by Dr. Steven Buchthal and Dr. Jan den Hollander at the University of Alabama at Birmingham (UAB). The UAB group has extensive publications with human, cardiac P-31 NMR spectroscopy beginning with Dr. den Hollander's work in Leiden, The Netherlands and continuing with work in Birmingham, Alabama. Their analysis was performed using FITMASTER™. Post-processing techniques at UF were also evaluated using the available software of Sage_IDL™, MRUI™, EXCEL™ (Microsoft), FELIX™ and a header modification program created with help from Dr. Marian Buszko, UF Department of Microbiology and Cell Sciences. A detailed explanation of how each program was used to process data, in addition to comparative data analysis, can be found in Appendix E.

Experience in post-processing human, in-vivo cardiac P-31 spectra was provided via a collaborative working arrangement with Dr. Jan den Hollander and Dr. Steven Buchthal at the University of Alabama at Birmingham (UAB). As part of an NIH contract on Women's Ischemic Syndrome Evaluation (WISE), 4 sites including UF and UAB took part in a study of women with chest pain, but not severe stenosis, in the major arteries of their heart as determined by cardiac catheterization. Both UAB and UF gathered MRS cardiac data on women in the WISE population, at rest and at exercise at 1.5 T and 3.0 T. All WISE data were sent to UAB for post-processing. UAB has a 1.5 T Philips system with

exceptional capabilities for performing localized phosphorus spectroscopy. This system is in the Cardiology Division of the Department of Medicine at UAB and has been optimized for MR uses related to the heart. Dr. den Hollander originally came to UAB as an employee of Philips to work with UAB in optimizing their cardiac MRI and MRS capabilities. As part of his work with Philips, he helped create a post-processing program, called FITMASTER™. FITMASTER™ is optimized to do an excellent job of post-processing cardiac P-31 spectra, especially in terms of having the added ability to do linear prediction and fit the missing data at the start of the FID. Using FITMASTER™, Dr. Buchthal has been able to do an excellent job at post-processing the cardiac spectra for the WISE study, as was demonstrated by a very flat subtracted noise baseline of the FITMASTER™ fitted spectra for both 1.5 and 3.0 T. For all in-vivo cardiac P-31 spectroscopy figures the program that was used to post-process the data is noted in the appendix. Unfortunately, Philips only provides FITMASTER™ with the purchase of their magnet. The software cannot be purchased individually. Fortunately, we had the opportunity to work with UAB and get some results for this dissertation, which was analyzed by a group both experienced with cardiac P-31 spectroscopy and using the more sophisticated post-processing methods. This provides a standard to which the post-processing methods available at UF can be compared.

As part of UAB's methodology for fitting the low SNR cardiac P-31 spectra, they first co-add all P-31 spectra obtained in the same study (rest, exercise, and recoveries). The summed data is then fit via back extrapolation to replace the initial, missing section of the FID.

Fitting the beginning of the FID corrects for the baseline curve and creates a flat baselined spectrum. This higher SNR spectrum is then fit for each peak and the software is then primed with initial peak locations and widths. Next, spectra are individually fitted using the initial guesses for fit based on the summed spectra, but allowing just the peak heights to change, except for Pi which is allowed to change frequency position (as would be expected with a change in pH). This method takes advantage of optimizing SNR while obtaining the best results for even low SNR cardiac P-31 spectra. Other details of their post-processing include the use of Gaussian 15 Hz line broadening, and the fitting assumption that all three ATP peaks are of equal area. Unfortunately, we have found that the FITMASTER™ program's fitting routine is sensitive to SNR and does not work well with low SNR data. In one example, shown in Appendix E, a low SNR spectrum where each peak area was individually fit with SAGE_IDL™ was found to not be contaminated by skeletal muscle based on a [PCr]/[ATP] ratio of ~1.0. The same spectrum, processed and automatically peak area fit by FITMASTER™, was found incorrectly to be a skeletal muscle contaminated spectrum based on a skewed [PCr]/[ATP] ratio of ~2.00, when the true problem was low SNR. This is further proven visually by looking at the example spectra in the appendix, where the PCr peak is clearly altered from being shorter than ATP to being much larger. As shown in the next chapter, this may account for why the DRESS sequence appears to be so often more highly contaminated by skeletal muscle when compared to UAB's ISIS results. Despite this fault, this program has been designed to be extremely flexible and powerful in terms of post-processing cardiac P-31 MRS.

Locally, the GE Signa Advantage™ system comes with a program designed to post-process spectroscopy data obtained on a GE system. This software, called Sage_IDL™, is provided free to the user with the magnet. Like Microsoft Word runs on Windows 98, Sage_IDL™ runs on IDL™ (Interactive Data Language by Research Systems, Inc) a licensed program installed at the UNIX station. Sage_IDL™ requires the user first to convert the header of the GE data file using the "sdhm" command at the UNIX prompt. Once the new header has been created, the Sage_IDL™ program can be run to do a variety of spectral post-processing tasks including apodization, zero-filling, fft, phase, basic baseline correction, peak picking, curve fitting, and spectral analysis. In addition, Sage_IDL™ can input and correlate images with multivoxel CSI data to overlay the voxels on the image for precise localization. Unfortunately, Sage_IDL™ does not have many options for baseline corrections. Missing is a method for performing time domain linear prediction and interpolation of missed data at the beginning of an FID, which is a necessary correction for localized cardiac spectroscopy acquisitions on the GE systems. Time domain extrapolation of the missing start of the FID has even been dealt with in a separate program by Schaefer et al.,¹⁶¹ due to the lack of its availability in most spectroscopy post-processing software. In addition, in Sage_IDL™ the available baseline corrections in the frequency domain are based on a simple user input of points matching the spectral noise that represent the true baseline. For data with low SNR, such as cardiac P-31 MRS, points picked along the noisy baseline are jaggedly placed, creating unrepeatable and undesirable warpage rather than straightening of the baseline. This feature works well for spectra with high SNR and mostly

flat baselines, but does very poorly for cardiac P-31 spectra which are inherently low SNR and have a non-flat baseline due to the loss of data at the start of the FID.

The next viable software option for cardiac spectroscopy post-processing is MRUI™ (Magnetic Resonance User Interface, the result of a collaborative project sponsored by the European Community). Since this software was developed as part of a research project, the licensure was free assuming a research agreement was signed. MRUI™ is designed to process data in the time domain, rather than the frequency domain. Like Sage_IDL™, MRUI™ is able to do simple functions such as apodize, zero-fill, fft, phase, and fit spectra. As Sage_IDL™ ran from the IDL™ platform, MRUI™ runs from a Matlab™ (The Mathworks, Inc.) version 4X platform. Unfortunately, the most updated version of MRUI™ available (97.1 released September 1997) is not able to perform linear prediction and back fit the missing data at the start of the FID. Again, this fit when done using FITMASTER™ corrects for the distortion in the cardiac P-31 baseline caused by the cutoff of the start of the FID signal. In addition, because this software is designed for time domain fitting, frequency domain baseline correction methods are not available.

FELIX™ (of Molecular Simulations, Inc) is the final post-processing program available locally that has been evaluated in attempts to find the best software for post-processing cardiac P-31 spectra. FELIX™ runs on an SGI workstation, and standalone can be purchased at around \$6,000 to \$10,000 per site-license. At UF, FELIX™ is available for a single user at a rate of \$160/quarter via the Brain Institute (David Parks, system administrator), as a shared expense site licensure. Along with the other standard spectroscopy post-processing

techniques, such as apodization, zero-fill, fft, and phase, FELIX™ does have the ability to do linear prediction in a limited fashion. The linear prediction in the FELIX™ software is designed not to add missing points to the start of an FID, but to replace points at the start of an FID that have been corrupted by eddy currents. It appears that most spectroscopy acquisition systems acquire the entire FID and leave the choice of eliminating the beginning of the FID up to the operator during post-processing. The GE system, on the other hand, doesn't collect the start of the FID during acquisition that leads to problems, but their post-processing software does not provide a fix for these problems. To compound the problems with FELIX™ linear prediction, the utility for performing this task does its own peak selection based on the user inputting the number of peaks expected. The system can make mistakes, especially with split peaks or low SNR, and does not allow for user intervention to correct the computer's guesses for incorrect peak positions. The system then examines the peaks it has selected in the frequency domain and predicts the shape and number of co-added decaying sinusoids in the time domain resulting in an FID. It is clear that this program would work best with data with good SNR to ensure proper auto-selection of peak positions. This can be best achieved with the cardiac data by co-adding all the spectra from one study together (rest, exercise, recovery 1 and recovery 2) to get ideal fit parameters for all spectra with similar peak positions and widths. For the same sample and shim, you can assume that the peak positions and peak widths will remain constant, except for π_i . Each individual spectrum from the study can be refit, based on the parameters obtained by fitting the summed spectrum, but now allowing only the peak heights to change.

This method is also used at UAB using FITMASTER™ to analyze cardiac spectroscopy data.

Skeletal Muscle

Skeletal muscle spectra contain the same phosphorus peaks as cardiac spectra, but in different quantities. The primary method for ensuring that there is no skeletal muscle contamination in the cardiac spectra is to use good methods of localization with an appropriate pulse sequence.⁵⁰ Simply put, too much skeletal muscle contamination in the cardiac spectrum invalidates the study. This is determined by first post-processing the spectra and looking at the resulting ratio of [PCr]/[ATP] in each spectrum. A ratio of 1.5 to 2 or higher is indicative of skeletal muscle contamination.

Blood Contamination

UAB has also determined a blood correction factor. All of the WISE data and the data in this dissertation has been blood corrected by using an [ATP]/[2,3-DPG] correction factor of 0.18 based on data obtained at UAB using a vial sample of fresh heparinized blood with the same protocol used to acquire human cardiac P-31 spectra.¹⁵⁵ This factor falls close in line with published values of 0.19⁵² and 0.21¹⁴⁸ where the correction factor was obtained in a similar fashion.

To correct for blood contamination for each cardiac P-31 spectra, first multiply the area of the 2,3-DPG peak in that spectrum with the [ATP]/[2,3-DPG] correction factor. Next, subtract the estimated blood contributions as shown in the following equations. The final equation

given as $[PCr/ATP]_{blood \ corrected}$ is listed because it is the form of the output of the FITMASTER™ software.

$$ATP_{blood} = 2,3DPG_{area} \times \left[\frac{ATP}{2,3DPG} \right]_{\text{correction factor}} \quad \text{Equation 6}$$

$$ATP_{corrected} = ATP_{contaminated} - ATP_{blood} \quad \text{Equation 7}$$

$$\left[\frac{PCr}{ATP} \right]_{\text{blood}} = \frac{PCr}{(ATP_{corrected})} \quad \text{Equation 8}$$

T₁ Relaxation Corrections

Relaxation corrections adjust for the loss of area of a metabolite peak due to acquisition at short TR times, without complete relaxation between excitations. Assuming equal T₁ relaxation times between subjects at the same magnetic field strength, an estimate for the correction factor can be obtained from one set of subjects and used to correct cardiac P-31 MRS obtained from future subjects. At a set TR time, the relaxation correction factor (RCF) is the ratio of the metabolite peak area value at long TR (fully relaxed condition) over short TR (the TR time used for the study). The peak area can also be substituted with a ratio of two peak areas, such as [PCr]/[ATP].

$$RCF = \frac{\text{Peak Area}_{\text{long TR acquisition}}}{\text{Peak Area}_{\text{short TR acquisition}}} \quad \text{Equation 9}$$

$$\text{Peak Area}_{\text{relaxation}} = \text{Peak Area}_{\text{short TR acquisition}} \times RCF_{\text{corrected}} \quad \text{Equation 10}$$

The RCF factor can also be determined based on the T_1 relaxation factor at a specific field strength expected for a specific tissue metabolite (X).

$$RCF_X(TR) = \frac{1}{1 - \exp(-TR / T_1)} \quad \text{Equation 11}$$

There are no literature values available for proper T_1 relaxation corrections of human cardiac muscle at 3.0 T. T_1 can, however, be measured at 3.0 T (or other field strength) by acquiring localized cardiac P-31 spectra at two or more TR times. If values from just two TR times are acquired they must be acquired from a short TR that is typically used to acquire the data and a long TR where conditions are fully relaxed. A single correction factor can then be calculated for that exact short TR value. When the TR is not constant from subject to subject, as in the case of a TR value dependent on heart rate gating, a single correction factor is not correct. Despite this fact, some human cardiac P-31 data in the literature is still corrected based on a single relaxation correction factor.³¹ This practice is done even when exercise is involved which will change the TR between resting and exercise acquisitions in the same subject.¹⁹⁵ With resting heart rates variable from 50 to 90 BPM, the TR value typically gated to every third or fourth heart beat will also vary between subjects, assuming a constant heart rate for each subject. Fortunately, acquisition of localized cardiac P-31 spectra for three or more different TR times (short, medium and long) provides enough data for an exponential fit and an estimation of the T_1 relaxation rate for each metabolite peak area (X) for each subject.

$$\text{Area}_x(\text{TR}) = a(b - \exp(-\text{TR} / T_1)) \quad \text{Equation 12}$$

where a and b are constants
 Area_x is the area of a metabolite at time TR
 TR and T₁ in seconds

Repeating this for several subjects and averaging provides a more reliable T₁ measure. The average T₁ relaxation rate can then be used to determine the RCF for any TR time, as shown above.

To estimate the value of T₁ for both PCr and ATP at 3.0 T, eight non-symptomatic subjects, from Table 14, without suspected ischemia (4 Males, 4 Females) were tested for one study each to obtain cardiac P-31 spectra at two to three different TR times. Two studies failed due to poor SNR (W.P.) and clausterphobia (C.S.). An additional study (T.B.) was incomplete due to obtaining data at only two TR times (as recommended by the literature) but was not repeated to obtain data at three TR times. An RCF for a single TR based on this single subject is provided in Appendix F. The total number of studies was limited based on advisement. Results of these studies can be found in the next chapter.

Calculations of pH

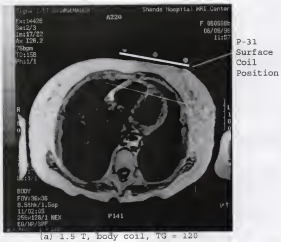
The measurement of pH on a phosphorus spectrum is proportional to the frequency difference, or chemical shift (cs) in ppm, between the Pi and PCr peaks.²²² This relationship has been simply described by the Henderson-Hasselbalch equation.^{223,224}

$$\text{pH} = 6.75 + \log_{10} \left[\frac{\text{cs} - 3.27}{5.69 - \text{cs}} \right] \quad \text{Equation 13}$$

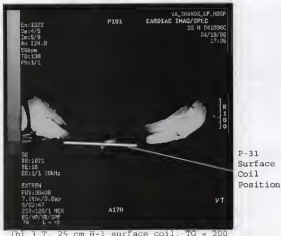
Locally, using oblique DRESS techniques at 1.5 T, the Pi peak is non-discriminable from the blood 2,3-DPG peaks, as shown in Figure 61 (a). In the same subject, on the same day, the oblique DRESS sequence was repeated at 3.0 T, and the Pi peak was detectable separate from the 2,3-DPG peaks as shown in Figure 61 (b). This provides an example of the capabilities of the 3.0 T to show the Pi peak due to greater spectral dispersion and thus allow for pH calculations, with a simple DRESS protocol (6 to 8 minutes, 128 acquisitions gated to every fourth heart beat).

Analysis

Based on the results from this chapter, the DRESS oblique slice localized cardiac P-31 spectroscopy will be the best option to consider for repeatability and reliability. DRESS oblique slice localization provides the best compromise between SNR, flexibility and quality in localization. In addition, a quadrature P-31 radio frequency (RF) coil provided additional SNR improvements over the single-turn coil of similar single-loop dimensions.



a) 1.5 T, body coil, TG = 120



(b) 3 T, 25 cm H-1 surface coil, TG = 200

Figure 45. Human cardiac imaging with the spin-echo pulse sequence at (a) 1.5 T with the body coil and at (b) 3.0 T with a surface coil. (Parameters: 1 echo, minimum full TE, TR each heart beat, 32kHz bandwidth, peripheral gated, 40 cm FOV, 7-8 mm thick, 3 mm space, scan time ~2:20; see Appendix B for more detail).



(a) 1.5 T, Gradient Echo, breathing



(b) 3 T, Gradient Echo, breathhold

Figure 46. Human cardiac imaging with the fast gradient echo pulse sequence at (a) 1.5 T with the body coil and at (b) 3.0 T with a surface coil. (Parameters: 60° flip angle, minimum full TE, TR each heart beat, 16kHz bandwidth, peripheral gated, 42 cm FOV, 7 mm thick, 1 mm space, scan time 0:20 per slice; see Appendix B for more detail).

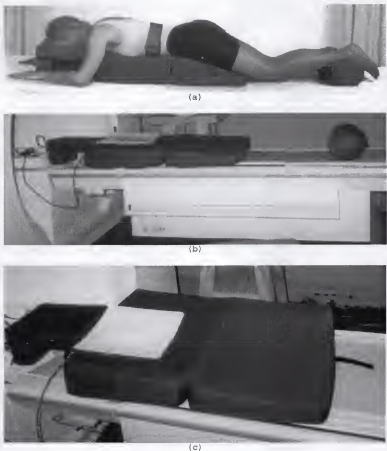


Figure 47. Prone positioner for in-magnet cardiac spectroscopy. (a) Prone massage M.A.T. by A2Z Possibilities, Inc. has a foam core with a removable and washable cover, along with a roll to place under the ankles. (b & c) The M.A.T. was trimmed a little in the side to side directions and then was perfect for prone positioning in the magnet.

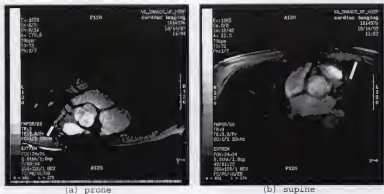


Figure 48. A comparison of the heart's position in the (a) prone and (b) supine positions, as shown from a 3.0 T axial slice. (Parameters: fast gradient echo, 60° flip angle, minimum full TE, TR each heart beat, 8kHz bandwidth, peripheral gated, 30 cm FOV, 8 mm thick, 1 mm space, scan time 0:20 per slice; see Appendix B for more detail)

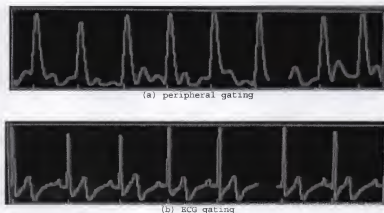


Figure 49. Waveforms of (a) peripheral gating and (b) ECG gating on the 3.0 T from a normal human volunteer (TEB) on Sept 20, 1998, displayed at a rate of 21 mm/sec.



Figure 50. A comparison of peripheral gating (pg) versus ECG gating, and breathing during the image versus breath-hold images. All images are fast gradient echo: (a) sagittal, peripheral gating, breath-hold; (b)sagittal, peripheral gating, breathing; (c) sagittal, ECG gating, breath-hold; (d) sagittal, ECG gating, breathing, (e) axial, peripheral gating, breath-hold, (f) axial, peripheral gating, breathing.

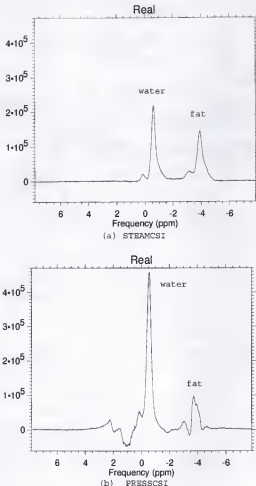


Figure 51. Human proton voxel localized spectroscopy of the heart and chest wall obtained during one volunteer's shim using the techniques of GE's (a) STEAMCSI and (b) PRESSCSI. (Parameters for both: 16 acquisitions, 1000 Hz spectral width, 2 sec TR, $4.1 \times 5.9 \times 3.0 \text{ cm}^3$ voxel, scan time of 0:40, 3 T, single-turn RF coil and no line-broadening; see Appendix B for more detail).

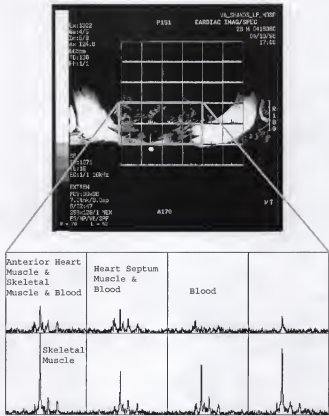


Figure 52. P-31 FIDCSI with CSI of a human subject at 3.0 T.
(Parameters: 128 acquisitions, 4000 Hz spectral width, TR gated every other heart beat, $3.5 \times 3.5 \times 3.0$ cm 3 voxels, scan time of 12 minutes, 10Hz line-broadening, & orient = transpose x-y, flip x; see Appendix B for more detail).

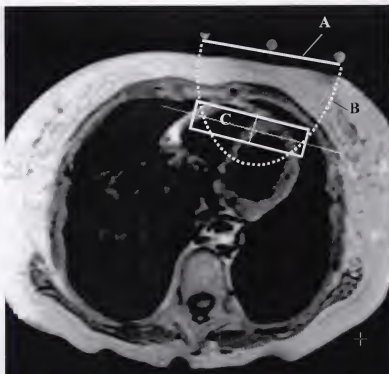


Figure 53. DRESS localization via oblique slice select combined with sensitivity region of coil. (A) Position of surface coil and the 3 vials of external standard. (B) Dashed line indicates the reception volume of the surface coil. (C) Cardiac P-31 DRESS spectroscopy is acquired from an oblique slice region.

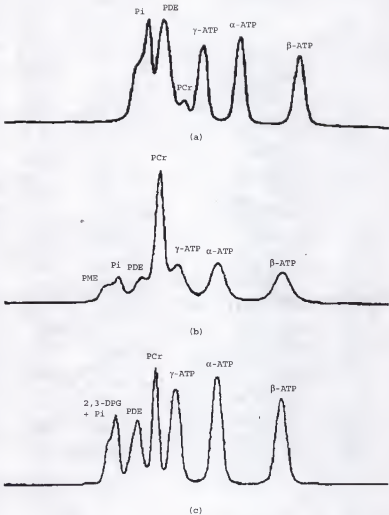


Figure 54. Examples of 1.5 T cardiac phosphorus spectra localization problems resulting in (a) liver contamination, or (b) skeletal muscle contamination, in comparison with (c) a non-contaminated cardiac spectrum.

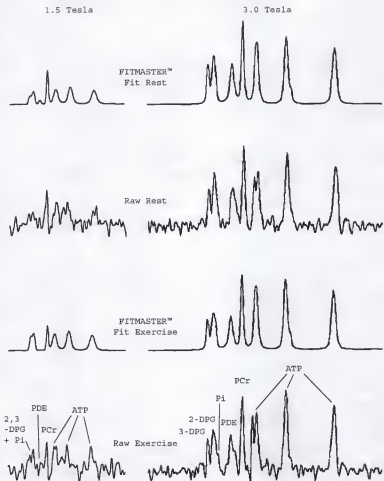


Figure 55. P-31 FIDCSI oblique slice localized human cardiac spectroscopy (oblique DRESS) of the same subject, at 1.5 and 3.0 T, on different days showing examples of resting and exercise spectra, raw and fitted. (Parameters: 128 acquisitions, 2000 & 4000 Hz spectral width for 1.5 and 3.0 T, TR gated every third heart beat, 25mm slice, scan time of 6 to 8 minutes, 15 Hz line-broadening; see Appendix B for more detail).

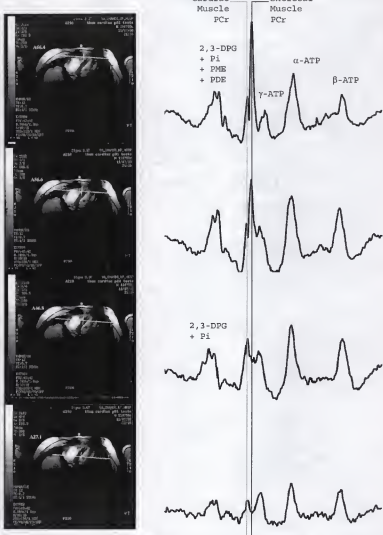
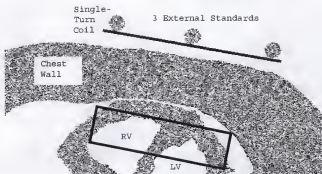
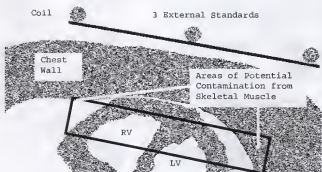


Figure 56. Series of cardiac region oblique DRESS spectra representing decreased skeletal muscle contamination with increase in depth of spectroscopy slice localization. Note the split in the PCr peak that designates the cardiac and skeletal muscle as separate peaks.



(a) 10 cm diameter single turn P-31 surface coil combined with oblique DRESS



(b) $16 \times 10 \text{ cm}^2$ quadrature P-31 surface coil combined with oblique DRESS

Figure 57. Relative size of oblique DRESS slice with (a) a 10-cm diameter single-turn P-31 surface coil and (b) a $16 \times 10 \text{ cm}^2$ quadrature P-31 surface coil.

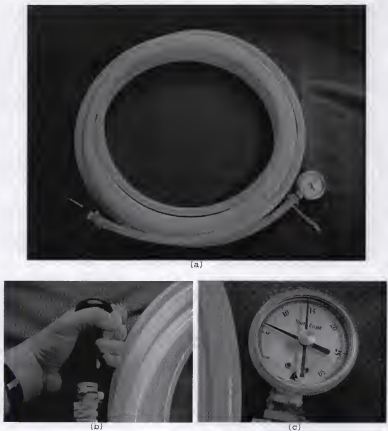


Figure 58. Water, hydraulic, hand-squeeze ergometer/static-exerciser, modified from original design by North Coast Medical (Bulb Dynamometer, Item # NC70154) by adding 30 ft hose between rubber squeeze ball and gauge, (a) coiled up for storage, (b) close up of rubber, hand-squeeze, and (c) close up of pressure gauge.

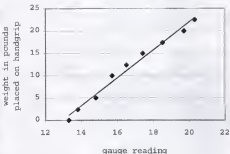


Figure 59. The linear response of the hydraulic handgrip to added weight on the rubber bulb is illustrated. Due to initial water pressure, that changes depending on the position of the tubing (a constant in any individual MRS exercise case), the gauge will read a value above zero even when no weight has been applied.



Figure 60. Dinamap™ blood pressure and pulse monitoring equipment.

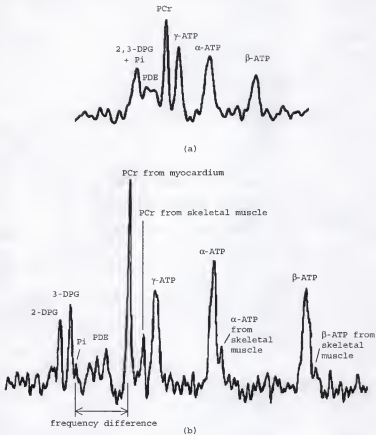


Figure 61. Myocardial pH is proportional to the frequency difference of the Pi and PCr peaks in the human, in-vivo phosphorus NMR spectrum.
 (a) At 1.5 T the Pi peak is hidden by blood 2,3-DPG. (b) At 3.0 T the Pi peak is discernible from the 2,3-DPG peak, allowing for the measurement of pH. Both spectra obtained on the same volunteer at rest using oblique DRESS. (Parameters: 128 Acquisitions, every third heart beat TR, Oblique DRESS, 25 mm thick slice, single-turn P-31 coil; see Appendix B for more detail).

CHAPTER 5
HUMAN DATA REPRODUCIBILITY

The previous chapter on human techniques allowed for an investigation of the best combination of pulse sequence and coils to be used at 3.0 T to achieve optimal acquisition of human, in-vivo, cardiac P-31 spectroscopy on the GE Signa Advantage™ 3.0 Tesla system at the University of Florida. Based on that chapter's investigations, the oblique DRESS sequence (via the FIDCSI GE sequence) provides the best compromise of the GE sequences between SNR, flexibility, accuracy in terms of localization over the desired region of the heart, and reasonable acquisition time. The oblique DRESS protocol will now be evaluated based on a number of human studies. The aim is to quantify reliability and repeatability specifically for the acquisition of human, in-vivo, cardiac P-31 spectroscopy.

This chapter addresses the reproducibility of this technique for cardiac spectroscopy P-31 measurement. It is a chapter of multiple acquisitions and evaluation designed to show that the protocol selected for 3.0 T cardiac phosphorus spectroscopy acquisitions is optimal. These results are based on studies locally at 1.5 and 3.0 T, with the locally constructed hydraulic handgrip in-magnet exercise. In addition, these local studies will be compared with similar studies being conducted at University of Alabama at Birmingham for the WISE studies, and other publications on human, in-vivo cardiac spectroscopy.

T₁ Relaxation Corrections

Six sets of resting P-31 cardiac spectra obtained with short (1RR), medium (3RR) and long (12RR or the closest time) TR times, were obtained on the 3.0 T. The protocol consisted of oblique DRESS, 128 acquisitions, and gated TR for each time interval. The data were sent to Birmingham for post-processing by Fitmaster™. The three ATP signal areas (γ -, α - and β -ATP) were "estimated" by the Fitmaster™ program to be approximately equal (whether truly correct or not), therefore only a single ATP area value is listed to represent all three peaks. The post-processed metabolite areas from each spectrum are shown in Table 16. Note that gating at every heart beat (1RR) and every third heart beat (3RR) was selected on the system, but the actual time that the system gated to was every other heart beat (2RR) and every fourth heart beat (4RR) based on recorded time between audible acquisition pulses. This also limits the minimum time that the system allows for a gated TR. A shorter TR time would have otherwise been preferred, especially when determining the relaxation rate of ATP. In this table, ATP is corrected for blood contamination using the equations specified in Chapter 4, resulting in blood corrected (BC) ATP values.

Table 16. Oblique DRESS Acquisition P-31 Metabolite Area Values Obtained with Different TR Gating Intervals for the Purpose of Relaxation Measurements (obtained by post-processing of spectra with Fitmaster™).

Subject	RR* (sec)	TR time	2,3-		PCr/ATP _{BC}	PCr	ATP _{BC}
			ATP/3	DPG/2			
T.B.	4	4.2	3.04E+06	1.15E+06	1.511	1.75	4.589E+06 2.622E+06
T.B.	12*	14.5	3.23E+06	1.08E+06	1.549	1.76	5.000E+06 2.841E+06
C.M.	2	1.7	8.80E+05	1.11E+05	1.544	1.617	1.359E+06 8.406E+05
C.M.	4	3.8	1.04E+06	1.72E+05	1.589	1.689	1.654E+06 9.794E+05
C.M.	12*	10.5	1.06E+06	1.77E+05	1.855	1.981	1.957E+06 9.879E+05
D.P.	2	2.5	9.74E+05	2.60E+05	1.146	1.268	1.117E+06 8.806E+05
D.P.	4	4.9	1.08E+06	2.47E+05	1.175	1.281	1.269E+06 9.906E+05
D.P.	12*	12.1	1.06E+06	2.58E+05	1.31	1.435	1.393E+06 9.704E+05
L.R.	2	1.8	1.59E+06	4.48E+05	1.444	1.606	2.300E+06 1.432E+06
L.R.	4	4	1.85E+06	4.85E+05	1.517	1.676	2.799E+06 1.670E+06
L.R.	12*	11.2	1.80E+06	2.65E+05	1.604	1.694	2.884E+06 1.702E+06
L.B.	2	1.5	7.06E+05	6.64E+04	0.551	5.703	3.891E+05 6.823E+04
L.B.	4	3.3	7.04E+05	8.37E+04	0.674	0.704	4.741E+05 6.736E+05
L.B.	12*	9.3	6.85E+05	1.13E+05	0.815	0.866	5.580E+05 6.444E+05
R.B.	2	2.6	6.10E+05	2.12E+05	2.054	2.348	1.253E+06 5.336E+05
R.B.	4	4.1	8.44E+05	2.60E+05	1.821	2.048	1.537E+06 7.505E+05
R.B.	12*	13.6	9.89E+05	3.48E+05	1.977	2.264	1.955E+06 8.636E+05

*Gated to every RR heart beat (requested value of 12xRR may be less than 12 within constraints of a 15 second system maximum TR time)
 BC = blood corrected

Five of the six studies (except T.B.) were exponentially fit to estimate the T_1 value for PCr and ATP_{BC}. The resulting equations and figures of the fits can be found in Appendix F. Based on these values, the cumulative result is shown in Table 17.

Table 17. Summary of Resulting T_1 values for PCr and ATP_{BC}.

Subject	T_1 (PCr)	T_1 (ATP _{BC})
C.M.	3.47	0.74
D.P.	3.23	0.45
L.R.	1.85	1.67
L.B.	2.83	0.23
R.B.	3.16	1.59
Average	2.91	0.94
Std Dev	0.63	0.66

Abbreviations: BC = blood corrected

Based on the average T_1 (PCr) and average T_1 (ATP_{BC}), new equations for relaxation for each can be derived based on a relative signal scale of 0 to 1, specific to 3.0 T.

$$\text{PCr(TR)} = 1 - \exp(-\text{TR} / 2.91) \quad \text{Equation 14}$$

$$\text{ATP}_{\text{BC}}(\text{TR}) = 1 - \exp(-\text{TR} / 0.94) \quad \text{Equation 15}$$

The T_1 relaxation correction factor (RCF) for any TR can then be calculated for each peak or for the ratio of [PCr]/[ATP].

$$\text{RCF}_{\text{PCr}}(\text{TR}) = \frac{1}{1 - \exp(-\text{TR} / 2.91)} \quad \text{Equation 16}$$

$$\text{RCF}_{\text{ATP}}(\text{TR}) = \frac{1}{1 - \exp(-\text{TR} / 0.94)} \quad \text{Equation 17}$$

$$\text{RCF}_{[\text{PCr}/\text{ATP}]}(\text{TR}) = \frac{1 - \exp(-\text{TR} / 0.94)}{1 - \exp(-\text{TR} / 2.91)} \quad \text{Equation 18}$$

The resulting RCF for [PCr]/[ATP] has been graphed in Figure 62.

Overall Reproducibility of the Oblique DRESS Method

The overall reproducibility of the oblique DRESS protocol can be obtained by looking at both 1.5 and 3.0 T data acquired for the WISE

study, and by looking at studies on the 3.0 T of group data at rest, and individuals repeated at 3.0 T.

The opportunity of the WISE (Women's Ischemic Syndrome Evaluation) study to look at the same type of patients with 1.5 T cardiac P-31 spectroscopy at both UAB and UF has allowed for a unique comparison of techniques. The data from each site is evaluated at UAB using the same criteria and the Philips Fitmaster™ program for post-processing of data. As shown in Table 18, the magnet systems and techniques are slightly different at each facility, which may account for the difference in degrees of success.

At UF, use of the oblique DRESS protocol, which relies partially on the surface coil to perform some of the localization, has proved to be less than ideal in terms of perfect localization. Too often, it is difficult to place the slice to adequately reduce skeletal muscle contamination and get good SNR, thus being a difficult protocol for good reproducibility requirements.

The ISIS sequence can work well when it can be placed obliquely for maximum flexibility in placement and localization, as can be accomplished on the Philips Gyroscan™ system at UAB. After local modifications of the ISIS sequence for the 3.0 T GE Signa Advantage™ at UF, non-oblique ISIS voxels should be a more reliable and flexible tool for future use. Use of the oblique ISIS voxel has given UAB an advantage in terms of successful studies, compared to a less reliable localization at UF, as shown in Table 18. The criteria for a successful study is the lack of skeletal muscle contamination, represented by $[PCr]/[ATP] > 2.0$ or an SNR low enough that the FITMASTER™ will not process the data due to confusion about which peak

is relevant. UF's success rate is lower, also due to the fact that this data includes the first patient cardiac P-31 acquisitions done at UF, and therefore the learning curve could account for some of the low numbers of successes. Unfortunately, large patients, typical for heart patients, and some difficulties in not having more flexible localization procedure than oblique DRESS capable of localizing to a smaller voxel volume, has meant that failures do occur. Of the last 15 studies done, the success rate was 67% or 10/15 studies successful, which is statistically the same as the overall success rate of 66%.

Table 18. WISE 1.5 T Cardiac Spectroscopy Acquisition Success Rate.

	UF	UAB
System Used	GE Signa Advantage™	Philips Gyroscan™
P-31 Acquisition Method	Oblique DRESS Slice	Oblique ISIS Voxel
Total Studies (as of Jan/99)	32	43
Number of Successful Studies	21	40
% Success	66%	93%
Average Resting [PCr]/[ATP]	1.27	Data Not Available
Standard Deviation of Average	0.48	Data Not Available

At 3.0 T, cardiac P-31 MRS was obtained at rest from nine studies as shown in Table 19. This excludes five studies where the spectra had poor SNR (W.P.) or were contaminated by excess skeletal muscle, demonstrated by a [PCr]/[ATP] value greater than 2.0 after relaxation and blood corrections (T.B., C.M, R.B., & L.R.). It is also interesting to note that three of the four with skeletal muscle contamination (from Table 17) also had longer T₁ relaxation times for ATP. Three of the non-excluded studies were obtained on the same individual, K.S., on different days. This data was obtained with cardiac gating option of "3xRR" on the GE software, which actually gated on every fourth heartbeat. Most data in the literature points to

a normal resting [PCr]/[ATP] ratio for mild ischemia and infarction, therefore it is assumed that the resting values of different individuals will be equivalent.

Table 19. 3.0 T Cardiac P-31 Spectroscopy at Rest Only, 3xRR Gating.

Subject	TR	RCF	Raw Resting	Blood	Relax and
			[PCr]/[ATP]	Corrected [PCr]/[ATP]	Blood Corrected [PCr]/[ATP]
K.S. (Aug 1998)	3.7	1.36	0.867	1.02	1.39
K.S. (Oct 1998)	3.8	1.35	0.623	0.72	0.97
K.S. (Nov 1998)	3.7	1.36	0.925	1.025	1.40
D.P.	4.9	1.22	1.18	1.281	1.56
L.B.	3.3	1.43	0.67	0.704	1.01
E.O.	4.1	1.31	0.926	0.993	1.30
				Average:	1.27
				Std Dev:	0.24

As can be seen, the standard deviation of these six rest [PCr]/[ATP] ratios acquired at 3.0 T (0.24 from Table 19) is half the value of the standard deviation at 1.5 T (0.48 from Table 18). Part of the reason for this reduction in standard deviation of results may be due to having the same operator and shorter duration of the studies allowing for a more standard method of testing.

Of 11 total tests at 3.0 T, five had problems with SNR or skeletal muscle contamination resulting in a success ratio of 55% which is similar to the 66% success rate at 1.5T. Therefore, there was not an increase in successful acquisitions at 3.0 T with the oblique DRESS method.

In terms of repeatability, one ischemic volunteer was tested three separate times at 3.0 T with an average [PCr]/[ATP] ratio of 1.25 ± 0.24 (blood and relaxation corrected), which has the same standard

deviation of the person to person variability of 1.28 ± 0.23 (n=4).

Regardless, this is highly variable data due to the conditions of obtaining data from a moving heart, with a small volume to acquire from while excluding external volumes that may present potential contamination.

The last issue to consider for the protocol developed to obtain in-vivo, cardiac P-31 spectroscopy at 3.0 T is the use of a single-turn or quadrature coil. The quadrature coil provides greater SNR, but can be a hindrance with oblique DRESS. The quadrature coil's broader profile leads to large volumes of acquisition and therefore more difficulty in localizing to cardiac muscle, as described in Chapter 4. In general, comparing single turn coils at 1.5 and 3.0 T, approximately the same volume could be acquired at each field strength, with some displacement error due to chemical shift. This displacement error between PCr and β -ATP is estimated at 2.8 mm at 1.5 T and 4.9 mm at 3.0 T, based on calculations from Ordidge et al.⁷² During the studies, use of a quadrature coil required a longer time for trying out proper placement of the oblique DRESS slice in order to avoid skeletal muscle contamination. The slice would continuously have to be repositioned at deeper and deeper depths to prevent the tall skeletal muscle PCr peak from appearing in the spectrum. From a study perspective, it seems that the quadrature coil is harder to use during the study with greater potential skeletal muscle contamination unless extra efforts are made to place the slice deeper, just posterior to the anterior wall of the heart, as explained in Chapter 4. In a few studies performed with the quadrature coil, however, the skeletal muscle contamination was eventually avoided. Comparing single to quadrature coils at 3.0 T,

again the slice must be placed still deeper from the quadrature coil to obtain a spectrum without skeletal muscle contamination with DRESS. The quadrature coil, therefore may be more ideally suited for an ISIS protocol where the coil is not relied on to be part of the localization procedure. Some tests were performed at 3.0 T with both the quadrature and single turn coils and the results are shown in Table 20. Notice that the average $[PCr]/[ATP]$ ratio (blood and relaxation corrected) for the quadrature coil group is slightly lower than for the single turn coil group although not significantly different ($p=0.16$ using a t-test). This shows that the quadrature coil is equally good at avoiding skeletal muscle contamination in practice, although the slice should be placed deeper to do so as was done in these examples. The tall skeletal muscle PCr peak that is seen more often with the quadrature coil may even be a good feedback mechanism, because more often the skeletal muscle contamination was avoided with the quadrature coil rather than the single turn coil. This peak is most likely obtained from the skeletal muscle to the left of the heart, where the larger periphery of the quadrature coil will reach. With the single turn coil, a slight amount of skeletal muscle contamination is hard to perceive at the time of acquisition, but does show up after post-processing. This is demonstrated for subjects C.M., R.B., L.R., T.B., who had a blood and relaxation corrected $[PCr]/[ATP]$ value greater than 2.0.

Table 20. 3.0 T Cardiac P-31 Results Categorized by P-31 Surface Coil.

Subject	P-31 Coil Type	Relax and Blood Corrected [PCr]/[ATP]
K.S. (Aug 1998)	Quadrature	1.38
K.S. (Oct 1998)	Quadrature	0.96
T.B.	Quadrature	2.24*
	Average:	1.53
	Std Dev:	0.65
K.S. (Nov 1998)	Single Turn	1.38
C.M.	Single Turn	2.50*
D.P.	Single Turn	1.55
L.R.	Single Turn	2.20*
L.B.	Single Turn	1.00
R.B.	Single Turn	2.64*
E.O.	Single Turn	1.29
	Average:	1.79
	Std Dev:	0.64

*Includes data with skeletal muscle contamination

Adequacy of the Hydraulic, In-Magnet, Handgrip Exerciser

Thirty separate individuals tested the hydraulic handgrip, most during scheduled studies for WISE at 1.5 T. The resulting resting and peak exercise, heart rate and systolic blood pressure for each participant is shown in Table 21. All participants are grouped, regardless of medical history, assuming that presence or absence of myocardial ischemia does not affect the response the heart will have to handgrip exercise. The resulting average values for rate pressure product (heart rate times systolic blood pressure) is comparable with the isometric handgrip responses in the literature.⁴⁹ Statistically, the values from Weiss et al.⁴⁹ of 9600 and 12600 for the rate pressure product for rest and exercise, is not statistically different ($p=0.46$ and $p=0.32$ using a t-test assuming equal variance) from the average rate pressure product values shown in Table 21.

Table 21. Heart Rate (HR) and Systolic Blood Pressure (SBP) Response from 30% of Maximum Effort Isometric Hydraulic Handgrip.

Initials	Resting HR	Rest SBP	Rest HR*SBP	Peak Exer HR	Peak Exer SBP	Peak Exer HR*SBP	HR*SBP (Exer-Rest)
E.Q.	53	104	5512	100	161	16100	10588
S.P.	76	120	9120	88	150	13200	4080
A.B.	60	100	6000	72	130	9360	3360
K.S.	62	145	8990	84	219	18396	9406
E.O.	64	124	7936	72	160	11520	3584
G.N.	76	105	7980	92	145	13340	5360
B.H.	70	120	8400	78	160	12480	4080
S.E.	70	124	8680	100	175	17500	8820
S.H.	84	135	11340	108	200	21600	10260
E.K.	84	140	11760	92	166	15272	3512
E.B.	96	160	15360	116	200	23200	7840
H.P.	60	176	10560	72	250	18000	7440
S.J.	96	170	16320	100	200	20000	3680
S.A.	84	120	10080	104	160	16640	6560
J.G.	75	120	9000	100	111	11100	2100
L.C.	80	143	11440	84	146	12264	824
J.F.	86	142	12212	90	179	16110	3898
H.T.	64	136	8704	63	143	9009	305
J.D.	72	156	11232	82	188	15416	4184
R.S.	57	110	6270	67	132	8844	2574
M.P.	65	141	9165	70	153	10710	1545
G.O.	81	122	9882	102	199	20298	10416
E.W.	76	200	15200	79	241	19039	3839
G.A.	77	112	8624	86	133	11438	2814
A.S.	82	114	9348	90	147	13230	3882
K.G.	83	128	10624	86	154	13244	2620
N.W.	70	127	8890	76	151	11476	2586
M.A.	54	117	6318	58	136	7888	1570
L.H.	72	113	8136	76	164	12464	4328
D.M.	86	142	12212	96	158	15168	2956
Average:	74	132	9843	86	167	14477	4634
Std Dev:	11	23	2642	14	33	3998	2924

Another comparison for the adequacy of the stress level that the handgrip stress puts on the heart can be obtained by looking at data available through the WISE study. Each WISE participant who was tested with cardiac P-31 MR spectroscopy exercised in the magnet using the hydraulic handgrip in-magnet exerciser. On some WISE participants,

there is also data on heart rate (HR) and systolic blood pressure (SBP) response from dobutamine (drug induced stressor) and aerobic exercise, treadmill tests. As shown in Table 22, the isometric handgrip exercise produced on average a smaller increase in heart rate but a greater increase in systolic blood pressure than both the dobutamine and treadmill tests were able to do on the same individuals. The blood pressure product (heart rate times systolic blood pressure) is lower for handgrip exercise due mostly to the lesser increase in heart rate.

Table 22. Handgrip Exercise Compared to Dobutamine and Treadmill Responses for Known WISE Studies.

Subject	Handgrip			Dobutamine			Treadmill		
	Max HR	SBP	HRxSBP	Max HR	SBP	HRxSBP	Max HR	SBP	HRxSBP
B.H.	80	138	11040	136	131	17816	147	160	23520
S.E.	100	175	17500	138	150	20700	110	120	13200
G.N.	90	140	12600	147	130	19110	156	160	24960
C.F.	80	230	18400	97	161	15617	100	185	18500
S.H.	108	200	21600	139	200	27800	138	170	23460
L.C.	84	146	12264	153	156	23868	147	170	24990
J.F.	90	179	16110	134	178	23852	131	166	21746
Average	90	173	15645	135	158	21252	133	162	21482
Std Dev	10	34	3843	18	25	4182	21	20	4282

Reproducibility of the Hydraulic Handgrip

The reproducibility of the level of stress provided by the hydraulic handgrip is also very steady, as shown in Table 23. The same volunteer was MR tested on three separate dates in the 3.0 T. Each time the maximum effort was measured for that day and a regimen of 30% of the maximum sustained by the volunteer during the isometric handgrip exercise. As can be seen from the results, the average exercise heart rate was close for all three days. The average diastolic blood

pressure was different at the first date, but similar the last two dates. In contrast, the systolic blood pressure was similar for the first two dates but slightly different for the third date. The resting blood pressure was also different for the first date. This may explain the slight difference in the blood pressure results from day to day.

Table 23. Handgrip 30% Maximum Effort Isometric Exercise Results of K.S. Subject Tested Repeatedly.

Date of Study	Rest HR	Exercise HR	Rest BP	Exercise BP	Rest HR*SPB	Exercise HR*SPB
8/10/98	65	77	162/76	178/97	10530	13706
10/12/98	63	77	145/75	191/95	9135	14707
11/11/98	65	79	149/68	195/103	9685	15405
Average	64	78	152/73	188/98	9783	14606
Std Dev	1	1	9/4	9/4	703	854

No Drop in [PCr]/[ATP] During Exercise with Reference Volunteer

As explained earlier in the literature review on ischemia, data is available from three sources on the percent change in [PCr]/[ATP] with handgrip exercise on groups of reference subjects without cardiac ischemia. From that data the threshold for significant drop in the percent change in [PCR]/[ATP] with handgrip exercise is -20.6% (UAB, n=17),⁴⁵ -14% (Weiss et al., n=11),⁴⁶ or -18% (Yabe et al., n=11)¹² based on two standard deviations. The study at UAB involved using non-ischemia symptomatic subjects, but none of the reference subjects were tested clinically for silent ischemia. The results at UAB may therefore include silent ischemic subjects, and this may explain the higher standard deviation compared to the other sites. Since threshold data was available, and because locally there was not funding to clinically test volunteers for possible silent ischemia prior to

cardiac P-31 MRS, no non-clinically tested subjects were subjected to in-magnet exercise for the purpose of determining a standard deviation and threshold. Funding is being sought from NIH to perform adequate cardiac evaluations of reference group subjects prior to testing via cardiac P-31 MRS for the near future. The true threshold for studies at UF performed with oblique DRESS may be lesser or greater than the published values. The larger standard deviation threshold of -20.6 \pm will be used to estimate statistical significance of [PCr]/[ATP] with handgrip exercise at this time.

One subject who appeared quite healthy (E.Q.) but also was not clinically tested was, however, tested to demonstrate the ability of the handgrip exercise and P-31 measurement. This subject was tested at 1.5 T and substantially raised her heart rate and blood pressure during the exercise portion of the study, as detailed in Table 24. Despite the subject's significant response to the handgrip exercise, there is no significant difference in the rest versus exercise spectra with the small change of +2.84%. As duplicated in the literature, this study's result demonstrates that without cardiac ischemia one cannot lower the [PCr]/[ATP] ratio of the myocardium with in-magnet exercise of isometric handgrip at 30 \pm maximum.

Table 24. Results from 1.5 T Cardiac P-31 Exercise Study on Reference Normal Volunteer.

Acq	Avg	Avg	HR	Blood		Blood &
	HR	BP	*	Raw	Corrected	Relaxation
			SBP	[PCr]/[ATP]	[PCr]/[ATP]	[PCr]/[ATP]
Rest	53	104/64	5512	0.605	0.762	0.986
Exercise	83	136/86	11288	0.647	0.792	1.014
Recovery 1	55	105/62	5775	0.773	1.005	1.286
Recovery 2	55	105/62	5775	0.682	0.828	0.828
				% change		+2.84%

Drop in [PCr]/[ATP] Seen with the Handgrip Exerciser with Ischemia

To prove that the hydraulic handgrip exerciser can produce a drop in [PCr]/[ATP] in the ischemic heart, subjects were tested that were thought to be ischemic. The first subject, K.S., had been shown by treadmill ECG to be mildly ischemic with high intensity exercise. The second subject, E.O., was a WISE study participant, meaning that microvascular ischemia was suspected based on symptoms and catheterization results. As shown in Table 25, K.S. was tested four times, once at 1.5 T. In three of the five cases, a significant drop in [PCr]/[ATP] was measured, again based on the UAB data where a -20.6% drop was considered significant. The second study showed a large drop (-13.95%) but was not significant based on the data from UAB, although it could almost be considered significant based on the threshold determined from reference studies by Weiss et al.¹⁷ The fourth study did not show a drop, but this 3.0 T study was performed after and on the same day as the 1.5 T study. Perhaps some unknown factor prevents the cardiac study from being repeated on the same day reliably. There could be some degree of acidosis in the myocardium from stress earlier that day that changed the energy to a anaerobic state sooner, as will

be further described in the section on pH measurements at 3.0 T. The second volunteer, a participant in the WISE study with chest pain and suspected of having microvascular ischemia, also showed a significant drop (-29.13% > -20%) in [PCr]/[ATP] with in-magnet, handgrip exercise.

Table 25. Ischemic and WISE Studies at 3.0 T Show Drop in [PCr]/[ATP] with Handgrip Exercise.

Subject	Study Date	Field	Resting	Exercise	% Change
		Strength	[PCr]/[ATP]	[PCr]/[ATP]	
K.S.	11/11/98	1.5 T	1.61	1.24	-23.25
K.S.	8/10/98	3.0 T	1.15	0.99	-13.95
K.S.	10/12/98	3.0 T	0.81	0.57	-29.09
K.S.	11/11/98	3.0 T	1.16	1.14	-1.55
E.O.	2/25/99	3.0 T	1.13	0.80	-29.13

Myocardial pH Measured at 3.0 T

At 3.0 T it is possible to differentiate the Pi peak from the blood 2,3-DPG peaks. Myocardial pH is proportional to the chemical shift difference in ppm between Pi and PCr. For seven (3 repeated with K.S. and 4 more on separate subjects) of the 3.0 T studies performed, the Pi peak was visible and the Pi to PCr ppm difference was recorded. Based on this, the pH was measured using the 3.0 T system, as described in the Human Techniques chapter, resulting in an average resting pH of 7.10 ± 0.14 , as listed in Table 26. Referring back to the values for cardiac pH typically found in the literature, as listed in Table 10 in the literature review chapter, the typical pH of the resting heart muscle has been shown to be around $7.15^{165,167}$. This average resting result measured at 3.0 T is not statistically different from the literature values ($p=0.41$ based on a t-test of two samples for means).

An ischemic subject (K.S.) was tested three times at 3.0 T and all three times pH was recorded during rest and exercise. On two of the occasions, the pH did not drop significantly with exercise ($p=0.45$ and $p=0.49$ based on t-test for two samples for means), but on a third occasion a significant drop was seen ($p=0.05$), as shown in Table 26. The reason for this drop is hypothesized to be associated with receiving a cardiac stressor earlier that same day of the pH drop, causing the heart to use more anaerobic cycles during the second stressor which caused pH shift.

Table 26. Myocardial pH as Measured on Human Volunteers using Oblique DRESS Cardiac P-31 MRS on the GE 3.0 T SIGNA® for those Studies where the Pi Peak was Discernible due to Adequate SNR.

Subject (Date)	Pi-PCr ppm at rest	pH at Rest	Pi-PCr ppm with handgrip exercise	pH with Handgrip Exercise
K.S. (Aug 1998)	4.945	7.10	4.873	7.04
K.S. (Oct 1998)	4.58	6.82	4.588	6.83
K.S. (Nov 1998)	4.949	7.11	3.839	6.24*
C.M.	4.898	7.06	-	-
D.P.	5.006	7.15	-	-
L.B.	5.101	7.24	-	-
R.B.	5.101	7.24	-	-
Average:	4.94	7.10		
Std Dev:	0.18	0.14		

* Denotes significant drop ($p=0.05$) in pH compared to resting value with handgrip exercise

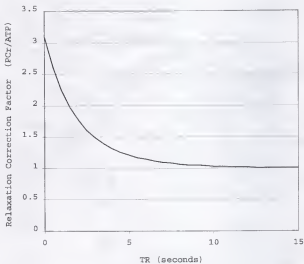


Figure 62. Relaxation correction factors at 3.0 T for cardiac $[PCr]/[ATP]$ values based on repetition time (TR) values.

CHAPTER 6
SUMMARY AND CONCLUSIONS

Phosphorus, in-vivo, human, cardiac spectroscopy over the anterior region of the heart is not only possible at 3.0 Tesla, but eminently feasible. The 3.0 T GE Signa Advantage™ system at the University of Florida has been carefully evaluated in terms of imaging and spectroscopic capabilities, for gathering P-31 spectroscopy data of the heart. Advantages and disadvantages of such imaging and spectroscopy techniques such as spin echo imaging, multivoxel CSI and ISIS have been explored and a protocol for the 3.0 T GE Signa Advantage™ has been recommended. This protocol included using gradient echo imaging, PRESS proton spectroscopy for shimming, and oblique DRESS slice selection for cardiac P-31 acquisitions. A 25 x 25 cm² square, single loop, proton surface coil was utilized for imaging and shimming. Two P-31 RF coils, a 9.5 cm diameter single-turn and a 10 x 16 cm² quadrature design, were created and utilized. It was found that the quadrature coil has potential to provide greater SNR than the single turn RF coil, but at the price of needing to acquire a deeper slice when used with the oblique DRESS protocol.

In addition, a hydraulic handgrip exerciser was designed and tested in the magnet. This in-magnet exercise was found to evoke a similar response, in terms of blood pressure and heart rate, when compared to similar literature studies and other types of cardiac stress such as drug induced dobutamine stress and treadmill exercise.

In addition, three out of five cases of subjects with known or suspected ischemia showed a significant drop (-23.25%, -29.09% and -29.13%), of greater than 20% in their [PCr]/[ATP] ratios with the handgrip exercise. On two occasions where the drop was not greater than -20% there was still a large drop of -13.95% in [PCr]/[ATP], which falls between the first and second standard deviations (-10% and -20%) statistically based on studies of random volunteers not tested for ischemia. It is expected that future studies with more carefully controlled subjects who have been screened for the lack of cardiac ischemia, will provide tighter standard deviations. The final evaluation did not show a drop in [PCr]/[ATP], however, it did show a significant drop in pH ($p=0.05$). This may be the result of use of the anaerobic energy cycle due to stressing the heart earlier on the same day.

As previously reported in the literature, volunteers not thought to have ischemia did not show a change in the [PCr]/[ATP] ratio with exercise. No other volunteers were tested due to the lack of cardiac medical testing that would have ruled out ischemia. The handgrip exercise test was also shown to work on a linear scale and to be repeatable and equally stress the heart each time it is used. In short, the protocol that has been designed here to obtain cardiac P-31 spectra at 3.0 T, on the GE Signa Advantage™ is adequate for continued use in testing more WISE patients and will be used with future cardiac patient studies.

Implications for Future Research

More extensive work should be done to improve the RF profiles for use at 3.0 T. All work done for this dissertation used the generic GE pulse sequences, with a few minor changes in EPIC by Dr. Kim. The consequence of this is that the RF pulse was the same as that designed for 1.5 T, resulting in more contamination from outside the slice at 3.0 T.

As of the date of this writing, an upgrade for the 3.0 T GE Sigma Advantage™ at the University of Florida has been ordered. The upgrade will include increasing the gradient strength to 4 Gauss/cm up from the current 1 Gauss/cm. The increased gradient should provide for more accurate ISIS localization, especially with planned improvements to the ISIS pulse sequence.

Improvements in the image quality were not focused on more sophisticated coil designs that provide a more homogeneous, volume excitation. The image quality in this work was good enough for spectroscopy localization purposes, but improving the image quality could help move toward more diagnostically acceptable images and techniques.

It was the intention of this work to create a protocol that could be used to investigate cardiac function for the purpose of investigating ischemia, although this technique could easily be expanded to look at other types of cardiac disease states. Most of the WISE participants already studied at 1.5 T could be immediately restudied at 3.0 T, taking advantage of the visibility of the Pi peak, making pH measurement possible, in addition to increased SNR and spectral dispersion. In addition, the microvascular ischemia study can

be extended to both male and female patients at the Veteran's Affairs Hospital to test the viability of P-31 spectroscopy as a screening test for microvascular ischemia. In a broader sense, the protocol can be used to study any type of cardiac problem where the cardiac metabolism is thought to be altered. In the literature, this has included disease states such as ischemia, infarction, cardiomyopathy, hypertrophy and heart transplants. This list could be expanded to looking at drug therapies and the cardiac muscle's response to intense exercise, studies that have been done on skeletal muscle. Further roles in research could also include investigating the heart with other nuclei such as H-1 and C-13, where there are opportunities to learn more about glycolytic and citric acid cycle energy metabolism as well as the tissue oxygenation status of the heart. Currently, research has also started on cardiac H-1 spectroscopy where creatine depletion is thought to be a measure of cardiac necrosis.²²⁶ Bottomley et al.²²⁶ studied 10 subjects with myocardial infarction and 10 controls. The study conjectures that not only does spatially localized H-1 MRS measure total creatine non-invasively in the heart, but that the detection of regional creatine depletion may provide a metabolic means to distinguish healthy from infarcted myocardium, as P-31 MRS offers with the drop in $[PCr]/[ATP]$ and pH with exercise.

In order for cardiac P-31 spectroscopy to advance from the research to the clinical arena, much work must be done. First, there must be improvements in pulse sequence localization to the anterior myocardium without as much risk of skeletal muscle contamination. Second, there must be more studies to increase the statistical relevance of this testing procedure. Although reports of human, in-

vivo, cardiac spectroscopy have been published for about 10 years, and data seems to clearly show a relationship between P-31 metabolite changes and ischemia, most studies are very small in number and have inherently large variability in resulting [PCr]/[ATP] values. In addition, diseases other than ischemia and infarction have shown wide variations in the literature in terms of being a marker for metabolic changes in cardiomyopathy or heart transplant cases. In addition, since in-vivo, cardiac spectroscopy is currently limited to the anterior portion of the heart due to SNR difficulties with depth, the abilities to look at the whole heart will also determine clinical viability. Such advancements may be obtained through improvements in coils (such as phased array designs), localized pulse sequence optimizations for cardiac spectroscopy, and increased gradient strength. Unfortunately, these advancements will be difficult to take advantage of due to obstacles such as increased sensitivity to motion, larger bandwidths of the required RF pulses, and limitations with specific absorption rate (SAR) guidelines.² Another roadblock for clinical use of human, in-vivo, cardiac P-31 spectroscopy is the simple implementation of the technique. The moving heart is a challenge, especially in the motion sensitive MR environment.

Advances in computing may also assist in the ability and increased accuracy of cardiac P-31 spectroscopy to move beyond peak metabolite ratios and provide metabolite concentrations. This can be closer to being accomplished when the true volume of myocardium that is contributing to the spectroscopy signal can be defined with little error using computer models based on empirical MR images. This will be useful for looking at infarction, where dead tissue contributes no

signal, but also does not change [PCr]/[ATP] ratio with exercise. In the case of infarction, a reduction in metabolite concentration in an area of interest will define the affected region. Advanced computer programs and graphics can also assist with the complicated post-processing needed to show an image of the heart in terms of a map of metabolite concentrations. This would show an image very comparable to SPECT nuclear medicine studies. At this point, some attempts at calculating metabolite concentrations in the heart and mapping the concentrations have been started, but are still crude, error prone and in need of improvements. Advancements in computer technology certainly will assist in this endeavor.

While human, in-vivo, cardiac P-31 spectroscopy has yet to define a precise position in the diagnosis and treatment of heart disease, the technique has proved valuable in the measurement of cardiac function via the myocardial energy metabolites.

APPENDIX A
IRBS AND SCREENING FORMS

University of Florida Institutional Review Board (IRB) Informed Consent
Forms and MRI Screening Forms for 1.5 and 3.0 Tesla Volunteers for
Human, In-Vivo, MR Spectroscopy Cardiac Studies

IRB Protocols

This dissertation was covered under three separate IRB protocols.

1. IRB #459-97: Human In-Vivo Cardiac Phosphorus NMR Spectroscopy at 3.0 Tesla

The first IRB covered all of the 3.0 T cardiac spectroscopy work on men and women volunteers for the period of time from the start of work up until January 9, 1999. This IRB was specifically designed for use with this dissertation with the principal investigator listed as Dr. Katherine N. Scott (IRB # 459-97). Most of the volunteer data in this work is covered by this IRB. The current IRB informed consent which is valid until 1/9/99 is included in this appendix.

2. IRB #376-96: Evaluation of Ischemic Heart Disease in Women - Clinical Centers (EIHDC)

Women patient and volunteer studies at 1.5 T were originally covered under the IRB for the WISE study with the principal investigator listed as Dr. Carl Pepine (IRB # 376-96). This IRB was

later expanded to include 3.0 T. The current IRB informed consent which is valid until 10/7/99 is included in this appendix.

3. IRB #452-98: P-31 Magnetic Resonance Evaluation of 3.0 T Ischemic Heart Disease in Men

Men patients and volunteers for study at 3.0 T are covered under this IRB with Dr. Katherine N. Scott listed as the principal investigator (IRB #452-98). This IRB was created in late 1998 to cover preliminary tests of men's ischemic heart disease in the 3.0 T whole body system. The current IRB informed consent which was valid until 1/9/99 is included in this appendix.

Screening Forms

In addition, an example of the screening forms used at the 1.5 and 3.0 T systems are shown. These screening forms are necessary to rule out a patient history that would indicate metal in the body, and thus make the MR system unsafe for that patient.

1. IRB #459-97: Human In-Vivo Cardiac Phosphorus NMR Spectroscopy at
3.0 Tesla

IRB# 459-97

Informed Consent to Participate in Research

The University of Florida
Health Science Center
Gainesville, Florida 32610

You are being invited to participate in a research study. This form is designed to provide you with information about the study to help you understand your decisions. If you have any questions or concerns about the informed consent process or the research study, please contact the
Committee on Review Board (COB), the committee that protects human subjects, at (352) 392-
1454.

1. Name of Subject:

2. Title of Research Study

Human In-Vivo Cardiac Phosphorus NMR Spectroscopy at 3.0 Tesla

3. a. Principal Investigator(s) and Telephone Number(s)

Katherine N. Scott PhD
Professor of Radiology, University of Florida, Box 100374
8. Cancer Research Scientist, Veterans Affairs Medical Center
(352) 273-1611, X5066

b. Sponsor or the Study (if any)

None

4. The Purpose of the Research

Magnetic resonance imaging (MRI) creates pictures of the body with magnets rather than x-rays. Magnetic resonance spectroscopy (MRS) uses a technique similar to MRI to gather chemical information in the form of spectra about the tissues in your body. We will be doing MRI and MRS of your heart, while you rest, to do exercises in the regional. The ultimate goal of this work is to provide diagnostic information about the health of your heart. You might also be asked to provide a sample of blood for chemical analysis.

APPROVED

From John F. To John F.
heretofore we have found John F.

Received 8/1/97

5. Procedures for this Research

Chemical information about your heart and tissues of your body will be obtained in the same fashion that an ordinary MRI scan would be done. The 3.0 Tesla scanner is similar to an ordinary MRI scanner, except that it has a higher strength of the magnetic field. Pictures and/or graphics will be obtained and the effectiveness of the scanner and the procedure will be evaluated from this information. You may be asked to have a second scan with a different "tagging" on the scanner such as twisting or pulling against a device, possibly garments while in the MRI scanner such as a vest or tie down or more. However, the number of scans will differ from one test to another. This 3T MRI scanner is currently considered an investigational device by the Food and Drug Administration.

You will be asked to provide up to 96 cups of blood for chemical analysis. This volume is necessary to suffice demands arising when the blood sample is checked in the MRI scanner. A person qualified to handle raw blood (a Venipuncturist) will perform this procedure. If you do not consent to blood testing, you will not have this procedure, but you still can participate in the program.

You wish to provide a sample of blood for chemical analysis

YES NO

Signature of Subject or Representative

Date

Received 8/1/97

Potential Health Risks or Discomforts Biological, Chemical, Electrical, and Physical Hazards to Others

If you are the first or sole author of this study, **you will be the principal investigator**. MFL and MHS are co-authors and who alone will be responsible for the design and conduct of the study, analysis and interpretation of the data, and the preparation and submission of manuscripts for publication. All other authors (including MFL and MHS) will be listed as co-authors. You will be the primary contact for all correspondence regarding this study. You will be responsible for the day-to-day management of the study, including recruitment of participants, collection and analysis of data, and interpretation of results. You will be responsible for the preparation and submission of manuscripts for publication. You will be responsible for the day-to-day management of the study, including recruitment of participants, collection and analysis of data, and interpretation of results. You will be responsible for the preparation and submission of manuscripts for publication.

The minimal risks of the arm's eye scanner were similar to those of the current MRI scanner. When this radio receiver string or array was higher than the conventional MRI scanner, there was a small chance of damage to the ear canal of your skin. All of these adverse localized incidents of loss of hearing have been specifically designed to prevent this from occurring.

The risks of taking a blood sample include discomfort at the site of the puncture, possible bruising and swelling, merely an infection, and, uncommonly, faintness from the procedure.

Digitized by srujanika@gmail.com

Gesamt-Durchschnitt

In the unlikely event of you suffering a physical or physiological injury which is presently caused by this study:
 professional medical; OR professional dental; OR professional osteopathic

can be received at the University of Florida Health Science Center will be provided without

You will not have to pay hospital expenses if you are being treated at the Veterans Administration Medical Center (VAMC) and sustain any physical injury during participation in VAMC-administered exercises.

12. Attitudes to Participating in this Research Study

Answers to Participating in This Research Study

You are free not to participate in this study. If you choose to participate, you are free to withdraw your consent and discontinue participation in this research study at any time without this decision affecting your medical care. If you have any question regarding your rights as a subject, you may phone the Institutional Review Board (IRB) office at (352) 846-

If you believe that your participation in this research project along with other volunteers will pose a risk to you or others, you have been invited to participate in this study or not may not affect your rights as a participant in this study. Your participation in this study is voluntary and you are free to withdraw from or not to participate at any time without penalty.

POLISH FOLK TALES

There is no charge to you as a volunteer for this study.

participation in this study is voluntary and anonymous.

If you believe that your participation in this study or your decision to withdraw from or to not participate in this study has imposed any significant burden on you, you should discuss this with the principal investigator or a member of the research team.

16. Signatures

Subject's Name _____

If you wish to stop your participation in this research study for any reason, you should contact: Kishimoto, H. Scott, M.D., [252] 305-1811 and 50568... You may also contact the Institutional Review Board (IRB) Office at [252] 848-1494.

13. Withdrawal From This Research Study

If you wish to stop your participation in this research study for any reason, you should contact: Kishimoto, H. Scott, M.D., [252] 305-1811 and 50568... You may also contact the Institutional Review Board (IRB) Office at [252] 848-1494.

14. Confidentiality

The University of Florida and the Veterans Administration Medical Center will protect the confidentiality of your records to the extent provided by Law. You understand that the Study Sponsor, Food and Drug Administration and the Institutional Review Board have the legal right to review your records.

Signature of Principal or Co-Principal
Investigator or Researcher (or obtaining consent)

Date

Signature of Subject or Representative

Date

If you are not the subject, please print your name _____
Indicate one of the following:

15. Assistant Procedure (if applicable):

Not Applicable.

 The subject's parent The subject's guardian A surrogate A durable power of attorney A proxy Other, please indicate: _____

Signature of Witness

Date

If a nonrelative signs and incorporates, the subject of this research should indicate by signing below.

Y

Signature of Signator

Date

1. IRB #376-96: Evaluation of Ischemic Heart Disease in Women - Clinical Centers (EIHDW)

What will you do if you take part in this research study?

IRB Condition Nr. 10/2/96
 Revision 5/2/97
 Review 1/15/98
 IRB Credential #229

Informed Consent to Participate in Research

The University of Florida
 Health Science Center
 Gainesville, Florida 32610

You are being asked to participate in a research study. This form provides you with information about the study. The Principal Investigator (the person in charge of this research) or his/her representative will also describe this study to you and answer all of your questions. Read the information below and ask questions about anything you don't understand before deciding whether or not to take part. Your participation is entirely voluntary and you can refuse to participate without penalty or loss of benefits to which you are otherwise entitled.

Name of the Subject

Title of Research Study

Evaluation of Ischemic Heart Disease in Women - Clinical Centers (EIHDW)

Principal Investigator(s) and Telephone Number(s)

Carl J. Pepine, M.D.
 (352) 344-0630

Sponsor of the Study

National Heart, Lung, and Blood Institute

What is the purpose of this study?

The purpose of this study will be to better understand chest pain in women, and to develop diagnostic tools that improve a physician's ability to accurately determine which women with chest pain have disease in the arteries that supply blood to your heart.

APPROVED

From: Carl J. Pepine To: Carl J. Pepine
 Institutional Review Board (I.R.B.) Date: 1/15/98

Approved

Page 1 of 8

Revised 1998

admission will be referred as a bolus in the coronary artery and the blood flow through the vessel will be measured. The administration of the nitroprusside and atergactoline will prolong the procedure by approximately 15 minutes.

After the cardiac catheterization, pertinent recommendations will be given to you based on the results of these tests. These may include the recommendations for medical therapy, procedures such as balloon angioplasty or bypass surgery, or referrals to other specialists such as gastroenterologists for further evaluation of the test.

After the cardiac catheterization, a series of images will be taken to undergo imaging of the heart muscle in a special magnet. This test is called Magnetic Resonance Spectroscopy (MRS). This is a method of determining the energy levels at the muscles of your heart with an imaging device similar to a CT scan but without the x-ray. During this test, you will be asked to lie in the magnet for a resting period while baseline images are obtained. You will then be asked to squeeze a handgrip repetitively until your become fatigued. Images will be taken during the exercise and after exercise is completed. The testing period will last approximately one hour. This test will be done in one of two different strength magnetics, the 1.5 T or the 3.0 T.

Regardless of the recommendations you receive, you will be asked to return to the office annually for a brief physical examination and assessment of your current medical status for the next four years and will be contacted by phone every six months to see how you are doing. If medically indicated, scans or all of the procedures may be repeated over that next 3-4 years. The lectures to review the tests will be made between you and your physician. With your permission we will obtain the information obtained from these tests to provide a more complete picture of your cardiac status.

At the final visit at the end of your year, you will be asked to have a repeat physical examination, ECG, exercise stress test, quality of life assessment, and forearm study.

The Carotid Catherization, exercise stress test, and forearm studies are part of your standard care. The Dobutamine stress test and Doppler flow measures, in some patients, will also be part of standard care. All other testing is for study purposes only.

Your participation in this study can be terminated, without your consent, by your physician. Participants may be terminated by your physician if you fail to follow the directions of your physician.

If you decide not to participate in this study, your alternative is to continue your evaluation and treatment here with the doctors in the cardiology clinic, or with your private doctor. If you do not have a doctor, we will refer you to a doctor here or in your community.

What are the possible discomforts and risks?

ECC (Electromagnetic): No risks are involved.

Dobutamine Stress Echocardiogram: This procedure involves the administration of dobutamine so as to dilate through a catheter placed in your vein. This medication is increased gradually over a 20 minute period and results in a gradual increase your heart rate, similar to what would occur if you were to exercise. During the infusion a probe will be placed on your chest which will provide ultrasound or sound waves to view the structure and function of the heart in baseline and in response to the medication. There are no risks involved with the Doppler machine. Dobutamine may be associated with nausea, sweating, palpitations, and flushing. There have been rare reports (<1%) of severe chest pain and heart attack.

Lipoprotein Cloning: This procedure involves the use of ultrasound or sound waves to view the structure and function of the heart. No risks are involved.

Exercise Treadmill Test (ETT): There are potential risks (approximately 2-3 per 10,000) associated with the exercise stress testing to be done. These include episodes of temporary lightheadedness, feelings of chest pain, shortness of breath, palpitations, and very rarely, heart attack. The checkup before the test, administration of qualified personnel during the test, and emergency treatment readily available are all part of the safeguards included in the procedure.

Hemangioma: Atergactoline has been used in the coronary arteries in over 1000 patients (1.1 has also been used in the arm arteries in over 1000 patients) as well without any serious side effects or permanent side effects. There is the possibility with any medication given directly into the heart of side effects including chest pain, blockage of blood flow in the artery, or arrhythmia heart beat. The cause of these side effects is usually related to rates (concentration) of the drug. This is uncommon (5% of patients). The drug is easily removable with dialysis/catheter. Any unexpected side effects such as heart attack or stroke can occur with any heart medication. Any unexpected side effects that might occur with atergactoline can be treated with the catheterization laboratory. Having this catheter will increase the catheterization risk (approximately 1% patients). This increase in risk does not expose you to any additional risk above that already exposed to you.

Adalatine: The side effects associated with adalatine include chest pain, headache, shortness of breath, flushing and nausea. They are extremely short-lived (seconds) because of the short duration of adalatine. One or more of these side effects occurs in 30% of patients overall.

Intracoronary Doppler: The Doppler catheter and Doppler wire are FDA approved for intracoronary use. The trials indicate, but are unverified in, possible perforation (tear) of the blood vessel wall. A blood clot could form in the blood vessel, the blood vessel could become occluded as a result of the catheter. The use of these catheters does not increase the risk of catheterization above the known risk of 1-2 per 1000 of serious complications like stroke, heart attack or death.

Blood Draw: The risks of drawing blood from a vein include dislodgment at the site of injection possible bruising and swelling around the angio line (newly an adhesive, and, unconsciously, fatalities from the procedure. Blood drawn each time will be approximately 2 tablespoons. The total amount drawn during the study will be approximately 8 tablespoons.

Quality of Life Questionnaire. Some of the questions in the quality of life questionnaires may ask you to consider areas of your life about which you may not currently think about. There are no physical risks from completing the survey, but the questions could cause you concern or emotional distress.

46. Hair Follicle Monitors: Broken no risks and only occasional skin irritation due to the adhesive for electrode placement.

Femoral Ultrasound: The ultrasound test involves placing a probe on the artery to measure the blood flow in your arm. This test requires the withdrawal of a blood pressure cuff which may result in some temporary mild discomfort. There are no risks to the procedure.

Magnetic Resonance Spectroscopy (MRS): This is a procedure which allows your doctor to look at internal body parts using a scanner that sends out a strong magnetic field and radio waves. This is a routine medical procedure and a very safe for most people. However, if you have any type of metal embedded in your body, you may not be able to have the MRS. Sometimes we will ask you questions before you have the procedure. You will not be able to have the study if you have any metallic devices (such as a heart pacemaker) in your eyes, or certain types of hearing devices and brain aneurysm clips. In addition, the MRS scanner produces a "harmonica" noise which has been reported to have produced hearing loss in a very small number of patients. You will be given pamphlets to further reduce this risk. It is possible that you develop chest pain during the duration of the study. Study patients have experienced discomforts (a few of which are traced) which is relieved by getting out of the magnet. You will be monitored during the entire study.

If you wish to discuss items of any other discomforts you may experience, you may call Dr. Poppe at (312) 446-0230.

What are the possible benefits to you or to others?

The benefits which you might reasonably expect from taking part in this study are first being evaluated and having your doctor a better picture of your heart condition. There is no guarantee that your participation will directly benefit you. Other patients with a similar condition may benefit from information obtained in this study.

If you choose to take part in this study, will it cost you anything?

There are no financial risks associated with your participation in this study. The financial obligations incurred for the testing are not different from what would be charged for a routine evaluation. The exercise test, echocardiogram, and cardiac catheterization are considered standard procedures to evaluate patients with chest pain. Your insurance will be billed as is normally done for this type of evaluations. The magnetic resonance screening (MRS) will be paid for by the study.

Will you receive compensation for your participation in this study?

The 48 hour ambulatory monitor, quality of life assessments, blood drawn for female hormones, electrolyte checks and doppler catheter during the catheterization, and MRS imaging will be provided at no charge to you.

***You will receive some of the tests at no charge to you.**

What if you are injured because of the study?

If you experience an injury that is directly caused by this study, only professionals medical —— professionals in detail, —— professional caregivers can treat you. At the University of Florida Health Science Center will be provided without charge. However, legal expenses will have to be paid by you or your insurance provider. No other compensation is offered.

You will not have to pay hospital expenses if you are being treated at the Veterans Administration Medical Center (VAMC) and experience any physical injury during participation in a VAMC-approved study.

You will not have to pay hospital expenses if you are being treated at the Veterans Administration Medical Center (VAMC) and experience any physical injury during participation in a VAMC-approved study.

If you do not want to take part in this study, what other options or treatments are available to you?

You are free set to participate in this study. If you choose to participate, you are free to withdraw your consent and discontinue participation in this research study at any time without this decision affecting your medical care. Alternative treatment would be to consult with standard medical therapy currently currently in use for your disease. If you have any questions regarding your rights as a subject, you may please the Institutional Review Board (IRB) office at (312) 446-1444.

How can you withdraw from this research study?

If you wish to withdraw from participation in this research study for any reason, you should contact Dr. Carl Pepke at (312) 446-0230. You are free to withdraw your consent and stop participation in this research study at any time without penalty or loss of benefits in which you are otherwise entitled. Throughout this study, the researchers will notify you of new information that may become available and that might affect your decision to remain in the study.

In addition, if you have any questions regarding your rights as a research subject, you may phone the Institutional Review Board (IRB) office at (312) 446-1444

How will your privacy and the confidentiality of your research records be protected?

Authorized persons from the University of Florida, the Hospital or clinic (if any) involved in this research, and the Institutional Review Board have the legal right to review your research records if the project is sponsored or if it is being conducted under the authority of the United States Food and Drug Administration (FDA), than the sponsor, the sponsor's agent, and the FDA also have the legal right to review your research records. Otherwise, your research records will not be reviewed without your consent unless required by law or a court order.

If the results of this research are published or presented at scientific meetings, your identity will soon be disclosed.

Will the researchers benefit from your participation in this study (by need publishing or presenting the results)?

There is no conflict of interest involved with this study beyond the professional benefit from academic publication or presentation of the results. [Year name and personal information will not appear in print or be presented in a manner which could identify you.]

Signatures

As a representative of this study, I have explained the purpose, the procedures, the benefits, and the risks that are involved in this research study.

[Signature]

[Date]

[Signature of person obtaining consent]

[Date]

[Signature of witness]

[If available]

[Date]

3. IRB #452-98: P-31 Magnetic Resonance Evaluation of 3.0 T Ischemic Heart Disease in Men

In frequency coil) will be placed on your chest, over your heart. A computer locates the radio waves passing through your heart and constructs pictures and chemical information of your heart. The total procedure will last approximately 90 minutes. While you are at the magnet, we will also use to acquire a fluid-filled rubber bulb. This will exercise your heart, and will let us see how your heart responds to exercise.

APPROVED

The University of Florida
Health Sciences Center
Gainesville, Florida 32610
Date: 10/22/98
Signature: [Signature]

You are being invited to participate in a research study. This form provides you with information about the study. The Principal Investigator (the person in charge of this research) or his/her representative will fully describe this study to you and answer all of your questions. Read the information below and ask questions about anything you don't understand before deciding whether or not to take part. Your participation is entirely voluntary and you can refuse to participate without penalty or loss of benefits to which you are otherwise entitled.

*Name of the Subject:

>

Title of Research Study

P-31: Magnetic Resonance Evaluation of 3.0 T of Ischemic Heart Disease in Men

Principal Investigator(s) and Telephone Number(s)

Katherine N. Scott, Ph.D., Telephone: (352)392-1611, Extension 1046

Sponsor of the Study

Venetech Affairs Medical Research Service

What is the purpose of this study?

This is a part of a research project to learn more about the behavior of your heart. Our aim is to test pictures of your heart without the use of X-rays. That part of the test is called magnetic resonance angiography or MRA. Then we will get information about the chemistry of your heart without the use of dyes and laboratory tests. This part of the test is called magnetic resonance spectroscopy or MRS.

What will be done if you take part in this research study?

You will lie on a bed, which rolls into the opening of a large magnet. A flat coil of wire (a radio

Informal Consent to Participate in Research

Date: 9/5/98

At a later date, (1 month or 1 year later) the procedure will be repeated. This will let us see whether the chemistry of your heart is changing.

The chemical information part of the test is experimental. We have been able to many volunteers and patients at other institutions. It has been done under Dr. Scott's guidance on male and female volunteers and on female patients at the University of Florida and the VA Medical Center.

We plan to compare the results of this test with the results of other tests that your doctor has ordered, such as blood tests, ventriculogram (ECG), treadmill ECG, nuclear medicine scans, and cardiac catheterization. We ask your permission to obtain this information from your medical records.

You give us permission to obtain this information from your medical records.

YES _____

NO _____

Signature of Subject _____

Date _____

If you are a healthy volunteer (a reference subject), you did not have any other tests done. Therefore, we are not asking your permission to obtain information from your medical records.

You are a healthy volunteer (a reference subject).

YES _____

Signature of Subject _____

Date _____

What are the possible disadvantages and risks?

Your hand will get tired from squeezing the (filled) rubber bulb, but there is no other discomfort associated with the procedure.

The risk of this study to you will be minimal. MRI and MRS are very safe for most people. However, if you have any type of metal implanted into your body, you may not be able to have the MRI/MRS. Someone will ask you questions before you have the MRI/MRS. You will not be

Assent 3.0

Document 3.0

able to have the study if you have any pacemakers, devices such as a hearing aid, metal in your eye, any bone structure clips, or certain types of heart valves. Likewise, metal objects such as steel, glasses, hairpins, jewelry, and needles should not be present when you go into the scanner.

In addition, the MRI scanner produces a "humming" noise, which has been reported to have produced learning loss in a very small number of patients. You will be given earplugs to further reduce this risk. You will be instructed during the entire study because of the small space made by the MRI scanner, you may require sedation (sedation is when you sleep) if you are uncomfortable in small spaces. If you do require sedation, you will not be able to drive a car or perform other serial tasks for 4-6 hours afterwards because of drowsiness.

The radio waves of this magnetic scanner are similar to those of the conventional MRI scanner. The radio waves may or may not be stronger than those for a conventional MRI scanner. We hope the heating effects within the guiders will be the same. All of the controls used on the scanner and in this study have been specifically designed to prevent this from occurring. However, if you feel any localized heating sensations, simply tell the operator, and the scan will be stopped immediately.

If you wish to discuss the information above or any other questions you may experience, you may ask questions now or call our Principal Investigator later on the first page of this document.

What are the possible benefits to you or to others?

There is a chance that the information we get from this scan may provide a better understanding of your disease. There is also a chance that you may not receive a direct benefit. If the test is useful, it may provide information about the severity of your bone, vertebrae, the use of energy and laboratory tests. Future bone patients may also benefit from the added information that we obtain from this study.

If you choose to take part in this study, will it cost you anything?

This scan will be performed at no cost to you.

Will you receive compensation for your participation in this study?

You will not receive monetary compensation for participating in this study.

What if you are injured because of the study?

If you experience an injury that is directly caused by this study, one _____, _____ professional medical, or _____ professional dental, or _____ professional care that you receive at the University of Florida Health Science Center will be provided without

charge. However, hospital expenses will have to be paid by you or your insurance provider. No other compensation is offered.

You will have to pay hospital expenses if you are being treated at the Veterans Affairs Medical Center (VAMC) and expenses for surgical injury during participation in a VAMC-approved study.

If you do not want to take part in this study, what other options or treatments are available to you?

Participation in this study is entirely voluntary. You are free to refuse to be in the study, and your refusal will not influence earned or future health care you receive at this institution.

How can you withdraw from this research study?

If you wish to stop your participation in this research study for any reason, you should contact the Principle Investigator, Katherine N. Scott, PhD, at (312) 3716-6111. Extramural grants 5016. You are free to withdraw your consent and stop participation in this research study at any time without penalty or loss of benefits to whom you are otherwise entitled. Throughout the study, the researchers will notify you of new information that may become available and that might affect your decision to remain in the study.

In addition, if you have any questions regarding your rights as a research subject, you may phone the Institutional Review Board (IRB) office at (312) 343-1494.

How will your privacy and the confidentiality of your research records be protected?

Administrative Review Board have the legal right to review your research records and will preserve the confidentiality of those records to the extent permitted by law. If the research project is sponsored or if it is being conducted under the authority of the United States Food and Drug Administration (FDA), then the sponsor, the sponsor's agent, and the FDA also serve the legal right to review your research records. Otherwise, your research records will not be released without your consent unless required by law or a court order.

If the results of this research are published or presented at scientific meetings, your identity will not be disclosed.

Will the researchers benefit from your participation in this study (beyond publishing or presenting the results)?

The researchers will benefit from your participation in this study by learning more about the chemistry of your bone and, in the future, the needs of other patients like you. Otherwise, the results, which will derive are other benefit from your participation in this study.

Signatures

As a representative of this study, I have explained the purpose, the procedures, the benefits, and the risks this are involved in this research study.

Signature of person obtaining consentDate

You have been informed about this study's purpose, procedures, possible benefits and risks, and you have received a copy of the Form. You have been given the opportunity to ask questions before you sign. All your have been told that you can ask other questions at any time. You voluntarily agree to participate in this study. By signing this form, you are not waiving any of your legal rights.

Signature of subjectDate

**Signature of Witness
(If available)**

Date

Screening Forms:

SHANDS		University of Florida																									
Department of Radiology																											
MRI Screening Form																											
<input type="checkbox"/> Inactive <input type="checkbox"/> Occupant <input type="checkbox"/> Impaired <input type="checkbox"/> Unknown		PATIENT NAME: _____ AGE: _____ PATIENT WEIGHT: _____ TELEPHONE NUMBER: _____																									
<p>PLEASE INDICATE IF THE PATIENT HAS ANY OF THE FOLLOWING:</p> <p>Tattoo or permanent eyeliner? <input type="checkbox"/></p> <p>Anemia? <input type="checkbox"/></p> <p>Cardsitic implants? <input type="checkbox"/></p> <p>Implanted disc, infusion device or pump? <input type="checkbox"/></p> <p>Artificial heart valve prosthesis? <input type="checkbox"/></p> <p>Any type of pacemaker/defibrillator? <input type="checkbox"/></p> <p>Any type of bone growth stimulator? <input type="checkbox"/></p> <p>Ocular implants or similar ear prosthesis? <input type="checkbox"/></p> <p>Clamshell placeholder? <input type="checkbox"/></p> <p>Any intramedullary canal, filter or stents? <input type="checkbox"/></p> <p>Shrapnel or bullet injury? <input type="checkbox"/></p> <p>Any metallic joint prosthesis, rods, or plates? <input type="checkbox"/></p> <p>21 yrs or less how long ago was surgery? _____</p> <p>Sickle cell disease? <input type="checkbox"/></p> <p>Rheumatologic disease? <input type="checkbox"/></p> <p>Kidney disease? <input type="checkbox"/></p> <p>Allergies? <input type="checkbox"/></p> <p>Fragrant or breast feeding (female patients)? <input type="checkbox"/></p> <p>If yes to any above, comment: _____</p> <p>Has patient ever had metal in eyes or worked in machine shop or similar environment? <input type="checkbox"/></p> <p>If yes, have x-ray or CT of the orbits been done? <input type="checkbox"/></p> <p>Radiologist: _____</p> <p>Source of information _____</p> <p>The above information is true to the best of my knowledge. Patient or Next of kin (circle one): _____ Date: _____</p> <p>Signature of patient _____</p> <p>Are there any complaints/leads affecting from scan? If yes, please list below _____</p> <p>I attest the information is correct to the best of my knowledge. Patient or Next of kin (circle one): _____ Date: _____</p> <p>Signature: _____</p> <p>Hospital: _____</p> <p>Scanning: Whole-Body and/or Head _____</p>																											
<p>Magnetic Resonance Imaging (MRI) is a diagnostic procedure used to image various organs and tissues inside the body. It can be a useful to detect soft tissue abnormalities in any area of the body. MRI operates with a magnetism field and a large magnet and a large magnet. No x-rays or implants by are involved. Because of the high magnetic field certain metallic implants or devices are not permitted. Some implants, while not hazardous to the patient, may degrade a MRI images. On the left side of the page, the implants, while not hazardous to the patient, causing a potentially life threatening condition, an internal injury, or heating of the object within the body.</p>																											
<p>Please indicate if you have any of the following items?</p> <table border="0"> <tr> <td>Yes</td> <td>No</td> </tr> <tr> <td><input type="checkbox"/> Back pain</td> <td><input type="checkbox"/> Any heterotopic bone (fibrous or cartilaginous)</td> </tr> <tr> <td><input type="checkbox"/> Stomach or bowel</td> <td><input type="checkbox"/> Spine (for good back)</td> </tr> <tr> <td><input type="checkbox"/> Kidney disease</td> <td><input type="checkbox"/> Spine or bones (fracture)</td> </tr> <tr> <td><input type="checkbox"/> Liver disease</td> <td><input type="checkbox"/> Any other metal implants or devices?</td> </tr> <tr> <td><input type="checkbox"/> Heart disease</td> <td><input type="checkbox"/> Pacemakers or defibrillators</td> </tr> <tr> <td><input type="checkbox"/> Cardiac (heart) pacemaker</td> <td><input type="checkbox"/> Allergies</td> </tr> <tr> <td><input type="checkbox"/> Artificial heart valve</td> <td><input type="checkbox"/> Other</td> </tr> <tr> <td><input type="checkbox"/> Arteriovenous fistula</td> <td><input type="checkbox"/> Are you pregnant, or do you suspect you might be?</td> </tr> <tr> <td><input type="checkbox"/> Implanted drug delivery device or pump</td> <td><input type="checkbox"/> Are you breast feeding?</td> </tr> <tr> <td><input type="checkbox"/> Any type of heterotopic bone (fibrous and cartilaginous)</td> <td><input type="checkbox"/> Any other implants or devices?</td> </tr> <tr> <td><input type="checkbox"/> Cocaine problems or amphetamine use</td> <td><input type="checkbox"/> Any other comments?</td> </tr> </table>				Yes	No	<input type="checkbox"/> Back pain	<input type="checkbox"/> Any heterotopic bone (fibrous or cartilaginous)	<input type="checkbox"/> Stomach or bowel	<input type="checkbox"/> Spine (for good back)	<input type="checkbox"/> Kidney disease	<input type="checkbox"/> Spine or bones (fracture)	<input type="checkbox"/> Liver disease	<input type="checkbox"/> Any other metal implants or devices?	<input type="checkbox"/> Heart disease	<input type="checkbox"/> Pacemakers or defibrillators	<input type="checkbox"/> Cardiac (heart) pacemaker	<input type="checkbox"/> Allergies	<input type="checkbox"/> Artificial heart valve	<input type="checkbox"/> Other	<input type="checkbox"/> Arteriovenous fistula	<input type="checkbox"/> Are you pregnant, or do you suspect you might be?	<input type="checkbox"/> Implanted drug delivery device or pump	<input type="checkbox"/> Are you breast feeding?	<input type="checkbox"/> Any type of heterotopic bone (fibrous and cartilaginous)	<input type="checkbox"/> Any other implants or devices?	<input type="checkbox"/> Cocaine problems or amphetamine use	<input type="checkbox"/> Any other comments?
Yes	No																										
<input type="checkbox"/> Back pain	<input type="checkbox"/> Any heterotopic bone (fibrous or cartilaginous)																										
<input type="checkbox"/> Stomach or bowel	<input type="checkbox"/> Spine (for good back)																										
<input type="checkbox"/> Kidney disease	<input type="checkbox"/> Spine or bones (fracture)																										
<input type="checkbox"/> Liver disease	<input type="checkbox"/> Any other metal implants or devices?																										
<input type="checkbox"/> Heart disease	<input type="checkbox"/> Pacemakers or defibrillators																										
<input type="checkbox"/> Cardiac (heart) pacemaker	<input type="checkbox"/> Allergies																										
<input type="checkbox"/> Artificial heart valve	<input type="checkbox"/> Other																										
<input type="checkbox"/> Arteriovenous fistula	<input type="checkbox"/> Are you pregnant, or do you suspect you might be?																										
<input type="checkbox"/> Implanted drug delivery device or pump	<input type="checkbox"/> Are you breast feeding?																										
<input type="checkbox"/> Any type of heterotopic bone (fibrous and cartilaginous)	<input type="checkbox"/> Any other implants or devices?																										
<input type="checkbox"/> Cocaine problems or amphetamine use	<input type="checkbox"/> Any other comments?																										
<p>If yes, comment: _____</p> <p>Have you ever worked in a machine shop or similar environment where they may have been subjected to small metal shavings which may have gone in your eyes or elsewhere? <input type="checkbox"/> Yes <input type="checkbox"/> No</p> <p>If you have had metal shavings in your eyes or elsewhere, we recommend x-rays of your head be performed prior to the MRI since shavings may react.</p> <p>X-rays of the head required? <input type="checkbox"/> Yes <input type="checkbox"/> No</p> <p>Results _____</p> <p>Reviewed _____</p>																											

APPENDIX B
FIGURE ACQUISITION PARAMETERS

List of MR Acquisition Parameters for Figures

Figure 5. Gate-able-Phantom images, (a) axial, (b) coronal and (c) sagittal views, as imaged with 25cm square proton coil.

Head 1st, prone, extremity coil, axial or coronal or sagittal
2D, gradient echo, extended dynamic range, fast (graphic Rx for
coronal and sagittal)
60° flip angle, minimum full TE, 200 msec TR
autoshim, water auto center frequency, 8 kHz bandwidth
36 cm FOV, 5 mm thick, 0 mm space, I40-S40 for axial with 17
slices, 256 x 128, R/L, 1 NEX, scan time = 0:58
R1 = 7, R2 = 30, TG = 200, power = 8.1
Date: 092397, axial: series 1 image 12, coronal: series 3 image
7, sagittal: series 2 image 12
Magnet: 3.0T; Coil: single-turn HI; phantom: gate-able

Figure 7. Depth-Changing-Phantom images, (a) axial, (b) coronal and (c) sagittal views, as imaged with 25cm square proton coil.

Head 1st, prone, extremity coil, axial or coronal or sagittal
2D, gradient echo, extended dynamic range, fast (graphic Rx for
coronal and sagittal)
60° flip angle, minimum full TE, 200 msec TR
autoshim, water auto center frequency, 8 kHz bandwidth

36 cm FOV, 5 mm thick, 0 mm space, I40-S40 for axial with 17 slices, 256 x 128, R/L, 1 NEX, scan time = 0:58
R1 = 7, R2 = 30, TG = 200, power = 8.7
Date: 070298, axial: series 1 image 7, coronal: series 4 image 6,
sagittal: series 2 image 6
Magnet: 3.0T; Coil: single-turn H1; phantom: depth

Figure 19. Axial images of gate-able phantom comparing images obtained on 3.0 T using a 25 cm square proton surface coil with the image pulse-sequences of (a) spin echo, (b) fast spin echo, (c) gradient echo and (d) fast gradient echo imaging.

(a) spin echo:

Head 1st, supine, nasion, extremity coil, axial
2D, Spinecho, no options, 1 echo, minimum full TE, 2000 msec TR
autoshim, water auto center frequency, 16kHz receive bandwidth
36 cm FOV, 5 mm thick, 0 mm space, I20-S20 (9 slices)
256 x 128, A/P, 1 NEX, scan time = 4:40

R1 = 7, R2 = 15, TG = 200, power = 6.1

Date: 091098a, series 4, image 5

Magnet: 3.0T; Coil: single-turn H1; phantom: gate-able

(b) fast spin echo:

Head 1st, supine, nasion, extremity coil, axial
2D, Spinecho, fast, fse optimization on
4 echo train length, 1 echo, 17 msec TE, 3000 msec TR
autoshim, water auto center frequency, 32kHz receive bandwidth
36 cm FOV, 5 mm thick, 0 mm space, I20-S20 (9 slices)
256 x 128, R/L, 1 NEX, scan time = 1:48

R1 = 7, R2 = 15, TG = 200, power = 14.9

Date: 091098a, series 3, image 5

Magnet: 3.0T; Coil: single-turn H1; phantom: gate-able

(c) gradient echo:

Head 1st, supine, nasion, extremity coil, axial

2D, gradient echo, extended dynamic range

60° flip angle, 1 echo, minimum full TE, 250msec TR

autoshim, water auto center frequency, 8kHz receive bandwidth

36 cm FOV, 5 mm thick, 0 mm space, I20-S20 (9 slices)

256 x 128, R/L, 1 NEX, scan time = 0:36

R1 = 7, R2 = 30, TG = 200, power = 5.6

Date: 091098a, series 2, image 32

Magnet: 3.0T; Coil: single-turn H1; phantom: gate-able

(d) fast gradient echo:

Head 1st, supine, nasion, extremity coil, axial

2D, gradient echo, extended dynamic range, fast

60° flip angle, minimum full TE, 200msec TR

autoshim, water auto center frequency, 8kHz receive bandwidth

36 cm FOV, 5 mm thick, 0 mm space, I20-S20 (9 slices)

256 x 128, R/L, 1 NEX, scan time = 0:29

R1 = 7, R2 = 30, TG = 200, power = 5.6

Date: 091098a, series 2, image 23

Magnet: 3.0T; Coil: single-turn H1; phantom: gate-able

Figure 22. Frequency domain of (a) PRESSCSI voxel localized phosphorus spectroscopy

Head 1st, prone, nasion, extremity coil, axial

Spectro, spinecho, extended dynamic range, graphic roi, psd file

= presscsi

2000 spectral width, 1024 points, console freq = P-31, spectro

mode 1, 128 acquisitions, 1 x 1 x 1 CSI

40 msec TE, 2000msec TR, water auto center frequency
24 cm FOV, 20 mm thick, 20 x 20 x 20 mm voxel
256 x 128, R/L, 2 NEX, scan time = 4:24
R1 = 7, R2 = 30, TG = 200
Change cv's: pibbandfilt = 0, pixmtband = 1
Postprocessed with Sage_IDL™: apodize exponential 10Hz line
broadening, spectral zero-fill, fft, phase
Date: 091098, series 7, file = G00325
Magnet: 3.0T; Coil: quadrature P-31; phantom: gate-able

Figure 23. Frequency domain of (a) STEAMCSI voxel localized phosphorus spectroscopy with (b) diagram demonstrating localization.

Head 1st, prone, nasion, extremity coil, axial
Spectro, spinecho, extended dynamic range, graphic roi, psd file
= steamcsi
2000 spectral width, 2048 points, console freq = H1 (back room
frequency P-31), spectro mode 1, 32 acquisitions, 1 x 1 x 1 CSI
10 msec TE, 2000msec TR, peak auto center frequency
36 cm FOV, 20 mm thick, 20 x 20 x 20 mm voxel
256 x 128, R/L, 2 NEX, scan time = 1:14
R1 = 7, R2 = 30, TG = 200
Change cv's: sup = 0; suppress = 0; asfov = 420; GAM = 1723.5;
sharp = 1
Postprocessed with Sage_IDL™: apodize exponential 10Hz line
broadening, spectral zero-fill, fft, phase (zero order 180°, first
order 98°)
Date: 102897a, series 8, file = G00525
Magnet: 3.0T; Coil: quadrature P-31; phantom: gate-able

Figure 25. Frequency domain of (a) ECHOSI voxel localized phosphorus spectroscopy with (b) diagram demonstrating localization.

```

Head 1st, prone, nasion, extremity coil, axial
Spectro, spinecho, extended dynamic range, psd file = echocsi
2000 spectral width, 2048 points, console freq = H1 (back room
frequency P-31), spectro mode 1, 256 acquisitions, 8 x 8 x 1 CSI,
soft pulse (1)

35 msec TE, 2000msec TR, peak auto center frequency
36 cm FOV, 20 mm thick, 256 x 128, R/L, 4 NEX, scan time = 8:44
R1 = 7, R2 = 30, TG = 200

Change cv's: sup = 0; suppress = 0; asfov = 420; GAM = 1723.5;
sharp = 1, opfov 33

Postprocessed with Sage_IDL™: apodize exponential 30Hz line
broadening, spectral zero-fill, fft, phase (zero order -59°, first
order -59°)

Date: 102897a, series 8, file = G00526

Magnet: 3.0T; Coil: quadrature P-31; phantom: gate-able

```

Figure 28. Frequency domain of SPINECHO CSI multivoxel localized phosphorus spectroscopy

```

Head 1st, prone, nasion, extremity coil, axial
Spectro, spinecho, extended dynamic range, psd file = spinecho
2000 spectral width, 2048 points, console freq = H1 (back room
frequency P-31), spectro mode 1, 512 acquisitions (doesn't
matter), 11 x 11 x 1 CSI, soft pulse (1)

2000msec TR, peak auto center frequency
33 cm FOV, 33 mm thick, 0 space, 1 slice
256 x 128, R/L, 8 NEX, scan time = 32:40
R1 = 7, R2 = 30, TG = 140

```

```
Change cv's: sup = 0; suppress = 0; asfov = 420; GAM = 1723.5;
spec_chopletson = 0

Postprocessed with Sage_IDL™: apodize exponential 30Hz line
broadening, spectral zero-fill, fft

Date: 102497a, series 3, file = P25600

Magnet: 3.0T; Coil: quadrature P-31; phantom: gate-able
```

Figure 30. Frequency domain of (a) ISISCSI slice localized phosphorus spectroscopy

```
Head 1st, prone, nasion, extremity coil, axial
Spectro, spinedcho, extended dynamic range, graphic roi, psd file
= isiscsi
2000 spectral width, 1024 points, console freq = P-31, spectro
mode 1, 256 acquisitions, 1 x 1 x 1 CSI, soft pulse (1), plane
(2)
2000msec TR, peak auto center frequency
24 cm FOV, 20 mm thick slice
256 x 128, R/L, 2 NEX, scan time = 8:44
R1 = 7, R2 = 30, TG = 200
Change cv's: pibbandfilt = 0; pixmtband = 1
Postprocessed with Sage_IDL™: apodize exponential 10Hz line
broadening, spectral zero-fill, fft, phase (zero order = -106.51,
first order = 170.84)
Date: 091098a, series 7, file = G00327
Magnet: 3.0T; Coil: quadrature P-31; phantom: gate-able
```

Figure 31. Frequency domain of (a) ISISCSI column localized phosphorus spectroscopy

```
Head 1st, prone, nasion, extremity coil, axial
```

Spectro, spinecho, extended dynamic range, graphic roi, psd file
= isiscsci

2000 spectral width, 1024 points, console freq = P-31, spectro
mode 1, 256 acquisitions, 1 x 1 x 1 CSI, soft pulse (1), col (4)
2000msec TR, peak auto center frequency
24 cm FOV, 20 mm thick, 20 x 20 mm column
256 x 128, R/L, 4 NEX, scan time = 8:44
R1 = 7, R2 = 30, TG = 200
Change cv's: pibbandfilt = 0; pixmtband = 1
Postprocessed with Sage_IDL™: apodize exponential 10Hz line
broadening, spectral zero-fill, fft, phase (zero order = -68.545,
first order = 43.919)
Date: 091098a, series 7, file = G00328
Magnet: 3.0T; Coil: quadrature P-31; phantom; gate-able

Figure 32. Frequency domain of (a) ISISCSI voxel localized phosphorus
spectroscopy

Head 1st, prone, nasion, extremity coil, axial
Spectro, spinecho, extended dynamic range, graphic roi, psd file
= isiscsci

2000 spectral width, 1024 points, console freq = P-31, spectro
mode 1, 256 acquisitions, 1 x 1 x 1 CSI, soft pulse (1), vox (8)
2000msec TR, peak auto center frequency
24 cm FOV, 20 mm thick, 20 x 20 x 20 mm voxel
256 x 128, R/L, 8 NEX, scan time = 8:52
R1 = 7, R2 = 30, TG = 200
Change cv's: pibbandfilt = 0; pixmtband = 1

Postprocessed with Sage_IDL™: apodize exponential 10Hz line
broadening, spectral zero-fill, fft, phase (zero order = -187.97,
first order = 486.52)
Date: 091098a, series 7, file = G00329
Magnet: 3.0T; Coil: quadrature P-31; phantom: gate-able

Figure 34. Frequency domain of (a) modified ISISCSI localized voxel sequence for phosphorus

Head 1st, prone, nasion, extremity coil, axial
Spectro, spinecho, extended dynamic range, graphic roi, psd file
= isiscsi
2000 spectral width, 1024 points, console freq = P-31, spectro
mode 1, 64 acquisitions, 1 x 1 x 1 CSI, soft pulse (1), sin (1)
2000msec TR, peak auto center frequency
24 cm FOV, 20 mm thick, 20 x 20 x 20 mm voxel
256 x 128, R/L, 1 NEX, scan time = 2:13
R1 = 7, R2 = 30, TG = 200
Change cv's: pibbandfilt = 0; pixmtband = 1, THISISIS = 1 TO 8 (8
separate acquisitions
Postprocessed with Sage_IDL™: apodize exponential 10Hz line
broadening, spectral zero-fill, fft, phase, combine acquisitions
as such: Acq 1 = Acq 2 + Acq 3 - Acq 4 + Acq 5 - Acq 6 + Acq 7 -
Acq 8
Date: 071298a, series 7, file = G00005 - G00006 + G00007 - G00008
+ G00009 - G00010 + G00011 - G00012
Magnet: 3.0T; Coil: quadrature P-31; phantom: gate-able

Figure 38. Frequency domain of FIDCSI slice localized phosphorus spectroscopy of (a) gate-able phantom and (b) depth phantom

(a) gate-able phantom

Head 1st, prone, nasion, extremity coil, coronal
Spectro, spinecho, extended dynamic range, graphic Rx, psd file =
fidcsi
2000 spectral width, 2048 points, console freq = H1 (back room
frequency P-31), spectro mode 1, 128 acquisitions, 1 x 1 x 1 CSI,
soft pulse (1)
2000msec TR, peak auto center frequency, 36 cm FOV, 25 mm thick,
256 x 128, R/L, 2 NEX, scan time = 4:26, R1 = 7, R2 = 30, TG = 20
Change cv's: sup = 0; suppress = 0; asfov = 420; GAM = 1723.5
Postprocessed with Sage_IDL™: apodize exponential 10Hz line
broadening, spectral zero-fill, fft, phase (zero order -117°,
first order -210°)

Date: 012798, series 4, file = G00005

(b) depth phantom

Head 1st, supine, nasion, extremity coil, coronal
Spectro, spinecho, extended dynamic range, graphic Rx, psd file =
fidcsi
2000 spectral width, 1024 points, console freq = P-31, spectro
mode 1, 128 acquisitions, 1 x 1 x 1 CSI, soft pulse (1)
2000msec TR, peak auto center frequency
16 cm FOV, 25 mm thick, 256 x 128, R/L, 2 NEX, scan time = 4:26
R1 = 7, R2 = 30, TG = 50
Change cv's: pibbandfilt = 0, pixmtband = 1, pw_gph = 4msec
Postprocessed with Sage_IDL™: apodize exponential 10Hz line
broadening, spectral zero-fill, fft, phase
Date: 012798, series 5, file = G00034
Magnet: 3.0T; Coil: single-turn P-31 coil; phantom: gate-able and
depth phantoms

Figure 39. Multivoxel phosphorus FIDCSI plus CSI of the (a) gate-able phantom (b) depth phantom

(a) gate-able phantom

Head 1st, prone, nasion, extremity coil, axial
Spectro, spinecho, extended dynamic range, graphic ROI, psd file
= fidcsi
2000 spectral width, 1024 points, console freq = H1 (control room
frequency P-31), spectro mode 1, 128 acquisitions, 6x6x1 CSI,
soft pulse (1)
2000msec TR, peak auto center frequency
34 cm FOV, 25 mm thick, 256 x 128, R/L, 4 NEX, scan time = 4:59
R1 = 7, R2 = 30, TG = 30
Change cv's: suppress = 0; sup = 0; asfov = 480; GAM = 1723.5
Postprocessed with Sage_IDLTM: apodize exponential, spectral
zero-fill, fft, phase
Date: 022298a, series 3, file = P13824
Magnet: 3.0T; Coil: quadrature P-31; phantom; gate-able
(b) depth phantom
Head 1st, supine, nasion, extremity coil, axial
Spectro, spinecho, extended dynamic range, graphic ROI, psd file
= fidcsi
2000 spectral width, 1024 points, console freq = P-31, spectro
mode 1, 128 acquisitions, 8 x 8 x 1 CSI, soft pulse (1)
2000msec TR, peak auto center frequency
16 cm FOV, 30 mm thick, 256 x 128, R/L, 2 NEX, scan time = 4:26
R1 = 7, R2 = 30, TG = 125
Change cv's: pibbandfilt = 0, pixmtband = 1, pw_gph = 4msec

Postprocessed with Sage_IDL™: apodize exponential, spectral
zero-fill, fft, phase
Date: 073098b, series 3, file = P17920_b
Magnet: 3.0T; Coil: quadrature P-31; phantom: depth

Figure 40. Comparison of 1.5 to 3.0 Tesla results of phosphorus FIDCSI plus CSI localized voxel scaled by noise level.

(a) 1.5 T single-turn coil

Head 1st, supine, nasion, extremity coil, axial
Spectro, spinecho, extended dynamic range, graphic ROI, psd file
= fidcsi
1000 spectral width, 1024 points, console freq = P-31, spectro
mode 1, 256 acquisitions, 8 x 8 x 1 CSI, soft pulse (1)
2000msec TR, peak auto center frequency
16 cm POV, 25 mm thick, 1 slice
256 x 128, R/L, 4 NEK, scan time = 4:26, R1 = 7, R2 = 30, TG = 50
Postprocessed with Sage_IDL™: apodize exponential 10Hz line
broadening, spectral zero-fill, fft, phase (zero order = -79.393,
first order = 145.43), localized to voxel (4 to 4) x (4 to 4)

Date: 071198, series 5, file = P17408

Magnet: 1.5 T; Coil: single-turn P-31; phantom: depth

(b) 3.0 T single-turn P-31 coil

Head 1st, supine, nasion, extremity coil, axial
Spectro, spinecho, extended dynamic range, graphic ROI, psd file
= fidcsi
2000 spectral width, 1024 points, console freq = P-31, spectro
mode 1, 256 acquisitions, 8 x 8 x 1 CSI, soft pulse (1)
2000msec TR, peak auto center frequency

16 cm FOV, 20 mm thick, 1 slice
256 x 128, R/L, 2 NEX, scan time = 4:26
change cv's: pibbandfilt = 0, pixmtband = 1, pw_gph = 4msec
R1 = 7, R2 = 30, TG = 50
Postprocessed with Sage_IDL™: apodize exponential 10Hz line
broadening, spectral zero-fill, fft, phase (zero order = 128,
first order = 0), localized to voxel (5 to 5) x (3 to 3)
Date: 070998, series 8, file = P06144
Magnet: 3.0T; Coil: single-turn P-31; phantom: depth
(c) 3.0 T quadrature P-31 coil
Head 1st, supine, nasion, extremity coil, axial
Spectro, spinecho, extended dynamic range, graphic ROI, psd file
= fidcsi
2000 spectral width, 1024 points, console freq = P-31, spectro
mode 1, 256 acquisitions, 8 x 8 x 1 CSI, soft pulse (1)
2000msec TR, peak auto center frequency
16 cm FOV, 20 mm thick, 1 slice
256 x 128, R/L, 2 NEX, scan time = 4:26
change cv's: pibbandfilt = 0, pixmtband = 1, pw_gph = 4msec
R1 = 7, R2 = 30, TG = 50
Postprocessed with Sage_IDL™: apodize exponential 10Hz line
broadening, spectral zero-fill, fft, phase (zero order = -11,
first order = 0), localized to voxel (5 to 5) x (4 to 4)
Date: 071298, series 6, file = P04608
Magnet: 3.0T; Coil: quadrature P-31; phantom: depth

Figure 41. Comparison of 1.5 to 3.0 Tesla results of phosphorus,
modified ISISCSI localized voxel (created from eight separate

acquisitions, added and subtracted appropriately during post-processing).

(a) 1.5 T single-turn P-31 coil

Head 1st, supine, nasion, extremity coil, axial

Spectro, spinecho, extended dynamic range, graphic ROI, psd file = isisccsi

1000 spectral width, 1024 points, console freq = P-31, spectro mode 1, 256 acquisitions, 1 x 1 x 1 CSI, soft pulse (1), sin (1) 2000msec TR, peak auto center frequency

16 cm FOV, 20 mm thick, 20 x 20 x 20 mm voxel

256 x 128, R/L, 1 NEX, R1 = 7, R2 = 30, TG = 200

Change CV's: THISISIS = 1 to 8 for 8 separate acquisitions

Postprocessed with Sage_IDL™: apodize exponential 10Hz line broadening, spectral zero-fill, fft, phase, sum of spectra = Acq 1 - Acq 2 + Acq 3 - Acq 4 + Acq 5 - Acq 6 + Acq 7 - Acq 8

Date: 071198, series 6, file = G00769 - G00770 + G00771 - G00772 + G00773 - G00774 + G00775 - G00776

Magnet: 1.5 T; Coil: single-turn P-31; phantom: depth

(b) 3.0T single-turn P-31 coil

Head 1st, supine, nasion, extremity coil, axial

Spectro, spinecho, extended dynamic range, graphic ROI, psd file = isisccsi

2000 spectral width, 1024 points, console freq = P-31, spectro mode 1, 256 acquisitions, 1 x 1 x 1 CSI, soft pulse (1), sin (1) 2000msec TR, peak auto center frequency

16 cm FOV, 20 mm thick, 20 x 20 x 20 mm voxel

256 x 128, R/L, 1 NEX, R1 = 7, R2 = 30, TG = 200

Change CV's: pibbandfilt = 0, pixmtband = 1, pw_gph = 4msec, THISISIS = 1 to 8 for 8 separate acquisitions

```
Postprocessed with Sage_IDL™: apodize exponential 10Hz line
broadening, spectral zero-fill, fft, phase, sum of spectra = Acq
1 - Acq 2 + Acq 3 - Acq 4 + Acq 5 - Acq 6 + Acq 7 - Acq 8
Date: 070998, series 9, file = G00234 - G00235 + G00236 - G00237
+ G00238 - G00239 + G00240 - G00241
(c) 3.0T quadrature P-31 coil
Head 1st, supine, nasion, extremity coil, axial
Spectro, spinecho, extended dynamic range, graphic ROI, psd file
= isiscsi
2000 spectral width, 1024 points, console freq = P-31, spectro
mode 1, 256 acquisitions, 1 x 1 x 1 CSI, soft pulse (1), sin (1)
2000msec TR, peak auto center frequency
16 cm FOV, 20 mm thick, 20 x 20 x 20 mm voxel
256 x 128, R/L, 1 NEK, R1 = 7, R2 = 30, TG = 200
Change CV's: pibbandfilt = 0, pixmtband = 1, pw_gph = 4msed,
THISISIS = 1 to 8 for 8 separate acquisitions
Postprocessed with Sage_IDL™: apodize exponential 10Hz line
broadening, spectral zero-fill, fft, phase, sum of spectra = Acq
1 - Acq 2 + Acq 3 - Acq 4 + Acq 5 - Acq 6 + Acq 7 - Acq 8
Date: 071298, series 7, file = G00005 - G00006 + G00007 - G00008
+ G00009 - G00010 + G00011 - G00012
```

Figure 42. 1.5 T, P-31 single turn RF coil signal from a set of 25 mm thick, oblique DRESS slices (FIDCSI oblique slice) moved across the internal phosphoric acid vial in the Slice Profile Phantom.

Head 1st, supine, nasion, extremity coil, oblique
Spectro, spinecho, extended dynamic range, graphic Rx, psd file =
/usr/g/genesis/fidobl

2000 spectral width, 1024 points, console freq = P-31, spectro
mode 1, 32 acquisitions, 1 x 1 x 1 CSI, soft pulse (1)
1000msec TR, peak auto center frequency
14 cm FOV, 25 mm thick, 256 x 128, S/I, 2 NEX, scan time = 0:37
R1 = 7, R2 = 30, TG = 170; ax = 25868906
Postprocessed with Sage_IDL™: apodize exponential 10Hz line
broadening, spectral zero-fill, fft, phase (zero order = auto,
first order = 0)
Date: 101298; Magnet: 1.5 T; Coil: single-turn P-31 coil;
phantom: slice profile

Figure 43. 3.0 T, P-31 single turn RF coil signal from a set of 25 mm
thick, oblique DRESS slices (FIDCSI oblique slice) moved across the
internal phosphoric acid vial in the Slice Profile Phantom.

Head 1st, supine, nasion, extremity coil, oblique
Spectro, spinecho, extended dynamic range, graphic Rx, psd file =
/usr/g/genesis/fidobl
2000 spectral width, 1024 points, console freq = P-31, spectro
mode 1, 32 acquisitions, 1 x 1 x 1 CSI, soft pulse (1)
1000msec TR, peak auto center frequency
14 cm FOV, 25 mm thick, 256 x 128, S/I, 2 NEX, scan time = 0:37
control variables: pibbandfilt = 0, pixmtband = 1
R1 = 7, R2 = 30, TG = 100; ax = 21287799, back room freq =
30427790
Postprocessed with Sage_IDL™: apodize exponential 10Hz line
broadening, spectral zero-fill, fft, phase (zero order = auto,
first order = 0)
Date: 101098; Magnet: 3.0T; Coil: single-turn P-31 coil; phantom:
slice profile

Figure 44. 3.0 T, P-31 quadrature RF coil signal from a set of 25 mm thick, oblique DRESS slices (FIDCSI oblique slice) moved across the internal phosphoric acid vial in the Slice Profile Phantom.

```
Head 1st, supine, nasion, extremity coil, oblique
Spectro, spinecho, extended dynamic range, graphic Rx, pad file =
/usr/g/genesis/fidobl
2000 spectral width, 1024 points, console freq = P-31, spectro
mode 1, 32 acquisitions, 1 x 1 x 1 CSI, soft pulse (1)
1000msec TR, peak auto center frequency
14 cm FOV, 25 mm thick, 256 x 128, S/I, 2 NEX, scan time = 0:37
control variables: pibbandfilt = 0, pixmtband = 1
R1 = 7, R2 = 30, TG = 100; ax = 21287799, back room freq =
30427790
Postprocessed with Sage_IDL™: apodize exponential 10Hz line
broadening, spectral zero-fill, fft, phase (zero order = auto,
first order = 0)
Date: 102398; Magnet: 3.0T; Coil: quadrature P-31 coil; phantom:
slice profile
```

Figure 45. Human cardiac imaging with the spin-echo pulse sequence at (a) 1.5 T with the body coil and at (b) 3.0 T with a surface coil.

```
(a) 1.5 T with the body coil
Head 1st, supine, body coil, axial
2D, spin echo, gating, no phase wrap, graphic Rx (based on
previous sagittal scout)
1 echo, minimum full TE
autoshim, water auto center frequency, default kHz bandwidth
peak auto center frequency, 32kHz bandwidth
```

gating menu, trigger type: ECG autolead, effective TR: 1xRR,
Trigger Delay = recommended, Trigger window = auto trigger,
intersequence delay = minimum, cardiac phases = single
40 cm FOV, 7 mm thick, 3 mm space, L70-R10 (I26.2)
256 x 128, A/P, 1 NEX, scan time = 2:22
R1 = 7, R2 = 30, TG = autoset
Date: 060698, series 2, image 17
Magnet: 1.5 T; Coil: body coil; volunteer: WISE#2
(b) 3.0T with a surface coil (update info)
Head 1st, supine, extremity coil, axial
2D, spin echo, gating, no phase wrap, graphic Rx (based on
previous sagittal scout)
1 echo, minimum full TE
autoshim, water auto center frequency, 16 kHz bandwidth
peak auto center frequency, 32kHz bandwidth
gating menu, trigger type: ECG autolead, effective TR: 1xRR,
Trigger Delay = recommended, Trigger window = auto trigger,
intersequence delay = minimum, cardiac phases = single
36 cm FOV, 7 mm thick, 3 mm space, L70-R10 (I26.2)
256 x 128, A/P, 1 NEX, scan time = 2:47
R1 = 6, R2 = 15, TG = 179
Date: 041898, series 4, image 5
Magnet: 3.0T; Coil: 25cm square proton coil; volunteer: TB

Figure 46. Human cardiac imaging with the fast gradient echo pulse sequence at (a) 1.5 T with the body coil and at (b) 3.0 T with a surface coil.

(a) 1.5 T with the body coil
head 1st, supine, sternal notch, body coil, axial

2D, gradient echo, gating, no phase wrap, graphic Rx, fast arrhythmia rejection = 0, 60° flip angle, minimum full TE autoshim, water auto center frequency, 16kHz bandwidth gating menu, trigger type: peripheral gating, Trigger window = auto trigger window

42 cm FOV, 7 mm thick, 2.5 mm space

256 x 128, A/P, 2 NEX, scan time = 6:18

R1 = 7, R2 = 30, TG = 200, power = 10.8

Date: 040599, series 3

Magnet: 1.5T; Coil: body coil; volunteer: TB

(b) 3.0T with a surface coil

feet 1st, supine, sternal notch, extremity coil, axial

2D, gradient echo, gating, flow comp, extended dynamic range, fast, variable bandwidth

arrhythmia rejection = 0, 60° flip angle, minimum full TE

autoshim, water auto center frequency, 32kHz bandwidth

gating menu, trigger type: peripheral gating, effective TR: 1xRR, Trigger Delay = recommended, Trigger window = auto trigger window, intersequence delay = even

42 cm FOV, 7 mm thick, 1 mm space, I31.8

256 x 128, A/P, 1 NEX, scan time = 0:20; breathold

R1 = 7, R2 = 30, TG = 200, power = 10.8

Date: 020599, series 6; image 4

Magnet: 3.0T; Coil: square H1; volunteer: Relax#5 LR

Figure 48. A comparison of the heart's position in the (a) prone and (b) supine positions, as shown from a 3.0 T axial slice.

(a) prone position:

Head 1st, prone, extremity coil, axial

2D, gradient echo, gating, flow comp, extended dynamic range,
fast, variable bandwidth
60° flip angle, minimum full TE, 200 msec TR
autoshim, water auto center frequency, 8 kHz bandwidth
peak auto center frequency
gating menu, trigger type: peripheral gating, effective TR: 1xRR,
Trigger Delay = recommended, Trigger window = auto trigger
window, intersequence delay = even, cardiac phases = single
30 cm FOV, 8 mm thick, 1 mm space, I20 to S20
256 x 128, R/L, 1 NEX, scan time = 1:22
R1 = 7, R2 = 30, TG = 200, power = 11.2
Date: 101497B, series 2; breathhold
Magnet: 3.0T; Coil: square H1; volunteer: HK
(b) supine position:
Head 1st, supine, extremity coil, axial
2D, gradient echo, gating, flow comp, extended dynamic range,
fast, variable bandwidth
60° flip angle, minimum full TE, 200 msec TR
autoshim, water auto center frequency, 8 kHz bandwidth
peak auto center frequency, 32kHz bandwidth
gating menu, trigger type: peripheral gating, effective TR: 1xRR,
Trigger Delay = recommended, Trigger window = auto trigger
window, intersequence delay = even, cardiac phases = single
30 cm FOV, 8 mm thick, 1 mm space, I20 to S20
256 x 128, R/L, 1 NEX, scan time = 0:20
R1 = 7, R2 = 30, TG = 200, power = 9.3
Date: 101497B, series 2; breathhold
Magnet: 3.0T; Coil: square H1; volunteer: HK

Figure 50. A comparison of peripheral gating (pg) versus ECG gating, and breathing during the image versus breath-hold images. All images are fast gradient echo: (a) sagittal, peripheral gating, breath-hold; (b) sagittal, peripheral gating, breathing; (c) sagittal, ECG gating, breath-hold; (d) sagittal, ECG gating, breathing, (e) axial, peripheral gating, breath-hold, (f) axial, peripheral gating, breathing.

(a) sagittal, peripheral gating, breath-hold

Head 1", prone, extremity coil, sagittal

2D, gradient echo, gating, flow comp, extended dynamic range,
fast, variable bandwidth

arrythmia rejection = 0, 60° flip angle, minimum full TE
autoshim, water auto center frequency, 32kHz bandwidth
gating menu, trigger type: peripheral gating, effective TR: 1xRR,
Trigger Delay = recommended, Trigger window = auto trigger
window, intersequence delay = even

24 cm FOV, 8 mm thick, R10

256 x 128, S/I, 1 NEX, scan time = 0:16; breathold

R1 = 7, R2 = 30, TG = 200, power = 9.6

Date: 101497A, series 2; image 23

Magnet: 3.0T; Coil: square HI; volunteer: DP

(b) sagittal, peripheral gating, breathing

Head 1", prone, extremity coil, sagittal

2D, gradient echo, gating, flow comp, extended dynamic range,
fast, variable bandwidth

arrythmia rejection = 0, 60° flip angle, minimum full TE
autoshim, water auto center frequency, 32kHz bandwidth
gating menu, trigger type: peripheral gating, effective TR: 1xRR,
Trigger Delay = recommended, Trigger window = auto trigger
window, intersequence delay = even

24 cm FOV, 8 mm thick, R10
256 x 128, S/I, 1 NEX, scan time = 0:16
R1 = 7, R2 = 30, TG = 200, power = 9.6
Date: 101497A, series 2; image 28
Magnet: 3.0T; Coil: square H1; volunteer: DP
(c) sagittal, ECG gating, breath-hold
Head 1st, prone, extremity coil, sagittal
2D, gradient echo, gating, flow comp, extended dynamic range,
fast, variable bandwidth
arrythmia rejection = 0
60° flip angle, minimum full TE
autoshim, water auto center frequency, 32kHz bandwidth
gating menu, trigger type: ECG autolead, effective TR: 1xRR,
Trigger Delay = recommended, Trigger window = auto trigger
window, intersequence delay = even
24 cm FOV, 8 mm thick, R10
256 x 128, S/I, 1 NEX, scan time = 0:16; breathold
R1 = 7, R2 = 30, TG = 200, power = 9.6
Date: 101497A, series 2; image 18
Magnet: 3.0T; Coil: square H1; volunteer: DP
(d) sagittal, ECG gating, breathing
Head 1st, prone, extremity coil, sagittal
2D, gradient echo, gating, flow comp, extended dynamic range,
fast, variable bandwidth
arrythmia rejection = 0, 60° flip angle, minimum full TE
autoshim, water auto center frequency, 32kHz bandwidth
gating menu, trigger type: ECG autolead, effective TR: 1xRR,
Trigger Delay = recommended, Trigger window = auto trigger
window, intersequence delay = even

24 cm FOV, 8 mm thick, R10

256 x 128, S/I, 1 NEX, scan time = 0:16

R1 = 7, R2 = 30, TG = 200, power = 9.6

Date: 101497A, series 2; image 13

Magnet: 3.0T; Coil: square H1; volunteer: DP

(e) axial, peripheral gating, breath-hold

feet 1st, supine, sternal notch, extremity coil, axial

2D, gradient echo, gating, flow comp, extended dynamic range,
fast, variable bandwidth

arrythmia rejection = 0, 60° flip angle, minimum full TE

autoshim, water auto center frequency, 32kHz bandwidth

gating menu, trigger type: peripheral gating, effective TR: 1xRR,
Trigger Delay = recommended, Trigger window = auto trigger
window, intersequence delay = even

42 cm FOV, 7 mm thick, 1 mm space, I31.8

256 x 128, A/P, 1 NEX, scan time = 0:20; breathold

R1 = 7, R2 = 30, TG = 200, power = 10.8

Date: 020599, series 6; image 4

Magnet: 3.0T; Coil: square H1; volunteer: Relax#5 LR

(f) axial, peripheral gating, breathing

feet 1st, supine, sternal notch, extremity coil, axial

2D, gradient echo, gating, flow comp, extended dynamic range,
fast, variable bandwidth

arrythmia rejection = 0, 60° flip angle, minimum full TE

autoshim, water auto center frequency, 32kHz bandwidth

gating menu, trigger type: peripheral gating, effective TR: 1xRR,
Trigger Delay = recommended, Trigger window = auto trigger
window, intersequence delay = even

42 cm FOV, 7 mm thick, 1 mm space, I31.8

256 x 128, A/P, 1 NEX, scan time = 1:48
R1 = 7, R2 = 30, TG = 200, power = 10.8
Date: 020599, series 5; image 52
Magnet: 3.0T; Coil: square H1; volunteer: Relax#5 LR

Figure 51. Human proton voxel localized spectroscopy of the heart and chest wall obtained during one volunteer's shim using the techniques of GE's (a) STEAMCSI and (b) PRESSCSI.

(a) STEAM

Feet 1st, supine, sternal notch, extremity coil, axial
Spectro, spinecho, gating, extended dynamic range, graphic ROI,
psd file = steamcsi
1000 spectral width, 1024 points, console freq = H1, spectro mode
1, 16 acquisitions, 1 x 1 x 1 CSI
2000msec TR, TE = 40msec, water auto center frequency
gating menu, trigger type: peripheral gating, effective TR: 2xRR,
Trigger Delay = recommended, Trigger window = auto trigger
window, intersequence delay = even, cardiac phases = single
34 cm FOV, 30 mm thick, 16.5, 41.0 mm x 59.1 mm x 30 mm voxel
256 x 128, A/P, 4 NEX, scan time = 0:40
R1 = 7, R2 = 30, TG = 70; depth = 66mm

Change cv's: suppress = 0, sup = 0

Postprocessed with Sage_IDL™: fft, phase (52.734, 0)
Date: 021299a, series 6, file = 3.0 T_RELAX#7_proton_shim_steam
Magnet: 3.0T; Coil: 25cm square proton, volunteer: relax#7 CS

(b) PRESS

Feet 1st, supine, sternal notch, extremity coil, axial
Spectro, spinecho, gating, extended dynamic range, graphic ROI,
psd file = presscsi

1000 spectral width, 1024 points, console freq = H1, spectro mode
1, 16 acquisitions, 1 x 1 x 1 CSI
2000msec TR, TE = 40msec, water auto center frequency
gating menu, trigger type: peripheral gating, effective TR: 2xRR,
Trigger Delay = recommended, Trigger window = auto trigger
window, intersequence delay = even, cardiac phases = single
34 cm FOV, 30 mm thick, 16.5, 41.0 mm x 59.1 mm x 30 mm voxel
256 x 128, A/P, 4 NEX, scan time = 0:40
R1 = 7, R2 = 30, TG = 70; depth = 66mm
Change cv's: suppress = 0, sup = 0
Postprocessed with Sage_IDL™: fft, phase (52.734, 0)
Date: 021299a, series 6, file = 3.0 T_RELAX#7_proton_shim_press
Magnet: 3.0T; Coil: 25cm square proton, volunteer: relax#7 CS

Figure 52. P-31 FIDCSI with CSI of a human subject at 3.0 T.

Head 1st, prone, sternal notch, extremity coil, axial
Spectro, spinecho, gating, extended dynamic range, graphic ROI,
pad file = /usr/g/genesis/fidfovH
4000 spectral width, 1024 points, console freq = P-31, spectro
mode 1, 128 acquisitions, 6x6x1 CSI, soft pulse (1)
2000msec TR, peak auto center frequency
gating menu, trigger type: ECG autolead, effective TR: 2xRR,
Trigger Delay = recommended, Trigger window = auto trigger
window, intersequence delay = even, cardiac phases = single
20 cm FOV, 30 mm thick, voxel 35 x 35 x 30 mm³
256 x 128, A/P, 8 NEX, scan time = 12 minutes
R1 = 7, R2 = 30, TG = 50
Change cv's: squeeze = 1, pibbandfilt = 0, pixmtband = 1

AX= 21287137, back room freq = 30427790, true frequency =
51.714927 MHz, resting heart rate = 50
Postprocessed with Sage_IDL™: apodize exponential 10Hz line
broadening, spectral zero-fill, fft, orient = transpose x-y &
flip x, magnitude plot (can not phase all parts of csi equally
correctly)
Date: 041898c, series 5, file = P05632
Magnet: 3.0T; Coil: quadrature P-31; volunteer: TB

Figure 54. Examples of 1.5 T cardiac phosphorus spectra localization problems resulting in (a) liver contamination, or (b) skeletal muscle contamination, in comparison with (c) a non-contaminated cardiac spectrum.

(a) liver contamination

Head 1st, supine, sternal notch, extremity coil, oblique
Spectro, spinecho, gating, extended dynamic range, graphic Rx,
psd file = /usr/g/genesis/fidobl
2000 spectral width, 1024 points, console freq = P-31, spectro
mode 1, 128 acquisitions, 1 x 1 x 1 CSI, soft pulse (1)
3000maec TR, peak auto center frequency
gating menu, trigger type: ECG autolead, effective TR: 3xRR,
Trigger Delay = recommended, Trigger window = auto trigger
window, intersequence delay = even, cardiac phases = single
14 cm FOV, 25 mm thick
256 x 128, Not Swapped, 4 NEX, scan time = 6 to 8 minutes
R1 = 7, R2 = 30, TG = 185, Depth = 69mm
resting heart rate = 83
Postprocessed with FITMASTER™ at UAB
Date: 022299, file = G00994

Magnet: 1.5 T; Coil: single-turn P-31; volunteer: WISE#33

(b) Skeletal muscle contamination

Head 1st, supine, sternal notch, extremity coil, oblique

Spectro, spinecho, gating, extended dynamic range, graphic Rx,

psd file = fidcsi

2000 spectral width, 1024 points, console freq = P-31, spectro

mode 1, 128 acquisitions, 1 x 1 x 1 CSI, hard pulse (0) → later

change to soft pulse

3000 msec TR, peak auto center frequency

gating menu, trigger type: ECG autolead, effective TR: 3xRR,

Trigger Delay = recommended, Trigger window = auto trigger

window, intersequence delay = even, cardiac phases = single

20 cm FOV, 30 mm thick, 0 space

256 x 128, S/I, 4 NEX, scan time = 6 to 8 minutes

R1 = 7, R2 = 30, TG = 185

Change cv's: squeeze = 0

Backup, review screen, users cv's to change to soft pulse,

scanning range to change to 20 thick, erase slice, and reselect

positioning and measure depth

Depth = 45mm

resting heart rate = 77

Postprocessed with FITMASTER™ at UAB

Date: 031498, file = G00540

Magnet: 1.5 T; Coil: single-turn P-31; volunteer: WISE#1

(c) quality cardiac spectra

Head 1st, supine, sternal notch, extremity coil, oblique

Spectro, spinecho, gating, extended dynamic range, graphic Rx,

psd file = /usr/g/genesis/fidobl

2000 spectral width, 1024 points, console freq = P-31, spectro
mode 1, 128 acquisitions, 1 x 1 x 1 CSI, soft pulse (1)
3000msec TR, peak auto center frequency
gating menu, trigger type: ECG autolead, effective TR: 3xRR,
Trigger Delay = recommended, Trigger window = auto trigger
window, intersequence delay = even, cardiac phases = single
14 cm FOV, 25 mm thick
256 x 128, Not Swapped, 4 NEX, scan time = 6 to 8 minutes
R1 = 7, R2 = 30, TG = 110, Depth = 55mm
resting heart rate = 84
Postprocessed with FITMASTER™ at UAB
Date: 052598, file = G00693
Magnet: 1.5 T; Coil: single-turn P-31; volunteer: WISE#14

Figure 55. P-31 FIDCSI oblique slice localized human cardiac
spectroscopy (oblique DRESS) of the same subject, at 1.5 and 3.0 T, on
different days showing examples of resting and exercise spectra

(a) 1.5 T
Head 1st, supine, sternal notch, extremity coil, oblique
Spectro, spinecho, gating, extended dynamic range, graphic Rx,
psd file = /usr/g/genesis/fidobl
2000 spectral width, 1024 points, console freq = P-31, spectro
mode 1, 128 acquisitions, 1 x 1 x 1 CSI, soft pulse (1)
3000msec TR, peak auto center frequency
gating menu, trigger type: ECG autolead, effective TR: 3xRR,
Trigger Delay = recommended, Trigger window = auto, intersequence
delay = even, cardiac phases = single
14 cm FOV, 25 mm thick, 256 x 128, not swapped, 4 NEX, scan time
= 6:38

```
control variables: pibbandfilt = 0, pixmtband = 1  
R1 = 7, R2 = 30, TG = 165; ax = 25868826  
Postprocessed with FITMASTER at UAB  
Date: 111198; Magnet: 1.5 T; Coil: single-turn P-31 coil;  
phantom: slice profile  
(b) 3.0T  
Head 1st, supine, sternal notch, extremity coil, oblique  
Spectro, spinecho, gating, extended dynamic range, graphic Rx,  
psd file = /usr/g/genesis/fidobl  
4000 spectral width, 1024 points, console freq = P-31, spectro  
mode 1, 128 acquisitions, 1 x 1 x 1 CSI, soft pulse (1)  
3000msec TR, peak auto center frequency  
gating menu, trigger type: ECG autolead, effective TR: 3xRR,  
Trigger Delay = recommended, Trigger window = 10%, intersequence  
delay = even, cardiac phases = single  
20 cm FOV, 30 mm thick, 256 x 128, swapped, 4 NEX, scan time rest  
= 6:38  
control variables: pibbandfilt = 0, pixmtband = 1  
R1 = 7, R2 = 30, TG = 60; ax = 21287249, back room freq =  
30427790  
Postprocessed with FITMASTER at UAB  
Date: 081098; Magnet: 3.0T; Coil: single-turn P-31 coil
```

Figure 56. Series of cardiac region oblique DRESS spectra representing decreased skeletal muscle contamination with increase in depth of spectroscopy slice localization. Note the split in the PCr peak that designates the cardiac and skeletal muscle as separate peaks.

(a) Images

head 1st, supine, sternal notch, extremity coil, axial

2D, gradient echo, gating, flow comp, extended dynamic range,
fast, variable bandwidth, graphic Rx (based on sagittal image)
arrythmia rejection = 0
60° flip angle, minimum full TE
autoshim, water auto center frequency, 32kHz bandwidth
gating menu, trigger type: peripheral gating, effective TR: 1xRR,
Trigger Delay = recommended, Trigger window = auto trigger
window, intersequence delay = even
42 cm FOV, 5 mm thick, 1 mm space, I31.8
256 x 128, A/P, 1 NEX, scan time = 4:15
R1 = 7, R2 = 30, TG = 200, power = 10.8
Date: 0110798, series 2
Magnet: 3.0T; Coil: square H1; volunteer: Relax#5 TB
(b) Spectroscopy (update details)
Head 1st, supine, sternal notch, extremity coil, oblique
Spectro, spinecho, gating, extended dynamic range, graphic Rx,
psd file = /usr/g/genesis/fidobl
2000 spectral width, 1024 points, console freq = P-31, spectro
mode 1, 256 acquisitions, 1 x 1 x 1 CSI, soft pulse (1)
3000msec TR, peak auto center frequency
gating menu, trigger type: peripheral gating, effective TR: 3xRR,
Trigger Delay = recommended, Trigger window = auto trigger,
window, intersequence delay = even, cardiac phases = single
20 cm FOV, 30 mm thick: 4 separate acquisitions and slice
positions, Tilt = 274°
256 x 128, R/L, 4 NEX, scan time = 4:26
change cv's: pibbandfilt = 0, pixmtband = 1, pw_gph = 4msec
R1 = 7, R2 = 30, TG = 115 ; depth varies

Postprocessed with Sage_IDL™: apodize exponential 10Hz line
broadening, spectral zero-fill, fft, phase (zero order = -11,
first order = 0), localized to voxel {5 to 5} x {4 to 4}
Date: 110798, series 5, files = G00634, G00628, G00633, G00635
Magnet: 3.0T; Coil: quadrature P-31; phantom: depth

Figure 61. Myocardial pH is proportional to the frequency difference of the Pi and PCr peaks in the human, *in-vivo* phosphorus NMR spectrum.

(a) At 1.5 T the Pi peak is hidden by blood 2,3-DPG. (b) At 3.0 T the Pi peak is discernible from the 2,3-DPG peak, allowing for the measurement of pH. Both spectra obtained on the same volunteer at rest using oblique DRESS. (Parameters: 128 Acquisitions, every third heart beat TR, Oblique DRESS, 25 mm thick slice, single-turn P-31 coil; see Appendix B for more detail).

(a) 1.5 T

Head 1st, supine, sternal notch, extremity coil, oblique Spectro, spinecho, gating, extended dynamic range, graphic Rx, pad file = /usr/g/genesis/fidobl
2000 spectral width, 1024 points, console freq = P-31, spectro mode 1, 128 acquisitions, 1 x 1 x 1 CSI, soft pulse (1)
3000msec TR, peak auto center frequency
gating menu, trigger type: ECG autolead, effective TR: 3xRR,
Trigger Delay = recommended, Trigger window = auto, intersequence delay = even, cardiac phases = single
14 cm FOV, 25 mm thick, 256 x 128, not swapped, 4 NEX, scan time = 6:38
control variables: pibbandfilt = 0, pixmtband = 1
R1 = 7, R2 = 30, TG = 165; ax = 25868826

Postprocessed with FITMASTER at UAB
Date: 111198; Magnet: 1.5 T; Coil: single-turn P-31 coil;
phantom: slice profile
(b) 3.0T
Head 1st, supine, sternal notch, extremity coil, oblique
Spectro, spinecho, gating, extended dynamic range, graphic Rx,
ped file = /usr/g/genesis/fidobl
2500 spectral width, 1024 points, console freq = P-31, spectro
mode 1, 128 acquisitions, 1 x 1 x 1 CSI, soft pulse (1)
3000msec TR, peak auto center frequency
gating menu, trigger type: ECG autolead, effective TR: 3xRR,
Trigger Delay = recommended, Trigger window = 10%, intersequence
delay = even, cardiac phases = single
20 cm POV, 30 mm thick, 256 x 128, swapped, 4 NEX, scan time rest
= 6:38
control variables: pibbandfilt = 0, pixmtband = 1
R1 = 7, R2 = 30, TG = 60; ax = 21287249, back room freq =
30427790
Postprocessed with FITMASTER at UAB
Date: 111198; Magnet: 3.0T; Coil: single-turn P-31 coil

APPENDIX C
HYDRAULIC HANDGRIP

Assembly Instructions for Hydraulic Handgrip

Parts to purchase:

1. Bulb Dynamometer from North Coast Medical:
 - Includes rubber bulb and gauge already assembled
 - Part number NC70154
 - Phone: 1-800-821-9319 or 408-283-1900; fax: 408-283-1950
 - ~ \$80 + tax and shipping
2. 40 feet of stiff $\frac{1}{2}$ " inner diameter tubing
 - 5/8" outer diameter: 5/8" OD x $\frac{1}{2}$ " ID poly
 - purchased locally at Home Depot
 - ~ \$10
3. clear silicone (as used in bathrooms to water seal edges)
 - 1 tube purchased at Home Depot
 - ~ \$5
4. brass connector : I.D. Barb Splicer $\frac{1}{2}$ " by $\frac{1}{2}$ "
 - 1 piece purchased at Home Depot in plumbing department
 - ~ \$1.50
5. tie wraps or other magnetically safe circular clamp (check with a refrigerator magnet if unsure)
 - up to 10

Directions for assembly:

1. The bulb dynamometer comes in the mail with the bulb attached directly to the gauge with a metal flashing at the neck. Remove the metal flashing and discard, as this piece is not magnet safe. Pour out the liquid contents. The liquid contents are believed to be just diluted soap, to prevent growth.
2. Dry off the rubber bulb and gauge. Dab silicone over one end of the brass connector. Be careful not to silicone the opening in the brass connector; just silicone the sides of the connector where it will have contact with the rubber neck of the bulb. Insert the siliconed brass connector into the neck of the rubber bulb. Use three tie wraps to secure in place. Move the tie wrap connection for each so that they are placed at thirds around the circumference of the neck of the rubber bulb.
3. Heat up one end of the stiff $\frac{1}{8}$ " ID tube. It is recommended to submerge it in boiling water for 30 seconds to a minute. If the tube is not heated enough to soften it sufficiently it will crack and leak later. Also, coat the other end of the brass connector (sticking out of the rubber bulb) with silicone. Once the tubing is hot and soft, quickly place it over the siliconed brass connector (don't silicone the opening, just the sides where the tubing and connector will contact). Use 2 to 3 (or what you have space for) tie wraps to secure the tube in place while soft.
4. Add more silicone to the cracks to make sure that there are no easy leak spots.
5. Leave this to set overnight to be sure of a good seal.
6. Find the liquid you want to fill the contraption with. The liquid can be just water or water with soap or other antigrowth additive. Just be sure that you aren't creating more bubbles, as soap can tend

to do. Water can also be used but may need to be refilled if algae growth occurs.

7. Fill the tube with the liquid using two people and a set of stairs. One person stands at the top of the stairs and pours the liquid into the open end of the tube. The second person stands at the bottom of the stairs with the rubber bulb end of the tube and encourages the liquid to move down and the bubbles to move up (using gravity).
8. After the tubing is almost completely full of liquid, again put the remaining open end of the tube in boiling water to soften. Also put silicone over the threads of the gauge fitting, careful again not to silicone the opening. Quickly pour the liquid up to the top (heat this remaining bit of liquid first before topping off to reduce the heat loss from the softened tubing, but not so hot as to cause skin burns). Next, screw the gauge into the soft tubing, being careful not to strip the path the threads make (i.e. don't keep screwing once it is all the way in). Liquid will spill to the side, but that is ok. This will keep the bubbles to a minimum.
9. Tightly tie-wrap this end of the tubing in place and silicone around the base.
10. Again, let this sit overnight before putting any more stress on it. The next day it should be ready to work.

TIPS:

If liquid starts to leak out and/or air cavities are forming, the leak must be found and fixed. Experience has shown that it is usually at the gauge end where the leak occurs. Cut off just enough tubing to start fresh (a few inches) and reapply the connections with more heat (put the tube in near boiling water for 30 seconds) to make sure the

tube was soft enough when the connections are made. Then reapply the silicone and tie wraps and leave the handgrip in a place where it can rest for 12 hours and set.

Optional Data Recorder

The analog gauge can be replaced with a digital gauge in which the signal can be outputted and electronically recorded.

APPENDIX D
3.0 T CARDIAC ACQUISITION PROTOCOL

Instructions for Obtaining Gated Cardiac P-31 Spectra on a GE 3.0 T
SIGNA™ " Version 5.4 with In-Magnet Exercise via Handgrip

I. Setup:

1. Before the patient arrives:
 - a. Reboot the 3.0 T system. Do this via utilities, shutdown, yes. When a prompt appears after shutdown, type "b" to reboot.
 - b. Remove all coils from the magnet table and replace with padding that extends the length of the table. Over padding, place egg-foam crate material and cover with a sheet. Place a pillow in a pillowcase on the table.
 - c. Place the narrow white elastic strap on the table in the position where the patient's heart will be. Later you will use this strap to hold the P-31 coil in place. Also, attach the GE gray strap (the thinner one) to the table. This will act to hold the proton coil in place and discourage motion or movement during the scanning.
 - d. Setup the Dinamap™ monitor on a magnet-safe pole inside the magnet room such that the monitor is facing the scanning room window by the console. You will then be able to see the output of the monitor during scanning. Attach the 20 ft blue airhose and blood pressure cuff to the monitor.
 - e. Uncoil the handgrip exerciser so that the handgrip end is by the magnet table and the gauge end is by the console. Using 1 to 3

- clamps, hold the gauge in place on the back of a chair or cart where it is easily visible to the person running the scanner.
- f. Get all paperwork together (IRB consent form, MRI screening form, WISE study forms, or other), check the protocol and place a set of earplugs out for the patient/volunteer.
2. First talk the patient/volunteer through the IRB informed consent form. Have the patient/volunteer sign the form, and then have study representative sign the form. Signing this form means that the patient/volunteer understands the study parameters and their role in the study.
3. Talk the patient/volunteer through the MRI screening form. Have the patient/volunteer sign the form, and then have the study representative sign the form. Signing this form means that the information given by the patient/volunteer is correct. If there are any adverse problems noted by this questionnaire, they should be addressed before letting the patient/volunteer into the scan room.
4. If necessary, have the patient/volunteer change from the waist up into a hospital gown. This is necessary if the patient/volunteer is wearing a button up shirt (removed for comfort purposes), a bra (metal must be removed and bra will add distance to heart from coil position on exterior of chest), or any nice clothing (laying in the magnet may wrinkle clothes). NOTE: when the patient/volunteer is changing, encourage them to use the bathroom, since they may be in the magnet for up to 2 hours without a break.
5. Two options for positioning are available:
- a. Peripheral gating on the big toe: Place the patient/volunteer head first, face up on the magnet table. Put the peripheral gating device over the big toe, being careful to have the foam side on the nail side of the big toe, to ensure pulse signal is

reaching the sensor on the opposite side. (If not needing to do in-magnet exercise and/or measure blood pressure you also have the option of feet first, face up with the peripheral gating from a finger).

- b. ECG gating on back: You will be placing the patient/volunteer feet first, face up on the magnet table. This is the position recommended by GE for optimal ECG gating. Before the patient lies down, place the ECG electrodes on their back in the arrangement as pictured below. Also be sure to keep the ECG leads as straight as possible as they can add noise to the system, or pick up noise if they are not straight. Also, place a pad between the ECG wires and the patient/volunteer's skin to prevent possible burns.

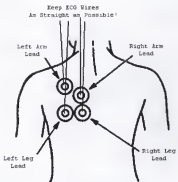


Figure 63. ECG lead placement for 3.0 T gating.

6. Place a pillow or blanket under the patient/volunteer's knees for lower back comfort. Also, check patient/volunteer temperature comfort levels. You may need to add a blanket and/or turn the

magnet fan on or off. Make sure you also give the patient/volunteer a set of earplugs and they insert them.

7. Place the P-31 coil on the chest at an estimated position over the heart. This can be estimated by a position 2/3 down the sternum and about 5 to 7 cm to the patient/volunteer's left. Use the white elastic band to keep this coil in place. Note that for the feet first positioning, you will need to use the extension for the cable to reach the end-of-bore RF coil connector.
8. Next place the 25 cm square proton coil on the chest over the P-31 coil. Be careful not to hit the patient/volunteer's chin with this coil. Note that for the feet first positioning, you will need to use the extension for the cable to reach the end-of-bore RF coil connector.
9. Check with the patient/volunteer if they are ok with exercising with their right hand and getting blood pressure from their left arm. Sometimes, medical reasons will change this default. Place the blood pressure monitor on the left arm (typically) and have the patient hold the handgrip in the right hand (typically) in a comfortable position. While the patient holds the handgrip, carefully tape the hose to the end of the table for support during the study. Make sure there are no kinks in the handgrip hydraulic hose.
10. Landmark at the center position of the P-31 coil, or as close to it as possible. Send the patient/volunteer into the magnet.
11. Once the patient/volunteer is in the magnet. Check that the Dinamap^{*} blood pressure/heart rate monitor can function. This can be a problem, sometimes, with larger patients/volunteers where the arm and blood pressure cuff are squeezed against the inside of the

magnet bore. In addition, if you get any error messages, check for leaks in the airhose connections.

II. Scanning Protocol: (for head first protocol with peripheral gating; change as needed)

1. Sagittal Scout Parameters

head 1°, supine, sternal notch, extremity coil, sagittal
2D, grad echo, flow comp, gating, extended dynamic range, fast,
variable bandwidth
arrythmia rejection = 0, flip angle = 60°, TE = min full
auto center frequency = water, 32 kHz receive bandwidth,
peripheral gating, auto trigger window
42 cm field of view, 8 mm thick, 1 mm space, L20-L60, 6 slices
256x128, A/P, 1 NEX (1:48)
R=7 R=30 TG=200 power = 11.7

2. Axial Scout

(a) Parameters:

Head first, supine, sternal notch, extremity coil, axial
3D, gradient echo, flow comp, gating, extended dynamic range,
fast, variable bandwidth, graphic Rx,
arrythmia rejection = 0, flip angle = 60°, TE = min full
auto center frequency = water, 32 kHz receive bandwidth
peripheral gating, autotrigger window,
42 cm field of view, 7 mm thick, 1 space, fallback
256x128, A/P, 1 NEX (1:48)
R1=7 R2=30 TG=200 power = 12.0

(b) After successful first acquisition of sagittal and axial images,
move coil as necessary to position over heart (refer to figures in
chapter on human techniques). After the coil is in the correct

position, and the approximate correct slice has been located, repeat the axial fast gradient echo acquisition for just one slice with breathhold (10 to 20 seconds, depending on heart beat).

3. PRESS Shim

(a) Parameters:

Head first, supine, sternal notch, extremity coil, axial
Spectro, spin echo, gating, extended dynamic range, graphic ROI,
psd=presscsci
2000 spectral width, 1024 points, console freq = H1, spectro mode
1, 16 acquisitions, 1 x 1 x 1 CSI
TE=40 msec, TR = 1000 msec
Auto center frequency = water,
gating menu, trigger type: peripheral gating, effective TR: 2xRR,
Trigger Delay = recommended, Trigger window = auto trigger
window, intersequence delay = even, cardiac phases = single
34 cm field of view, 30 mm thick, pick approximately 30 to 70 mm
rectangle over anterior heart, directly in line with surface coil
256x128, A/P, 2 NEX (0:40)

(b) change cv's: sup = 0 , suppress = 0,

(b) Spectro, start single

use dx (if necessary) to center water peak

(d) Gradient shim, autoshim, select region, 3D shim, write down numbers for x,y and z as well as set the window to 1 and move the level up and down to find the minimum and maximum points where the center column circles disappear. The difference between the two level values is a measure of the shim quality.

(e) Manual shim to sharpen the auto-picked values. Start single and set up the window for manual vertical zooming (vz): vz Y vo -45 vm Se-7 (or the vertical multiplier that works best). Then go into

gradient shim and adjust the x, y and z gradients manually to maximize the height of the water peak. It is suggested to jump by steps of 10 or 20.

(f) After optimal shimming, get an average saved; ent avg avg.

4. Oblique DRESS

(a) Parameters:

Head first, supine, sternal notch, extremity coil, oblique Spectro, spinecho, gating, extended dynamic range, graphic Rx, pad = /usr/g/genesis/fidobl
2500 spectral width, 2048 points, console freq = P-31, spectro mode 1, 128 acquisitions, 1 x 1 x 1 CSI, soft pulse (1)
TR = 2000msec, autocenter frequency = peak
gating menu, trigger type: peripheral gating, effective TR:
3xRR, Trigger Delay = recommended, Trigger window = auto trigger window, intersequence delay = even, cardiac phases = single
30 cm field of view, 25 mm thick, 0 mm space, place the slice as shown in figures from human techniques chapter
256x128, swapped, 2 NEX(6 to 8 minutes)

(b) Go to the magnet and disconnect the proton coil and connect the P-31 coil to the end of the magnet bore where the RF coils plug in.

(c) Go to the computer room and switch 4 spots: 1. Change the frequency to read 20.427790, 2. change the switch box to P-31, 3. Change the connector from head to spectro, and 4 change a connection at the penetration panel to the P-31 receiver.

(d) change cv's: pibbandfilt = 0, pixmtband = 1
spectro, r1 = 7, R2 = 30, TG = ? (will depend on type of coil and depth from the coil... see charts in chapter on phantom techniques)

- (e) "ent avg avg", will start average of 128 acquisitions. Use line broadening, phasing and other on the fly techniques to display the real data and try to examine for quality of spectra and reduced contamination from skeletal muscle and liver.
 - (f) Take a resting spectrum, 128 average with at least 2 resting values of blood pressure and heart rate (with 2 minute break between) with Dinamap™ monitor.
 - (g) Get the volunteer/patient to squeeze the handgrip as hard as they can. Record the gauge value at rest and during maximum squeeze. Take the difference of these two values, get 30 % of the difference and add to the resting value. This is the value to use for 30% of maximum isometric exercise.
 - (h) Get the patient/volunteer to start squeezing the handgrip at the 30% point, coaching via microphone if adjustments in squeezing need to be made. After 45 seconds to 1 minute of pre-squeezing, start the exercise 128 average acquisition. Take heart rate and blood pressure measurements every two minutes.
 - (i) After the exercise acquisition has completed, allow the patient/volunteer to stop squeezing, wait another minute and then record a first 128 acquisition recovery session followed by a second recovery 128 acquisition session.
5. Fill in all necessary paperwork, save all data and let the patient go. If for WISE study, send data and copies of forms (always keep a copy of all forms) to UAB for processing.

APPENDIX E
SPECTROSCOPY POST-PROCESSING INSTRUCTIONS

Instructions for Post-Processing Cardiac P-31 Spectra obtained using
Oblique FIDCSI (DRESS) on GE 3.0 T SIGNA™ Version 5.4

Introduction

There are two types of files created by the GE 3.0 T SIGNA™ version 5.4 system: G-files and P-files. The G-files consist of a single spectrum that is the result of an average of one or more spectra. The P-files are more complex data files, which are formatted depending on their originating pulse-sequence. For example, a 6x6 CSI data set would consist of a P-file organized under a header that identifies the file is not just one spectrum, but 36 spectra organized into a 6x6 matrix of set dimension. All oblique DRESS files are G-files.

Most of the data from this dissertation was analyzed with the "gold standard" for cardiac P-31 post-processing using FITMASTER™ (Philips) programmed and run by Dr. Jan den Hollander, with post-doctoral student Dr. Steven Buchthal. Dr. Jan den Hollander, a previous employee of Philips and current faculty at UAB, helped to develop this software and post-processing techniques partially for the purpose of optimized cardiac acquisitions. I was very fortunate to have his services in analyzing this data. Note, however, that FITMASTER™ requires a spectrum with good signal-to-noise ratio (SNR) to adequately operate. An example at the end of this description shows how poorly FITMASTER™ can perform when the SNR is poor.

This section is a description of how to try and accomplish the same post-processing tasks accomplished with FITMASTER™ but using the software available in Gainesville, Florida. This includes the use of the following software packages: Sage_IDL™ (GE), MRUI™ (project funded by the European Community), FELIX™ (Molecular Simulations Inc.) and a header modification program created by Dr. Marian Buzko, UF Department of Microbiology and Cell Sciences.

Take for example the post-processing of a 3.0 T P-31 cardiac spectrum obtained on 11/11/98. The original G-file was renamed as FLA3T_REST_111198. It is located on tesla at /angela/cardiac/3tcardiac/111198/.

FITMASTER™ (Philips)

The data file was FTPed to UAB. At UAB, Steve Buchthal processed the data using FITMASTER™.

To process the spectra, the rest, exercise, recovery 1 and recovery 2 data files from the same subject were first co-added. A Gaussian apodization with 15 Hz line-broadening, followed by Fourier transform, frequency flip and phasing. The fit of the summed spectra is then back extrapolated to fit the missing part of the start of the FID to achieve a flat baseline and remove the baseline roll. The sum of the spectra with the back extrapolation is then fit. The fit makes the assumption that the three ATP peaks are of equal area. The individual spectra are then individual fit based on the group fit, but now only allowing for the peak heights to change and fixing the peak positions and peak widths. The result for the resting spectrum is shown below. The bottom line shows the raw spectrum. Notice the flat baseline and the visibility of the Pi peak. The middle line is the fit of the data and the top line is the difference between the fit and the

raw data. The peak labels are added to this document only and are not part of the FITMASTER™ output.

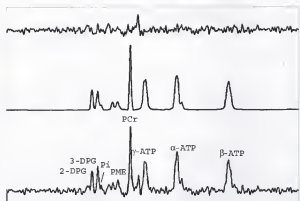


Figure 64. Example 3.0 T data set analyzed by FITMASTER™.

In addition, the FITMASTER™ program outputs the following useful data.

Pi-PCr	= 4.832e+00 [ppm]	(SD = 8.049e-02, Pi-PCr)
ATP total/3	= 3.016e+06	(SD = 4.066e+04, ATP total)
ATP-gamma	= 3.016e+06	(SD = 7.043e+04, ATP-gamma)
ATP-alfa	= 3.016e+06	(SD = 7.043e+04, ATP-alfa)
ATP-beta	= 3.015e+06	(SD = 7.042e+04, ATP-beta)
23-DPG total/2	= 9.549e+05	(SD = 6.958e+04, 23-DPG total)
PCr/Ptot	= 1.660e-01	(SD = 6.349e-03, PCr/Ptot)
ATP-gamma/Ptot	= 1.995e-01	(SD = 6.410e-03, ATP-gamma/Ptot)
Pi/PCr	= 8.816e-02	(SD = 3.595e-02, Pi/ATP)
[PCr] / [ATP]	= 8.323e-01	(SD = 2.831e-02, [PCr] / [ATP])
[PCr] / [ATP]-gamma	= 8.323e-01	(SD = 3.245e-02, [PCr] / [ATP]-gamma)
[PCr] / [ATP]	= 9.394e-01	(blood corrected

From this data, pH can also be calculated based on the ppm difference between Pi and PCr (line 1).

$$\text{pH} = 6.75 + \log_{10} \left[\frac{\text{cs} - 3.27}{5.69 - \text{cs}} \right] = 6.75 + \log_{10} \left[\frac{4.832 - 3.27}{5.69 - 4.832} \right] = 7.01$$

The following three programs are available locally and were used to process the 3T cardiac spectrum as a comparison.

SAGE_IDL™ (GE)

1. Data Conversion

(a) To convert the GE G-file to a file that SAGE_IDL™ can read you first must convert the data file. At the unix prompt, type the following:

- (i) cd /cardiac/3tcardiac/ [enter]
- (ii) sdbsm -c -q FLA3TREST_111198 [enter]
- (iii) accept all prompts except:
- (iv) change site to Signa_3.0T_VA_SHANDS_UF_HOSP
- (v) change center_freq to 51.71

2. Data Processing

(a) Follow these commands to process the data in Sage_IDL™, starting by loading the program at the unix prompt with "sage" and [enter].

(b) File - load - SAGEData

- (i) Click on "Signa_3.0T_VA_SHANDS_UF_HOSP"
- (ii) Click on "111198b"
- (iii) Click on "2125"
- (iv) Click on "5"
- (v) Click on "FLA3TREST_111198.shf"
- (vi) "load data"
- (vii) "dismiss"

(c) Processing - spectral apodize

- (i) Function - "exponential"
- (ii) LB - "15" Hz
- (iii) "Apodize"
- (iv) "dismiss"

(d) Processing - zero-fill

- (i) "zero-fill"
- (ii) "dismiss"

(e) Processing - Fourier transform (FFT)

- (i) For a G-file type, simply hit "transform" because the spatial dimensions are not relevant for a single spectrum
- (ii) "dismiss"

(f) Processing - Phasing

- (i) "phase zero/first"
- (ii) Use the "-90" and "+90" buttons and slide bar to phase
- (iii) In this case the phasing used was 158 for zero and -2215 for first order.
- (iv) "apply phase"
- (v) "dismiss"
- (vi) The results of the phased data are as the following figure.

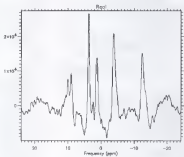


Figure 65. Example 3.0 T data set analyzed by Sage_IDL™.

(g) Processing - baseline correct

(i) "pick BL pts"

(ii) The following baseline points were picked (look carefully at the baseline of the spectrum shown for grayed "x" signs):

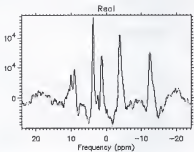


Figure 66. Example 3.0 T data set analyzed by Sage_IDL™ with baseline correction points selected.

(iii) Next button to push: "correct BL"

(iv) The result of a baseline correction with points manually picked to be the baseline are shown in the following figure. Note that the role of the baseline is not entirely fixed, as can be seen by the comparison of the baseline corrected spectrum with the FITMASTER™ extrapolation corrected spectrum.

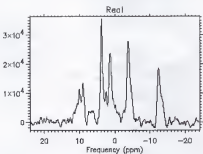


Figure 67. Example 3.0 T data set analyzed by Sage_IDL™ with baseline correction.

(h) Analysis - Create Peak Table

(i) Threshold = 35%, pick peaks

(ii) 6 peaks (the 6 highest) are picked with the following ppm values: (10.06, 9.09, 3.73, 1.25, -3.80, -12.44)
 (iii) Note that this method of analysis does not allow the Pi peak to become visible.

(i) Analysis - Marquardt fitting

(i) Function - Gaussian

(ii) Fit

(iii) The following parameters result (ppm from create peak table):

<u>Peak</u>	<u>ppm</u>	<u>Amplitude</u>	<u>Area</u>
1 (2-DPG)	10.06	8359.4	1.1361e6
2 (3-DPG)	9.09	7391.6	2.285e5
3 (PCr)	3.73	31197	1.2486e6
4 (γ -ATP)	1.25	17149	1.9791e6

5 (α-ATP)	-3.80	24718	1.8318e6
6 (β-ATP)	-12.44	16926	1.2354e6

MRUI™ (Magnetic Resonance User Interface, funded by European Community)

1. Conversion of data: All data conversion for MRUI™ is done within the program. To start the program, at the unix prompt type

(a) "matlab" [enter]

(b) If MatLab™ starts but does not start MRUI™, type MRUI™ at the MatLab™ prompt.

(c) Once in MRUI™ use the following commands to convert the GE G-file:

(i) Conversion - GEdata - 5xfiles - Gfile

(ii) /export/home/angela/cardiac/3tcardiac/111198

(iii) select file FLA3TREST_111198

(iv) save file as FLA3TREST_111198_mrui.dat

2. Data Processing

(a) Follow these commands to process cardiac P-31 spectra in MRUI™. Also remember to always use the dismiss button. Exiting out of any window in MRUI™ by closing the window itself will result in MRUI™ no longer working and requires restarting the program.

(b) Database - SETUP - experimental

(i) File - load - file - FLA3T_REST_111198_mrui.dat

(ii) SETUP

(iii) Nucleus = P-31

(iv) B0 = 3.0 T

(v) Transmit freq = 51.71

(c) Next - Peak Pick

(i) File - load - file - FLA3TREST_111198_mrui.dat

- (ii) When the data is opened, at the bottom of the window adjust the line-broadening to 15 Hz.
- (iii) At the top of the window adjust the phase, in this case phzero = 242.2 and tbegin = 2.651.
- (iv) This results in the following spectrum:

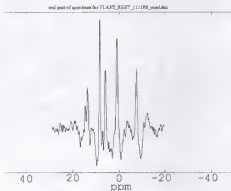


Figure 68. Example 3.0 T data set processed by MRUI™.

- (d) Peakpick - start peakpick - peakpick until {done}
 - (i) Pick 6 peaks.
- (e) Next - InputVARPRO
 - (i) Input - done
- (f) Next - InputAMARES
 - (i) Input - done
- (g) Next - VARPROMARES
 - (i) Go!
- (h) The result of a Varpro fit as shown as follows where the bottom line is the initial data, the middle line is the fit and the top line is the difference between the fit and the original data.

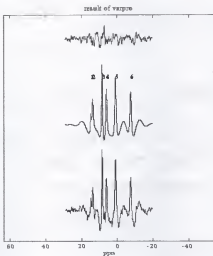


Figure 69. Example 3.0 T data set analyzed by MRUI™.

(i) In addition, the following data was outputted:

<u>Peak</u>	<u>Freq</u>	<u>Line Width</u>	<u>Amplitude</u>	<u>Std Dev</u>
1 (2-DPG)	14.723	10.759	57.39	16.57
2 (3-DPG)	13.677	33.104	215.99	59.52
3 (PCr)	8.434	12.923	289.02	17.57
4 (γ -ATP)	6.013	31.226	326.30	50.00
5 (α -ATP)	0.999	35.046	435.12	58.70
6 (β -ATP)	-7.491	43.927	416.29	83.48

(j) Unfortunately, the Pi peak was too small to be found with this software, as was also true for Sage/IDL. Provided that it had been found, the frequency difference between PCr and Pi can be converted to ppm and then the pH calculated.

(h) Note that MRUI™ is a time domain post-processing and fit tool and therefore does not come with baseline corrections, which is a frequency domain fit tool. In addition, neither Sage_IDL™ nor MRUI™ come with back extrapolation or any method for fitting the missing start of the FID.

FELIX™ (Molecular Simulations Inc.)

FELIX™ is a program that does not run on "tesla" but on a SGI computer at the Brain Institute. An account can be setup by David Parks or Haiquan Dai.

1. File Conversion

(a) First, while still on "tesla" you must convert the data so that FELIX™ can read it. You will accomplish this through a combination of using MRUI™, MatLab™ (which MRUI™ runs from), ws-ftp on your PC, and excel™.

(b) If you haven't already, convert the file to an MRUI™ compatible .dat file as shown in the above MRUI™ conversion section. This process will also create a .mat file.

(b) Quit MRUI™, but keep MatLab™ running. At the MatLab™ prompt type "la2b". Follow the instructions and convert the .mat file to a .gnu file.

(c) Go to the PC and use ws-ftp to grab the .gnu file to the PC.

(d) Open Microsoft Excel™ on the PC and open .gnu file. Select and delete the first column of data (the time). The next two columns represent real and imaginary data. Flip these two column positions. Save the file as a short file name .txt like FLAREST.txt.

(e) Use the PC tool, ws-ftp, to put the 3Trest.txt file back on tesla.

(f) In angela's account on tesla there is an executable file called ascii2felix or angela. To run these files type "ascii2felix" or "./angela" to get the prompt and instructions on format.

(i) ascii2felix filename filesize basewidth(Hz) freq(MHz)

(ii) As an example, to convert the 3TREST.txt to a FELIX™ type .dat file, type the following at the command prompt.

(iii) Ascii2felix 3TREST.txt 1024 2500 51.71

(iv) FLAREST.dat is created.

(g) Ftp this file to the computer that runs FELIX™.

2. Data Processing

(a) Connect to the computer with FELIX™ and ftp the .dat FELIX™ file to that computer as follows:

(i) Xhost +

(ii) telnet brain.ufbi.ufl.edu

(iii) login and password

(iv) setenv DISPLAY tesla.xray.ufl.edu:0.0

(v) cd data

(vi) ftp 128.227.164.247

(vii) login and password

(viii) bin

(ix) cd /cardiac/3tcardiac/111198

(x) get FLAREST.dat

(xi) by

(b) at the prompt, type "felix" [enter]

(c) at this point, don't open a database

(i) file - open

(ii) felix new data (*.dat)

(iii) FLAREST.dat

- (d) Process - Window Function
 - (i) Exponential - ok
 - (ii) Spectral width = 2500
 - (iii) Line broadening = 15, Ok
- (e) Process - transform -complex fft - ok
- (f) Process - Phase correction
 - (i) Real time - OK
 - (ii) Drag bars for phase 0 and phase 1
 - (iii) In this case, phase 0 = 207.1 & phase 1 = -2208.5
 - (iv) "keep"
 - (v) Here is the result for this example:

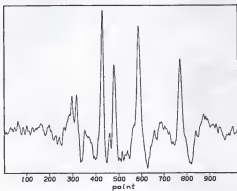


Figure 70. Example 3.0 T data set processed by FELIX™.

- (g) Peakpick - PickAll
 - (i) Cursor selection
 - (ii) 1st put a line at the threshold of the peaks and it automatically peaks all peaks above the threshold

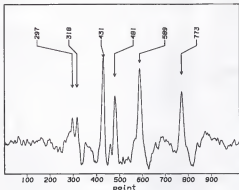


Figure 71. Example 3.0 T data set processed by FELIX™ with peaks picked.

(h) Process - Baseline Correct

- (i) Baseline Point - Pick points via cursor, Ok
- (ii) [esc] when done

(i) Process - Baseline Correct

- (i) Baseline Correct - Automatic w/abl
- (ii) Noise size (#pts) = 4
- (iii) Peak size (points) = 40

(iv) The baseline correction was not optimal for the ATP peaks.

It had a hard time with wide based peaks with uneven baselines to either side of the peak (due to missing start of FID causing rolling baseline).

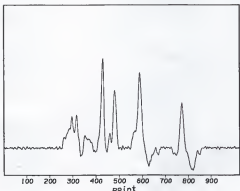


Figure 72. Example 3.0 T data set processed by FELIX™ with baseline correction.

- (j) Peaks - Optimize - Optimize (to fit a spectrum)
- (i) Start - wait to complete
- (ii) Use "previous" and "next" buttons to go through each peak.

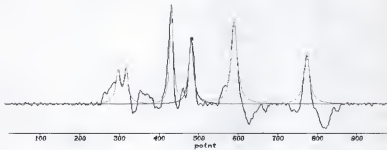


Figure 73. Example 3.0 T data set analyzed by FELIX™.

- (iii) The output from FELIX™ is as follows (for baseline correction):

<u>Peak</u>	<u>Center (Freq)</u>	<u>Height</u>	<u>Width</u>	<u>Integral (Areal)</u>
1 (2-DPG)	298.0	2613.5	14.0	56974.609
2 (3-DPG)	318.0	2695.5	12.0	50429.828
3 (PCr)	432.0	7915.5	10.0	1.236e5
4 (g-ATP)	481.0	5093.2	14.0	1.110e5
5 (a-ATP)	590.0	6655.3	18.0	1.861e5
6 (b-ATP)	773.0	3979.8	18.0	1.113e5

Final Comparison of All Methods:

Based on these results as shown in Table 27, it appears that in this case for a cardiac spectrum with good SNR, the locally applied methods were adequate at duplicating the FITMASTER™ result, with MRUI™ being the closest at getting the right value based on good fit algorithms. Note, that this FELIX™ routine was performed with baseline correction but without the fit of the initial missing part of the FID. FELIX™ does have a routine, called linear prediction, for fitting of the beginning of the FID but it is designed to replace data but not add data to the start of the FID.

Table 27. Comparison of Cardiac P-31 Post-Processing Software.

Method	Average	2,3-DPG	PCr	[PCr]/[ATP]	Blood	and Relaxation Corrected
	ATP	/2		[TP]	Raw	
FITMASTER™ (areas)	3016000	954900	-	0.8323	0.9394	1.0052
Sage IDL™ before Baseline Correction (areas)	723507	287065	6.71E+05	0.9279	1.0825	1.1583
Sage IDL™ after Baseline Correction (areas)	1682100	171055	1.25E+06	0.7423	0.7705	0.8244
MRUI™ (no area/amplitudes only)	392.57	136.69	289.02	0.7362	0.8417	0.9007
FELIX™ (integral areas)	136133.3	53702.2	1.24E+05	0.9079	1.0582	1.1323

An Example Where Poor SNR caused FITMASTER™ to Fail:

1. Sage_IDL™

- (a) Here is a 1.5 T WISE oblique DRESS P-31 Cardiac study where the SNR was low and there was no skeletal muscle contamination as shown in this figure from SAGE_IDL™.

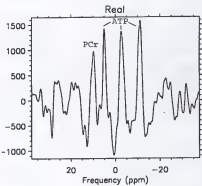


Figure 74. Example 1.5 T data set with low SNR analyzed by SAGE_IDL™.

(b) Here is the data output from SAGE_IDL™:

Peak	ppm	amplitude	area
1 (DPG)	19.65	327.01	9188.5
2 (DPG)	17.95	364.12	16940
3 (DPG)	16.63	376.60	9443.8
4 (PCr)	9.62	984.90	36049
5 (γ -ATP)	4.79	1464.90	50305
6 (α -ATP)	-3.25	1336.70	60765
7 (β -ATP)	-11.50	1721.0	75723

(c) Based on this output, which seems to fit well with the spectrum, the PCr peak is below the average ATP peaks.

$$(i) \text{ Avg_ATP} = \frac{50305 + 60765 + 75723}{3} = 62264.3$$

$$(ii) \text{ Total_DPG} = 9188.5 + 16940 + 9443.8 = 35572.3$$

$$(iii) [\text{PCr}] / [\text{ATP}] (\text{raw}) = 36049 / 62264.3 = 0.58$$

(iv)

$$\text{PCr / ATP}_{\text{blood}}_{\text{corrected}} = \frac{\text{PCr}}{\text{ATP} - \text{Total_DPG} * \text{blood_correction_factor}}$$

$$(v) \text{ PCr / ATP}_{\text{blood}}_{\text{corrected}} = \frac{36049}{62264.3 - 35572.3 * 0.18} = 0.6453$$

$$(vi) \text{ PCr / ATP}_{\text{blood}}_{\text{and saturation corrected}} = 0.6453 * 1.1 = 0.71$$

(d) Therefore, with all of the correction factors included (which increase the [PCr]/[ATP] ratio) the maximum value of [PCr]/[ATP] is 0.71. And the baseline correction necessary does not look to be extreme enough to double the height of the PCr.

(2) FITMASTER™

(a) Despite the results of Sage_IDL™, FITMASTER™ incorrectly corrected for and fitted in missing part of the FID to incorrectly enhance the PCr peak height, shown in the solution from the FITMASTER™ as below.

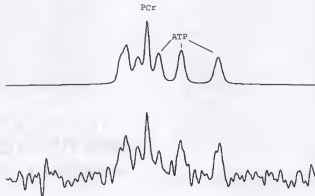


Figure 75. Example 1.5 T data set with low SNR analyzed by FITMASTER™.

(b) The numerical output from the FITMASTER™ program are listed below:

- (i) $\text{Pi-PCr} = 4.535 \pm 0.15 \text{ ppm}$
- (ii) $\text{ATP total/3} = 3.817 \times 10^5 \pm 2.11 \times 10^4$
- (iii) $\text{23-DPG total/2} = 1.724 \times 10^5 \pm 3.47 \times 10^4$
- (iv) $[\text{PCr}]/[\text{ATP}] = 1.324 \pm 0.15$
- (v) $[\text{PCr}]/[\text{ATP}] \text{ (blood corrected)} = 1.58$
- (vi) $[\text{PCr}]/[\text{ATP}] \text{ (blood and relaxation corrected (1.28))} = 2.024 \pm 0.31$

(c) Their spectrum and numerical result puts the corrected $[\text{PCr}]/[\text{ATP}]$ ratio at 2.024. This is due to the large amount of

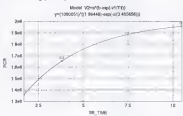
noise in the spectrum (low SNR) creating a situation that was difficult to correctly fit the missing part of the FID. Therefore, the resulting spectrum is incorrectly labeled as skeletal muscle contamination when the true cause of the problem is low SNR.

APPENDIX F
HUMAN T_1 RELAXATION DATA

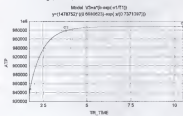
Results of fitting data to T_1 relaxation equation with Statistica software (StatSoft, Inc.).

Subject C.M.

(a) PCR Fit ($r=1.0$)
 $T_1(\text{PCR}) = 3.47$ seconds

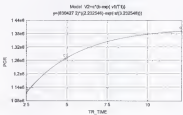


(b) ATP_{sc} Fit ($r=1.0$)
 $T_1(\text{ATP}) = 0.74$ seconds

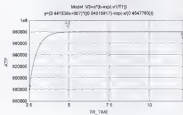


Subject D.P.

(a) PCR Fit ($r=1.0$)
 $T_1(\text{PCR}) = 3.23$ seconds



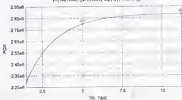
(b) ATP_{sc} Fit ($r=0.98$)
 $T_1(\text{ATP}) = 0.45$ seconds



Subject L.R.(a) PCr Fit ($r=1.0$)
 $T_1(\text{PCr}) = 1.85 \text{ seconds}$

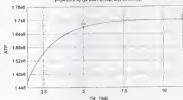
$$\text{Model: } V0=a/(b-\exp(-c/T))$$

$$y=(1321854/(1.218406)-\exp(a/(1.848877)))$$

(b) ATP_{sc} Fit ($r=1.0$)
 $T_1(\text{ATP}) = 1.67 \text{ seconds}$

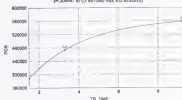
$$\text{Model: } V0=a/(b-\exp(-c/T))$$

$$y=(86531.4/(2.0421)-\exp(a/(1.669985)))$$

Subject L.B.(a) PCr Fit ($r=1.0$)
 $T_1(\text{PCr}) = 2.8 \text{ seconds}$

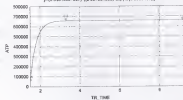
$$\text{Model: } V0=a/(b-\exp(-c/T))$$

$$y=(308847.8/(2.857308)-\exp(a/(2.853550)))$$

(b) ATP_{sc} Fit ($r=0.99$)
 $T_1(\text{ATP}) = 0.30 \text{ seconds}$

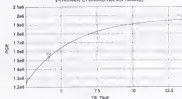
$$\text{Model: } V0=a/(b-\exp(-c/T))$$

$$y=(3.642118e+007/(3.00793/0.995)-\exp(a/(3.008156)))$$

Subject R.B.(a) PCr Fit ($r=1.0$)
 $T_1(\text{PCr}) = 3.16 \text{ seconds}$

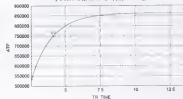
$$\text{Model: } V0=a/(b-\exp(-c/T))$$

$$y=(1853404/(1.208838)-\exp(a/(3.165250)))$$

(b) ATP_{sc} Fit ($r=1.0$)
 $T_1(\text{ATP}) = 1.47 \text{ seconds}$

$$\text{Model: } V0=a/(b-\exp(-c/T))$$

$$y=(1801817/(2.4545033)-\exp(a/(1.466548)))$$



At least three points are needed to fit a nonlinear function. Therefore, the two TR data acquisitions obtained on T.B. will not be used to estimate the T_1 value of PCr and ATP. However, a ratio of the metabolite area values for short and long TR can be used as a correction factor provided the TR for the acquisition is the same as the short TR value for T.B., namely a TR of 4.2 seconds. The relaxation correction factor (RCF) is then given by the metabolite area value of the long TR time over that for the short TR time, for a given P-31 metabolite or ratio, using the blood corrected (BC) value for ATP.

$$RCF(PCr) = \frac{PCr_{longTR}}{PCr_{shortTR}} = \frac{5.000e6}{4.589e6} = 1.09$$

$$CF(ATP_{BC}) = \frac{ATP_{BC,longTR}}{ATP_{BC,shortTR}} = \frac{2.841e6}{2.622e6} = 1.08$$

$$CF\left(\frac{PCr}{ATP_{BC}}\right) = \frac{[PCr / ATP_{BC}]_{longTR}}{[PCr / ATP_{BC}]_{shortTR}} = \frac{5.000e6 / 2.841e6}{4.589e6 / 2.622e6} = 1.01$$

Therefore, 1.01 is a single measure approximation for the T_1 relaxation correction factor for the TR time of 4.2 seconds.

APPENDIX G
T₁ RELAXATION RATES OF DEPTH PHANTOM

Relaxation rates of MDPA in the depth phantom were measured on both the 1.5 and 3.0 T systems using an FIDCSI 35 cm slice.

Model v2=a*(b-exp(-v1/T1))
 $y=(288.2954)*(1.014155)\exp(-x/(5.527841))$

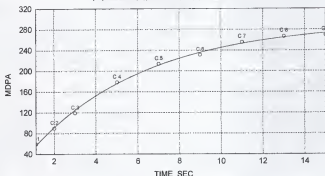


Figure 76. 1.5 T T₁ relaxation curve for MDPA (T₁ = 5.53 sec)

Model v2=a*(b-exp(-v1/T1))
 $y=(497698.8)*(1.157486)\exp(-x/(6.041721))$

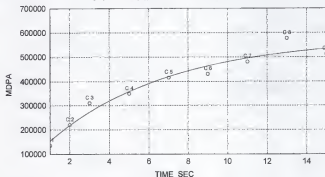


Figure 77. 3.0 T T₁ relaxation curve for MDPA (T₁ = 6.04 sec)

REFERENCES

1. AHA, The official web site of the American Heart Association. 1997, AHA: www.amhrt.org.
2. DeBakey, M.E. and A.M. Gotto, *The New Living Heart*. 1997, Holbrook, Massachusetts: Adams Media Corporation.
3. Bemiller, C.R., C.J. Pepine, and A.K. Rogers, *Long-term observations in patients with angina and normal coronary arteriograms*. *Circulation*, 1973. 47(1): p. 36-43.
4. Pepine, C., personal communication. January 1998 - July 1999.
5. Nunnally, R. and P. Bottomley, *Assessment of pharmacological treatment of myocardial infarction by phosphorus-31 NMR with surface coils*. *Science*, 1981. 211(4478): p. 177-180.
6. Flaherty, J.R., M.L. Weisfeldt, B.H. Bulkley, T.J. Gardner, V.L. Gott, and W.E. Jacobus, *Mechanisms of ischemic myocardial cell damage assessed by phosphorus-31 nuclear magnetic resonance*. *Circulation*, 1982. 65(3): p. 561-570.
7. Bottomley, P., *MR Spectroscopy of the human heart: the status and the challenges*. *Radiology*, 1994. 191: p. 593-612.
8. de Roos, A. and E.E. van der Wall, *Evaluation of ischemic heart disease by magnetic resonance imaging and spectroscopy*. *Radiol Clin North Am*, 1994. 32(3): p. 581-92.
9. Bottomley, P.A., *Noninvasive study of high-energy phosphate metabolism in human heart by depth-resolved 31P NMR spectroscopy*. *Science*, 1985. 229(4715): p. 769-772.
10. Jung, W.-I., S. Widmaier, U. Seeger, M. Bunse, A. Staubert, L. Sieverding, K. Straubinger, F. van Erkelens, F. Schick, G. Dietze, and O. Lutz, *Phosphorus J coupling constants of ATP in human myocardium and calf muscle*. *J Magn Reson Series B*, 1996. 110: p. 39-46.
11. Hardy, C.J., R.G. Weiss, P.A. Bottomley, and G. Gerstenblith, *Altered myocardial high-energy phosphate metabolites in patients with dilated cardiomyopathy*. *Am Heart J*, 1991. 122(3 Pt 1): p. 795-801.
12. Yabe, T., K. Mitsunami, M. Okada, S. Morikawa, T. Inubushi, and M. Kinoshita, *Detection of myocardial ischemia by 31P magnetic resonance spectroscopy during handgrip exercise*. *Circulation*, 1994. 89(4): p. 1709-1716.

13. Kuno, S.-y., T. Ogawa, S. Katsuta, and Y. Itai, In vivo human myocardial metabolism during aerobic exercise by phosphorus-31 nuclear magnetic resonance spectroscopy. *Eur J Appl Physiol*, 1994. 69: p. 488-91.
14. Neubauer, S., T. Krahe, R. Schindler, H. Hillenbrand, C. Entzeroth, M. Horn, W. Bauer, T. Stephan, K. Lackner, A. Haase, and G. Ertl, Direct measurement of spin-lattice relaxation times of phosphorous metabolites in human myocardium. *Magn Reson Med*, 1992. 26(2): p. 300-307.
15. Matson, G.B., D.B. Twieg, G.S. Karczmar, T.J. Lawry, J.R. Gober, M. Valenza, M.D. Boska, and M.W. Weiner, Application of image-guided surface coil P-31 spectroscopy to human liver, heart and kidney. *Radiology*, 1988. 169: p. 541-547.
16. Hetherington, H.P., D.J. Luney, J.T. Vaughan, J.W. Pan, S.L. Ponder, O. Tschendel, D. Twieg, and G.M. Pohost, 3D 31P spectroscopic imaging of the human heart at 4.1 T. *Magn Res Med*, 1995. 33: p. 427-431.
17. Menon, R.S., K. Hendrich, X. Hu, and K. Ugurbil, 31P NMR spectroscopy of the human heart at 4T: detection of substantially uncontaminated cardiac spectra and differentiation of subepicardium and subendocardium. *Magn Res Med*, 1992. 26: p. 268-276.
18. Loeffler, R., R. Sauter, H. Kolem, A. Haase, and M. von Kienlin, Localized spectroscopy from anatomically matched compartments: improved sensitivity and localization for cardiac 31P MRS in humans. *J Magn Reson*, 1998. 134(2): p. 287-299.
19. Mitsunami, K., T. Yabe, S. Inoue, M. Kinoshita, S. Morikawa, and T. Inubushi, Left ventricular systolic and diastolic function and NMR-visible myocardial inorganic phosphate content determined by 31P NMR spectroscopy in hypertrophied human heart, in *Proceedings of the International Society for Magnetic Resonance in Medicine: Fifth Scientific Meeting & Exhibition*, B. Vancouver, Canada, 1997, SMRM: Berkeley, CA, USA. p. 1282.
20. Bottomley, P.A., E. Atalar, and R.G. Weiss, Human cardiac high-energy phosphate metabolite concentrations by 1D-resolved NMR spectroscopy. *Magn Reson Med*, 1996. 35(5): p. 664-670.
21. Miali-Allen, V.M., G.J. Kemp, B. Rajagopalan, D.J. Taylor, G.K. Radda, and S.G. Haworth, Magnetic resonance spectroscopy in congenital heart disease. *Heart*, 1996. 75: p. 614-619.
22. Pluim, B.M., J.C. Chin, A. De Roos, J. Doornbos, H.M. Siebelink, A. Van der Laarse, H.W. Vliegen, R.M. Lamerichs, A. Bruschke, and E.E. Van der Wall, Cardiac anatomy, function and metabolism in elite cyclists assessed by magnetic resonance imaging and spectroscopy. *Eur Heart J*, 1996. 17(8): p. 1271-1278.
23. Buchthal, S., J. den Hollander, C. Katholi, J. Caulfield, G. Pohost, and W. Evanochko, Clinical cardiac rejection assessed by

- P-31 MRS: the final phase I analysis, in *Proceedings of the Society of Magnetic Resonance in Medicine: Fourth Scientific Meeting & Exhibition*, N. New York, 1996, SMRM: Berkeley, CA, USA. p. 1011.
24. Herfkens, R., H. Charles, R. Negro-Vilar, and P. van Trigt, *In vivo phosphorus-31 NMR spectroscopy of human heart transplants*, in *Book of Abstracts, Society of Magnetic Resonance in Medicine, 7th Annual Scientific Meeting & Exhibition*, C. San Francisco, USA, 1988, SMRM: Berkeley, CA, USA. p. 827.
 25. Conway, M., J. Bristow, M. Blackledge, B. Rajagopalan, and G. Radda, *Cardiac metabolism during exercise measured by magnetic resonance spectroscopy (letter)*. *Lancet*, 1988. ii: p. 692.
 26. Weiss, R., *A clinical perspective of cardiac NMR spectroscopy*, in *Book Of Abstracts, Society of Magnetic Resonance in Medicine, 10th Annual Scientific Meeting & Exhibition*, C. San Francisco, USA, 1991, SMRM: Berkeley, CA, USA. p. 327.
 27. Yabe, T., K. Mitsunami, M. Okada, M. Kinoshita, S. Morikawa, and T. Inubushi, *Quantitative measurements of phosphorus metabolites in coronary artery diseases by 31P slice-selected one-dimensional chemical shift imaging*, in *Proceedings of the Society for Magnetic Resonance in Medicine: 2nd Annual Scientific Meeting*, C. San Francisco, USA, 1994, SMRM: Berkeley, CA, USA. p. 1220.
 28. Lamb, H., J. Doombos, J. den Hollander, H. Beyerbach, and A. de Roos, *Strategies for cardiac 31P -MR spectroscopy at rest and during dobutamine stress: a study of reproducibility*, in *Proceedings of the Society of Magnetic Resonance: 3rd Scientific Meeting & Exhibition & The European Society for Magn Reson & Biol: 12th Annual Meeting & Exhibition*, F. Nice, 1995, SMRM: Berkeley, CA, USA. p. 96.
 29. Health Care Finance Administration, *National Physician Fee Schedule Relative Value File*; <http://www.hcfa.gov/stats/cpt/rvudown.htm>. 1999, Department of Health and Human Services: Washington, DC.
 30. Nunnally, R.L., ed. *NMR spectroscopy for in vivo determination of metabolism: An overview*. *NMR in medicine: The instrumentation and clinical applications*, ed. S.R. Thomas and R.L. Dixon. 1986, American Institute of Physics, Inc.: New York, New York. 249-268.
 31. Bushberg, J.T., J.A. Seibert, E.M. Leidholdt, and J.M. Boone, *The Essential Physics of Medical Imaging*. 1994, Baltimore, Maryland: Williams & Wilkins.
 32. Ernst, R., G. Bodenhausen, and A. Wokaun, *Principles of Nuclear Magnetic Resonance Spectroscopy in One and Two Dimensions*. 1987, Oxford, UK: Oxford University Press.
 33. Brey, W., ed. *Pulse Methods in 1D and 2D Liquid Phase-NMR*. 1988, Academic: San Diego, CA.

34. Scott, A.I. and R.L. Baxter, *Applications of C-13 to metabolic studies*. Ann Rev Biophys Bioeng, 1981. 10: p. 151-174.
35. Bruhn, H., J. Frahm, M.L. Gyngell, K.D. Merboldt, W. Hanicke, R. Sauter, and C. Hamburger, *Cerebral metabolism in man after acute stroke: new observations using localized proton NMR spectroscopy*. Radiology, 1989. 9(1): p. 126-131.
36. Negengark, W., *Studies of human tumors by MRS: a review*. NMR Biomed, 1992. 5(5): p. 303-324.
37. Ng, T.C., Y.G. Comair, M. Xue, N. So, A. Majors, H. Kolem, H. Luders, and M. Modic, *Temporal lobe epilepsy: presurgical localization with proton chemical shift imaging*. Radiology, 1994. 193: p. 465-472.
38. Salibi, N. and M.A. Brown, *Clinical MR Spectroscopy: First Principles*. 1998, New York, NY: Wiley-Liss.
39. Hayes, C.E., *Radio frequency coils*, in *Medical Physics Monograph No. 14: NMR in Medicine: The Instrumentation and Clinical Applications*, S.R. Thomas and R.L. Dixon, 1986, American Institute of Physics, Inc.: New York, NY.
40. Robitaille, P.-M., H. Merkle, E. Sublett, K. Hendrick, B. Lew, G. Path, A.H.L. From, R.J. Bache, M. Garwood, and K. Ugurbil, *Spectroscopic imaging and spatial localization using adiabatic pulses and applications to detect transmural metabolite distribution in the canine heart*. Magn Reson Med, 1989. 10: p. 14-37.
41. Hoffenberg, E.F., P. Kozlowski, T.A. Salerno, and R. Deslauriers, *Evaluation of cardiac 31P magnetic resonance spectroscopy: reviewing NMR principles*. J Surg Res, 1996. 62: p. 135-143.
42. Moseley, M.E., ed. *Imaging techniques: Pulse sequences from spin-echo to diffusion*. Magnetic Resonance Imaging of the Body, ed. C.E. Higgins, H. Hricak, and C. Helms. 1992, Raven Press: New York, New York. 157-174.
43. Hutchinson, J., B. Sutherland, and J. Mallard, *Three dimensional NMR imaging using selective excitation*. J Phys, 1978. 1: p. 217.
44. Crooks, L., *Selective irradiation line-scan techniques of NMR imaging*. IEEE Trans Nucl Sci, 1980. 27: p. 1239.
45. Bottomley, P.A., T.B. Foster, and R.D. Darrow, *Depth-resolved surface-coil spectroscopy (DRESS) for in vivo 1H, 31P, and 13C NMR*. J Magn Reson, 1984. 59: p. 338-342.
46. Bottomley, P., L. Smith, W. Leue, and C. Charles, *Slice-interleaved depth resolved surface-coil spectroscopy (SLIT DRESS) for rapid 31P NMR in vivo*. J Magn Reson, 1985. 64: p. 347-351.
47. Bottomley, P.A., B.P. Drayer, and L.S. Smith, *Chronic Adult Cerebral Infarction Studied by Phosphorus NMR Spectroscopy*. Radiology, 1986. 160: p. 763-766.

48. Blackledge, M.J., B. Rajagopalan, R.D. Oberhaensli, N.M. Bolas, P. Styles, and G.K. Radde, Quantitative studies of human cardiac metabolism by $P-31$ rotating frame NMR. Proc Natl Acad Sci, USA, 1987. 84: p. 4283-4287.
49. Weiss, R.G., P.A. Bottomley, C.J. Hardy, and G. Gerstenblith, Regional myocardial metabolism of high energy phosphates during isometric exercise in patients with coronary artery disease. N. Engl. J. Med., 1990. 323(23): p. 1593-1600.
50. Hartiala, J., H. Sakuma, and C. Higgins, Magnetic resonance imaging and spectroscopy of the human heart. Scand J Clin Lab Invest, 1993. 53: p. 425-437.
51. Mitsunami, K., T. Yabe, M. Okada, S. Endoh, M. Kinoshita, S. Morikawa, and T. Inubushi, Cardiac high-energy phosphate metabolism before and after percutaneous transluminal coronary angioplasty, in Proceedings of the Society for Magnetic Resonance in Medicine: 2nd Annual Scientific Meeting, C. San Francisco, USA, 1994, SMRM: Berkeley, CA, USA. p. 1229.
52. Okada, M., K. Mitsunami, T. Yabe, M. Kinoshita, S. Morikawa, and T. Inubushi, Quantitative comparison of cardiac $31P$ NMR Spectroscopy and $201Tl$ SPECT imaging in patients with old myocardial infarction, in Proceedings of the Society of Magn Reson in Medi: 12th Annual Scientific Meeting & Exhibition, N. New York, 1993, SMRM: Berkeley, CA, USA. p. 1090.
53. Mitsunami, K., T. Yabe, M. Okada, S. Inoue, M. Kinoshita, S. Morikawa, and T. Inubushi, Quantitative analysis of myocardial phosphate metabolism in idiopathic cardiomyopathy by $31P$ NMR spectroscopy, in Proceedings of the Society of Magnetic Resonance: 3rd Scientific Meeting & Exhibition & The European Society for Magn Reson & Biol: 12th Annual Meeting & Exhibition, F. Nice, 1995, SMRM: Berkeley, CA, USA. p. 1441.
54. Yabe, T., K. Mitsunami, M. Okada, S. Endoh, H. Miura, T. Inubushi, and M. Kinoshita, Detection of myocardial ischemia by $31P$ -magnetic resonance spectroscopy during hand-grip exercise. J Am Coll Cardiol, 1993. 21: p. 113A.
55. Sakuma, H., K. Takeda, T. Tagami, Y. Kinoshita, T. Nakagawa, Okamoto, T. Konishi, and T. Nakano, $P-31$ MR spectroscopy in hypertrophic cardiomyopathy with correlation of blood contamination: Comparison with $Tl-201$ myocardial perfusion imaging, in Book Of Abstracts, Society of Magnetic Resonance in Medicine, 10th Annual Scientific Meeting & Exhibition, C. San Francisco, USA, 1991, SMRM: Berkeley, CA, USA. p. 75.
56. Sakuma, H., K. Takeda, K. Yamakado, Y. Kinoshita, T. Nakagawa, S. Okamoto, T. Konishi, T. Nakano, Y. Okamoto, and K. Nagasawa, $P-31$ NMR spectroscopy in patients with hypertrophic cardiomyopathy, in Book Of Abstracts, Society of Magnetic Resonance in Medicine, 9th Annual Scientific Meeting & Exhibition, N. New York, 1990, SMRM: Berkeley, CA, USA. p. 248.

57. Conway, M., R. Ouwerkerk, B. Rajagopalan, G. Radde, and P. Bottomley, Low PCR/ATP ratio in eccentric hypertrophy in severe mitral regurgitation, in *Proceedings of the Society for Magnetic Resonance in Medicine: 2nd Annual Scientific Meeting*, C. San Francisco, USA, 1994, SMRM: Berkeley, CA, USA. p. 1218.
58. Conway, M., R. Ouwerkerk, B. Rajagopalan, and G. Radde, ³¹P MRS of the human heart in 172 patients, in *Proceedings of the Society of Magnetic Resonance: 3rd Scientific Meeting & Exhibition & The European Society for Magn Reson & Biol: 12th Annual Meeting & Exhibition*, F. Nice, 1995, SMRM: Berkeley, CA, USA. p. 94.
59. Bastin, M., A. Blamire, and P. Styles, Numerical calculation of saturation factors in ³¹P human cardiac spectroscopy, in *Proceedings of the Society of Magnetic Resonance in Medicine: Fourth Scientific Meeting & Exhibition*, N. New York, 1996, SMRM: Berkeley, CA, USA. p. 1010.
60. Yabe, T., K. Mitsunami, i.T. Imabush, and M. Kinoshita, Quantitative measurements of cardiac phosphorous metabolites in coronary artery disease by ³¹P magnetic resonance spectroscopy (see comments). *Circulation*, 1995. 92: p. 15-23.
61. Sakuma, H., S.J. Nelson, D.B. Vigneron, J. Hartials, and C. Higgins, B, Measurement of T1 relaxation times of cardiac phosphate metabolites using BIR-4 adiabatic RF pulses and a variable mutation method. *Magn Reson Med*, 1993. 29: p. 688-691.
62. Bottomley, P.A. and R.G. Weiss, Reductions in creatine kinase metabolite concentrations in infarcted myocardium by noninvasive MRS, in *Proceedings of the International Society for Magnetic Resonance in Medicine: Fifth Scientific Meeting & Exhibition*, B. Vancouver, Canada, 1997, SMRM: Berkeley, CA, USA. p. 480.
63. Bottomley, P.A., R.G. Weiss, C.J. Hardy, and G. Gerstenblith, Assessment of myocardial ischemia in patients with coronary artery disease by ³¹P NMR stress-testing: Response to therapy, in *Book Of Abstracts, Society of Magnetic Resonance in Medicine, 9th Annual Scientific Meeting & Exhibition*, N. New York, 1990, SMRM: Berkeley, CA, USA. p. 244.
64. Schaefer, S., G.G. Schwartz, S. Steinman, D.J. Meyerhoff, B. Massie, and M.W. Weiner, Metabolic response of the heart to increased work: ³¹P NMR spectroscopy of normal and cardiomyopathic myocardium in man, in *Book Of Abstracts, Society of Magnetic Resonance in Medicine, 9th Annual Scientific Meeting & Exhibition*, N. New York, 1990, SMRM: Berkeley, CA, USA. p. 245.
65. Sieverding, L., J. Breuer, A. Staubert, W. Jung, S. Widmaier, U. Seeger, G. Dietze, O. Lutz, and J. Apitz. Proton decoupled myocardial ³¹P -NMR-spectroscopy reveals decreased PCR/PI in patients with severe hypertrophic cardiomyopathy. in *Proceedings of the Society of Magn Reson: 3rd Scientific Meeting & Exhibition & the European Society for Magn Reson & Biol: 12th Annual meeting and exhibition*. 1995. Berkeley, Calif: Society of Magn Reson.

66. Jung, W., M. Bunse, S. Widmaier, F. Schick, K. Kuper, G. Dietze, and O. Lutz, Localized ^{31}P MRS of the human heart: decreasing errors in PCr signal intensities in 2D-CSI spectroscopy, in *Proceedings of the Society of Magn Reson in Med: 12th Annual Scientific Meeting & Exhibition*, N. New York, 1993, SMRM: Berkeley, CA, USA. p. 1097.
67. Bottomley, P.A., C.H. Hardy, and P.B. Roemer, Phosphate metabolite imaging and concentration measurements in human heart by nuclear magnetic resonance. *Magn Reson Med*, 1990. 14(3): p. 425-434.
68. Loeffler, R., M. von Kienlin, K. Wicklow, A. Haase, and R. Sauter, ^{31}P spectra of the human heart *in vivo* with reduced spectral contamination using prior knowledge from MRI, in *Proceedings of the Society for Magnetic Resonance in Medicine: 2nd Annual Scientific Meeting*, C. San Francisco, USA, 1994, SMRM: Berkeley, CA, USA. p. 1171.
69. Campbell, C.M., R.T. Thompson, J. Sykes, and G. Wisenberg, Pharmaceutical moderation of myocardial metabolism during ischemia and reperfusion, in *Proceedings of the International Society for Magnetic Resonance in Medicine: Fifth Scientific Meeting & Exhibition*, B. Vancouver, Canada, 1997, SMRM: Berkeley, CA, USA. p. 1281.
70. Bottomley, P.A. and C.J. Hardy, ^{31}P spectroscopic imaging of the human heart, in *Book of Abstracts, Society of Magnetic Resonance in Medicine, 7th Annual Scientific Meeting & Exhibition*, C. San Francisco, USA, 1988, SMRM: Berkeley, CA, USA. p. 832.
71. Kolem, H., R. Sauter, M. Friedrich, M. Schneider, K. Wicklow, and K. Bachmann, A double-oblique 3D CSI technique for ^{31}P cardiac spectroscopy applied to patients with coronary artery disease, in *Proceedings of the Society of Magn Reson in Med: 12th Annual Scientific Meeting & Exhibition*, N. New York, 1993, SMRM: Berkeley, CA, USA. p. 1096.
72. Tsakos, N.V., Comprehensive evaluation of cardiac physiology with magnetic resonance imaging and spectroscopy methods (myocardial perfusion, heart wall motion). 1995, University of Minnesota.
73. Rosch, C., M.v. Kienlin, M. Horn, S. Neubauer, and A. Haase, Quantitative determination of phosphate distribution and infarct size in chronically infarcted rat heart using three-dimensional ^{31}P spectroscopic imaging, in *Proceedings of the International Society for Magnetic Resonance in Medicine: Fifth Scientific Meeting & Exhibition*, B. Vancouver, Canada, 1997, SMRM: Berkeley, CA, USA. p. 479.
74. Cho, Y.K., H. Merkle, N.V. Tsakos, J. Zhang, and K. Ugurbil, Noninvasive ^{31}P 3D-CSI of the canine heart at 9.4 T, in *Proceedings of the International Society for Magnetic Resonance in Medicine: Fifth Scientific Meeting & Exhibition*, B. Vancouver, Canada, 1997, SMRM: Berkeley, CA, USA. p. 1288.

75. Jaffer, F., H. Wen, R. Balaban, and S. Wolff, A method to improve the B_0 homogeneity of the heart *in vivo*. *Magn Reson Med*, 1996. 36(3): p. 375-383.
76. Menon, R., X. Hu, K. Hendrich, and K. Ugurbil. A 3-D fourier series window approach to ^{31}P spectroscopy. in *Proceedings of the Society of Magn Reson in Med: 12th Annual Scientific Meeting*. 1993. Berkeley, Calif: Society of Magn Reson in Med.
77. Bottomley, P., Spatial localization in NMR spectroscopy *in vivo*. *Ann NY Acad Sci*, 1987. 508: p. 333-348.
78. Bottomley, P.A. and C.J. Hardy, PROGRESS in efficient three-dimensional spatially localized *in vivo* ^{31}P NMR spectroscopy using multidimensional spatially selective pulses. *J Magn Reson*, 1987. 74: p. 550-556.
79. Haase, A. and J. Frahm, Multiple chemical-shift-selective NMR imaging using stimulated echoes. *J Magn Reson*, 1985. 64: p. 94-102.
80. Hetherington, H., D. Luney, J. Vaughan, J. Pan, S. Ponder, O. Tschendel, D. Twieg, and G. Pohost, 3D ^{31}P spectroscopic imaging of the human heart at 4.1T, in *Proceedings of the Society for Magnetic Resonance in Medicine: 2nd Annual Scientific Meeting*, C. San Francisco, USA, 1994, SMRM: Berkeley, CA, USA. p. 86.
81. Luney, D., J. den Hollander, W. Evanochko, L. Johnson, and G. Pohost, ^{31}P nuclear magnetic resonance spectroscopy of human myocardial scar, in *Proceedings of the Society of Magn Reson in Med: 12th Annual Scientific Meeting & Exhibition*, N. New York, 1993, SMRM: Berkeley, CA, USA. p. 1091.
82. Neubauer, S., T. Krahe, R. Schindler, M. Horn, H. Hillenbrand, C. Entzeroth, H. Mader, E.P. Kromer, G.A. Riegger, K. Lackner, and G. Ertl, ^{31}P magnetic resonance spectroscopy in dilated cardiomyopathy and coronary artery disease: altered cardiac high-energy phosphate metabolism in heart failure. *Circulation*, 1992. 86(6): p. 1810-1818.
83. Schaefer, S., J. Gober, M. Valenza, G.S. Karczmar, G.B. Matson, S.A. Camacho, E.H. Botvinick, B. Massie, and M.W. Weiner, Nuclear magnetic resonance imaging-guided phosphorous-31 spectroscopy of the human heart. *J Am Coll Cardiol*, 1988. 12: p. 1449-1455.
84. Bottomley, P., CRISIS Pulse Sequence, . 1988: US.
85. Kim, H., The development of phosphorus-31 *in vivo* human cardiac spectroscopy. 1996, University of Florida.
86. Moonen, C.T.W., M. von Kienlin, P.C.M. van Zijl, J. Cohen, J. Gillen, P. Daly, and G. Wolf, Comparison of single-shot localization methods (STEAM and PRESS) for *in vivo* proton NMR spectroscopy. *NMR in Biomedicine*, 1989. 2(5/6): p. 201-208.
87. Yongbi, N.M., G.S. Payne, D.J. Collins, and M.O. Leach, Quantification of signal selection efficiency, extra volume

- suppression and contamination for ISIS, STEAM, and PRESS localized H-1 NMR spectroscopy using an EEC localization test object. *Phys Med Biol*, 1995. 40: p. 1293-1303.
88. Jung, W.-I., K. Kuper, F. Schick, M. Bunse, M. Pfeffer, K. Pfeffer, G. Dietze, and O. Lutz, Localized phosphorus NMR spectroscopy: a comparison of the FID, DRESS, CRYSIS/CODEX, and STEAM methods *in vitro* and *in vivo* using a surface-coil. *Magn Reson Imaging*, 1992. 10(4): p. 655-662.
89. Frahm, J., T. Michaelis, K.-D. Merboldt, W. Hanicke, M.L. Gyngell, D. Chien, and H. Bruhn, Localized NMR spectroscopy *in vivo*: Progress and problems. *NMR Biomed*, 1989. 2(5-6): p. 188-195.
90. Cady, E.B., M. Nylezinska, J. Penrice, A. Lorek, and P. Amess, Quantitation of phosphorus metabolites in newborn human brain using internal water as reference standard. *Magn Reson Imaging*, 1996. 14(3): p. 293-304.
91. GE, *Signa Advantage Spectroscopy Research Accessory Release 5.4 Operator's Manual*. 1995, Milwaukee, Wisconsin: General Electric Medical Systems.
92. Ordidge, R., A. Connelly, and J. Lohman, Image-selected *in vivo* spectroscopy (ISIS): a new technique for spatially selective NMR spectroscopy. *J Magn Reson*, 1986. 66: p. 283-294.
93. Lawry, T., G. Karczmar, M. Weiner, and G. Matsno, Computer simulation of MRS techniques: an analysis of ISIS. *Magn Reson Med*, 1989. 9: p. 299-314.
94. Bendall, M. and D. Pegg, Uniform sample excitation with surface coils for *in vivo* spectroscopy by adiabatic rapid half passage. *J Magn Reson*, 1986. 67: p. 376.
95. de Graaf, R.A., Y. Luo, M. Terpstra, H. Merkle, and M. Garwood, A new localization method using an adiabatic pulse, BIR-4. *J Magn Reson B*, 1995. 106(3): p. 245-252.
96. de Graaf, R.A., Y. Luo, M. Terpstra, and M. Garwood, Spectral editing with adiabatic pulses. *J Magn Reson B*, 1995. 109(2): p. 184-193.
97. FDA, *Magnetic Resonance Diagnostic Devices Criteria for Significant Risk Investigations* (at www.fda.gov), . 1997, Food and Drug Administration (FDA) Center for Devices and Radiological Health (CDRH): Washington, DC.
98. Brown, J.J., S.A. Mirowitz, J.C. Sandstrom, and W.H. Perman, MR spectroscopy of the heart. *AJR*, 1990. 155: p. 1-11.
99. Briggs, R., personal communication. May, 1999.
100. Neubauer, S., M. Horn, H. Mader, D. Lubke, M. Godde, W. Kaiser, D. Hahn, and G. Ertl, Hemodynamic correlates of impaired cardiac high-energy phosphate metabolism in patients with dilated

- cardiomyopathy, in *Proceedings of the Society for Magnetic Resonance in Medicine: 2nd Annual Scientific Meeting*, C. San Francisco, USA, 1994, SMRM: Berkeley, CA, USA. p. 90.
101. van Dobbenburgh, J., N. de Jonge, C. Klopping, J. Lahpor, S. Woolley, and C. van Echten, Altered myocardial energy metabolism in heart transplant patients: consequence of rejection or a postischemic phenomenon?, in *Proceedings of the Society of Magn Reson in Med: 12th Annual Scientific Meeting & Exhibition*, N. New York, 1993, SMRM: Berkeley, CA, USA. p. 1093.
102. Evanochko, W., J. den Hollander, D. Luney, G. Blackwell, and G. Pohost, ³¹P MRS in human heart transplants: a clinical update, in *Proceedings of the Society of Magn Reson in Med: 12th Annual Scientific Meeting & Exhibition*, N. New York, 1993, SMRM: Berkeley, CA, USA. p. 1092.
103. Evanochko, W., A. Bouchard, J. Kirklin, R. Bourge, D. Luney, and G. Pohost, Detection of cardiac transplant rejection in patients by ³¹P NMR spectroscopy, in *Book Of Abstracts, Society of Magnetic Resonance in Medicine, 9th Annual Scientific Meeting & Exhibition*, N. New York, 1990, SMRM: Berkeley, CA, USA. p. 246.
104. Horn, M., M. Cramer, K. Harre, T. Pabst, D. Hahn, and S. Neubauer, 6 years experience with ³¹P -MR spectroscopy of the human myocardium: 209 examinations in 163 patients, in *Proceedings of the Society of Magnetic Resonance in Medicine: Fourth Scientific Meeting & Exhibition*, N. New York, 1996, SMRM: Berkeley, CA, USA. p. 1009.
105. Neubauer, S., M. Horn, H. Mader, and et al., Clinical and hemodynamic correlates of impaired cardiac high-energy phosphate metabolism in patients with aortic valve disease, in *Proceedings of the Society of Magn Reson in Med: 12th Annual Scientific Meeting & Exhibition*, N. New York, 1993, SMRM: Berkeley, CA, USA. p. 355.
106. Dell' Italia, L., W. Evanochko, G. Blackwell, J. den Hollander, H. Singleton, and G. Pohost, Dissociation between mechanics and PCr/ATP in patients with volume overload hypertrophy, in *Proceedings of the Society of Magn Reson in Med: 12th Annual Scientific Meeting & Exhibition*, N. New York, 1993, SMRM: Berkeley, CA, USA. p. 356.
107. Keesil, S., M. Lewis, J. Garbutt, I. Huggo, E. Baker, and P. Garlick, In vivo phosphorous-31 NMR spectroscopy of the myocardium in children with congenital heart abnormalities, in *Proceedings of the Society of Magn Reson in Med: 12th Annual Scientific Meeting & Exhibition*, N. New York, 1993, SMRM: Berkeley, CA, USA. p. 1095.
108. Luyten, P.R., A. de Roos, L.J.M.J. Oosterwaal, J. Doornbos, and J.A. den Hollander, PCr/ATP ratio changes and pH values in dilated and hypertrophic cardiomyopathy patients determined by ³¹P NMR heart spectroscopy, in *Book Of Abstracts, Society of Magnetic Resonance in Medicine, 16th Annual Scientific Meeting &*

- Exhibition, C. San Francisco, USA, 1991, SMRM: Berkeley, CA, USA. p. 74.
109. Neubauer, S., M. Horn, M. Goedde, K. Harre, A. Laser, W. Bauer, T. Pabst, D. Hahn, I. Reis, J. Ingwall, and G. Ertl, In patients with dilated cardiomyopathy abnormal cardiac energy metabolism can be detected invasively (endomyocardial biopsy) and non-invasively ($31P$ -MR spectroscopy), in Proceedings of the Society of Magnetic Resonance: 3rd Scientific Meeting & Exhibition & The European Society for Magn Reson & Biol: 12th Annual Meeting & Exhibition, F. Nice, 1995, SMRM: Berkeley, CA, USA. p. 93.
 110. Sharp, J.C. and M.O. Leach, Conformal NMR spectroscopy: Accurate localization to noncuboidal volumes with optimum SNR. *Magn Reson Med*, 1989. 11: p. 376.
 111. Neubauer, S., M. Horn, M. Godde, D. Lubke, B. Jilling, D. Hahn, and G. Ertl, Contributions of $31P$ -magnetic resonance spectroscopy to the understanding of dilated heart muscle disease. *Eur-Heart-J*, 1995. 16(Supplement O): p. 115-118.
 112. Lamb, H., H.P. Beyerbach, J. Doornbos, B.E. van der Wall, and A. de Roos, Evidence for altered myocardial HEP metabolism in hypertensive cardiac hypertrophy, in Proceedings of the International Society for Magnetic Resonance in Medicine: Fifth Scientific Meeting & Exhibition, B. Vancouver, Canada, 1997, SMRM: Berkeley, CA, USA. p. 361.
 113. Neubauer, S., M. Horn, K. Harre, H. Stromer, T. Pabst, J. Sandstede, D. Hahn, and K. Kochsiek, Impaired cardiac high-energy phosphate metabolism in patients with aortic stenosis but not in patients with aortic regurgitation, in Proceedings of the International Society for Magnetic Resonance in Medicine: Fifth Scientific Meeting & Exhibition, B. Vancouver, Canada, 1997, SMRM: Berkeley, CA, USA. p. 1283.
 114. Lamb, H.J., R. Ouwerkerk, J. Doorbos, v.d. Laarse, and A. de Roos, Motion sensitivity of 3D-ISIS: effects on human cardiac $31P$ -MRS during stress, in Proceedings of the International Society for Magnetic Resonance in Medicine: Fifth Scientific Meeting & Exhibition, B. Vancouver, Canada, 1997, SMRM: Berkeley, CA, USA. p. 1290.
 115. Ye, J., J.K. Sun, J. Shen, R. Summers, T.A. Salerno, and R. Deskauriers, Localized magnetic resonance spectroscopy is a useful tool for continuous assessment of metabolism in both ventricles during warm blood cardioplegia, in Proceedings of the International Society for Magnetic Resonance in Medicine: Fifth Scientific Meeting & Exhibition, B. Vancouver, Canada, 1997, SMRM: Berkeley, CA, USA. p. 1291.
 116. Vermeulen, J.W.A.H., P.R. Lyuten, J.I. van der Heijden, and J.A. den Hollander, Uncovering the Pi signal in the *in vivo* $31P$ NMR spectra of the human heart, in Book of Abstracts, Society of Magnetic Resonance in Medicine, 7th Annual Scientific Meeting & Exhibition, C. San Francisco, USA, 1988, SMRM: Berkeley, CA, USA. p. 833.

117. Sauter, R., M. Friedrich, H. Requardt, J. Offermann, and A. Weikl, *Localized phosphorus spectroscopy of the human myocardium*, in *Book of Abstracts, Society of Magnetic Resonance in Medicine, 7th Annual Scientific Meeting & Exhibition, C. San Francisco, USA, 1988*, SMRM: Berkeley, CA, USA. p. 828.
118. Kantor, H.L., R.W. Briggs, K.R. Metz, and R.S. Balaban, *Gated in vivo examination of cardiac metabolites with 31P nuclear magnetic resonance*. Am J Physiol, 1986. **251**: p. H171-H175.
119. Humphrey, S.M. and P.B. Garlick, *NMR-visible ATP and Pi in normoxic and reperfused rat hearts: a quantitative study*. Am J Physiol, 1991. **260**: p. H6-H12.
120. Garlick, P. and R. Townsend, *NMR visibility of Pi in perfused rat hearts is affected by changes in substrate and contractility*. Am J Physiol, 1992. **263**: p. H497-H502.
121. Garlick, P., G. Radde, P. Seeley, and B. Chance, *Phosphorous NMR studies on perfused hearts*. Biochem Biophys Res Commun, 1977. **74**: p. 1256-1262.
122. Jacobus, W., G. Taylor, D. Hollis, and R. Nunnally, *Phosphorus nuclear magnetic resonance of perfused working rat hearts*. Nature (London), 1977. **265**(5596): p. 756-758.
123. Bottomley, P.A., R.J. Herfkens, L.S. Smith, S. Brazzamano, R. Binder, L.W. Hedlund, J.L. Swain, and R.W. Redington, *Noninvasive detection and monitoring of regional myocardial ischemia in situ using depth-resolved 31P NMR spectroscopy*. Proc Natl Acad Sci USA, 1985. **82**(24): p. 8747-8751.
124. Bottomley, P., L. Smith, S. Brazzamano, L. Hedlund, R. Redington, and R. Herfkens, *The fate of inorganic phosphate and pH in regional myocardial ischemia and infarction: a noninvasive 31P NMR study*. Magn Reson Med, 1987. **5**(2): p. 129-142.
125. Jasinski, A., P. Kozlowski, A. Urbanski, and J. Saunders, *Hexagonal surface gradient coil for localized MRS of the heart*. Magn Reson Med, 1991. **21**: p. 296.
126. Robitaille, P.M., H. Merkle, B. Lew, G. Path, K. Hendrich, P. Lindstrom, A.H. From, M. Garwood, R.J. Bach, and K. Ugurbil, *Transmural high energy phosphate distribution and response to alterations in workload in the normal canine myocardium as studied with spatially localized 31P NMR spectroscopy*. Magn Reson Med, 1990. **16**(1): p. 91-116.
127. Balaban, R.S., H.L. Kantor, L.A. Katz, and R.W. Briggs, *Relation between work and phosphate metabolism in the in vivo paced mammalian heart*. Science, 1986. **232**: p. 1121-1123.
128. Rehr, R.B., J.L. Tatum, J.I. Hirsch, L. Wetstein, and G. Clarke, *Effective separation of normal, acutely ischemic, and reperfused myocardium with P-31 MR spectroscopy*. Radiology, 1988. **168**: p. 81-89.

129. Levine, S.R., J.A. Helpern, K.M. Welch, A.M. Vande-Linde, K.L. Sawaya, E.B. Brown, N.M. Ramadan, R.K. Deveshware, and R.J. Ordidge, Human focal cerebral ischemia: evaluation of brain pH and energy metabolism with $P-31$ NMR spectroscopy. *Radiology*, 1992. 185(2): p. 537-544.
130. Rehr, R.B., B.B. Fuhs, F. Lee, J.L. Tatum, J.I. Hirsch, and R. Quint, Differentiation of reperfused-viable (stunned) from reperfused-infarcted myocardium at 1 to 3 days postreperfusion by *in vivo* phosphorus-31 nuclear magnetic spectroscopy. *Am Heart J*, 1991. 122: p. 1571-1582.
131. Jennings, R. and K. Reimer, Lethal myocardial ischemic injury. *Am J Pathol*, 1981. 102: p. 241-255.
132. Markiewicz, W., S. Wu, W.W. Parmley, C.B. Higgins, R. Sievers, T.L. James, J. Wikman-Coffelt, and G. Jasmin, Evaluation of the hereditary Syrian hamster cardiomyopathy by $31P$ nuclear magnetic resonance spectroscopy: improvement after acute verapamil therapy. *Circ Res*, 1986. 59(6): p. 597-604.
133. Camacho, S.A., J. Wikman-Coffelt, S. Wu, T.A. Watters, E.H. Botvinick, R. Sievers, T.L. James, G. Jasmin, and W.W. Parmley, Improvement in myocardial performance without a decrease in high-energy phosphate metabolites after isoproterenol in Syrian cardiomyopathic hamsters. *Circulation*, 1988. 77: p. 712-719.
134. Wu, S., R. White, J. Wikman-Coffelt, R. Sievers, M. Wendland, J. Garrett, C.B. Higgins, T. James, and W.W. Parmley, The preventative effect of verapamil on ethanol-induced cardiac depression: phosphorus-31 nuclear magnetic resonance and high-pressure liquid chromatographic studies of hamsters. *Circulation*, 1987. 75(5): p. 1058-1064.
135. Nicolay, K., W. Aue, J. Seelig, C. van Echteld, T. Ruigrok, and B. de Kruijff, Effects of the anti-cancer drug adriamycin on the energy metabolism of the rat heart as measured by *in vivo* $31P$ -NMR and implications for adriamycin-induced cardiotoxicity. *Biochim Biophys Acta*, 1987. 929: p. 5 - 13.
136. Kopp, S., L. Klevay, and J. Feliksik, Physiological and metabolic characterization of a cardiomyopathy induced by chronic copper deficiency. *Am J Physiol*, 1983. 245: p. H855-H866.
137. Afzal, N., P. Ganguly, K. Dhalla, G. Pierce, P. Signal, and N. Dhalla, Beneficial effects of verapamil in diabetic cardiomyopathy. *Diabetes*, 1988. 37: p. 936-942.
138. Schaefer, S., G.G. Schwartz, J.R. Gober, B. Massie, and M.W. Weiner, Magnetic resonance spectroscopy. Evaluation of ischemic heart disease. *Invest Radiol*, 1989. 24: p. 969-972.
139. Schaefer, S., S. Camacho, J. Gober, R.G. Obregon, M.A. DeGroot, E.H. Botvinick, B. Massie, and M.W. Weiner, Response of myocardial metabolites to graded regional ischemia: $31P$ NMR

- spectroscopy of porcine myocardium in vivo. *Circ Res*, 1989. 64(5): p. 968-976.
140. Schaefer, S., G.G. Schwartz, J.R. Gober, A.K. Wong, S.A. Camacho, B. Massie, and M.W. Weiner, Relationship between myocardial metabolites and contractile abnormalities during graded regional ischemia. *Phosphorus-31 nuclear magnetic resonance studies of porcine myocardium in vivo*. *J Clin Invest*, 1990. 85(3): p. 706-713.
 141. Von Kienlin, M. and R. Mejia, Spectral localization with optimal pointspread function. *J Magn Reson*, 1991. 94: p. 268-287.
 142. Neubauer, S., R. Schindler, T. Krahe, H. Hillenbrand, C. Entrereth, M. Horn, W. Bauer, T. Stephan, K. Lackner, G. Ertl, and A. Haase, Direct measurement of spin-lattice relaxation times of phosphorus metabolites in human myocardium, in *Works in Progress, Society of Magnetic Resonance in Medicine, 10th Annual Scientific Meeting & Exhibition*, C. San Francisco, USA, 1991, SMRM: Berkeley, CA, USA. p. 987.
 143. Loeffler, R., H. Kolem, K. Wicklow, A. Haase, and M. von Kienlin, Localized MR spectra in the human heart from anatomically matched compartments in three spatial dimensions, in *Proceedings of the Society of Magnetic Resonance: 3rd Scientific Meeting & Exhibition & The European Society for Magn Reson & Biol: 12th Annual Meeting & Exhibition*, F. Nice, 1995, SMRM: Berkeley, CA, USA. p. 334.
 144. Sieverding, L., W.I. Jung, J. Breuer, S. Widmaier, A. Staubert, P. van Erckelen, O. Schmidt, M. Bunse, T. Hoess, O. Lutz, G.J. Dietze, and A. J., Proton-decoupled myocardial ^{31}P NMR spectroscopy reveals decreased PCr/Pi in patients with severe hypertrophic cardiomyopathy. *Am J Cardiol*, 1997. 80(3A): p. 34A-40A.
 145. Neubauer, S., M. Horn, M. Cramer, K. Harre, J.B. Newell, W. Peters, T. Pabst, G. Ertl, D. Hahn, J.S. Ingwall, and K. Kochsiek, Myocardial phosphocreatine-to-ATP ratio is a predictor of mortality in patients with dilated cardiomyopathy. *Circulation*, 1997. 96(7): p. 2190-2196.
 146. Landschutz, W., M. Meiningen, M. Beer, T. Seyfarth, M. Horn, T. Pabst, A. Haase, D. Hahn, S. Neubauer, and M. von Kienlin, Concentration of human cardiac ^{31}P -metabolites determined by SLOOP ^{31}P -MRS. *MAGMA*, 1998. 6(2-3): p. 155-156.
 147. Masuda, Y., Y. Tateno, H. Ikehira, T. Hashimoto, F. Shishido, M. Sekiya, Y. Imazeki, H. Imai, S. Watanabe, and Y. Inagaki, High-energy phosphate metabolism of the myocardium in normal subjects and patients with various cardiomyopathies: the study using ECG gated MR spectroscopy with a localization technique. *Jpn Circ J*, 1992. 56(6): p. 620-626.
 148. Sakuma, H., K. Takeda, T. Tagami, T. Nakagawa, S. Okamoto, T. Konishi, and T. Nakano, ^{31}P MR spectroscopy in hypertrophic

- cardiomyopathy: comparison with Tl-201 myocardial perfusion imaging. Am Heart J, 1993. 125: p. 1323-1328.
149. Bottomley, P.A., R.J. Herfkens, L.S. Smith, and T.M. Bashore, Altered phosphate metabolism in myocardial infarction: P-31 MR spectroscopy. Radiology, 1987. 165(3): p. 703-707.
 150. Bottomley, P.A., R.G. Weiss, C.J. Hardy, and W.A. Baumgartner, Myocardial high-energy phosphate metabolism and allograft rejection in patients with heart transplants. Radiology, 1991. 181(1): p. 67-75.
 151. Bottomley, P., R. Weiss, C. Hardy, and G. Gerstenblith, 31P NMR stress testing in patients with coronary disease: evidence for myocardial PCr/Pi changes, in Book Of Abstracts, Society of Magnetic Resonance in Medicine, 10th Annual Scientific Meeting & Exhibition, C. San Francisco, USA, 1991, SMRM: Berkeley, CA, USA. p. 577.
 152. Hardy, C.J., P.A. Bottomly, K.W. Rohling, and P.B. Roemer, An NMR phased array for human cardiac 31P spectroscopy. Magn Res Med, 1992. 28: p. 54-64.
 153. Bottomley, P.A. and C.J. Hardy, Proton Overhauser enhancements in human cardiac phosphorous NMR spectroscopy at 1.5T. Magn Reson Med, 1992. 24: p. 384-390.
 154. Bottomley, P.A. and C.J. Hardy, Mapping creatine kinase reaction rates in human brain and heart with 4 tesla saturation transfer 31P NMR. J Magn Reson, 1992. 99: p. 443-448.
 155. Rajagopalan, B., M.J. Blackledge, W. McKenna, N. Bolas, and G.K. Radda, Measurement of phosphocreatine to ATP ratio in normal and diseased human heart by 31P magnetic resonance spectroscopy using the rotating frame-depth selection technique. Ann NY Acad Sci, 1987. 508: p. 321-332.
 156. Conway, M.A., J. Allis, R. Ouwerkerk, T. Niicka, B. Rajagopalan, and G.K. Radda, Detection of low phosphocreatine to ATP ratio in failing hypertrophied human myocardium by 31P magnetic resonance spectroscopy. Lancet, 1991. 338(8773): p. 973-976.
 157. Conway, M., J. Bristow, M. Blackledge, B. Rajagopalan, and G. Radda, Cardiac metabolism during exercise in healthy volunteers measured by 31P magnetic resonance spectroscopy. Br Heart J, 1991. 65: p. 25-30.
 158. Blamire, A.M., C. Liess, and B. Rajagopalan, Sine bell encoding and surface saturation techniques to obtain spectra from the whole human heart using a double surface coil, in Proceedings of the Society of Magnetic Resonance: 3rd Scientific Meeting & Exhibition & The European Society for Magn Reson & Biol: 12th Annual Meeting & Exhibition, F. Nice, 1995, SMRM: Berkeley, CA, USA. p. 1942.
 159. Blamire, A.M., C. Liess, G.K. Radda, and B. Rajagopalan, Measurement of myocardial pH by saturation transfer in man, in

- Proceedings of the Society of Magnetic Resonance: 3rd Scientific Meeting & Exhibition & The European Society for Magn Reson & Biol: 12th Annual Meeting & Exhibition, F. Nice, 1995, SMRM: Berkeley, CA, USA. p. 91.*
160. Conway, M., P. Bottomley, R. Ouwerkerk, G. Radda, and B. Rajagopalan, *Mitral regurgitation: impaired systolic function, eccentric hypertrophy, and increased severity are linked to lower phosphocreatine/ATP ratios in humans*. Circulation, 1998. 97(17): p. 1716-1723.
 161. Schaefer, S., J.R. Gober, G.G. Schwartz, D.B. Twieg, M.W. Weiner, and B. Massie, *In vivo phosphorous-31 spectroscopic imaging in patients with global myocardial disease*. Am J Cardiol, 1990. 65(16): p. 1154-1161.
 162. Auffermann, W., W.M. Chew, C.L. Wolfe, N.J. Tavares, W.W. Parmley, R.C. Semelka, T. Donnelly, K. Chatterjee, and C.B. Higgins, *Normal and diffusely abnormal myocardium in humans: functional and metabolic characterization with P-31 MR spectroscopy and cine MR imaging*. Radiology, 1991. 179: p. 253-259.
 163. Schaefer, S., G. Schwartz, S. Steinman, D. Meyerhoff, B. Massie, and M. Weiner, *Metabolic response of the human heart to inotropic stimulation: in vivo phosphorous-31 studies of normal and cardiomyopathic myocardium*. Magn Reson Med, 1992. 25(2): p. 260-272.
 164. van Dobbenburgh, J., C. Lekkerkerk, and C. van Echteld, *Saturation effects in human heart and chest wall muscle measured by 31P 1D spectroscopic imaging*, in *Book Of Abstracts, Society of Magnetic Resonance in Medicine, 10th Annual Scientific Meeting & Exhibition, C. San Francisco, USA, 1991, SMRM: Berkeley, CA, USA*. p. 988.
 165. de Roos, A., J. Doornbos, P. Luyten, L. Oosterwaal, E. van der Wall, and J. den Hollander, *Cardiac metabolism in patients with dilated and hypertrophic cardiomyopathy: assessment with proton-decoupled P-31 MR spectroscopy*. J Magn Reson Imaging, 1992. 2(6): p. 711-719.
 166. Lamb, H.J., J. Doornbos, J.A. den Hollander, P.R. Luyten, H.P. Beyerbach, E.E. van der Wall, and A. de Roos, *Reproducibility of human cardiac 31P-NMR spectroscopy*. NMR Biomed, 1996. 9(5): p. 217-227.
 167. Lamb, H.J., H.P. Beyerbach, R. Ouwerkerk, J. Doornbos, B.M. Pluim, E.E. van der Wall, A. van der Laarse, and A. de Roos, *Metabolic response of normal human myocardium to high-dose atropine-dobutamine stress studied by 31P-MRS*. Circulation, 1997. 96(9): p. 2969-2977.
 168. Pluim, B.M., H.J. Lamb, H.W. Kayser, F. Leujes, H.P. Beyerbach, A.H. Zwinderman, A. van der Laarse, H.W. Vliegen, A. de Roos, and E.E. van der Wall, *Functional and metabolic evaluation of the athlete's heart by magnetic resonance imaging and dobutamine*

- stress magnetic resonance spectroscopy.* Circulation, 1998. 97(7): p. 666-672.
169. den Hollander, J., W. Evanochko, L. Dell'Italia, and G. Pohost, ^{31}P NMR T1 inversion recovery measurements of the human heart, in *Proceedings of the Society of Magn Reson in Med: 12th Annual Scientific Meeting & Exhibition*, N. New York, 1993, SMRM: Berkeley, CA, USA. p. 1098.
 170. Doornbos, J., P. Luyten, M. Janssen, r.M. Wasse, and A. de Roos, P-^{31} MR spectroscopy of skeletal and cardiac muscle metabolism in patients with systemic sclerosis: a multiple case study. *J Magn Reson Imaging*, 1994. 4: p. 165-8.
 171. Ponder, S.L. and D.B. Twieg, A novel sampling method for ^{31}P spectroscopic imaging with improved sensitivity, resolution, and side lobe suppression. *J Magn Reson, Series B*, 1994. 104: p. 85-88.
 172. Whitman, G.J.R., B. Chance, H. Bode, J. Maris, J. Hasselgrove, R. Kelley, B.J. Clark, and A.H. Harken, Diagnosis and therapeutic evaluation of a pediatric case of cardiomyopathy using phosphorous-31 nuclear magnetic resonance spectroscopy. *J Am Coll Cardiol*, 1985. 5(3): p. 745-749.
 173. Kalil-Filho, R., C.P. de Albuquerque, R.G. Weiss, A. Mocellim, G. Bellotti, G. Cerri, and F. Pileggi, Normal high energy phosphate ratios in "stunned" human myocardium. *J Am Coll Cardiol*, 1997. 30(5): p. 1228-1232.
 174. Brunner, A., H.-W. Kim, A. Boyette, C. Pepine, S. McGorray, S. Buchthal, J. den Hollander, and K. Scott, Human *in vivo* cardiac imaging and phosphorus DRESS spectroscopy of women with suspected microvascular dysfunction using the 1.5 T GE Signa, in *International Society for Magnetic Resonance in Medicine Seventh Scientific Meeting and Exhibition*, P. Philadelphia, 1999, MRM: Berkeley, CA. p. 281.
 175. Brunner, A., H.W. Kim, D. Peterson, J. Fitzsimmons, C. Pepine, S. Buchthal, J. den Hollander, and K. Scott, Improvements in human *in-vivo* cardiac phosphorus spectroscopy at 3.0 Tesla in comparison with 1.5 Tesla for ischemic heart disease, in *International Society for Magnetic Resonance in Medicine Seventh Scientific Meeting and Exhibition*, P. Philadelphia, 1999, MRM: Berkeley, CA. p. 1488.
 176. Memon, R.S., K. Hendrich, X. Hu, and K. Ugurbil, ^{31}P NMR spectroscopy of the human heart at 4 T: detection of substantially uncontaminated cardiac spectra and differentiation of subepicardium and subendocardium. *Magn Res Med*, 1992. 26(2): p. 368-376.
 177. Ackerman, J., T. Grove, G. Wong, D. Gadian, and G. Radda, Mapping of metabolites in whole animals by ^{31}P NMR using surface coils. *Nature*, 1980. 283: p. 167-170.

178. Buchthal, S.D., W.J. Thoma, J.S. Taylor, S.J. Nelson, and T.R. Brown, *In vivo* Ti values of phosphorus metabolites in human liver and muscle determined at 1.5T by chemical shift imaging. NMR in Biomedicine, 1989. 2(5/6): p. 298-304.
179. Hubesch, B., D.J. Meyerhoff, S. Naruse, Gober, T.J. Lawry, M.D. Bosck, G.B. Matson, and M.J. Weiner, Noninvasive quantitation of phosphorus metabolites in human tissue by NMR spectroscopy. J Magn Reson, 1989: p. 299-311.
180. Luyten, P., J. Groen, J. Vermeulen, and J. den Hollander, Experimental approaches to image localized human ^{31}P NMR spectroscopy. Magn Reson Med, 1989. 11: p. 1-21.
181. Bailes, D., D. Bryant, G. Bydder, H. Case, A. Collins, I. Cox, P. Evans, R. Harman, A. Hall, S. Khenia, P. McArthur, A. Oliver, M. Rose, B. Ross, and I. Young, Localized phosphorus-31 NMR spectroscopy of normal and pathological human organs *in vivo* using phase encoding techniques. J Magn Reson, 1987. 74: p. 158-170.
182. Cox, I.J., D.J. Bryant, A.G. Collins, P. George, R.R. Harman, A.S. Hall, H.J.F. Hodgson, S. Khenia, P. McArthur, D.H. Spencer, and I.R. Young, Four-dimensional chemical shift MR imaging of phosphorus metabolites of normal and diseased human liver. J Comput Assist Tomogr, 1988. 12: p. 369-376.
183. Brown, T.R., S.D. Buchthal, J. Murphy-Boesch, S.J. Nelson, and J.S. Taylor, A multi-slice sequence for ^{31}P *in vivo* spectroscopy. 1-D chemical shift imaging with an adiabatic half-passage pulse. J Magn Reson, 1989. 82: p. 629-633.
184. Blackledge, M.J., R.D. Oberhaensli, P. Styles, and G.K. Radda, Measurement of *in vivo* ^{31}P relaxation rates and spectral editing in human organs using rotating-frame depth selection. J Magn Reson, 1987. 71: p. 331-336.
185. Hayes, C.E. and L. Axel, Noise performance of surface coils for magnetic resonance imaging at 1.5 T. Med Phys, 1985. 12(5): p. 604-607.
186. Bendall, M., J. McKendry, I. Creashull, and R. Ordidge, Active detune switch for complete sensitive volume localization in *in vivo* spectroscopy using multiple rf coils and depth pulses. J Magn Reson, 1984. 60: p. 473-478.
187. Weiner, M.W. Magnetic Resonance Spectroscopy of Cardiac and Skeletal Muscle. in ISMRM 4th Scientific Meeting, Educational Course Syllabus. 1996, April 28th.
188. Constantinides, C.D., C.R. Westgate, O.D.W. G, E.A. Zerhouni, and E.R. McVeigh, A phased array coil for human cardiac imaging. Magn Reson Med, 1995. 34(1): p. 92-98.
189. Fayad, Z., T. Connick, and L. Axel, An improved quadrature or phased-array coil for MR cardiac imaging. Magn Reson Med, 1995. 34(2): p. 186-193.

190. Bottomley, P.A. and C.H. Olivieri, What is the optimum phased-array coil design for cardiac magnetic resonance?, in *Proceedings of the Society of Magnetic Resonance in Medicine: Fourth Scientific Meeting & Exhibition*, N. New York, 1996, SMRM: Berkeley, CA, USA. p. 248.
191. Chen, C.N., D.I. Hoult, and V.J. Sank, Quadrature detection coils -- A further $\sqrt{2}$ improvement in sensitivity. *Journal of Magn Reson*, 1983. 54: p. 324-327.
192. Mitsunami, K., M. Okada, T. Inoue, M. Hachisuka, M. Kinoshita, and T. Inubushi, *In vivo* 31P nuclear magnetic resonance spectroscopy in patients with old myocardial infarction. *Jpn Circ J*, 1992. 56: p. 614-619.
193. Okada, M., K. Mitsunami, T. Yabe, M. Kinoshita, S. Morikawa, and T. Inubushi, Quantitative measurements of phosphorus metabolites in normal and diseased human hearts by 31P NMR spectroscopy, in *Proceedings of the Society of Magn Reson in Med: 11th Annual Scientific Meeting & Exhibition*, 1992, SMRM: Berkeley, CA, USA. p. 2305.
194. Rozenman, Y. and H.L. Kantor, Heterotropic transplanted rat heart: a model for *in vivo* determination of phosphorus metabolites during ischemia and reperfusion. *J Magn Reson Med*, 1990. 13(3): p. 450-457.
195. den Hollander, J. and S. Buchthal, personal communication. 1998.
196. Buchthal, S., J. den Hollander, E.T. Martin, W.J. Rogers, and G. Pohost, Ischemia by P-31 MR spectroscopy in women without CAD: Pilot phase data from WISE, in *World Congress of Cardiology 1998*.
197. Yoshida, T., H. Watari, and K. Tagawa, Effects of active and passive recoveries on splitting of the inorganic phosphate peak determined by 31P -nuclear magnetic resonance spectroscopy. *NMR in Biomedicine*, 1996. 9: p. 13-19.
198. Brown, B.G., A.B. Lee, E.L. Bolson, and H.T. Dodge, Reflex constriction of significant coronary stenosis as a mechanism contributing to ischemic left ventricular dysfunction during isometric exercise. *Circulation*, 1984. 70: p. 18-24.
199. Widmaier, S., W.-I. Jung, M. Bunse, F. van Erckelens, G. Dietze, and O. Lutz, Change in chemical shift and splitting of 31P gamma-ATP signal and human skeletal muscle during exercise and recovery. *NMR in Biomedicine*, 1996. 9: p. 1-7.
200. Minakami, S., C. Suzuki, T. Saito, and H. Yoshikawa, Studies on erythrocyte glycolysis. I Determination of the glycolytic intermediates in human erythrocytes. *J Biochem*, 1965. 58: p. 543-550.
201. Ting, T., S. Naccarato, A. Qualtieri, G. Chidichimo, and C. Brancati, *In vivo* metabolic studies of glucose, ATP and 2,3-DPG in thalassaemia intermedia, heterozygous beta-thalassaemic and

- normal erythrocytes: ^{13}C and ^{31}P MRS studies. *J of Haematology*, 1994. 88: p. 547-554.
202. Ambruso, D.R., B. Hawkins, D.L. Johnson, A.R. Fritzberg, W.C. Klingensmith, and E.R.B. McCabe, Measurement of adenosine triphosphate and 2,3-diphosphoglycerate in stored blood with ^{31}P nuclear magnetic resonance spectroscopy. *Biochemical Medicine and Metabolic Biology*, 1986. 35: p. 376-383.
203. Moon, R.B. and J.H. Richards, Determination of intracellular pH by ^{31}P magnetic resonance. *The Journal of Biomedical Chemistry*, 1973. 248(20): p. 7276-7278.
204. Henderson, T.O., A.J.R. Costello, and A. Omachi, Phosphate metabolism in intact human erythrocytes: determination by phosphorus-31 nuclear magnetic resonance spectroscopy. *Proc Nat Acad Sci USA*, 1974. 71(6): p. 2487-2490.
205. Tehrani, A.Y., Y.-F. Lam, A.K.L.C. Lin, S.F. Dosch, and C. Ho, Phosphorus-31 nuclear magnetic resonance studies of human red blood cells. *Blood Cells*, 1982. 8: p. 245-261.
206. Lam, Y.-F., A.K.L.C. Lin, and C. Ho, A phosphorus-31 nuclear magnetic resonance investigation of intracellular environment in human normal and sickle cell blood. *Blood*, 1979. 54(1): p. 196-209.
207. Gupta, R.K., J.L. Benovic, and Z.B. Rose, The determination of the free magnesium level in the human red blood cell by ^{31}P NMR. *The Journal of Biological Chemistry*, 1978. 253(17): p. 6172-6176.
208. Gunther, H., *NMR Spectroscopy*. 1980, New York, NY: John Wiley & Sons.
209. Bottomley, P.A., C.J. Hardy, and R.G. Weiss, Correcting human heart ^{31}P NMR spectra for partial saturation: evidence that saturation factors for PCr/ATP are homogeneous in normal and disease states. *J Magn Reson*, 1991. 95: p. 341-355.
210. Bottomley, P., The true T₁ values of myocardial high-energy phosphates (letter)? *Magn Reson Med*, 1993. 29: p. 145-146.
211. Evelhoch, J.L., C.S. Ewy, B.A. Siegfried, J.J.H. Ackerman, D.W. Rice, and R.W. Briggs, ^{31}P spin-lattice relaxation times and resonance linewidths of rat tissue *in vivo*: Dependence upon the static magnetic field strength. *Magn Reson Med*, 1985. 2: p. 410-417.
212. Sakuma, H., S. Nelson, D. Vigneron, and C. Higgins, in *Proceedings of the Society of Magn Reson in Med: 11th Annual Scientific Meeting & Exhibition 1992*, SMRM: Berkeley, CA, USA. p. 2306.
213. Martin, J.P., B.D. Guth, R.H. Griffey, and D.E. Hoekenga, Myocardial creatine kinase exchange rates and ^{31}P NMR relaxation rates in intact pigs. *Magn Reson Med*, 1989. 11: p. 64-72.

214. Howe, F.A. and J.R. Griffiths, A two-compartment phosphate-doped gel phantom for localized spectroscopy. *Magn Reson Imag*, 1992. 10: p. 119-126.
215. Boylestad, R.L., *DC/AC: The Basics*. 1989, Columbus, Ohio: Merrill Publishing Company. 771.
216. Bottomley, P.A. and C.J. Hardy, Strategies and protocols for clinical ^{31}P research in the heart and brain. *Phil Trans R Soc Lond A*, 1990. 333: p. 531-544.
217. Lim, K., J. Pauly, P. Webb, R. Hurd, and Macovský, Short TE phosphorus spectroscopy using a spin-echo pulse. *Magn Reson Med*, 1994. 32: p. 98-103.
218. Cooper, J.W., *An Introduction to Fourier Transform NMR and the Nicolet 1080 Data System*. 1973, Madison, Wisconsin: Nicolet Instrument Corporation.
219. Field, S.A. and F.W. Wehrli, *Sigma Applications Guide: Volume I*. 4th ed. Vol. 1. 1990, Milwaukee, Wisconsin: GE.
220. Fitzsimmons, J., personal communication. June 1999.
221. Cohen, E. and A. McDermott, Who's fat? New definition adopted, <http://cnn.com/HEALTH/9806/17/weight.guidelines/index.html>, . 1998, CNN: Atlanta, GA.
222. Frohlich, O. and M.A. Wallert, Methods of measuring intracellular pH in the heart. *Cardiovasc Res*, 1995. 29: p. 194-202.
223. Arnold, D.L., P.M. Matthews, and G.K. Radda, Metabolic recovery after exercise and the assessment of mitochondrial function in vivo in human skeletal muscle by means of ^{31}P NMR. *Magnetic Resonance in Medicine*, 1983. 1: p. 307-315.
224. Graham, R., A. Taylor, and T. Brown, A method for calculating the distribution of pH in tissues and a new source of pH error from the P-31 NMR spectrum. *Am J Physiol*, 1994. 266(2): p. R638.
225. Bottomley, P. and R. Weiss, Non-invasive magnetic-resonance detection of creatine depletion in non-viable infarcted myocardium. *Lancet*, 1998. 351(9104): p. 714-718.

BIOGRAPHICAL SKETCH

Angela Properzio Bruner attended the Georgia Institute of Technology (Georgia Tech) in Atlanta, Georgia, where she graduated with a bachelor's degree in mechanical engineering in 1993. During her time at Georgia Tech she participated in the cooperative work program and swapped each quarter with work at Critikon, a Johnson & Johnson company in Tampa, Florida. Her work at Critikon continued after graduation, in the Division of Research and Development including work on the Dinamap™ vital signs monitor (in use in hospitals from clinics to intensive care and operating rooms) for its design, development, manufacture and FDA approval. Her work also overlapped with the quality control and design of blood pressure cuffs and equipment. In pursuit of a Ph.D. in the summer of 1994 she enrolled in the medical physics program in the departments of nuclear engineering and radiology at the University of Florida. She started working with Dr. Katherine Scott in the area of MRI and MRS, with special interest in human patient studies. Including the research presented in this dissertation, she was also able to work with MRI and proton and phosphorus MRS in a variety of patient studies where MR provided both diagnostic and treatment feedback. This experience included patients with cardiac heart failure, peripheral vascular disease, tumor, stroke, Sturge Weber syndrome, schizophrenia and cardiac syndrome-X. In addition, Angela shared her time with the

medical physicists at Shands at UF in annual physics tests, acceptance tests, and general quality control within the department of radiology.

In June 1996, Angela Marie Properzio married Thom Bruner, an architect/graphic artist and computer programmer from Tuscaloosa, Alabama.

I certify that I have read this study and that in my opinion it conforms to acceptable standards of scholarly presentation and is fully adequate, in scope and quality, as a dissertation for the degree of Doctor of Philosophy.

KN Scott

Katherine N. Scott, Chair
Professor of Nuclear and
Radiological Engineering

I certify that I have read this study and that in my opinion it conforms to acceptable standards of scholarly presentation and is fully adequate, in scope and quality, as a dissertation for the degree of Doctor of Philosophy.

Jeff R. Fitzsimmons
Jeffrey R. Fitzsimmons
Professor of Nuclear and
Radiological Engineering

I certify that I have read this study and that in my opinion it conforms to acceptable standards of scholarly presentation and is fully adequate, in scope and quality, as a dissertation for the degree of Doctor of Philosophy.

David E. Hintenlang
David E. Hintenlang
Associate Professor of Nuclear
and Radiological Engineering

I certify that I have read this study and that in my opinion it conforms to acceptable standards of scholarly presentation and is fully adequate, in scope and quality, as a dissertation for the degree of Doctor of Philosophy.

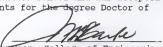
Christine B. Stopka
Christine B. Stopka
Associate Professor of Exercise
and Sport Sciences

I certify that I have read this study and that in my opinion it conforms to acceptable standards of scholarly presentation and is fully adequate, in scope and quality, as a dissertation for the degree of Doctor of Philosophy.

James R. Ballinger
James R. Ballinger
Assistant Professor of Radiology

This dissertation was submitted to the Graduate Faculty of the College of Engineering and to the Graduate School and was accepted as partial fulfillment of the requirements for the degree Doctor of Philosophy

August 1999



C. W. Stark

Dean, College of Engineering

Dean, Graduate School

LD
1780
1999
.B894

-997-9

UNIVERSITY OF FLORIDA



3 1262 08554 4780